MONASH University

PU.1 and maturational plasticity in acute myeloid leukaemia

Ethan Paul Oxley

A thesis submitted for the degree of Doctor of Philosophy at

Monash University in 2021

Australian Centre for Blood Diseases

Melbourne, Australia

Copyright notice

I certify that I have made all reasonable efforts to secure copyright permissions for third-party content included in this thesis and have not knowingly added copyright content to my work without the owner's permission.

Abstract

Acute myeloid leukaemia (AML) is a disease characterised by the accumulation of transformed immature myeloid blasts. This aggressive malignancy occurs following the acquisition of mutations that block normal myeloid differentiation and enhance proliferation and survival. There is a wide spectrum of recurrent genetic lesions, however compared to other cancers relatively few mutations are required for leukaemic transformation. Interestingly, many of the differentiation blocking mutations are acquired mutually exclusively, suggesting that they may converge to disrupt a similar gene or pathway.

AML patients routinely receive cytotoxic chemotherapy, and although the regime often induces remission, this is short lived and patients eventually relapse. A notable exception is in the treatment of the AML subtype acute promyelocytic leukaemia (APL), characterised by the PML-RARA fusion protein resulting from the t(15;17) translocation. The vitamin A analogue all-*trans*-retinoic-acid (ATRA) is capable of binding and degrading PML-RARA, triggering myeloid differentiation and engaging normal cell clearance mechanisms. The use of ATRA has revolutionised APL outcomes, fuelling the development of novel differentiation therapies targeting other recurrently mutated genes.

PU.1 is a myeloid transcription factor required for normal haematopoiesis. Although rarely sustaining direct mutations, normal PU.1 function is frequently disabled in AML by other recurrent mutations such as the APL fusion protein PML-RARA. Previously in the Dickins laboratory, a murine AML model termed AML246 was developed driven by reversible shRNA-based knockdown of endogenous PU.1. Upon PU.1 restoration AML246 cells homogeneously undergo myeloid differentiation coupled with a loss of clonogenicity and leukaemogenicity, mimicking ATRA-induce differentiation of APL. Surprisingly when PU.1 suppression is reengaged in these mature AML-derived cells, approximately 5% revert to their immature state and reacquire clonogenicity, demonstrating that AML246 maturation can be a plastic process.

Using RNA-seq, PU.1-ChIP-seq, and ATAC-seq, dynamic changes in AML246 transcription, PU.1 binding, and chromatin remodelling were tracked during differentiation and subsequent de-differentiation. This allowed the identification of 804 genes whereby PU.1 acts as a

pioneering transcription factor, binding nearby regulatory elements to open chromatin and upregulate transcription in a reversible manner. This demonstrates that PU.1 expression not only upregulates target genes to initiate myeloid differentiation, but sustains their expression to maintain the mature myeloid state.

Expanding on the reversible differentiation of AML246, de-differentiation of mature human APL cell lines NB4 and HT93 *in vitro* and primary patient samples *ex vivo* was examined through the treatment and withdrawal of the differentiation agent ATRA. Following withdrawal of ATRA, mature APL cells undergo immunophenotypic and morphologic de-differentiation, restoring both clonogenicity and viability.

To further examine the role of PU.1 in APL and myeloid differentiation, NB4 cells were stably transduced with inducible PU.1 shRNA. Remarkably, PU.1 suppression prevents ATRA-induced differentiation of NB4 cells. Furthermore, PU.1 knockdown alone can maintain the AML differentiation block following CRISPR/Cas9 deletion of PML-RARA in NB4 cells.

Ultimately, this data reveals that AML maturation is a plastic process driven in large part through the modulation of PU.1 function.

Declaration

This thesis is an original work of my research and contains no material which has been accepted for the award of any other degree or diploma at any university or equivalent institution and that, to the best of my knowledge and belief, this thesis contains no material previously published or written by another person, except where due reference is made in the text of the thesis.

Ethan Oxley
Mar 2021

Publications

McKenzie MD*, Ghisi M*, **Oxley EP* [*equal contributors]**, Ngo S, Cimmino L, Esnault C, Liu R, Salmon JM, Bell CC, Ahmed N, Erlichster M, Witkowski MT, Liu GJ, Chopin M, Dakic A, Simankowicz E, Pomilio G, Vu T, Krsmanovic P, Su S, Tian L, Baldwin TM, Zalcenstein DA, DiRago L, Wang S, Metcalf D, Johnstone RW, Croker BA, Lancaster GI, Murphy AJ, Naik SH, Nutt SL, Pospisil V, Schroeder T, Wall M, Dawson MA, Wei AH, De The H, Ritchie ME, Zuber J, Dickins RA. Interconversion between tumorigenic and differentiated states in acute myeloid leukemia. *Cell Stem Cell* 25, 258-272 (2019) [Commentary in *Cell Stem Cell* 25:167-8 (2019), profiled in *Cancer Discovery* 9:1157 (2019)] IF 20.96

Carmichael CL, Wang J, Nguyen T, Kolawole O, Benyoucef A, De Mazière C, Milne A, Samuel S, Gillinder K, Hediyeh-zadeh S, Vo A, Huang Y, Knezevic K, McInnes WRL, Shields B, Mitchell H, Ritchie ME, Lammens T, Lintermans B, Van Vlierberghe P, Wong N, Haigh K, Thoms JAI, Toulmin E, **Oxley EP**, Dickins RA, Beck D, Perkins A, McCormack M, Davis MJ, Berx G, Zuber J, Pimanda JE, Kile BT, Goossens S, Haigh JJ. The EMT modulator SNAI1 contributes to AML pathogenesis via its interaction with LSD1. *Blood* 136, 957-973 (2020) IF 17.543

Van Thillo Q, De Bie J, Seneviratne JA, Demeyer S, Omari S, Balachandran A, Zhai V, Tam WL, Sweron B, Geerdens E, Gielen O, Provost S, Segers H, Boeckx N, Marshall G, Cheung B, Isobe K, Kato I, Takita J, Amos T, Deveson I, McCalmont H, Lock R, **Oxley EP**, Garwood MM, Dickins RA, Uyttebroeck A, Carter DR, Cools J, de Bock CE. Oncogenic cooperation between the novel TCF7-SPI1 fusion and NRAS-G12D requires β-catenin activity to drive T-cell acute lymphoblastic leukemia. *Nature Communications*, in press (2021) IF 13.610

Acknowledgements

Starting with Honours in the Dickins Lab in 2016, the past 5 years have been an incredible learning experience that would not be possible without the aid of a multitude of people. Firstly, I must thank my supervisor Ross Dickins, who gave me the opportunity to join the lab, to stay on for a PhD, and was wholeheartedly involved with all my projects. Through his guidance the lab was a comfortable yet productive environment, fuelling me with a genuine interest in science that I hope sticks with me for the foreseeable future. Secondly, I'd like to thank Margherita Ghisi who supervised me when I first joined the lab, teaching me not only the foundational experimental techniques I continue to use to this day, but also represented a shining example how to perform good science. I can only hope to one day come close to her credibility as a scientist.

Additionally, I would like to thank members of the Dickins lab over the years who have provided both friendship and aid in a variety of ways. In particular I'd like to thank Steven Ngo who, as 1-year ahead of me in the PhD, was a valuable mentor in my first steps in the scientific environment. Additionally, nothing but my deepest gratitude to the research assistants, and my friends, Emilia Simankowicz, Thao Nguyen, and Max Garwood who all worked tirelessly in the background over the years to keep the rest of us productive and the lab functional. Furthermore, I would like to acknowledge the numerous others in the department that gave help when needed and were valuable friends, particularly Maria Selvadurai and Kelsey Man who welcomed me in as a housemate without hesitation.

Of course, I would never have made it this far without the encouragement and support of my family, particularly my parents Paul and Denise Oxley. Without their positive attitude to life, study, and work, as well as the lengths they will go to help us at any moment, I doubt I would have made it this far and thus I dedicate everything to them.

TABLE OF CONTENTS

Chapter 1. Literature Review

1.1 Acute Myeloid Leukaemia

Haematopoiesis is a tightly controlled process of differentiation from haematopoietic stem cells (HSCs) to increasingly committed and non-proliferative cell types ranging from red blood cells and platelets to myeloid and lymphoid immune cells. Importantly, the fate of the progenitors relies on a complex interwork of numerous transcription factors, cytokines, and niche signals. Dysregulation of this ordered process can lead to a variety of disorders, many of which remain incompletely understood and poorly treated. Acute myeloid leukaemia (AML) is a blood cancer characterised by abnormal myeloid progenitors with enhanced proliferation and impaired differentiation. The accumulation of these transformed leukaemic blasts in the bone marrow disrupts the normal development of haematopoietic progenitors and is rapidly fatal in the absence of therapy.

1.1.1 Incidence and prognosis

Over 1000 individuals are diagnosed with AML each year within Australia making it the most common acute leukaemia in adults (AIHW 2018). The malignancy most often occurs in those over 60 with a median age of incidence of 64, however it can appear in individuals of all ages (De Kouchkovsky and Abdul-Hay 2016). Typically arising as a *de novo* disease, the development of AML has also been attributed to prior exposure to chemotherapeutic or radiation therapies, as well as resulting from various genetic disorders.

When combining all subtypes, AML harbours the worst prognosis of all leukaemia and currently accounts for almost 2% of cancer related deaths. With few exceptions, currently available treatments for a majority of AML patients are inadequate, with the Surveillance, Epidemiology and End Results program (SEER) documenting a 5-year relative survival rate of only 28.7% (Hankey, Ries, and Edwards 1999). However, there has been a gradual trend towards improved survival rates owing to better management of standard therapies and the development of novel therapeutic agents.

1.1.2 Standard Therapy

For the majority of AML patients, the standard of care remains induction chemotherapy, 7-day cytarabine treatment followed by 3 days of anthracycline, otherwise known as the 7+3 regime.

Approximately 50-75% of patients that undergo this therapy will enter complete remission, however less than a third will achieve long-term disease-free survival (Litzow 2004). While chemotherapeutic agents target proliferative leukaemic cells, they also have significant off-target effects by killing normal dividing cells (Plenderleith 1990). The toxicity of chemotherapy means that many are ineligible for induction therapy, with the often-elderly patients more likely to suffer from treatment-related mortality (TRM). Additionally, elderly patients are more likely to harbour complex karyotype AML that can be resistant to chemotherapeutic agents (De Kouchkovsky and Abdul-Hay 2016).

Following induction therapy, consolidation therapy can be provided to combat any potential residual disease. This can involve further chemotherapy or allogeneic haematopoietic stem cell transplant (HSCT). Despite improvements in techniques and patient care, HSCT remains a risky procedure with a high TRM (Cornelissen and Blaise 2016). Nevertheless, it is preferentially considered as the first-line consolidation therapy in patients harbouring adverse-risk AML as they cannot be guaranteed a second remission. While these frontline treatments currently do not provide certain therapeutic success, the development of novel targeted strategies such as FLT3 inhibitors (Midostaurin) and mutant IDH1/2 inhibitors (Enasidenib/Ivosidenib) are showing encouraging results (discussed further in §1.4) (Yanada et al. 2005).

1.2 AML Genomics

Compared to other cancers, AML genomes harbour relatively few somatic gene mutations, with a single case of AML averaging 5 recurrent mutations (Cancer Genome Atlas Research et al. 2013). On a broader level however, the genetic landscape is considerably heterogeneous, with a variety of regularly occurring genetic lesions. This may highlight the fragility of normal haematopoiesis and the requirement for controlled regulation of the various differentiation factors.

1.2.1 AML genetic subtypes

Before the use of diagnostic DNA sequencing, AML subtypes were classified based on disease progression and maturation status of the cells as seen under the microscope with the French-American-British (FAB) classification scheme. Unfortunately, this system did not provide sufficient prognostic outlook, and an updated version has been developed by the World Health

Organisation (WHO classification) (Arber et al. 2016). This system includes genetic subtype classification, specifying some of the distinct genetic lesions that define individual cases of AML. Also included are AML cases arising in the context of myelodysplasia, previous therapies, Down syndrome, myeloid sarcomas, or otherwise unspecified. Ultimately, each and every AML harbour slight variations and should be considered on a case-to-case basis, with the sum of all co-occurring lesions providing the most prognostic information.

1.2.2 Categories of Driving Mutations

Identifying and categorising somatic mutations allows for more effective diagnostic, therapeutic, and prognostic management of individual patients. The classification of certain mutations was historically based on the theory that mutations in each of two classes were required for leukaemic transformation. This two-hit hypothesis centred around class I mutations that enhanced proliferation, namely in components of cytokine receptor signalling such as *FLT3*, *NRAS* or *KIT*, as well as class II mutations that blocked myeloid differentiation mostly through rearrangement of transcription factors such as *PML-RARA*, *RUNX1-RUNXT1* (*AML1-ETO*), or *MLL-X* (Kelly and Gilliland 2002). This genetic classification was centred around Sanger sequencing and karyotypic analysis of gross chromosomal rearrangements, and therefore limited in scope.

This classification has been expanded upon with the advent of modern gene analysis tools like next generation sequencing, allowing for the first cancer genome, an AML, to be sequenced in 2008 (Ley et al. 2008). This was soon followed up by a large-scale analysis of 200 AML patients in 2013 (Cancer Genome Atlas Research et al. 2013), and 1540 AML patients in 2016 (Papaemmanuil et al. 2016). Genetic lesions are now separated into eleven distinct gene categories, including transcription factor fusions, mutations in *NPM1*, tumour suppressors, DNA methylators, signalling proteins, chromatin-modifiers and chromatin, transcription factors, cohesion-complex proteins, and spliceosome components.

1.2.3 Co-occurrence and Mutual Exclusivity of Genetic Lesions

An intriguing aspect of AML genetics is that many of the recurrent mutations are mutually exclusive (Figure 1.1) (Cancer Genome Atlas Research et al. 2013; Papaemmanuil et al. 2016). This is especially evident for the rearranged transcription factors *PML-RARA, MYH11-CBFB, RUNX1-RUNX1T1*, and *MLL-X*, as well as direct mutations in *NPM1, RUNX1, TP53*, and

CEBPA. Mutations in these genes occur in over 70% of AML cases, and the mutually exclusivity suggests that they may converge to functionally disrupt common downstream targets or pathways in order to promote leukaemogenesis (§1.3). Further separation is also observed in the mutations acquired in kinases and the *RAS* family. These occur in 59% of AML patients, almost half of which are in the *FLT3* receptor tyrosine kinase. Additional mutual exclusivity is observed between mutations in other myeloid transcription factors, cohesion-complex proteins, and chromatin modifiers.

Interestingly, certain mutations are also more likely to co-occur together. Mutations in epigenetic regulators, such as *DMNT3A, IDH1/2*, and *TET1/2* are in a category of their own, but typically are found with other class I and II mutations (Cancer Genome Atlas Research et al. 2013). One particularly common example is the *FLT3/NPM1c/DNMT3A* co-mutation pattern. Advancement in single cell sequencing have allowed in-depth investigation into the clonal evolution of AML, identifying that co-operating mutations often occur sequentially, with pre-leukaemic early clonal expansion mostly driven by mutations in epigenetic regulators before the acquisition of certain signalling activation mutations (Miles et al. 2020; Morita et al. 2020). With resolution of co-operating genetic mutations currently limited by the number of patient samples able to be single cell sequenced, along with epigenomic and transcriptomic analysis of leukaemia progression, more co-operating states are likely to be characterised in the near future.

These findings of exclusivity and co-occurrence expand upon the class I and class II model, giving credence to the idea that critical aspects of haematopoiesis, the regulation of growth, differentiation, and survival, need to be individually disrupted for AML transformation.

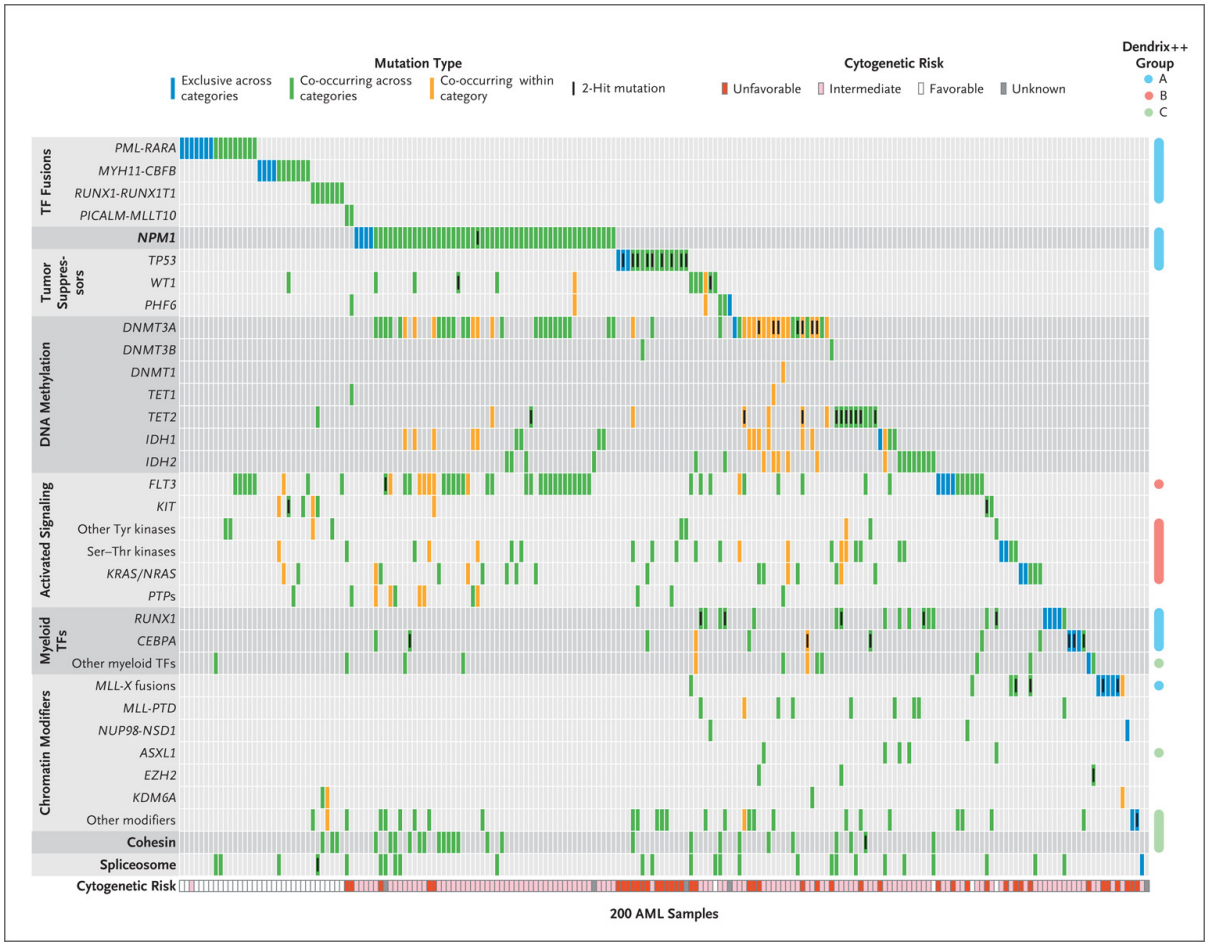

Figure 1.1: Molecular subgroups of recurrently mutated genes in AML
Stratification of the somatic mutations identified in 200 AML patients (Cancer Genome Atlas Research et al. 2013).

1.3 PU.1 Dysfunction in AML

There is increasing evidence that dysfunction of the myeloid transcription factor PU.1 (SPI1) contributes to the pathogenesis of multiple AML subtypes. Although PU.1 itself is rarely mutated in AML, numerous studies have identified links between some of the recurrent drivers of leukaemia and the direct downregulation or inhibition of PU.1, accounting for over 50% of AML cases. This may suggest that preventing normal PU.1 function is one of the crucial factors in the differentiation block required for leukaemogenesis.

1.3.1 The Myeloid Transcription Factor PU.1

PU.1 is a member of the ETS transcription factor family and is crucial for both myeloid and lymphoid lineage development. This transcription factor directly regulates the expression of over 1000 key genes for haematopoietic differentiation and commitment, including cytokine receptors for *G-CSF, GM-CSF, M-CSF*, as well as many key genes for granulocytic and macrophage functional pathways (Gupta et al. 2009). Additionally, PU.1 carries out its own autoregulation, positively inducing expression through the upstream regulatory element (URE) (Okuno et al. 2005). On a wider scale, PU.1 is known to indirectly modulate the expression of over 3000 genes in haematopoietic cells (Burda, Laslo, and Stopka 2010). It is highly expressed in monocytic, granulocytic, and B cell lymphoid lineages, although PU.1 is present in various haematopoietic stem cells and progenitors with levels fluctuating between the different stages of development (Nutt et al. 2005). The dose-dependency of PU.1 influences the progression between multiple cell fates.

Another aspect that influences the versatility of PU.1 in haematopoiesis is through interactions with multiple binding partners. These partners, including co-activators, co-repressors, and other transcription factors form complexes in order to contribute to the specificity of PU.1 function (Gupta et al. 2009). The binding sites for PU.1 are often surrounded by recognition sites for the other transcription factors, suggesting combinatorial roles for enhancer activity. Through interactions with proteins such as Sp1, IRF4/8, RUNX-1, C/EBPa/b, c-Jun, and GATA-1/2, PU.1 is able to have a wide influence on haematopoietic differentiation, while at the same time carrying out defined functions (Gupta et al. 2009). This PU.1 activity is tightly regulated and the inhibition or enhancement of which is associated with several haematopoietic diseases (Gupta et al. 2009).

1.3.2 PU.1 Suppression in Murine Models

Loss of function studies in mice highlight the influence PU.1 dysfunction can have in leukaemogenesis. As PU.1 is required for HSC maintenance in addition to myelopoiesis, total loss results in neonatal lethality as haematopoiesis fails to be established (Kim et al. 2004). Using conditional knockouts of PU.1, the role of PU.1 can be determined later in haematopoiesis. While HSCs without PU.1 fail to grow or form lymphoid and myeloid progenitors all together, loss of PU.1 in granulocyte-monocyte progenitors (GMPs) exhibit a differentiation block without a loss of proliferation (Iwasaki et al. 2005). This is in contrast to the lymphoid lineage, where the conditional loss of PU.1 in lymphoid progenitors does not affect the ability to produce mature lymphocytes, highlighting PU.1 as a regulator of myeloid differentiation.

A heterozygous deletion of PU.1 has little impact on mouse haematopoiesis, however the deletion of regulatory elements that diminish PU.1 levels to approximately 20% of normal levels trigger a block of differentiation and facilitate leukaemic transformation (Rosenbauer et al. 2004; Will et al. 2015). Restoring PU.1 in these cells re-establishes normal myeloid differentiation, demonstrating that PU.1 dysregulation in not only initiating but sustaining the differentiation block. Importantly, several recurrent and mutually exclusive class II mutations in human AML have direct impact on PU.1 function, thereby suggesting PU.1 disruption may represent a convergence point for differentiation blocking mutations.

1.3.3 PML-RARA

Acute promyelocytic leukaemia (APL) is a subtype of AML that is driven by the recurrent oncoprotein fusion PML-RARA resulting from a t(15;17) translocation. This translocation occurs in 10-15% of AML patients (Cancer Genome Atlas Research et al. 2013).

The fusion of PML and RARA alters both of their standard functions. PML is involved in the assembly of PML nuclear bodies, nebulous sites involved in the regulation of DNA replication, transcription, senescence, and apoptosis (Lallemand-Breitenbach and de The 2010). Mice devoid of PML have impaired apoptosis following cellular stress and increased tumourigenesis, however they only exhibit minor issues with haematopoiesis and otherwise develop healthily (Wang et al. 1998; Nakahara, Weiss, and Ito 2014). In APL, the PML-RARA fusion exhibits

a dominant negative effect upon the untranslocated PML, resulting in the fragmentation and disruption of nuclear bodies, however little is known how this directly impacts leukaemogenicity (Koken et al. 1994; Zhu et al. 1997; Duprez et al. 2000).

RARA is a member of the retinoic acid receptor family (RARA, RARB, RARG) and is a nuclear receptor protein which dissociates from co-repressors and binds co-activators to promote the transcription of numerous haematopoietic differentiation genes upon liganding of retinoic acid (Kastner et al. 2001). Following the t(15;17) chromosomal translocation, the RARA moiety of PML-RARA obtains co-repressor functionality, binding and downregulating genes crucial for differentiation (de The 2018).

Importantly, PML-RARA both downregulates *PU.1* expression transcriptionally while also directly binding PU.1 to antagonise its function at a protein level (Mueller et al. 2006). Furthermore, the fusion protein binds multiple RARA enhancers that are located near PU.1 binding sites, repressing important PU.1 targets (Wang et al. 2010). The inhibition of PU.1 is crucial to sustaining the differentiation block induced by PML-RARA, with overexpression of PU.1 alone sufficient to overcome a PML-RARA mediate differentiation block in APL models (Mueller et al. 2006). Differentiation of APL is discussed in further detail in §1.4.1.

1.3.4 RUNX1-RUNX1T1 (AML1-ETO) and RUNX1 mutations

RUNX1 (AML1) is another important myeloid transcription factor required for normal haematopoiesis that is frequently mutated or fused with RUNX1T1 (ETO) through the t(8;21) translocation (RUNX1-RUNX1T1) in AML. RUNX1 binds to a number of coactivators and transcription factors to regulate gene expression during myeloid haematopoiesis. *PU.1* upregulation is a fundamental role of RUNX1, inducing expression to properly establish myeloid commitment (Imperato et al. 2015). Additionally, RUNX1 interacts with PU.1 protein to activate expression of downstream targets including the key myeloid cytokine receptors *GM-CSF* and *M-CSF*. Mutant RUNX1, a recurrent lesion in AML, downregulates *PU.1* transcription directly, and fails to act as a coactivator with PU.1 protein (Huang et al. 2008).

RUNX1T1 is a zinc-finger transcription factor and a member of the ETO family (RUNX1T1, ETO2, ETO3), with co-repressor activities (Davis, McGhee, and Meyers 2003). Although RUNX1 has been observed in fusions with all the members of the ETO family, RUNX1-

RUNX1T1 remains the most frequent combination. In addition to RUNX1 disruption, the RUNX1-RUNX1T1 fusion recruits RUNX1T1 as a co-repressor to RUNX1 target genes, such as *PU.1*, while also binding PU.1 protein and displacing coactivators such as c-Jun (Vangala et al. 2003). Thus RUNX1-RUNX1T1 establishes a differentiation block in part through direct PU.1 antagonism. As with PML-RARA-driven leukaemia models, over-expression of *PU.1* is sufficient to overcome RUNX1-RUNX1T1 and restore myeloid differentiation (Vangala et al. 2003). Differentiation of RUNX1-RUNX1T1 AML is discussed in further detail in §1.4.3.3.

1.3.5 NPM1c

Mutations in *NPM1* are present in 27% of AML patients making it the second most commonly mutated gene in AML (Cancer Genome Atlas Research et al. 2013). NPM1 normally functions as a nuclear protein chaperone that facilitates the nuclear transport of various components including ribosomal proteins, histones, DNA, and RNA. In AML, mutations occur near the C-terminus of NPM1 that result in the misfolding of the nuclear-localisation domain and forced localisation to the cytoplasm (NPM1c) (Verhaak et al. 2005).

Until recently, how NPM1c localisation in the cytoplasm conferred leukaemogenesis was unknown. New evidence has shown that NPM1 in normal myeloid cells interacts and binds with PU.1, and that NPM1c retains this PU.1 binding ability, relocating PU.1 to the cytoplasm (Gu et al. 2018). This prevents PU.1 from binding DNA and inducing the expression of the key myeloid differentiation genes. Furthermore, through downregulation of *NPM1c* or the nuclear export inhibitor selinexor, it was shown that PU.1 can be re-located to the nucleus, restoring myeloid differentiation in NPM1c patient-derived xenograft AML models (Gu et al. 2018). Differentiation of NPM1c AML is discussed in further detail in §1.4.3.2.

1.3.6 FLT3 mutations

FMS-like tyrosine kinase 3 (*FLT3*) is a cytokine receptor expressed on various haematopoietic cells that, upon binding of the ligand FLT3L, initiates a signal cascade promoting cellular survival and proliferation. *FLT3* is mutated in 28% of AML cases making it the most recurrent genetic lesion (Cancer Genome Atlas Research et al. 2013). Furthermore, mutations in *FLT3* confer a high leukaemic burden and a poor prognosis (Daver et al. 2019). Mutations are most often an internal tandem duplication (ITD) in the intracellular domain (25% of AML cases), however point mutations in the kinase domain and over-expression of wild type *FLT3* are also

frequent. These mutations constitutively activate the receptor, representing a class I mutation that enhances AML survival and growth (Daver et al. 2019). Interestingly, selective targeting of activated FLT3 induces apoptosis but can also induce differentiation, suggesting class II potential (Sexauer et al. 2012; Cortes et al. 2019; McMahon et al. 2019). Interestingly, it was recently demonstrated that one of the downstream targets of FLT3 is the micro RNA miR-155, and that miR-155 potently inhibits *PU.1* transcript (Gerloff et al. 2015). This further exemplifies the recurrent theme of PU.1 disruption by recurrent AML oncogenes. Differentiation of FLT3 AML is discussed in further detail in §1.4.2.1.

1.4 Differentiation Therapy in AML

For most AML patients, chemotherapy remains the frontline treatment of AML. However, chemotherapies are cytotoxic agents that indirectly target rapidly growing cells without discretion causing devastating adverse reactions and frequently result in relapse. In contrast, differentiation therapies are targeted therapies that trigger maturation and allow natural cell turnover, in essence a less toxic therapy through indirectly allowing for cancer cell death. A differentiation therapy involves re-establishing differentiation, causing maturation of the leukaemic blasts into committed progeny that are inherently non-proliferative and with limited lifespan. These AML cells lose the ability to self-renew and survive, eventually being cleared from the body and causing regression of the disease. There are several of these targeted differentiation therapies approved for use against distinct AML subtypes, with more currently under development.

1.4.1 Differentiation of Acute Promyelocytic Leukaemia

APL is an aggressive subtype of AML that, prior to differentiation therapy, had a 1 week prognosis (Coombs, Tavakkoli, and Tallman 2015). However, it is now one of the most effectively treated cancers following the discovery of all-*trans*-retinoic-acid (ATRA), the original differentiation therapy. ATRA is an analogue of vitamin A capable of binding retinoic acid receptors to induce expression of pro-differentiation targets. It also binds the RARA subunit of the PML-RARA fusion-protein, promoting its degradation and dissociation from co-repressors to reactivate transcription of target genes responsible for myeloid differentiation (Quignon, Chen, and de The 1997). Importantly, degradation of PML-RARA leads to the restoration of PU.1 expression and function, which is necessary for the efficacy of ATRA (Mueller et al. 2006). Engaging differentiation of APL leads to a robust differentiation and

clearance of the leukaemia burden. However, the ability to trigger APL terminal myeloid differentiation without stopping leukaemia-initiating potential using distinct retinoid analogues demonstrates a disconnect between myeloid differentiation and permanent clearance, suggesting ATRA enables clearance through additional means (Ablain et al. 2013). Unfortunately, remission following ATRA monotherapy is often transitory, and its use initially required combination chemotherapy.

Following the advent of ATRA, it was discovered that APL also responds to arsenic trioxide (ATO), which in contrast to ATRA cures 70% of patients as a single agent (Mathews et al. 2002). ATO binds the PML subunit and also promotes the degradation of the fusion protein, suppressing growth and inducing cell death. Although it does not directly activate RARA target genes, ATO does trigger partial myeloid differentiation of AML blasts (Camacho et al. 2000). When used in combination, ATRA and ATO ensure robust differentiation and clearance of the leukaemia, with complete remission in approximately 80-90% of APL patients (Shen et al. 2004; Tallman et al. 2002). These targeted differentiation therapies have reversed the prognosis of a previously notorious subtype of AML, fuelling the development of novel targeted agents against non-APL AML.

1.4.2 Novel approved differentiation therapies

Differentiation therapy has revolutionised outcomes for APL patients, promoting a surge in the development of targeted therapies for other AML subtypes. Several novel clinically-approved agents have recently become available that promote differentiation, interestingly however they do not target classical differentiation-blocking class II lesions.

1.4.2.1 FLT3 Inhibitors

As previously mentioned, mutational activation of FLT3 remains one of the most recurrent hallmarks in AML (Cancer Genome Atlas Research et al. 2013). Traditionally considered a class I mutation, activation of FLT3 promotes proliferation and survival, however more recently it has been demonstrated that FLT3 activation in part limits PU.1 function among other myeloid differentiation transcription factors (Gerloff et al. 2015; Radomska et al. 2006). Several FLT3 inhibitors have been developed, of which gilteritinib and midostaurin have received approval for clinical use. Although the capacity for differentiation is incompletely detailed for some agents, both gilteritinib and the yet-to-be approved quizartinib have shown

definitive terminal differentiation in patients with FLT3-mutant AML (Sexauer et al. 2012; Cortes et al. 2019; McMahon et al. 2019). Although achieving longer overall survival rates, much like ATRA monotherapy remission is often transitory and a significant proportion do not respond at all (Altman et al. 2018).

1.4.2.2 Mutant IDH1/IDH2 Inhibitors

The isocitrate dehydrogenase isoforms *IDH1* and *IDH2* are enzymatic genes involved in cellular metabolism, catalysing the production of alpha-ketoglutarate (α-KG) from isocitrate. A number of enzymes are dependent on α-KG to regulate histone and DNA methylation (Lu and Thompson 2012). Mutations in either *IDH1* or *IDH2* occur in 20% of AML patients (Cancer Genome Atlas Research et al. 2013). In AML, mutant IDH converts α-KG to R2-hydroxyglutarate (R2-HG), impairing the function of α-KG dependent enzymes. The deregulation of DNA and histone methylation confers epigenetic aberrations that alter the expression of growth and tumour suppressive genes, promoting leukaemic transformation (Nassereddine et al. 2017). However, these mutations are not sufficient to drive leukaemia alone, thus the mutant IDH1 and IDH2 are often implicated in the maintenance of pre-leukaemic HSCs, which acquire additional cooperative mutations before leukaemic transformation (Chan and Majeti 2013). Small molecule inhibitors that specifically target IDH1 or IDH2 mutants such as ivosidenib and enasidenib have been developed specifically to address residual chemotherapeutic-resistant pre-leukaemic HSCs implicated as a source of relapse. These inhibitors have been shown to reduce the abundance of R2-HG, reversing the changes in DNA and histone methylation (Birendra and DiNardo 2016). Importantly, this is sufficient to reverse the differentiation block and achieve complete remission in a subset of mutant IDH patients, particularly those with minimal co-operating receptor tyrosine kinase mutations (DiNardo et al. 2018). However, relapse again is a regular occurrence, most often from mutations in the drug binding sites or of the reciprocal IDH paralogue (Intlekofer et al. 2018; Quek et al. 2018).

1.4.3 Experimental differentiation therapies

Several druggable options have been shown to trigger AML differentiation in pre-clinical studies, however they currently have failed to have a successful follow up.

1.4.3.1 ATRA and non-APL leukaemia

ATRA has allowed for a remarkable reversal in APL prognoses, however it usually only exhibits mild efficacy in non-APL contexts. Even in the absence of PML-RARA, ATRA is a ligand for the retinoic acid receptor family which regulates the expression of various genes involved in myelopoiesis (Collins 2002). The efficacy of ATRA in the absence of PML-RARA has been most famously demonstrated in the AML cell line HL60 (Breitman, Selonick, and Collins 1980). Although originating from a patient harbouring APL, the derived cell line does not express the classical fusion oncogene yet retains full responsiveness to the differentiating agent. Furthermore, ATRA-induced differentiation of HL60 appears to be entirely dependent on signalling through the untranslocated retinoic acid receptors (Collins, Robertson, and Mueller 1990). In addition to the known role of the retinoid, there is evidence for the targeted degradation of mutant NPM1 by ATRA (Martelli et al. 2015). There also exists sporadic case-reports of the moderate ATRA responses in the treatment of non-APL AML (Chen et al. 2002; Forghieri et al. 2016). However, systemic analysis has shown minimal efficacy of ATRA when used in combination with chemotherapy in non-APL AML patients (Kuley-Bagheri et al. 2018). Although non-APL ATRA differentiation currently fails to translate to clinic successfully, there remains further investigation into retinoid signalling in AML.

1.4.3.2 NPM1c and Nuclear export inhibitors

As previously mentioned, the nuclear export inhibitor selinexor can re-stablish normal myeloid differentiation in models of AML harbouring NPM1c by restoring PU.1 localisation to the nucleus (Gu et al. 2018). Selinexor is currently under clinical investigation in a multitude of AML subtypes, particularly focusing on forced accumulation of tumour suppressors in the nucleus to trigger apoptosis and differentiation (Sweet et al. 2020). Interestingly, in a recently completed clinical trial of selinexor for refractory AML patients, the only patient to achieve complete remission also exhibited an NPM1c mutation, however the pro-differentiation effects of selinexor remains to be investigated in patients (Garzon et al. 2017).

1.4.3.3 Epigenetic inhibitors

Epigenetic regulators remain a particularly popular focus for targeted inhibition in AML, representing a major class of recurrently mutated or deregulated genes in AML (Cancer Genome Atlas Research et al. 2013; Papaemmanuil et al. 2016). One such case is the fusion protein RUNX1-RUNX1T1, which recruits a HDAC-containing repressor complex as a

component of disease progression (Gelmetti et al. 1998). Critically, the HDAC inhibitor panobinostat has been shown to induce myeloid differentiation in a RUNX1-RUNX1T1 driven mouse leukaemia model (Salmon et al. 2015; Bots et al. 2014). However, early clinical trials reveal minimal therapeutic efficacy of HDAC inhibitors (Quintas-Cardama, Santos, and Garcia-Manero 2011; Schaefer et al. 2009).

1.4.3.4 DHODH inhibitors

An emerging differentiation therapy is the use of inhibitors targeting dihydroorotate dehydrogenase (DHODH). DHODH is a metabolic enzyme normally involved in the biosynthesis of pyrimidines, ubiquitously expressed in all tissues. Inhibitors such as brequinar (BRQ) halt pyrimidine synthesis, restoring myeloid differentiation in human AML cell lines *in vitro*, as well as AML xenotransplants and mouse AML models *in vivo* (Sykes et al. 2016). However, DHODH is not typically associated with myelopoiesis, and the link between pyrimidine starvation and differentiation remains unclear (Sykes et al. 2016; Christian et al. 2019).

1.4.4 Differentiation Syndrome

Differentiation therapy is not without risks however, as the treatment features a unique adverse effect termed differentiation syndrome. With ATRA and ATO therapy, DS occurs within approximately one month of treatment in 25% of APL patients, whereby triggering differentiation of the large number of APL cells releases cytokines and generates a systemic inflammation (Montesinos et al. 2009). Differentiation syndrome has also been observed following the use of mutant IDH1, IDH2, and FLT3 inhibitors (Birendra and DiNardo 2016; Fathi et al. 2018). The adverse effects of DS can be partially alleviated with the cessation of differentiation therapy and treatment with the corticosteroid dexamethasone.

1.4.5 Differentiation therapy and relapse

Among the clinically approved differentiation therapies, there remains a common theme of impressive response rates yet only a temporary remission. While a majority of relapses following ATRA monotherapy or combination with chemotherapy occur within the first 2 years, late relapses (considered 4 years post-remission) are possible, with relapse as late as 17 years post-remission previously reported (Sakurai et al. 2018; Kelaidi et al. 2006). Interestingly, many of these late relapses remain sensitive to ATRA therapy (Kelaidi et al.

2006). These cases present the scenario in which a minor proportion of the cells persist post-therapy in a dormant state, raising the fundamental question of which cells are seeding relapse.

1.5 Cancer Heterogeneity

The spectrum of AML phenotypes and maturity states can be extremely variable between patients and within an individual tumour. A heterogeneous tumour bulk can differ in sensitivity to certain therapies as well as their tumour-initiating potential, therefore tumour heterogeneity is important consideration in the development of cancer therapeutics.

1.5.1 Leukaemia Stem Cell Model

The maturational heterogeneity of a single tumour is especially evident in AML, as the myeloid lineage has been extensively studied, categorised, and compartmentalised for the different stages of differentiation. Central to this was the use of flow cytometry analysis of surface markers to define maturational heterogeneity. Over the years, advances in single cell transcriptome sequencing have restructured our understanding of haematopoiesis into a more amorphous and continuous process of lineage determination (Weinreb et al. 2020). In 1994, the putative 'leukaemia stem cell' (LSC) was first identified (Lapidot et al. 1994). This LSC model postulates that the ability of leukaemia cells to engraft was dependent on immaturity, with the vast majority of tumour-derived cells not leukaemogenic as they are not capable of self-renewal. Rather, only a small subset of the tumour, the LSCs, had the capacity to initiate leukaemia through self-renewal. In theory, LSCs would self-renew as well as form differentiated leukaemia cells with limited proliferative potential that made up the bulk of the leukaemia. Furthermore, the LSC were defined based on cell surface markers: CD34+/CD38– were transplantable LSCs, CD34+/CD38+ or CD34– were the non-leukaemogenic progeny, though over time leukaemia-initiating cells have been revealed in more immunophenotypic compartments. Conceptually quiescent and therefore chemotherapeutically-resistant cells, LSC provide prognostic information in particular likelihood of initial therapy resistance, therefore their detailed characterisation is extremely appealing (Ng et al. 2016). This model has been expanded into the cancer stem cell (CSC) theory, as apparent tumour-initiating subpopulations were identified in more cancers (Al-Hajj et al. 2003). Based on the CSC theory, therapies were developed in order to specifically target the CSC, with the belief that following the elimination of the stem cells, the mature CSC progeny could not sustain the tumour (Shibata and Hoque 2019).

1.5.2 Maturation and Tumourigenic Potential

Recently the LSC model has begun to fall out of favour. The defined phenotypic range of the LSC compartment has continually expanded over the years through refinement of the analytical tools, chiefly mouse models that better replicate the *in vivo* conditions required for leukaemia engraftment (Buss and Ho 2011). Using these, leukaemic cells of more mature states are capable of recapitulating the entire parental phenotype, immature cells included (Sarry et al. 2011). Additionally, there are questions whether transplantation assays accurately represent the leukaemia-propagating cells in an established tumour, as they may skew results towards immaturity unintentionally.

On a broader scale, the CSC hypothesis has not made a significant impact in the clinical world, with direct targeting of the immature CSC remaining a mystery (Pollyea and Jordan 2017). In colorectal cancer models, the targeted ablation of the CSCs triggers reversion of differentiated cancer cells into the tumourigenic immature state to replace the CSC niche (de Sousa e Melo et al. 2017; Shimokawa et al. 2017). In AML, chemotherapy-treated xenografts whereby LSC are depleted during remission can still relapse, leaving the source of relapse a mystery (Boyd et al. 2018). This raises the concept of maturation plasticity by which a) AML maturation may not be inherently unidirectional, and b) through this the maturation state of a leukaemic cell may be distinct from its potential to self-renew. Such a concept could have important consequences in how LSCs are regarded as a therapeutic target, and in the origin of relapse in differentiation therapy. This thesis addresses the potential for plastic maturation in AML, specifically focusing on the role of the transcription factor PU.1.

1.6 Project Rationale and Aims

Restoring normal myeloid differentiation and clearance mechanisms is an attractive therapeutic option for AML. Differentiation agents display high rates of remission yet, barring combination ATRA and ATO in the treatment of APL, also often result in relapse raising the question as to the origin of relapse.

The aim of this study is to elucidate the potential for mature and therapy-responsive AML cells to regain leukaemia-propagating potential. Furthermore, we aim to characterise how the transcription factor PU.1 is involved in controlling the maturation state of AML cells. These topics are addressed in the following chapters:

Chapter 3: Maturational plasticity of a mouse AML model driven by reversible PU.1 knockdown

Chapter 4: Maturational plasticity of human APL following differentiation therapy

Chapter 5: Generating models of inducible PU.1 restoration in human APL

CHAPTER 2. Materials and methods

2.1 *In vitro* cell culture

2.1.1 Culture conditions

AML246 cells were cultured in Iscove's Modified Dulbecco's Medium (IMDM) (Gibco) with 10% Fetal Calf Serum (FCS) (Sigma-Aldrich), 100 U/mL penicillin-streptomycin (Pen-Strep) (Gibco) and 10 ng/mL IL-3 (Peprotech). Cells were plated at a concentration range between $1x10^5$ to $1x10^6$ cells per mL and incubated at 37°C, 10% CO_2.

The human APL cell lines NB4 (Lanotte et al. 1991) and HT93 (Kishi et al. 1998) were cultured in Roswell Park Memorial Institute Medium (RPMI 1640) (Gibco) with 10% FCS and 100 U/mL Pen-Strep. HT93 cultures were further supplemented with 50 ng/mL rhG-CSF (Filgrastim, Hospira). Cells were incubated at 37°C, 10% CO_2.

Human APL primary experiments were approved by the Alfred Hospital Human Research Ethics Committee. AML patients were consented according to institutional guidelines before obtaining bone marrow samples. Approximately 3 million Ficoll-purified primary APL cells were thawed and cultured in StemSpan SFEM II (StemCell Technologies, Inc.) supplemented with 50 ng/mL FLT3 ligand, 50 ng/mL rhSCF, 10 ng/mL rhIL-3, and 10 ng/mL rhIL-6 (all from R&D Systems).

293T cells were cultured in Dulbecco's Modified Eagle Medium (DMEM) (Gibco) with 10% FCS and 100 U/mL Pen-Strep. Cells were detached for passaging with Trypsin-EDTA (Gibco). Cells were incubated at 37°C, 10% CO_2.

2.1.2 Drug treatments

The tetracycline analogue Doxycycline (Dox) was used for inducible regulation of transgene expression. Dox (Sigma-Aldrich) was diluted to 1 μg/mL in media except where explicitly stated. Fresh Dox-treated media was utilised for every cell culture split, and cell cultures were thoroughly washed by centrifuging at 300 RCF for 5 minutes and resuspended in fresh Dox media every 5 days. For withdrawal experiments, cells were thoroughly washed twice with Phosphate Buffered Saline solution (PBS) (Sigma-Aldrich) to eliminate any residual Dox.

For the differentiation of human APL cell lines and primary cultures, the relevant media was treated all-*trans*-retinoic-acid (ATRA) (Sigma-Aldrich) to a final concentration of 1 μM (10 mM stock in ethanol) except where explicitly stated. All relevant controls were treated with the vehicle ethanol. Fresh ATRA-treated media was utilised for every cell culture split, and cell cultures were thoroughly washed by centrifuging at 300 RCF for 5 minutes and resuspended in fresh ATRA media every 5 days. Fresh aliquots of the ATRA stock were routinely utilised to circumvent the loss of activity resulting from repeated freeze-thaws. For withdrawal experiments, cells were thoroughly washed twice with PBS to eliminate any residual ATRA.

For ATO experiments, media was made up from 5 μM ATO stock to the relevant concentrations. Cells were washed every 4 days, during which the expended ATO-treated media was disposed as hazardous waste, and contaminated wastes disposed in genotoxic waste reciprocals.

For experiments requiring antibiotic selection, recently transduced cells were cultured in the relevant antibiotic (1 μg/mL puromycin (Sigma-Aldrich) or 1 mg/mL G418 (Sigma-Aldrich)) until total loss of viability of concurrent parental control culture.

2.2 Flow cytometry and cell sorting

Cells were pelleted by centrifugation at 300 RCF for 5 minutes and washed in PBS. Mouse leukaemia cells were incubated for 5 minutes on ice in FACS buffer (PBS with 10% FCS) with anti-CD16/CD32 (unlabelled, clone 2.4G2, WEHI). For analysis of human or mouse myeloid maturation markers, cells were stained with the following anti-mouse antibodies: CD11B-PE (clone M1/70, eBioscience), CD11B-BV711 (clone M1/70, eBioscience), CD16/CD32-Pacific Blue (clone 2.4G2, WEHI); or the following anti-human antibodies: CD11B-APC (clone Bear1, Beckman), CD15-PE (clone W6D3, BD Biosciences), CD16-Pacific Blue (clone 3G8, BD Pharmigen), CD34-PE-Cy7 (clone 581, BD Biosciences) for 30 minutes. Cells were washed with PBS and resuspended with 200 μL of FACS buffer. For viability staining, 1 μg/mL propidium iodide (Thermo Fisher Scientific) or 1 μg/mL SYTOX blue (Thermo Fisher Scientific) was added to the FACS buffer. For flow cytometry analysis, less than $1x10^6$ cells were resuspended in 200 μL FACS buffer, and were analysed on an LSRII machine (BD Biosciences).

For cell counting, 25,000 Sphero AccuCount Blank Beads (Spherotech) were added per tube to the FACS buffer and bead events were compared to viable cell count reads, with calculations adjusted for culture dilution factor over time.

For fluorescence-activated cell sorting (FACS), cells were resuspended in FACS buffer $1x10^7$ cells/mL. For single cell purification, GFP+ cells were sorted on a BD Influx (BD Biosciences) cell sorter into a 96-well plate with 100 µL of media per well. Sorting of GFP+/mCherry+ cells was performed on an Influx (BD Biosciences) cell sorter into collection tubes with 1mL media.

All AML246 cell sorting was done without refrigeration due to intolerance of cold temperatures.

2.3 *In vitro* CFU analysis

2.3.1 Semi-solid colony forming assays

For AML246 colony-forming assays 500 cells were plated into 1 mL cultures of untreated or Dox-treated methylcellulose (MethoCult GF M3434, StemCell Technologies, Inc.) supplemented with 10 ng/mL IL-3 in 35 mm culture dishes.

For NB4 and HT93 colony-forming assays, the specified number of cells based on treatment were plated into 1 mL cultures of untreated or ATRA-treated methylcellulose (MethoCult SF H423, StemCell Technologies, Inc.). HT93 methylcellulose was further supplemented with 50 ng/mL rhG-CSF (Filgrastim, Hospira).

Colony number and diameter was assessed 10 days after plating using a GelCount colony counter (Oxford Optromix).

2.3.2 Index-sorting single-cell clonogenic assays

For single-cell clonogenic assays with AML246, cells were single cell index sorted by Influx (BD Biosciences) into 96-well plates containing 200 µL of Dox-free or Dox-treated medium.

For NB4, cells were single cell index sorted by Influx (BD Biosciences) into 96-well plates containing 200 µL of untreated or ATRA-treated medium.

All plates were cultured for 3-4 weeks to allow clonal outgrowth.

2.4 Cytospins

Up to $1x10^5$ cells were harvested and washed twice with PBS before resuspension in 100 µL in PBS. Cells were spun onto SuperFrost Plus microscope slides (Menzel Gläser) at 800 RPM in a Shandon Cytospin Centifuge for 5 min. After drying, cytospins were placed in 100% methanol for 45 sec. After drying, slides were stained with May-Grunwald Giemsa, mounted, and imaged with the Aperio ScanScope XT microscope. Representative images were taken using Aperio ImageScope software v11.2 (Leica) and scored blind.

2.5 Leukaemia transplants

To verify the leukaemogenicity of index-sorted, de-differentiated AML246, ~$1x10^6$ cells were transplanted by tail vein injection into immunocompromised PtprcLy5.1 (Cd45.1) Rag1–/– recipient mice, 2 mice per sample. After approximately 4-6 weeks injection recipients developed GFP^+ AML246 leukaemia burden in the peripheral blood, spleen, and bone marrow.

2.6 Viral production and transduction

2.6.1 Calcium phosphate viral packaging

The calcium phosphate transfection procedure was used to package viral vectors. $3.6x10^6$ 293T cells were plated in 100 mm^2 polystyrene plates and incubated overnight.

To make the DNA plasmid mix for lentiviral vectors, 5 µg of the structural vector pMDL-GAG-POL, 3 µg of the envelope vector (either ECO or VSV-G), 2.5 µg of pRSV-Rev, and 10 µg of the transgene expression vector was added to 250 µL of HEPES H_2O (2.5mM HEPES, pH 7.3, Gibco).

To make the DNA plasmid mix for retroviral vectors, 5 µg of the structural vector pGAG-POL, 3 µg of the envelope vector (either ECO or VSV-G), and 14 µg of the transgene expression vector was added to 250 µL of HEPES H_2O (2.5mM HEPES, pH 7.3, Gibco).

To the plasmid mix, 250 µL of 0.5 M $CaCl_2$ was added. This plasmid solution was added dropwise to 500µL of HBS 2x concentrated (0.28 M NaCl, 0.05 M HEPES, 1.5 mM NO_2HPO_4, pH 7) whilst being bubbled with air by pipette. A DNA-calcium phosphate precipitate formed during 20 minutes of incubation at room temperature. The total volume was added dropwise to the 293T cell culture following addition of fresh media. Media was changed after at least 7 hours and replaced with 6 mL fresh media, and supernatant harvested twice over two sequential days.

2.6.2 Viral collection and transduction

The viral containing supernatant from §2.6.1 was passed through a 0.45 µm Minisart syringe filter unit into an Amicon Ultra-15 Centrifugal Filter Device, which was then centrifuged at 2,400 RCF for 15 minutes to concentrate the virus. Concentrated virus was collected and used for transduction immediately or stored at -80°C.

1mL of viral supernatant was added to $5x10^5$ target cells per FALCON polystyrene 15mL round bottom tube and spin infected by centrifuging at 2,400 RCF for 90 minutes. Cells were washed twice and plated at a concentration of $1x10^5$ cells/mL. After 72 hours, cells were washed twice again to eliminate any remaining viral particles.

2.7 Western blotting

Protein was extracted from $2x10^6$ cells. Cells were centrifuged at 300 RCF for 5 minutes and washed in 1 mL PBS (Sigma-Aldrich). Cells were pelleted again, and supernatant was aspirated. Cells were resuspended in 200 µL Laemmli solution (4% SDS, 20% glycerol, 10% β-mercaptoethanol, 0.004% bromophenol blue, 0.125M Tris HCl, pH 6.8). The lysate was vortexed and denatured for 5 minutes at 100°C. Protein lysate was quantified by NanoDrop 1000 spectrophotometer at 280 nm wavelength, and stored at -20°C.

To 35 µg of protein, 5 µL of loading dye (40% Bromphenol Blue 0.1%, 10% β-mercaptoethanol, 50% ddH_2O) was added. All samples were made up to 30 µL with Laemmli solution. Samples were boiled at 100°C for 5 minutes, then centrifuged for 3 minutes at 500 RCF before being loaded into Mini-protean pre-cast Gels 4-15% (BioRad). Electrophoresis was performed for 1 hour at 100V in running buffer (14.4 g Glycine, 3 g Tris and 1 g SDS in 1 L H_2O). PVDF membranes (Immobilon-P) were activated with methanol, then protein was

transferred from the gel to the PVDF membrane for 1 hour at 120V in transfer buffer (14.4g Glycine and 3 g Tris in 1 L H_2O 20% methanol).

Following transfer of protein, the membranes were washed with PBS (Sigma-Aldrich) with 0.1% Tween20 (PBS-Tween20) (EMD Chemicals Inc.) for 30 minutes on a mechanical shaker at room temperature. To prevent unspecific antibody binding, the membranes were blocked with 5% milk PBS-Tween20 overnight in 50 mL FALCON tubes on a mechanical roller at 4°C. Blocking solution was removed and the membrane was incubated overnight at 4°C with the primary antibody, either rabbit polyclonal anti-PU.1 (T-21, SantaCruz Biotechnology), mouse monoclonal anti-PU.1 (C-3, SantaCrus Biotechnology), mouse monoclonal anti-α-tubulin (clone B-5-1-2, Sigma-Aldrich), or rabbit anti-beta-actin (clone 13E5, Cell Singaling Technology) diluted 1:1000 in 5% milk PBS-Tween20. Membranes were washed with PBS-Tween20 for 10 minutes 3 times, then incubated for 1 to 2 hours with secondary polyclonal swine anti-rabbit (Dako) (1:2000) or polyclonal goat anti-mouse (Dako) (1:2000) HRP-conjugated antibodies in 5% milk PBS-Tween20 on a mechanical shaker at room temperature. Membranes were again washed with PBS-Tween20 for 10 minutes 3 times.

For band detection, 4 mL of Luminata Forte Western HRP substrate was dropped onto the membranes and the excess solution was drained. ChemiDoc Touch Imaging System (BioRad) was utilised to acquire both colorimetric and chemiluminescent signal readings.

2.8 Molecular biology

2.8.1 DNA extraction

Genomic DNA was extracted from approximately $1x10^6$ cells per sample with the use of the DNeasy Blood & Tissue Kit (Qiagen) as per manufacturer's instructions. Quantification was assessed by NanoDrop 1000 spectrophotometer analysis of 260/280nm wavelength absorption. DNA was stored at -20°C.

2.8.2 RNA extraction

Total RNA was extracted from $0.5x10^6$ to $5x10^6$ cells per sample with the use of the RNeasy Mini Kit (Qiagen) as per manufacturer's instructions. Quantification was assessed by NanoDrop 1000 spectrophotometer analysis of 260/280 nm wavelength absorption. RNA was stored at -80°C.

2.8.3 Reverse-transcription and quantitative PCR

Total RNA was extracted from cells. To reverse-transcribe the RNA to complementary DNA (cDNA), two mixes were made. Mix 1 featured 500-1000 ng of the total RNA, 2 µL random hexamers (100 µg/µL) (NEB), made up to 12 µL with H_2O DEPC. Mix 2 featured 5 µL M-MLV RT 5x buffer (NEB), 1.25 µL dNTPs (10 mM), 1 µL M-MLV RT (H-) (NEB), 0.25 µL RNAse inhibitor (NEB), and 5.5 µL H_2O DEPC. Mix 1 was incubated at 70°C for 5 minutes, then cooled to 4°C. Mix 2 was then added to Mix 1, and samples were incubated in a T100 Thermal Cycler (BioRad) at 23°C for 10 minutes, 50°C for 50 minutes, 95°C for 5 minutes, then cooled to 4°C.

Primers were designed flanking an intron of a target gene, distinguishing between long genomic DNA and a small section of the mRNA coding sequence (Table 2.1). Intended products were approximately 150 nucleotides in length. For qPCR, 10 µL of sample was used per well in a 96-well plate. Each well featured 2 µL cDNA from the retrotranscription reaction diluted between 1:2-1:5, 1 µL H_2O, 5 µL Promega Master Mix 2x, and 2 µL of primers. Plates were covered with film to prevent the samples from drying. qPCR was performed using a LightCycler 480 (Roche). Protocol involved 3-step PCR with the following programming: 95°C 3 minutes, (95°C 15 seconds, 60°C 30 seconds, 72°C 30 seconds) x 45 cycles, 4°C ∞. Relative transcript quantification was deduced from ΔΔCt.

2.8.4 Short guide RNA cloning

Short guide RNA (sgRNA) gene sequences were cloned into the lentiviral sgETN backbone vector provided by Professor Johannes Zuber. Oligomers were designed and ordered from Sigma-Aldrich with overhangs for direct cloning into the sgETN backbone (Table 2.2). To anneal, 1 µL of both forward and reverse sgRNA (100µM) were added to 1µL T4 DNA ligase, 1µL T4 PNK (NEB), and 6 µL H_2O. Mix was vortexed and annealed in the thermocycler: 37°C 30 min, 95°C 5', ramp down 5°C a min to 25°C (x14 cycles). Annealed sgRNA were diluted 1:250, and 1µL used for ligation: 100 ng backbone, 1 µL T4 ligase, 1 µL T4 ligase buffer, 1 µL annealed oligo and made up to 10 µL with H_2O. Mix was left for 1 hour at room temp and transformed into bacteria.

2.8.5 Short hairpin RNA cloning

miR-E short hairpin RNA (shRNA) 97-mer gene sequences were cloned into retroviral LENC, or lentiviral LT3-GEN or LT3-GEPIR backbone vectors provided by Professor Johannes Zuber.

Restriction digests were performed to cut backbone vectors, allowing for isolation of both the backbone and the shRNA. These plasmids harboured XhoI and EcoRI restriction sites flanking the shRNA sequence. 2.5 µg of plasmid DNA was incubated at 37°C for 90 minutes with 2 µL CutSmart Buffer 10x (NEB), 1 µL EcoRI (NEB), 1 µL XhoI (NEB), H_2O up to 20 µL. Restriction enzymes were inactivated at 65°C for 20 minutes. Annealed shRNA and digested plasmid backbone were separated by size with gel electrophoresis, then bands were removed from the agarose gel and extracted with DNA Gel Extraction Kit (Qiagen).

Oligomers were designed and ordered from Sigma-Aldrich (Table 2.3). The forward and reverse single strands were phosphorylated and then annealed in the same reaction. 2.5 µL of the forward oligonucleotide (40 µM) and 2.5 µL of the reverse oligonucleotide (40 µM) were added to a mix containing 5 µL Kinase Buffer 10x (NEB), 5 µL ATP (10mM), 1 µL of T4 polynucleotide Kinase (NEB), and 34 µL of H_2O. The solution was incubated at 37°C for 30 minutes, then 96°C for 10 minutes on a AccuBlock Digital Dry Bath. Samples were cooled slowly to 80°C over 1 hour on the heat block, and then rapidly cooled on ice. Annealing was kept to a high temperature to prevent secondary structure issues, a frequent issue when working with shRNA. Annealed oligonucleotides were made up to 1 mL with H_2O.

A ligation reaction was set up featuring 2 µL of cut vector (30 ng/µL), 8 µL of insert (annealed oligonucleotides, excised shRNA), 2 µL of Ligase Buffer 10x (NEB), 1 µL of T4 DNA Ligase (NEB), and 7 µL of H_2O. Ligation reactions were incubated overnight at 4°C.

2.8.6 Bacterial transformation

Plasmids were transformed into chemically competent bacteria. 2-5 µL of plasmid was incubated with 50 µL of competent bacteria on ice for 30 minutes. To heat shock the bacteria, they were placed at 42°C for 45 seconds then placed back on ice for 5 minutes. Bacteria was made up to 1 mL with LB broth and incubated at 37°C for 1 hour to recover. Depending on

plasmid concentrations, bacterial mixtures were diluted between 1:1-1:10 and 150 µL of bacteria were plated on 100 µg/mL Ampicillin agar plates.

2.8.7 Plasmid amplification

To amplify plasmids, transformed bacteria were grown in LB buffer with 100 µg/mL Ampicillin. Plasmid DNA was extracted from bacteria with the use of Plasmid Miniprep or Maxiprep Kits (Qiagen) as per manufacturer's instructions. Plasmids were quantified by NanoDrop 1000 spectrophotometer analysis of 260/280nm wavelength absorption. Plasmid samples were stored at -20°C.

2.9 DNA Sequencing

cDNA and plasmid sequencing was performed by the Micromon DNA Sequencing Facility at Monash University, where Sanger sequencing and electrophoresis capillary separation was performed. CRISPR/Cas9 knockout sequences were sequenced using the primers in Table 2.1

2.10 RNA sequencing

For *in vitro* AML246 gene expression time course analysis, duplicate samples (from parallel cultures) of viable (PI-negative) cells or Cd11b-high viable cells were flow sorted at each time point. Total RNA was extracted using the RNeasy Plus Mini Kit (QIAGEN, Valencia, CA). RNA libraries for *in vivo* and *in vitro* samples were prepared from 200 ng total RNA using the Illumina TruSeq Kit. Samples were transferred to the WEHI Genomics Hub and sequenced on NextSeq 500 (86 base single end reads).

Data was transferred to Prof. Matthew Ritchie, whereby reads were aligned to the mouse genome (mm10) using the subread algorithm (Liao, Smyth, and Shi 2013) then summarized at the gene-level using featureCounts (Liao, Smyth, and Shi 2014) from the Rsubread package. Genes with low expression (less than 0.5 counts per million in fewer than 3 samples) were removed from further analysis. Compositional differences between libraries were normalized using the trimmed mean of M-values (TMM) method (Robinson and Oshlack 2010). Differential expression analysis was performed using the limma package (Ritchie et al. 2015). Counts were transformed to log2-CPM values (with an offset of 0.5) with associated precision weights using voom (Law et al. 2014) or voom with sample quality weights (Liu et al., 2015). Linear models with effects for different treatments at different time-points were fitted.

Contrasts between conditions were estimated and differential expression was assessed using moderated t-statistics (Smyth 2004). Genes with false discovery rate (FDR) < 0.05 were considered differentially expressed.

Gene ontology analysis was performed using MetaCore software (https:// portal.genego.com/). Gene set testing used the roast method, allowing for statistical analysis of gene-wise correlation (Wu et al. 2010) for gene signatures obtained from the ImmGen expression database (GSE15907) (Heng, Painter, and Immunological Genome Project 2008) comparing neutrophils to common myeloid progenitors (CMPs – Derrick Rossi laboratory). For the ImmGen comparisons, the logarithmic fold change (logFC) of the ImmGen data were used as gene weights for roast and all differentially expressed genes (FDR < 0.05, jlogFCj > 1) were used. Heatmaps of the expression values on a log2 scale that were row-scaled were generated using the gplots package (https://cran.r-project.org/web/packages/gplots/index.html).

To determine genes whose expression correlated with Spi1 across the AML246 time course, linear model analysis was performed that included log2-CPM Spi1 expression as a covariate in the design matrix using the limma-voom pipeline described above. RNA-seq data is available through the Gene Expression Omnibus under accession number GSE108946.

2.11 Single-cell RNA sequencing

Single untreated or 14 day Dox-treated AML246 cells were flow sorted (PI-negative or PI-negative Cd11b-high cells respectively) into 384-well plates using a BD FACSAria III flow cytometer (BD Biosciences). These plates were transferred to the WEHI Single Cell Open Research Endeavour (SCORE) facility.

Single cell transcriptome libraries were generated using the CEL-Seq2 protocol (Hashimshony et al. 2016) with adaptations: second strand synthesis was performed using NEBNext Second Strand Synthesis Module in a final reaction volume of 8 mL, and NucleoMag NGS Clean-up and Size select magnetic beads (Macherey-Nagel) were used for DNA purification and size selection. CEL-Seq2 scRNA-sequencing reads were mapped to the GRCm38 mouse genome using the Rsubread aligner (Liao, Smyth, and Shi 2013) and assigned to genes using scPipe (http://bioconductor.org/packages/release/bioc/html/scPipe.html) with ENSEMBL v86 annotation. Gene counts were exported as a matrix by scPipe with UMI-aware counting and

imported into R. Cells were removed from further analysis if they failed to achieve 1000 total counts or 1000 total genes detected. Genes were filtered out if they failed to achieve 1 count in at least 20% of a particular cell condition group. Multi-dimensional scaling was performed on normalized log2-CPM expression values with size factors calculated by the computeSumFactors function in scran (Lun, Bach, and Marioni 2016). These data are available through the Gene Expression Omnibus under accession number GSE109100.

2.12 PU.1-ChIP sequencing

$1x10^7$ viable (PI-negative) or Cd11b-high viable AML246 cells were flow sorted using a FACSAria (BD Bioscience). Samples were then passed on to Dr. Michael Chopin at WEHI.

Cells were cross-linked for 10 min at room temperature in 0.1 volumes of fresh formaldehyde solution (11% formaldehyde, 1 mM EDTA, 0.5 mM EGTA, 50 mM HEPES-KOH, 100 mM NaCl). Formaldehyde was quenched with 0.1 volumes of 1.25 M glycine. Cross-linked cells were washed twice with PBS and snap-frozen. ChIP samples were prepared according to the modified Millipore/Upstate protocol using the polyclonal anti-PU.1 IgG (T-21 X, Santa Cruz Biotechnology: sc-352 X). Briefly, cells were lysed and the chromatin sonicated (Branson Sonifier) in SDS lysis buffer (1% SDS, 10 mM EDTA, 50 mM Tris-HCl pH 8.1) containing protease inhibitors (Roche). Sonicated chromatin was incubated at 4C overnight in dilution buffer (0.01% SDS, 1% Triton-X, 1.2 mM EDTA, 16.5 mM Tris-HCl pH 8.1, 165 mM NaCl) containing anti-PU.1 antibody and protease inhibitors, then for another hour with ProteinG DynaBeads. Immunoprecipitated chromatin was washed sequentially in low salt buffer (0.1% SDS, 1% Triton-X, 2 mM EDTA, 20 mM Tris-HCl pH 8.1, 150 mM NaCl), high salt buffer (low salt buffer with 500mM NaCl), LiCl buffer (1% NP-40, 1% Na deoxycholic acid, 1 mM EDTA, 10 mM Tris-Hcl pH 8.1, 0.25 M LiCl), then twice in TE buffer. Chromatin was eluted from DynaBeads by two rounds of incubation in elution buffer (1% SDS, 0.1 M NaHCO3) at 65°C for 15 min with occasional vortexing. Protein-DNA crosslinks were reversed by incubating the eluate at 65°C for 6 hours in the presence of 0.2 M NaCl and 0.02 mg/ml RNase A, followed by another hour of incubation at 45°C in the presence of 0.04 mg/ml Proteinase K, 10mM EDTA, and 40mM Tris-HCl. DNA was extracted using ChIP DNA clean and concentrator columns (Zymo Research). DNA libraries were prepared from 10 ng ChIP DNA using the Illumina TruSeq DNA Sample Kit and sequenced on NextSeq 500 (86 base single end reads). Reads were aligned to the mouse genome (mm10) using the Rsubread program and

bam files were sorted using SAMtools (Li et al. 2009). For in vivo ChIP samples, MACS2 (Feng et al. 2012) was used to identify differentially bound peaks between the Dox-treated and untreated samples by treating the latter samples as background and using a q-value cut-off of 0.05. Peaks were identified by MACS2 using an input control sample as background with a q-value cut-off of 0.05 and fold-enrichment < 10. Remaining peaks were plotted using Gviz (Hahne and Ivanek 2016) and assigned to genes from the RNA-seq analysis with TSS within ± 50 kb using GenomicRanges software (Lawrence et al. 2013). Peaks with low values for all samples were filtered out. Changes in PU.1 binding at particular genomic locations over time were determined using DiffBind (Ross-Innes et al. 2012), merging ChIP peaks across samples that overlap by at least one base then calculating reads within a binding site interval ('superpeak') for each sample. ChIP-seq data are available through the Gene Expression Omnibus under accession number GSE108945.

Table 2.1: Primers for sequencing and qRT

Primer target	Sequence	Product length
PML – Forward	TTTCGGACAGCTCAAGGGAC	1,982
PML – Reverse	CCCCAGGAGAACCCACTTTC	
PML-RARA – Forward	TCAGCTTCTCTTCACGCACT	1,370
PML-RARA – Reverse	GACCCCATAGTGGTAGCCTG	
PU.1 qRT – Forward	Hs02786711_m1 TaqMan	–
PU.1 qRT – Reverse	Hs02786711_m1 TaqMan	–
R18S – Forward	GTAACCCGTTGAACCCCATT	–
R18S – Reverse	CCATCCAATCGGTAGTAGCG	–

Table 2.2: Sequences of sgRNA oligos

sgRNA	Sequence
sgPML1 forward	caccAGGTGCAGACACACCCGCCC
sgPML1 reverse	aaacGGGCGGGTGTGTCTGCACCT
sgPML2 forward	caccCCGGCAGATTGTGGATGCGC
sgPML2 reverse	aaacGCGCATCCACAATCTGCCGG

Table 2.3: 97mer oligonucleotide sequences for shRNA with 5’ and 3’ miR-E linkers

sgRNA	5’ linker	97mer Forward Sequence	3’ linker
shRen.713	TCGAGAAGGTATAT	TGCTGTTGACAGTGAGCGCAGGAATTATAATGCTTATCTATAGTGAAGCCACAGATGTATAGATAAGCATTATAATTCCTATGCCTACTGCCTCGGA	CTTTCAAGGGGCTAG
shPU.1.200 (mouse)	TCGAGAAGGTATAT	TGCTGTTGACAGTGAGCGAATCGGATGACTTGGTTACTTATAGTGAAGCCACAGATGTATAAGTAACCAAGTCATCCGATGTGCCTACTGCCTCGGA	CTTTCAAGGGGCTAG
shPU.1.1293 (mouse)	TCGAGAAGGTATAT	TGCTGTTGACAGTGAGCGCAACCACTAAAGACAAGTAAAATAGTGAAGCCACAGATGTATTTTACTTGTCTTTAGTGGTTATGCCTACTGCCTCGGA	CTTTCAAGGGGCTAG
shPU.1.885 (human)	TCGAGAAGGTATAT	TGCTGTTGACAGTGAGCGCCCGCAAGAAGATGACCTACCATAGTGAAGCCACAGATGTATGGTAGGTCATCTTCTTGCGGTTGCCTACTGCCTCGGA	CTTTCAAGGGGCTAG
shPU.1.1384 (human)	TCGAGAAGGTATAT	TGCTGTTGACAGTGAGCGCAACAAGTAAAGTTATTCTCAATAGTGAAGCCACAGATGTATTGAGAATAACTTTACTTGTTTTTGCCTACTGCCTCGGA	CTTTCAAGGGGCTAG

CHAPTER 3. Maturational plasticity of a mouse AML model driven by reversible PU.1 knockdown

3.1 Introduction

All-*trans*-retinoic-acid (ATRA) has revolutionised the treatment of the AML subtype acute promyelocytic leukaemia (APL), however until recently there has been limited success in expanding differentiation therapies to other AML subtypes. As outlined in Chapter 1, APL is usually diagnosed by the presence of the t(15;17) translocation, resulting in the expression of the fusion protein PML-RARA, a class II mutation that drives the differentiation block in part through the dysregulation of the myeloid transcription factor PU.1. Restoring PU.1 function is critical for ATRA efficacy in APL. Importantly, PU.1 is directly inhibited by various mutually exclusive recurrent mutations in AML, suggesting they may functionally converge on disruption of the same pathway. To investigate PU.1 in the myeloid differentiation block, the Dickins Laboratory developed models of PU.1 suppression and restoration in mouse AML.

Dr. Mark McKenzie, a former member of the Dickins Laboratory, generated mouse models of AML whereby the differentiation block can be manipulated by reversible PU.1 knockdown. Mouse p53-null foetal haematopoietic stem and progenitor cells (HSPCs) were co-transduced with two vectors: one constitutively expressing the tet-off protein tet-transactivator (tTA), and another expressing a GFP-linked miR-E shRNA targeting *PU.1* under the control of a tet-responsive promoter (TRE3G) (Figure 3.1A). By engaging the TRE3G promoter, tTA induces expression of both *GFP* and the shRNA. This can be repressed through the addition of the tetracycline analogue Doxycycline (Dox), which binds tTA and inhibits expression (Figure 3.1A).

Lethally irradiated recipient mice reconstituted with HSPCs expressing the negative-control shRNA (Ren.713) eventually succumbed to a T cell malignancy resulting from the p53-null heterozygosity (Purdie et al. 1994). Conversely, mice reconstituted with HSPCs infected with shRNA targeting PU.1 (PU.1.200 and PU.1.1293) rapidly developed B cell and myeloid leukaemia (Figure 3.1B). Several primary leukaemias were further characterised, with AML246 identified as a cytogenetically normal AML harbouring an activating mutation (N824K) in the tyrosine kinase Kit.

Dr. Mark McKenzie found that AML246 cells transplanted into Rag1-/- immunocompromised secondary recipients engrafted and rapidly developed into aggressive leukaemia. Administrating Dox-treated food to the recipient mice led to downregulation of GFP in the AML (Figure 3.1C). This coincided with the loss of the PU.1 shRNA and subsequent restoration of endogenous PU.1 protein (Figures 3.1D). AML differentiation was evident by the upregulation of the pan-myeloid marker Cd11b and morphological maturation into neutrophil-like cells (Figures 3.1E-F). Remarkably, restoration of endogenous PU.1 alone was sufficient in driving disease regression followed by a period of undetectable AML burden, before an eventual relapse 1-2 months later in Dox-treated mice (Figure 3.1G).

AML246 cells also grew readily *in vitro* when supplemented with the cytokine interleukin-3 (IL3). *In vitro,* Dox triggered neutrophil-like differentiation coupled with the loss of proliferation and viability (Figure 3.1H). Exploiting the reversible nature of the tet-off system, the laboratory investigated the resulting effect of PU.1 re-suppression in mature AML246 through Dox withdrawal. Interestingly, re-engaging the PU.1 shRNA after 2 weeks of Dox treatment allowed the cells to revert to their original proliferating and clonogenic state, a finding that was recapitulated by a former member of the Dickins Lab Dr. Margherita Ghisi, who used colony forming unit (CFU) assays in the semi-solid medium methylcellulose to determine the frequency of reversion as 5% of $Cd11b^{HI}$ Dox-treated AML246 (Figures 3.1I-J).

The focus of this Chapter was to further characterise the capacity of de-differentiation in AML246, and the mechanism by which PU.1 controls maturational plasticity.

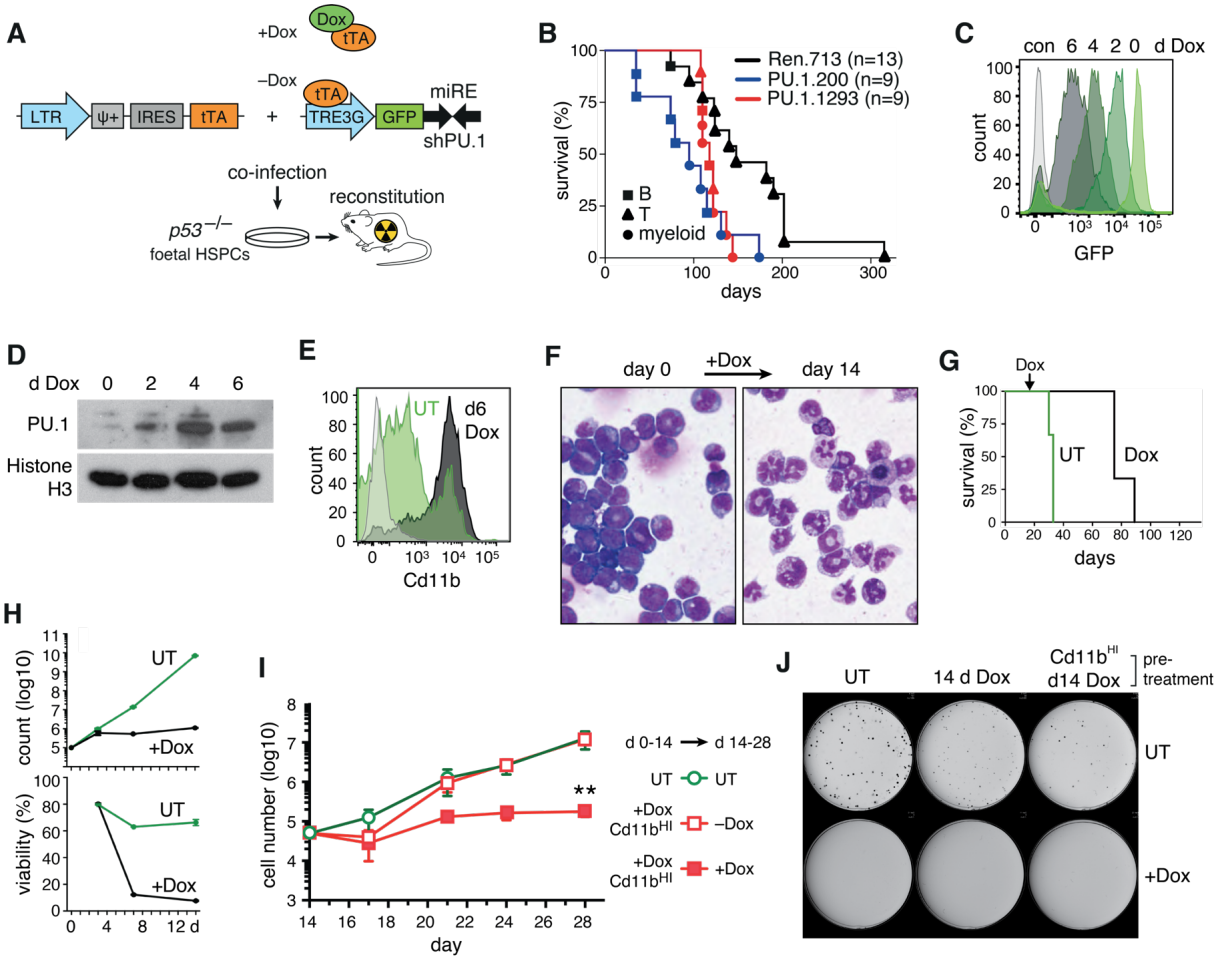

Figure 3.1: PU.1 expression reversibly controls maturation in the mouse AML cell line AML246

(A) Method to generate mouse AML cell lines driven by reversible PU.1 knockdown. (B) Kaplan-Meier survival analysis of lethally-irradiate mice reconstituted with $p53^{-/-}$ foetal livers co-infected with the tTA and one of the TRE3G Ren.713, PU.1.200, or PU.1.1293 shRNAs. (C) Flow cytometry analysis of GFP expression in $Rag^{-/-}$ secondary recipients bone marrow following AML246 engraftment and subsequent Dox treatment. (D) PU.1 protein in AML246 harvested from bone marrow before and after Dox treatment. (E) Cd11b flow cytometry of AML246 cells from peripheral blood. (F) MGG stain of AML246 cytospins derived from the bone marrow of mice before and after 14 days of Dox treatment. (G) Kaplan-Meier survival of secondary recipients of AML246 left untreated or treated with Dox. (H) Proliferation and viability counts of *in vitro* AML246 cultures with or without Dox. Mean ± SD of 3 technical replicates per time point. (I) Proliferation of AML246 cells over a 2-week period (days 14-28) in Dox-free (open symbols) or Dox (closed symbols) medium, following 2 weeks (days 0-14) pre-culture in Dox-free (circles) or Dox (squares) medium. Viable $Cd11b^{HI}$ cells: $**p < 0.01$ for – Dox versus + Dox at day 28; Student's t test with Welch's correction. (J) Methylcellulose colony formation of AML246 cells, untreated or containing Dox as indicated. Plated cells were pre-treated (days 0-14) with Dox as indicated and then 500 viable cells (total or $Cd11b^{HI}$) were plated and colonies imaged 10 days later (day 24).

3.2 AML246 homogeneously responds to Dox treatment

The Dickins laboratory had repeatedly observed that 5% of mature AML246 are capable of reacquiring clonogenicity following Dox withdrawal. Although Dox administration in AML246 results in upregulation of myeloid maturation markers, changes in morphology, and a loss of viability and proliferation consistent with *en masse* differentiation, these do not preclude the possibility of a rare and phenotypically distinct subpopulation seeding this clonogenicity due to incomplete Dox responses. Hence, we sought to verify the homogeneity of Dox responses in AML246.

To investigate, single cell RNA sequencing (scRNA-seq) was employed to observe the transcriptomic uniformity of Dox-treated AML246. AML246 cells were treated for two weeks with Dox *in vitro*, suppressing GFP expression and upregulating Cd11b (Figure 3.2A). Viable untreated AML246, $Cd11b^{HI}$ Dox-treated AML246, and $Cd11b^{+}/Ly6G^{+}$ wild type peripheral blood neutrophils were single cell sorted into 122 individual wells each of a 384-well plate (Figures 3.2A-B). Untreated and $Cd11b^{HI}$ Dox-treated AML246 were also simultaneously sorted in bulk and plated into untreated and Dox-treated methylcellulose, verifying that 5% of mature AML246 formed morphologically blast-like, albeit smaller, colonies when plated into untreated conditions (Figure 3.2C).

The 384-well plate was subsequently transferred to the Walter and Eliza Hall Institute (WEHI) Single Cell Open Research Endeavour (SCORE) facility for library preparation, sequencing, and analysis. Following analysis, 112 untreated AML246, 115 Dox-treated $Cd11b^{HI}$ AML246, and 107 $Cd11b^{+}/Ly6G^{+}$ peripheral blood neutrophils passed the quality control threshold.

Multidimensional scaling revealed that after 14 days of Dox treatment, $Cd11b^{HI}$ AML246 were not transcriptionally equivalent to mature peripheral neutrophils, however they did display a complete separation from their untreated counterparts (Figure 3.2D). Therefore, Dox-induced differentiation of AML246 occurs *en masse.*

Compared to untreated AML246, Dox-treated cells expectedly featured higher levels of Spi1 (PU.1) and Itgam (Cd11b) mRNA (Figure 3.2E). Additionally, increased PU.1 expression resulted in the upregulation of known targets such as *Tyrobp* and *Coro1a*, as well as genes for granulocyte function, for instance *Lyz1* and *Fcgr3* (Figure 3.2E). Many of these granulocyte

genes however were rarely expressed to quite the same levels found in the wild type neutrophils, though this may be in part driven by the *in vitro* milieu not fully replicating the conditions found in the *in vivo* niche.

Nevertheless, the clear distinction between Dox-treated and untreated AML246 demonstrated a homogeneous myeloid differentiation response, indicating that colonies arising following Dox withdrawal CFU experiments likely arise from transcriptionally mature AML246.

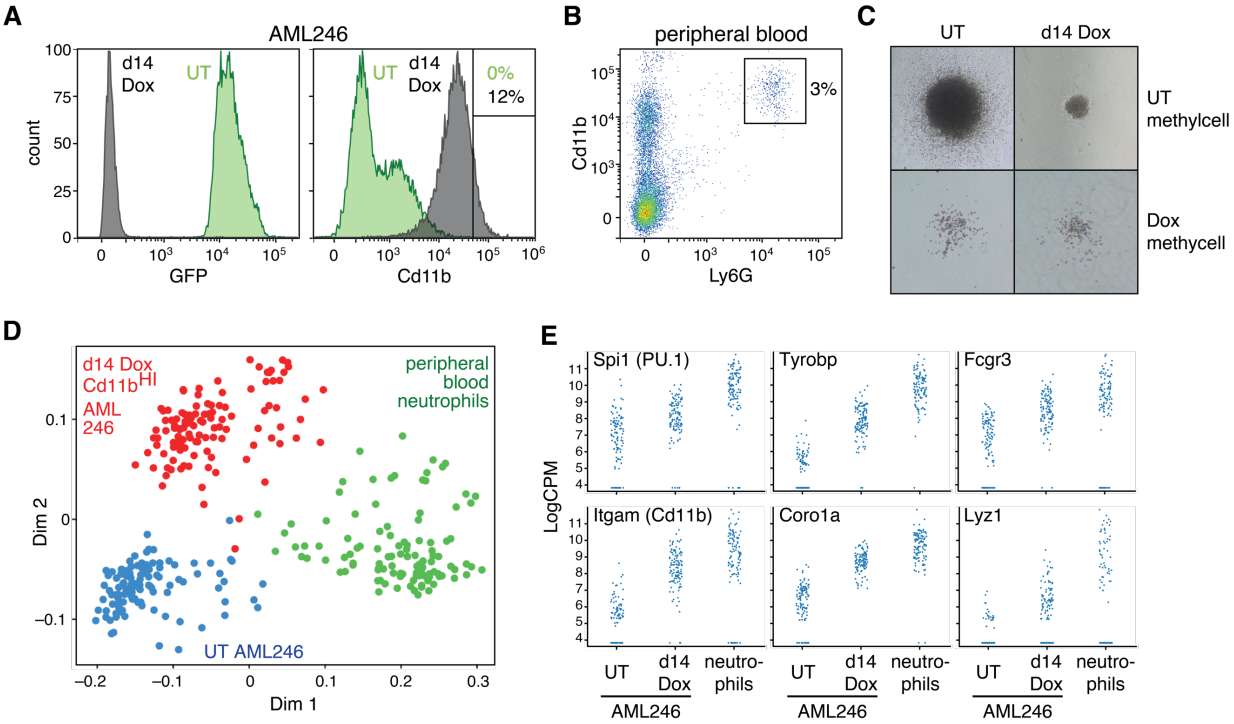

Figure 3.2: Dox treatment homogeneously restores endogenous PU.1 function in AML246
(A) Cd11b flow cytometry of untreated and 14 days Dox-treated AML246, with the $Cd11b^{HI}$ sort gate indicated. (B) Gating profile for wild type mouse peripheral blood neutrophils based on Cd11b and Ly6G expression. (C) Representative colonies from untreated or Dox-treated methylcellulose, in which AML246 derived adjacent to the single-cell sort were plated. (D) Multidimensional analysis of RNA-seq expression profiles for 112 untreated AML246 cells (blue), 115 14-day Dox-treated $Cd11b^{HI}$ cells (red), and 107 $Cd11b^{+}Ly6g^{+}$ peripheral blood neutrophils (green). (E) Single-cell mRNA expression levels in untreated AML246, 14 days Dox-treated AML246, or peripheral blood neutrophils for the genes *Spi1* (PU.1), *Tyrobp*, *Fcgr3*, *Itgam* (Cd11b), *Coro1a*, and *Lyz1*.

3.3 Reversion of mature AML246 at a single-cell level

Previous investigation of AML246 de-differentiation utilised Cd11b sort gates to enrich for the most mature cells. To further validate that clonogenicity following Dox withdrawal was arising from immunophenotypically mature AML246, we attempted to observe de-differentiation at a single cell level. This was possible through the use of FACS index sorting, whereby the immunophenotype of single sorted cells are recorded and linked to their individual target wells of 96-well plates. Subsequently, clonogenicity can be assessed and matched to the originating immunophenotype of the cell.

Untreated, or 6, 12, or 18 days Dox-pre-treated AML246 cells were index sorted into untreated or Dox-treated 96 well plates (Figure 3.3A). As expected, the viability of the cells prior to sort diminished as the length of Dox pre-treatment increased, complemented by increasing degrees of morphologic differentiation (Figures 3.3B-C). In addition to Cd11b upregulation, AML246 maturation was determined by the expression of the monocyte and granulocyte markers FcγR III and II (Cd16 and Cd32) (Gustafson et al. 2015). Upregulation of Cd11b and Cd16/32 was apparent within 6 days of Dox pre-treatment, with double-positive cells persisting for the duration of the time course (Figure 3.3C).

Overall, Dox pre-treatment diminished the proportion of clonogenic cells sorted into untreated plates, however colonies were still present up to 18 days pre-treatment (Figure 3.3D). Interestingly, the frequency of untreated AML246 clonogenicity was slightly higher compared to previous methylcellulose assays, possibly due to maintaining AML246 in liquid culture (Figure 3.3D). Regardless of pre-treatment, cells sorted into Dox-treated plates did not form colonies confirming that growth could not continue upon PU.1 restoration (Figure 3.3D).

Focusing on immunophenotypically mature AML246, Cd11b and Cd16/32 expression had no impact on the frequency of reversion of 6 and 12 days Dox-pre-treated cultures (Figure 3.3D). Importantly, representative $Cd11b^{+}/Cd16/32^{+}$-derived clones from 6 (6.2) or 12 (12.3) days pre-treatment reverted back to their immature immunophenotype, though retained both sensitivity to Dox and leukaemogenic potential (Figures 3.3E-F). This further demonstrates the remarkable plasticity of AML246 maturation through perturbation of PU.1 alone.

In contrast, 18 days Dox pre-treated $Cd11b^{+}/Cd16/32^{+}$ cells failed to form any colonies (Figures 3.3C-D). Although limited by the number of cells sorted, the lack of clonogenicity implies that there may exist a point of no return, beyond which differentiation is terminal.

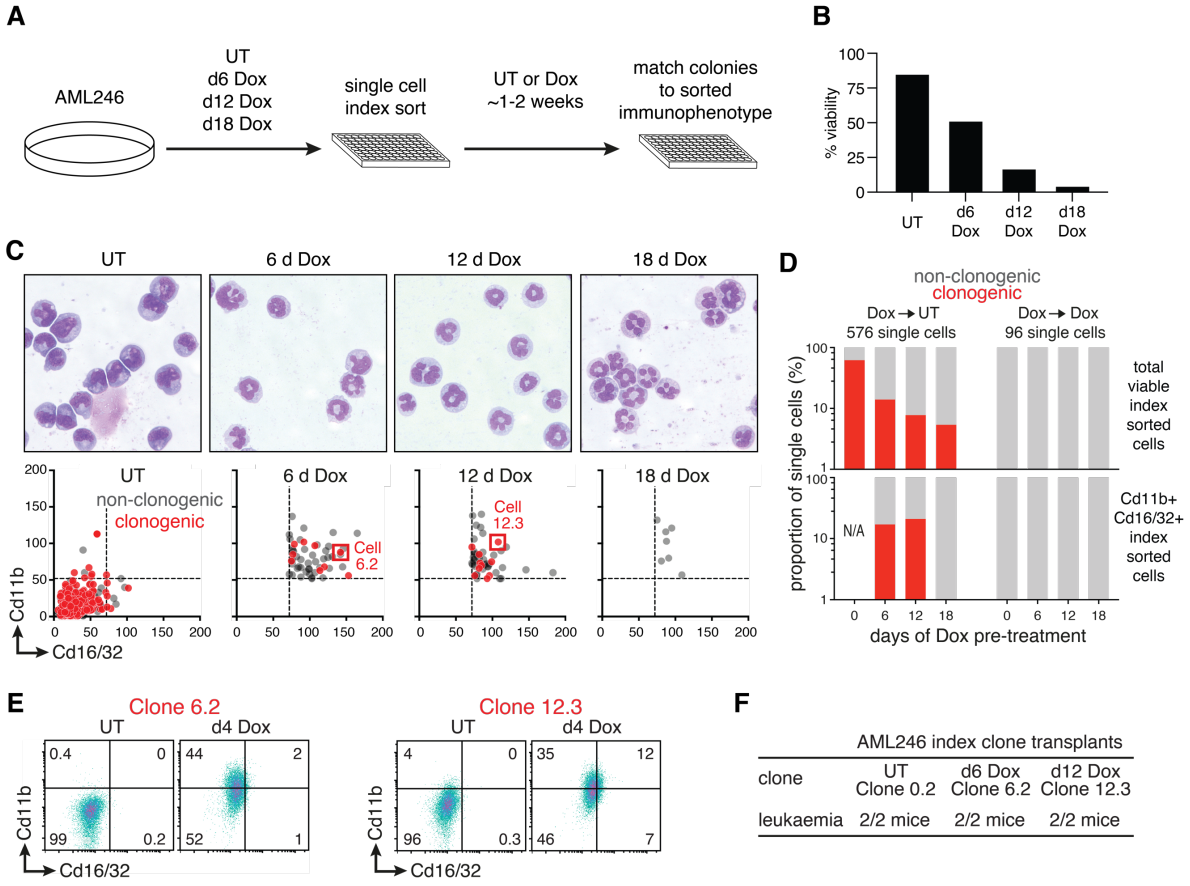

Figure 3.3: PU.1 suppression restores clonogenicity to single mature AML246 cells
(A) Procedure for index-sorting single AML246 cells across a time course of Dox treatment into untreated and Dox-treated 96-well plates. (B) Viability of AML246 cultures following 0, 6, 12, or 18 days Dox treatment. Data matches viability prior to index-sorting, and represents the singleton experiment. (C) Surface Cd11b and Cd16/32 expression (lower panels) of individual Dox-treated AML246 cells index-sorted into Dox-free culture medium in multiwall plates. Single cells subsequently forming clones are shown in red, non-clonogenic in black. Upper panels feature MGG stained cells for morphology. (D) Clonogenic frequency (red) of single index-sorted AML246 cells following a Dox treatment time course, plated into Dox-free (left) or Dox (right) medium, and showing total viable sorted cells (top) or $Cd11b^{+}Cd16/32^{+}$ cells (bottom). Data represents results from 1 experiment. (E) Cd11b and Cd16/32 profile of single cell clones from (C) expanded in Dox-free medium and Dox-treated for 4 days before analysis. (F) Fully penetrant leukaemogenesis upon transplant of untreated *Rag*$^{-/-}$ mice with AML246 clones derived from index-sorted single cells in (C).

3.4 Comprehensive time course of AML246 differentiation and de-differentiation

Before investigating the mechanisms of PU.1, we determined to characterise AML246 differentiation and de-differentiation in depth to demonstrate the optimal time points for Dox treatment and withdrawal.

AML246 cells were closely observed over 4-day intervals across a time course 12 days Dox treatment (0, 4, 8, 12) followed by a $Cd11b^{+}$ sort (12C), and then a further 12 days of Dox withdrawal (–4, –8, –12). Upon Dox administration, flow analysis revealed both a gradual loss of GFP and slow upregulation of Cd11b (Figure 3.4A). In contrast, Dox withdrawal resulted in a rapid upregulation of GFP, reaching maximal expression within 4 days (Figure 3.4B). While Cd11b expression continually rose during Dox treatment, upon Dox withdrawal the cells returned to an immature $Cd11b^{low}$ state within 8 days (Figure 3.4A-B). As expected, PU.1 protein closely correlated to the presence of Dox, immediately upregulating upon treatment, and returning to the suppressed state upon Dox withdrawal (Figure 3.4C). Both proliferation and viability, which dropped after approximately 8 days of Dox treatment, speedily recovered following removal of Dox (Figures 3.4D-E). Strikingly, MGG staining revealed that the morphologic changes observed during AML246 differentiation, including nuclei segmentation and the whitening of the cytoplasm, are seemingly reversed sequentially back through to the immature state (Figure 3.4F).

AML246 myeloid differentiation is apparent within the 12 days of Dox treatment, and by various metrics revert to their supposed original state following 12 days of Dox withdrawal, providing an adequate procedure for the investigation of PU.1 mechanisms during reversible maturation/de-differentiation.

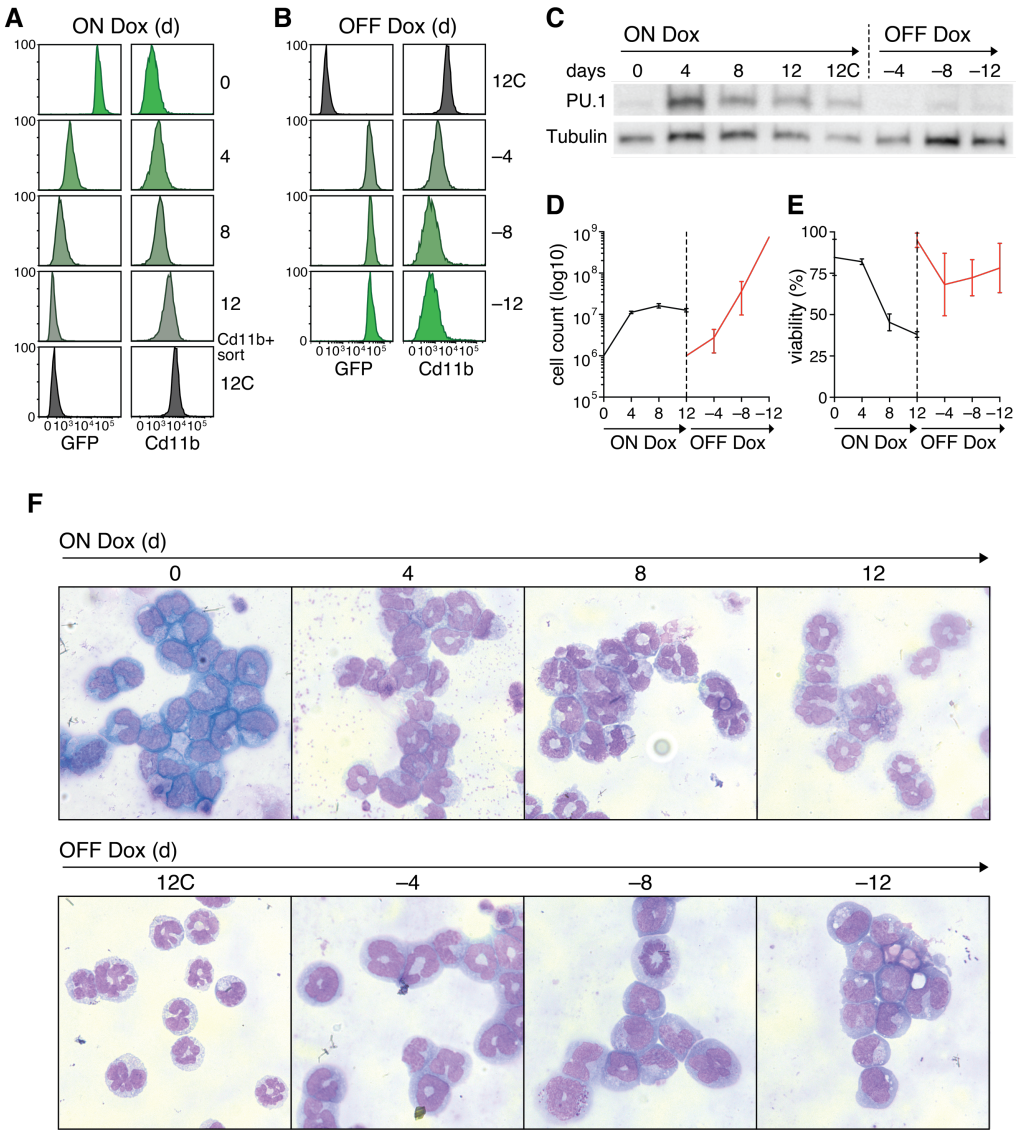

Figure 3.4: AML246 rapidly de-differentiates *en masse* following Dox withdrawal
(A) Flow cytometry of GFP and Cd11b expression in AML246 at 4 day intervals across a time course of 12 days Dox treatment and subsequent Cd11b^{HI} cells post-sort. (B) Flow cytometry of GFP and Cd11b expression of Cd11b^{HI} sorted AML246 at 4 day intervals across a time course of 12 days Dox withdrawal. PU.1 immunoblots (C), proliferation (D), viability (E), and MGG stained cytospins (F) of AML246 across the time course of Dox treatment and Dox withdrawal. Mean ± SD for at least 3 independent replicates for proliferation (days 0 to –8) and viability (days 0 to –12).

3.5 Transcriptional reversal on a global level following Dox withdrawal

The procedure described above was used to investigate the mechanisms of PU.1, whereby the time course of Dox treatment and withdrawal was staggered in such a way that each time point sample could be harvested concurrently. Subsequently, each sample was processed to identify dynamic changes in transcription (RNA-seq), PU.1 binding sites (PU.1-ChIP-seq), and chromatin remodelling (ATAC-seq) (Figure 3.5A).

RNA was harvested from duplicate samples at each time point, after which libraries were prepared using the Illumina TruSeq Kit. Transcriptome libraries were then passed on to the WEHI Genomics Hub for sequencing, with the resulting data transferred to A/Prof Matthew Ritchie for analysis. Validating the procedure, dynamic changes in PU.1 mRNA revealed a close correlation to PU.1 protein levels, with a 3.9-fold increase 4 days of Dox treatment that remained elevated on days 8 and 12, then reduced 3.9-fold 4 days after Dox withdrawal where it remained low (Figure 3.5B). Reassuringly, this degree of repression approximately resembles the 80% reduction of PU.1 in haematopoietic cells required to trigger murine leukaemogenesis (Rosenbauer et al. 2004).

As detailed in Chapter 1, PU.1 is a known master regulator transcription factor, as such restoring expression caused extensive transcriptomic changes, much of which was immediately reversed upon Dox withdrawal (Figure 3.5C). Maximal *PU.1* transcript upregulation and suppression occurred within 4 days of Dox treatment and withdrawal respectively, however global differential gene expression continued across subsequent time points representing the extensive transcriptomic restructuring occurring during myeloid differentiation and de-differentiation (Figure 3.5C). Interestingly, multidimensional scaling between time points suggested that much of the process of de-differentiation involved reversing changes that occurred within the first 4 days of PU.1 restoration, whereas some of the later effects of differentiation may be irreversible (Figure 3.5D). Focusing on acute differential gene expression, 2,306 of 3,863 genes (60%) upregulated in the first 4 days of differentiation were downregulated within the first 4 days of de-differentiation (Figure 3.5E). Importantly, differentiation and de-differentiation significantly correlated and contrasted respectively to the CMP to neutrophil transition derived from the ImmGen gene expression database (Heng, Painter, and Immunological Genome Project 2008) (Figure 3.5F).

PU.1 transcript levels positively correlated with 4056 genes across the time course, signifying that a large proportion of the myeloid transcriptome relies on continued PU.1 expression (Figure 3.5G). Interesting correlates included important granulocytic cytokine receptors such as *Csf2rb/Csf2rb2* (GM-CSF receptor), *Csf2r* (G-CSF receptor), and *Csf1r* (M-CSF receptor), and their downstream signalling components *Jak1, Jak2, Stat3*, and *Tyk2* (Figures 3.5G-H). Furthermore, genes involved in granulocyte function such as the integrins *Itgam* (Cd11b) and *Itgb2* (Cd18), adaptor *Tyrobp*, and signalling kinase *Syk* also correlated with *PU.1* expression (Figure 3.5H). Intriguingly, the proto-oncogene transcription factor *Myc* was strongly negatively-correlated with *PU.1* expression (Figure 3.5G-H). Frequently upregulated in human AML, restoration of *Myc* following Dox withdrawal and *PU.1* suppression may be an important component in re-establishing proliferation (Rayeroux and Campbell 2009; Jones et al. 2010).

Validating AML246 as a leukaemia model, many of the *PU.1*-correlated genes were conserved in human *PU.1*-correlated transcriptome data identified in a profiling study of 173 AML patients (Cancer Genome Atlas Research et al. 2013) (Figures 3.5I-J). As a further authentication, the RNAseq data was compared to the prior scRNA-seq experiment detailed in §3.2. Differentially expressed (DE) genes following the 12 days of Dox treatment significantly correlated with the scRNA-seq transcriptomic DE geneset (Figure 3.5K).

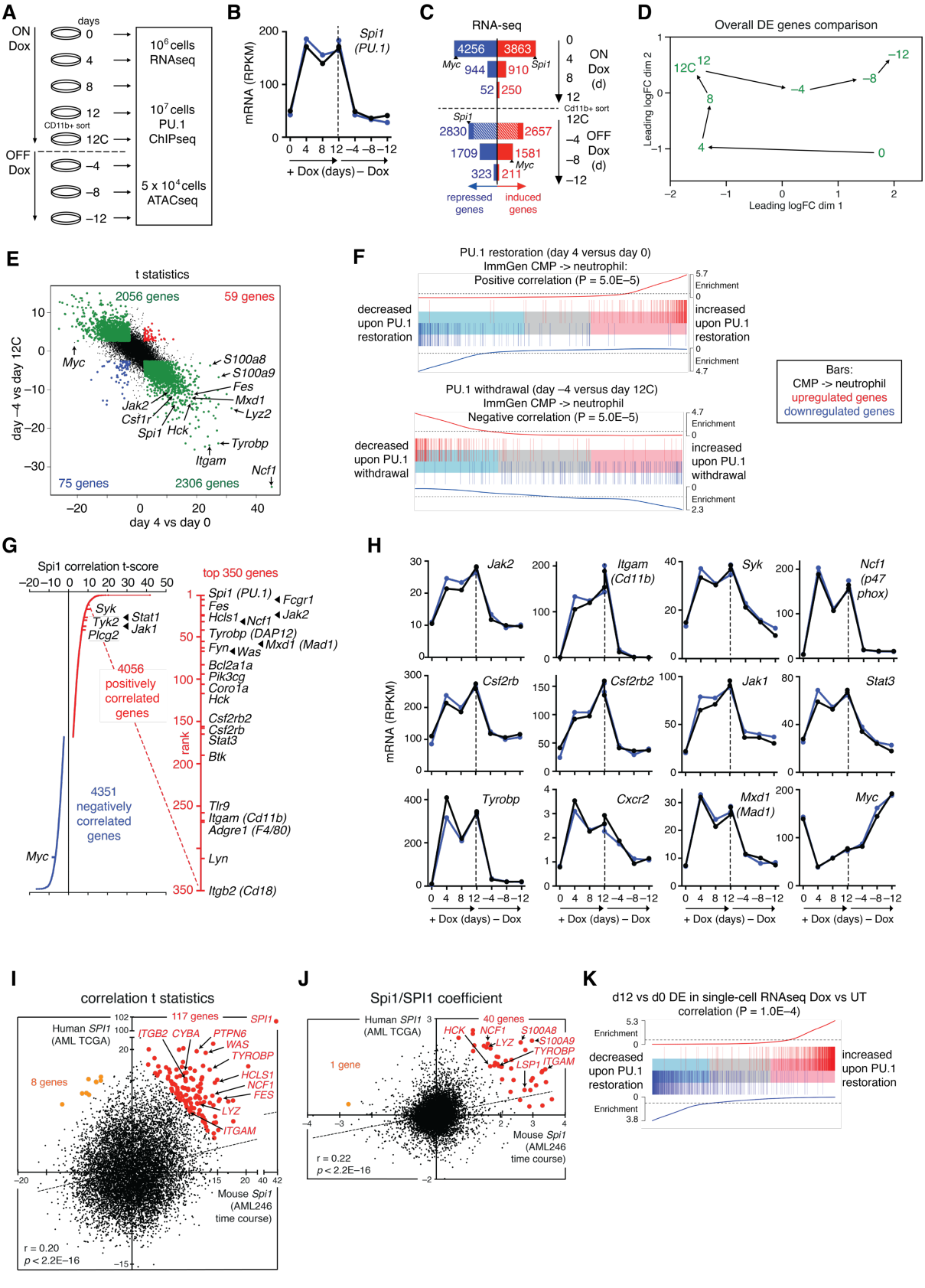
A
days
ON Dox
0
4
8
12
CD11b+ sort
12C
OFF Dox
–4
–8
–12
10^6 cells RNAseq
10^7 cells PU.1 ChIPseq
5 x 10^4 cells ATACseq
B
Spi1 (PU.1)
mRNA (RPKM)
+ Dox (days) – Dox
C
RNA-seq
4256
3863
Myc
944
910
Spi1
52
250
ON Dox (d)
Cd11b+ sort
2830
2657
1709
1581
323
211
OFF Dox (d)
repressed genes
induced genes
D
Overall DE genes comparison
Leading logFC dim 2
Leading logFC dim 1
E
t statistics
2056 genes
59 genes
75 genes
2306 genes
day –4 vs day 12C
day 4 vs day 0
S100a8
S100a9
Fes
Mxd1
Lyz2
Tyrobp
Itgam
Ncf1
Jak2
Csf1r
Spi1
Hck
Myc
F
PU.1 restoration (day 4 versus day 0)
ImmGen CMP -> neutrophil:
Positive correlation (P = 5.0E–5)
decreased upon PU.1 restoration
increased upon PU.1 restoration
Enrichment
PU.1 withdrawal (day –4 versus day 12C)
ImmGen CMP -> neutrophil
Negative correlation (P = 5.0E–5)
decreased upon PU.1 withdrawal
increased upon PU.1 withdrawal
Bars:
CMP -> neutrophil
upregulated genes
downregulated genes
G
Spi1 correlation t-score
top 350 genes
rank
4056 positively correlated genes
4351 negatively correlated genes
Spi1 (PU.1)
Fcgr1
Fes
Hcls1
Ncf1
Jak2
Tyrobp (DAP12)
Fyn
Was
Mxd1 (Mad1)
Bcl2a1a
Pik3cg
Coro1a
Hck
Csf2rb2
Csf2rb
Stat3
Btk
Tlr9
Itgam (Cd11b)
Adgre1 (F4/80)
Lyn
Itgb2 (Cd18)
Syk
Tyk2
Plcg2
Stat1
Jak1
Myc
H
mRNA (RPKM)
Jak2
Itgam (Cd11b)
Syk
Ncf1 (p47 phox)
Csf2rb
Csf2rb2
Jak1
Stat3
Tyrobp
Cxcr2
Mxd1 (Mad1)
Myc
+ Dox (days) – Dox
I
correlation t statistics
Human SPI1 (AML TCGA)
117 genes
8 genes
Mouse Spi1 (AML246 time course)
r = 0.20
p < 2.2E–16
SPI1
ITGB2
CYBA
PTPN6
WAS
TYROBP
HCLS1
NCF1
FES
LYZ
ITGAM
J
Spi1/SPI1 coefficient
Human SPI1 (AML TCGA)
40 genes
1 gene
Mouse Spi1 (AML246 time course)
r = 0.22
p < 2.2E–16
HCK
NCF1
S100A8
LYZ
S100A9
TYROBP
LSP1
ITGAM
K
d12 vs d0 DE in single-cell RNAseq Dox vs UT
correlation (P = 1.0E–4)
decreased upon PU.1 restoration
increased upon PU.1 restoration
Enrichment

Figure 3.5: Modulation of PU.1 triggers global and reversible transcriptional remodelling
(A) Strategy for harvesting AML246 across 12 days of differentiation, and 12 days of de-differentiation for RNAseq, PU.1-ChIPseq, and ATACseq analysis. (B) mRNA expression of Spi1 (PU.1) (RNAseq RPKM for two replicates), with a dotted line indicating Dox withdrawal. (C) Induced (red) and repressed (blue) changes in gene expression (5% FDR) at 4 day intervals across the time course. For 12C to day –4, shaded regions indicate the proportion of genes where changes in expression changes from day 0 to day 4. Day 12 to 12C only indicated 1 differentially expressed gene (5% FDR). (D) Multidimensional scaling (MDS) plot of RNA-seq expression profiles between time points, and the trajectory between samples. Data points indicate mean between 2 replicates. (E) Scatterplot of differential gene expression (t-statistics) in AML246 time course cells from day 0 to day 4 (acute Dox treatment) versus day 12C ($CD11b^{HI}$ sorted) to day –4 (acute Dox withdrawal) based on gene expression from 2 samples per time point. Genes where acute Dox-induced expression changes were reversed upon Dox withdrawal (5% FDR) are green, and genes upregulated or downregulated in both transitions are red and blue, respectively. (F) Gene set analysis barcode plots for RNAseq differential gene expression in the time course analysis, showing acute (4 days Dox) PU.1 restoration (top) and subsequent acute PU.1 suppression (4 days Dox withdrawal) (bottom). Differential expression is shown as a shaded rectangle with genes horizontally ranked by moderated t-statistic. Downregulated genes are shaded blue ($t < 1$) and upregulated genes pink ($t > 1$). Overlaid sets of the top 200 genes with higher (red bars) or lower (blue bars) expression in neutrophils relative to common myeloid progenitors (CMPs) from the ImmGen expression database. Red and blue traces above and below the barcode represent a moving average of relative enrichment calculated using a tri-cube weight function. p value was computed by the roast method using both up- and downregulated genes. (G) Genes where expression correlates with *Spi1* across the time course, ranked by t-statistic and with the top 350 genes detailed at the right. (H) Expression (RNAseq RPKM) of several key functional myeloid lineage genes across the time course, all barring *Myc* exhibiting a positive correlation with *Spi1*. (I) Scatter plot of t-statistics for mouse Spi1-correlated gene expression across the AML246 time course versus human SPI1-correlated gene expression across 173 human AML patient samples. Highlighted genes are significantly correlated with *Spi1/SPI1* in both species that fall beyond a diagonal line joining human $t = = 20$ and mouse $t = –20$ (orange) or $t = 20$ (red). (J) Scatter plot as described in I, but for *Spi1/SPI1* coefficient from the liner models instead of t-statistics. This plot indicates genes that are the most sensitive to differences in *Spi1/SPI1* expression, whereas the t-statistic plot indicates the most significantly correlated genes. (K) Barcode analysis plot for RNA-seq differential gene expression in the time course analysis from day 12 versus day 0, as compared to Dox-treated versus untreated AML246 differential genes identified in the single cell RNA-seq. Each bar (red = upregulated, blue = downregulated) represents a significantly differentially expressed gene from day 12 versus day 0, overlayed along the sorted logFC found in the single-cell experiment. p value was computed by the roast method using both up- and downregulated genes.

3.6 Reversibility of the pioneering functions of PU.1

PU.1-ChIP-seq was utilised to examine the dynamic binding of DNA by PU.1 (Figure 3.5A). Singlet samples from each time point described in §3.4 were harvested and transferred to Dr. Michael Chopin at WEHI for preparation, and analysed by A/Prof Matthew Ritchie at WEHI. As expected, the number of PU.1 binding sites closely correlated with Dox treatment and PU.1 restoration (Figure 3.6A-B). PU.1-bound genes, defined by PU.1-ChIP-seq peaks within 50kb of the transcription start site, also closely relating to PU.1 expression (Figures 3.6A-B). Acute treatment with Dox resulted in over 12,000 new PU.1 binding sites, with 13,538 genes gaining a PU.1 peak (Figures 3.6B-C). Conversely, Dox withdrawal and the subsequent PU.1 repression caused 12,437 genes to lose their complement PU.1 binding sites (Figure 3.6C). Importantly, a number of PU.1 sites remain in the absence of Dox, emphasising the point that PU.1 is repressed but not ablated by the shRNA.

Concurrent samples for each time point were harvested to investigate regions of open chromatin using ATAC-seq (Figure 3.5A). These were transferred to Charlie Bell in Prof Mark Dawson's Laboratory at the Peter MacCallum Cancer Centre for processing, and analysed by A/Prof Matthew Ritchie at WEHI. In contrast to PU.1-ChIP-seq, the amount of open chromatin peaks varied approximately 30% across the time course irrespective of treatment (Figure 3.6A).

The PU.1 upstream regulatory element (URE) is a known target of PU.1 itself, and served as a validation of the procedure (Okuno et al. 2005). Upon Dox withdrawal, PU.1-ChIP analysis shows several PU.1 binding sites reduced in intensity but not ablated, indicating a partial disruption on PU.1 auto-regulation (Figure 3.6D). However, there was minimal effect on chromatin accessibility (Figure 3.6D).

PU.1-ChIP-seq and ATAC-seq data was integrated with the prior RNA-seq experiment to identify genes where Dox treatment led to the binding of PU.1 within 50kb of the TSS, opening the chromatin, and upregulating the target gene, all of which was reversed following Dox withdrawal (Figure 3.6E). This approach identified 804 genes, a list enriched for pathway members involved in both myeloid differentiation and granulocyte function (Figures 3.6E-G). This includes the high-ranking PU.1-correlate gene and mediator of neutrophil migration *Cxcr2*, and transducer of myeloid cytokine signalling *Jak2* (Eash et al. 2010; Silvennoinen et al. 1993) (Figures 3.6H-I). These sites corroborate the known role of PU.1 as a pioneering

transcription factor, binding and opening regions of closed chromatin (Krysinska et al. 2007; Ghisletti et al. 2010; Barozzi et al. 2014). Importantly, the chromatin promptly condensed following PU.1 suppression, indicating that the continuous presence of PU.1 is required to maintain chromatin accessibility and the expression of hundreds of target genes responsible for a mature myeloid state and ensuring terminal differentiation.

A

Time point	0	4	8	12	–4	–8	–12
PU.1 ChIP peaks	402	12900	8334	15984	1195	1528	4302
ATAC-seq peaks	29314	28743	37314	28215	40411	33300	26127

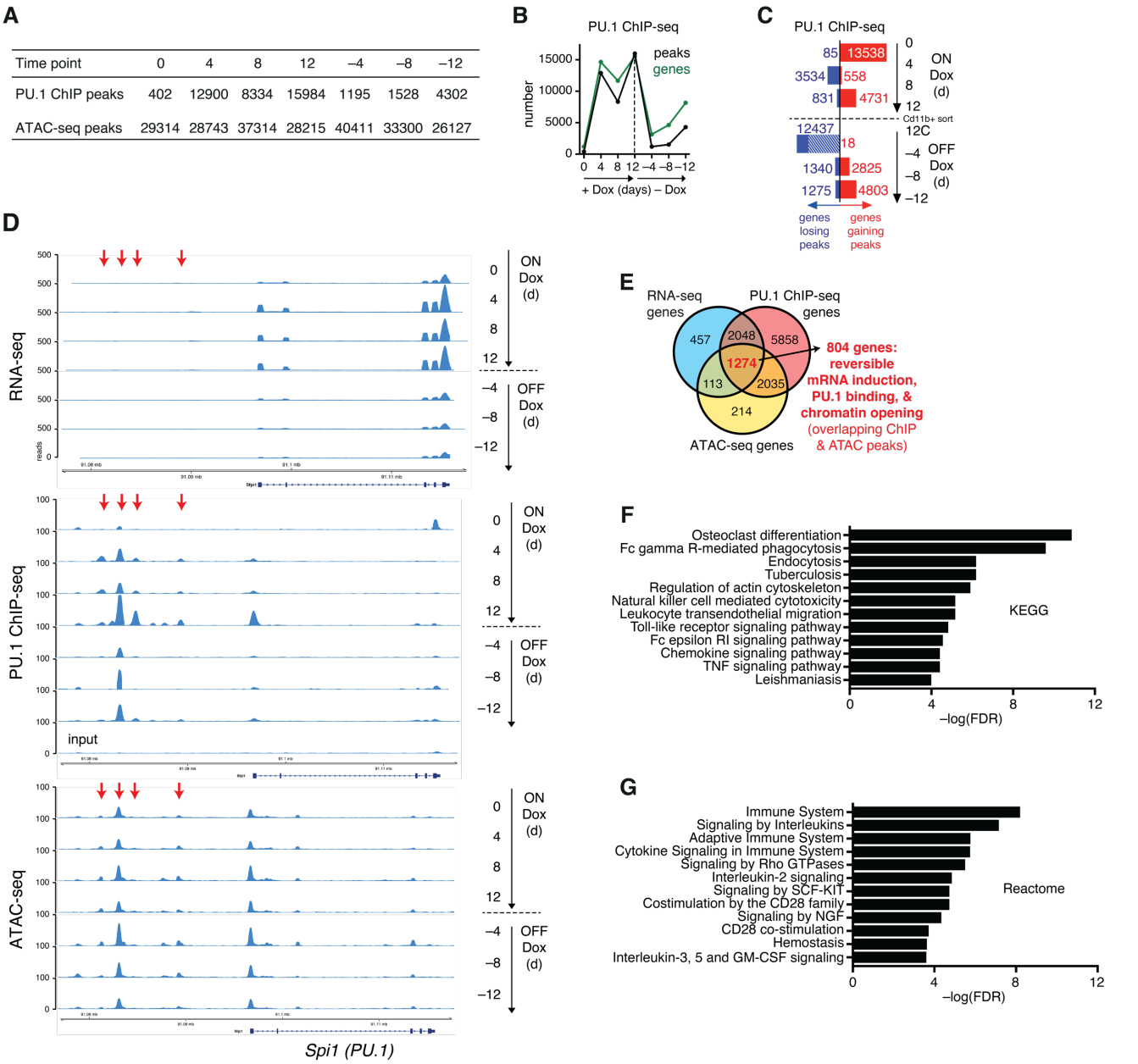

Figure 3.6: PU.1 acts as a pioneering transcription factor to reversibly regulate chromatin accessibility and expression of key target myeloid genes
(A) Number of PU.1-ChIPseq peaks and ATAC-seq peaks across the AML246 time course. (B) Number of PU.1-ChIPseq peaks corresponding number of gene TSS within 50kb of the peak. (C) Changes in PU.1 DNA binding during 4 day intervals across the time course. Shaded region indicates proportion of genes were binding is reversed. (D) RNA-seq (top), PU.1-ChIPseq (middle), and ATACseq (bottom) tracks for *Spi1*, showing dynamic PU.1 autoregulatory binding at several upstream enhancers. Arrows indicate enhancers at –7.5, –12, –13.6, and –15.4 kb relative to the transcription start site. The 3 upstream enhancers correspond to the URE. (E) Venn diagram showing "RNA-seq genes," where expression significantly rises by day 4 (staying up at days 8 and 12), and then falls at day –4 (staying down at day –8 and –12) and "ChIP-seq genes" and "ATAC-seq genes," where peaks are gained then lost at the same time points. For 804 of the common 1,274 genes, ATAC and ChIP peaks overlap, indicating PU.1 directly maintains open chromatin. (F) KEGG and (G) Reactome pathway enrichment of the 804 PU.1-regulated genes described in (E). (H) *Cxcr2* and (I) *Jak2* PU.1 ChIP-seq (left) and ATAC-seq (right) tracks. Time course samples are ordered top down with dotted line indicating Dox withdrawal. Arrows indicate enhancers with dynamic, overlapping ChIP and ATAC peaks.

3.7 Discussion and Conclusion

Using our model cell line AML246 we observed that endogenous PU.1 restoration triggers myeloid differentiation, and subsequently these mature AML-derived cells can revert to an immature, clonogenic, and leukaemogenic state upon PU.1 suppression through a process of de-differentiation. Furthermore, we tracked dynamic changes in transcription, PU.1 DNA-binding, and chromatin remodelling over 4 day intervals during 12 days of differentiation and 12 days de-differentiation. Using this data, we identified 804 genes whereby PU.1 acts as a pioneering transcription factor binding nearby regulatory elements to open chromatin and upregulate transcription in a reversible manner.

Overall, the maturational plasticity of AML246 has exciting implications in the use of differentiation therapy to treat APL, as well as wider considerations into the phenotypic plasticity of AML and the concept of leukaemic stem cells. In Chapter 4, this concept is recapitulated in a human APL context and is discussed in greater detail therein.

3.7.1 Mature AML246 can de-differentiate following Dox withdrawal

The addition of Dox to AML246 results in the restoration of endogenous PU.1, triggering a robust myeloid differentiation evident from upregulation of myeloid maturation markers, neutrophil-like morphological changes, and loss of proliferation and viability. Furthermore, withdrawing Dox from these mature AML246 reverts these phenotypic changes, restoring AML246 proliferative capacity.

Our original methylcellulose CFU assays did not provide the ability to discern whether the clonogenic cell of origin was indeed mature. Thus, there remained concerns that rare subpopulations may explain clonogenicity following Dox withdrawal due to incomplete Dox responses. This was addressed by observing both differentiation and de-differentiation at single cell levels.

In recent years, scRNA-seq has become a powerful platform for stratifying stages of haematopoiesis, a sensitive tool for uncovering slight transcriptomic variations within a population (Nestorowa et al. 2016). As such, we employed scRNA-seq to demonstrate the clear transcriptomic distinction between untreated and Dox-treated AML246, highlighting a population-wide response to Dox. Furthermore, close clustering of the Dox-treated AML246

single cells indicated a homogeneous response. Dox-treated AML246 were not transcriptionally equivalent to wild type peripheral blood neutrophils, however this may be due differences between an AML and wild type myeloid differentiation, the lack of functional p53 in AML246, mutant Kit, *in vitro* versus *in vivo* conditions, and general cell culture drift.

Index sorting was used to verify de-differentiation of mature AML246 at a single cell level. This method made possible the ability to match the mature immunophenotype with the potential for clonogenicity, at frequencies similar to that of earlier methylcellulose CFU experiments.

Taken together, these single cell approaches concluded that AML246 uniformly differentiates following Dox administration, and that mature cells can reacquire clonogenicity through Dox withdrawal, validating the reversion of AML246 observed in bulk cultures.

3.7.2 Myeloid de-differentiation is likely an AML-specific phenomenon

AML246 was generated through the introduction of PU.1 shRNA in *p53*$^{-/-}$ foetal HSCs. The differentiation block of AML246 is maintained by this suppression of PU.1, as Dox administration restored expression and triggered myeloid differentiation. The dependency of maturation via PU.1 function was further emphasised by the reversal of myeloid differentiation through Dox withdrawal and the re-suppression of PU.1.

However, our data does not suggest that plastic differentiation occurs in otherwise normal mature myeloid cells. In normal myelopoiesis, the regulation of transcription factors including PU.1 is tightly controlled through feed-forward loops that enforce unidirectional differentiation (Kueh et al. 2013). Furthermore, the presence of additional leukaemia-specific factors may encourage the plasticity observed in AML246. Genomic sequencing of AML often reveals several cooperating recurrent mutations (Cancer Genome Atlas Research et al. 2013; Papaemmanuil et al. 2016). AML models driven by retroviral introduction of PML-RARA, likewise with PU.1, endure a long latency suggesting the acquisition of additional cooperating mutations that enable leukaemic transformation (Riva et al. 2013). In the case of AML246, transcriptome sequencing revealed a likely activating mutation (N824K) in the receptor tyrosine kinase Kit, amongst others. These cooperating mutations presumably influence maturation plasticity in AML.

3.7.3 The pioneering functions of PU.1 are reversible

De-differentiation of mature AML246 is driven by the suppression of endogenous PU.1. By exploiting the reversibility of PU.1 restoration in AML246, we sought to identify the mechanisms by which PU.1 expression controls the myeloid differentiation state. This was explored through tracking the dynamic changes in transcription, PU.1 DNA-binding, and chromatin accessibility across the time course of differentiation and de-differentiation. These results were integrated to identify 804 genes whereby PU.1 bound closed regulatory elements to open the chromatin and induce expression, the majority of which was reversed upon PU.1 suppression.

The pioneering functions of PU.1 are well known, establishing the myeloid differentiation program by making regulatory elements accessible for additional transcription factors (Krysinska et al. 2007; Ghisletti et al. 2010; Barozzi et al. 2014). However, our work shows for the first time that the pioneering functions of PU.1 are reversible. Following acute Dox withdrawal and PU.1 suppression, open chromatin rapidly condensed and the target genes were immediately downregulated. This demonstrates that the presence of PU.1 is required not only to open these regulatory elements, but to sustain their accessibility. Through this, changes in PU.1 expression are capable of modulating the state of AML246 maturation.

It would be of interest to identify which co-operating transcription factors, co-activators or co-repressors, access these sites reversibly bound by PU.1. Attractive candidates include those known to interact synergistically or as co-activators with PU.1, such as Runx1, Cebpa, Crebbp, and c-Jun (Gupta et al. 2009). Critically, these transcription factors are highly expressed in both untreated and Dox-treated AML246. The AML246 model provides a convenient platform to investigate the role of these PU.1-interacting proteins in myeloid differentiation. Future experiments beyond the scope of this PhD may involve the use of loss-of-function to identify whether myeloid differentiation through PU.1 restoration is aided by any particular co-factors.

3.7.4 PU.1 initiates and sustains expression of 804 direct target genes

PU.1 restoration alone triggered robust myeloid differentiation in AML246, however this coincided with differential expression of over a third of the transcriptome. Our list of 804 direct

targets allows for future exploration into how PU.1 initiates and maintains myeloid differentiation.

Consistent with its expression in various myeloid lineages, PU.1 directly regulated the expression of multiple late term myeloid surface-expressed markers, including the pan-myeloid marker *Itgam* (Cd11b), monocyte and eosinophil marker Adgre1 (F4/80), and the eosinophilic marker *Siglec-f* (Lee et al. 2012). The morphology of Dox-treated AML246 resembled neutrophils, however the expression of these eosinophilic markers could imply multipotent differentiation given the right stimulus, for instance interleukin IL-5 (Esnault and Kelly 2016). However, the effect of lineage-specific cytokines upon AML246 differentiation remains to be investigated.

Importantly, PU.1 directly upregulated many of the receptors required during normal myeloid haematopoiesis. This included the cytokine receptor Csf1r, chemokine receptors Ccr2 and Ccr3, interferon receptors Ifnar1 and Ifnar2, and components of the interleukin receptors Il1, Il7, and Il10. These signalling pathways could be further augmented by PU.1 through the direct regulation of genes involved in cytokine transduction, including Jak1 and Jak2, Stat1 and Stat6, as well as the class I PI3K subunits Pik3cb and Pik3cd and adaptor Pik3ap1. Upregulation of these receptors and signalling pathways likely enhances their sensitivity, demonstrating that PU.1 is priming cells to be responsive to myeloid specific factors involved in differentiation and activation. Conversely, suppression of PU.1 in mature AML246 repressed expression of these pathways, the inhibition of which may be potentiating the process of de-differentiation.

Additionally, PU.1 directly upregulated the expression of genes involved in granulocyte function. These included Lyz1 and Lyz2 for lysozyme formation, and NADPH oxidase components Ncf1, Ncf2, Ncf4, and Rac2. Establishing granulocyte functionality may enhance the terminal cell fate, with NADPH oxidase one avenue of initiating neutrophil death and clearance *in vivo* (Frasch et al. 2008). Likewise, many factors involved in functional immune responses such as Tnf, Tlr1, Tlr6, Tlr9, Cxcr2, Ccr2, and Ccr3 were directly upregulated by PU.1, and effective granulocyte activation results in the upregulation clearance signalling molecules (Bratton and Henson 2011). Hence, maintaining high PU.1 expression may be fundamental to engaging clearance of tumour cells in AML differentiation therapies.

One of the more curious genes on the list of 804 PU.1-activated genes was the myeloid transcription factor Runx1. Expressed early during haematopoiesis, Runx1 establishes the expression of other transcriptional regulators of differentiation, including PU.1 (Huang et al. 2008). This may be an aspect of the feed-forward loop whereby PU.1 enhances its own expression to enforce terminal myeloid differentiation. Combined with co-operation between the transcription factors, the complementary upregulation of Runx1 and PU.1 further demonstrates the complexity in the regulation of myeloid master transcription factors during haematopoiesis (Imperato et al. 2015).

Unexpectedly, some known targets of PU.1 such as the granulocyte receptor Csf3r, granulocyte-monocyte receptor Csf2r, and PU.1 itself through auto-regulation did not meet the criteria to be included in the list of 804 genes (Smith et al. 1996; Okuno et al. 2005; Zhang et al. 1996). This may represent a limitation resulting from the use of the single model cell line, AML246. Additionally, AML246 has been adapted to *in vitro* culture, and may not entirely replicate the myeloid differentiation process accurately compared to the normal bone marrow niche. In the future, we intend to partially replicate this experiment to identify the targets of PU.1 in a human context, the generation of models for which forms the basis of Chapter 5.

It would be of interest to explore which downstream PU.1 targets are required for an effective myeloid differentiation. In future experiments, libraries of retroviral shRNA or CRISPR/Cas9 sgRNA targeting the 804 genes could be introduced into AML246 cells, and through loss-of-function and selection one could identify genes that aid or impede myeloid differentiation upon PU.1 restoration.

3.7.5 Conclusion

In conclusion, the restoration of endogenous PU.1 with Dox treatment triggered myeloid differentiation in the mouse AML cell line AML246, and withdrawal of Dox in mature AML246 allowed for reversion to an immature state and reacquisition of clonogenicity. Both the homogeneity of the Dox differentiation response and de-differentiation arising from mature AML246 cells were validated at a single cell level using scRNA-seq and FACS index sorting. Furthermore, the mechanisms by which PU.1 modulation controlled both differentiation and de-differentiation was assessed using RNA-seq, PU.1-ChIP-seq, and ATAC-seq, resulting in the identification of 804 PU.1-activated target genes whereby PU.1 bound closed regulatory

elements to open the chromatin and induce expression in a reversible manner, amongst thousands more differentially regulated by PU.1.

CHAPTER 4. Maturational plasticity of human APL following differentiation therapy

4.1 Introduction

The previous Chapter describes the validation of de-differentiation of our AML mouse cell line AML246, with reversion of myeloid maturation initiated by the knockdown of PU.1 in the mature cells. Maturational plasticity may influence how we regard differentiation in human cases of AML. As outlined in Chapter 1, APL is a subtype of AML characterised by the presence of the t(15;17) chromosomal translocation and its encoded fusion protein PML-RARA, which blocks normal myeloid differentiation in part through the dysregulation of PU.1. Administration of ATRA triggers myeloid differentiation following the degradation of PML-RARA, to some degree driven by the restoration of PU.1 expression and function. As mature AML246 cells de-differentiate upon PU.1 suppression following Dox withdrawal, we hypothesised that human APL maturation may also be a reversible process following the withdrawal of ATRA.

4.2 Basic Characterisation of ATRA-induced Differentiation of NB4 and HT93 cells

This Chapter relies on the use of two common APL cell lines, NB4 and HT93, as well as two patient-derived APL primary samples. NB4 cells readily grow in culture with a high capacity for single cell cloning. The cell line is karyotypically complex and are p53 deficient, however appreciable morphological differentiation and immunophenotypic induction of the myeloid marker CD11B reveal NB4 ATRA sensitivity in culture at concentrations as low as 100 nM (Figures 4.1A-C) (Mozziconacci et al. 2002). Unlike NB4 cells, HT93 cells harbour functional p53. Although HT93 cells are similarly sensitive to ATRA, HT93 exhibit a more robust morphological differentiation with the striking nuclear segmentation typical of human neutrophils (Figure 4.1D-F). Interestingly, G-CSF improves viability and growth of HT93 in the absence of ATRA, yet also potentiates ATRA responses (Kishi et al. 1998). As such, HT93 cultures are continuously supplemented with G-CSF in our experiments.

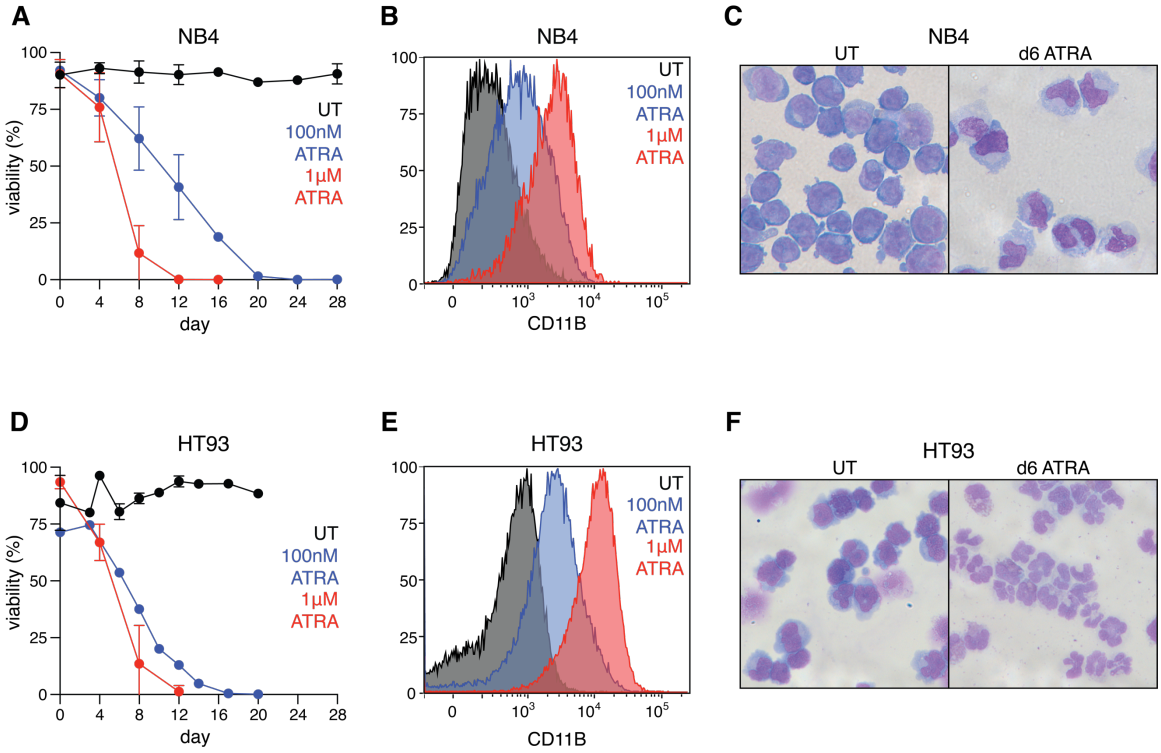

Figure 4.1: Administration of ATRA triggers myeloid differentiation and cell death in the human APL cell lines NB4 and HT93

(A) Viability of cultured NB4 cells untreated or treated with 100 nM or 1 µM ATRA. Mean ± SD of at least 3 independent experiments. (B) CD11B flow cytometry analysis of NB4 following 8 days untreated or ATRA-treated (100 nM and 1 µM). (C) Cytospins of NB4 following 6 days untreated or 1 µM ATRA treatment. (D) Viability of cultured HT93 untreated or treated with 100 nM or 1 µM ATRA. Mean ± SD of at least 3 independent experiments (untreated and 1µM ATRA only). The 100 nM ATRA-treated HT93 represent 1 experiment. (E) CD11B expression of HT93 after 8 days untreated, 100 nM or 1 µM ATRA treatment. (F) Cytospins of HT93 following 6 days untreated or 1 µM ATRA treatment.

4.3 De-differentiation of NB4 cells at a single cell level

The mouse model AML246 revealed that suppressing PU.1 in differentiated AML-derived cells could reverse maturation. To extend this to a human APL context, we examined whether differentiated NB4 cells could reacquire clonogenicity following the withdrawal of ATRA.

NB4 cells treated with ATRA rapidly upregulated immunophenotypic markers of differentiation, including the myeloid/neutrophil markers and mediators of adhesion/migration CD11B and CD15 (Figure 4.2A). As previously mentioned ATRA-induced changes in NB4 morphology can be subtle due to the absence of the characteristic segmented nucleus of neutrophils, however MGG staining revealed increased cytoplasm to nucleus ratio (Figure 4.1C, Figure 4.2A).

To investigate de-differentiation, NB4 cells were treated with ATRA for 4, 5, or 6 days, then $CD11B^+/CD15^+$ cells or viable untreated cells were sorted and plated into untreated or ATRA-treated methylcellulose to assess clonogenicity (Figure 4.2A). Untreated NB4 were particularly clonogenic with 50% of plated cells capable of forming a colony in untreated methylcellulose (Figure 4.2B). However, the clonogenicity of 4 days ATRA pre-treated cells reduced more than 10-fold in untreated methylcellulose (Figure 4.2B). Approximately 1% of mature NB4 cells were still capable of forming colonies even after 6 days of ATRA pre-treatment, indicating that de-differentiation is a rare but appreciable event (Figure 4.2B). Importantly, no colonies formed in methylcellulose supplemented with ATRA regardless of pre-treatment, verifying that clonogenicity was reliant on the withdrawal of the differentiation agent (Figure 4.2B).

Similar to AML246, the colonies arising from mature NB4 following ATRA withdrawal were significantly smaller than untreated cells regardless of how long they were pre-treated with ATRA, suggesting a lag time between therapy withdrawal and establishing proliferation (Figure 4.2C-D). Overall, these results indicated that withdrawal of ATRA in immunophenotypically mature, non-proliferative NB4 was sufficient to restore proliferation and survival in a minority of cells. As discussed in Chapter 1, PU.1 suppression is implicated in both PML-RARA oncogenesis and the therapeutic success of ATRA. A PU.1 immunoblot of NB4 cells following 6 days of ATRA and the subsequent 6 days ATRA withdrawal revealed striking correlation between the maturation state of the cells and PU.1 protein levels (Figure

4.2E). These results may suggest that both differentiation and de-differentiation of NB4 cells is driven by the modulation of PU.1.

Next, FACS index sorting was employed to validate de-differentiation at a single cell level by verifying immunophenotypic reversion of the resulting clones. As detailed in Chapter 3.3, FACS index sorting couples the immunophenotype of single sorted cells to their individual destination well of a 96-well plate, after which the potential for clonogenicity can be assessed and matched.

Extending ATRA treatment out to 8 days, samples from every second day were index sorted while recording their CD11B and CD15 profile. Untreated NB4 cells retained an efficient clonogenicity in the 96-well plate format, with 60% of the cells forming colonies (Figures 4.2F-G). Similar to ATRA-treated methylcellulose, ATRA in the destination wells of the 96-well plates prevented growth following all pre-treatment conditions (Figure 4.2F). Longer durations of ATRA treatment reduced the proportion of single cell clones emerging after ATRA withdrawal, however even after 8 days of ATRA treatment approximately 1% of cells retained clonogenic capacity (Figure 4.2F). Importantly, the clonogenic frequency of ATRA-treated NB4 was not impacted by the immunophenotypic profile of the cells, suggesting that differentiation markers of maturity could not adequately predict their clonogenic potential (Figures 4.2F-G). Furthermore, a representative clone derived from a $CD11B^{+}/CD15^{+}$ mature single cell had reverted back to an immature immunophenotype, yet retained ATRA sensitivity equivalent to an ATRA naïve NB4 clone (Figures 4.2G-H). Similar to the AML246 cell line, this result reinforces that AML maturation can be a plastic and reversible process.

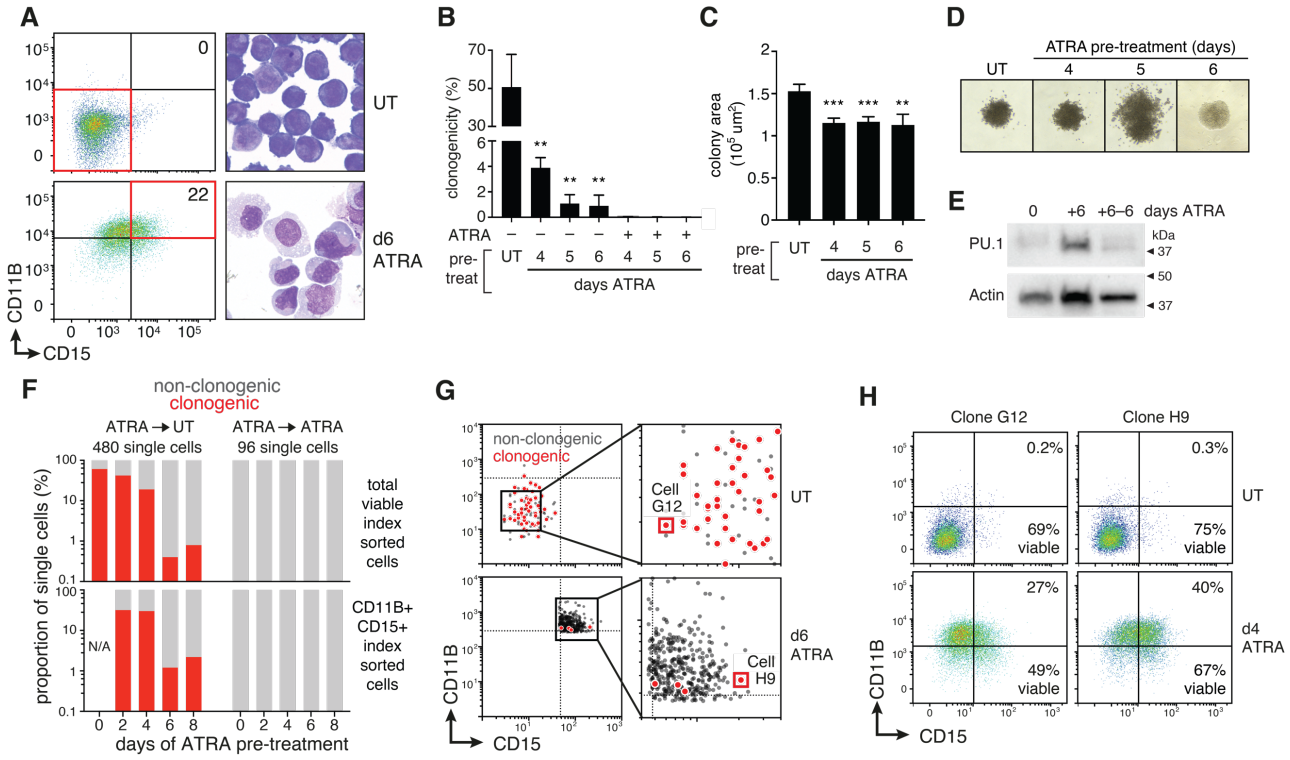

Figure 4.2: Cessation of ATRA-treatment is sufficient to drive de-differentiation at a single cell level in mature NB4

(A) CD11B/CD15 flow cytometry of untreated or 6 days ATRA-treated NB4 cells showing sort gates in red (left), and sorted cell morphology (right). (B) Methylcellulose colony frequency of 150 untreated NB4 cells, or 3750, 6000, or 12500 $CD11B^{HI}CD15^{HI}$ cells after 4, 5, or 6 days ATRA respectively, plated into untreated or ATRA-treated methylcellulose. Mean ± standard error of 2 independent experiments, each with duplicate plates for each condition. **$p < 0.01$ relative to untreated, Student's t test with Welch's correction. (C) Colony area for NB4 cells described in (B). Mean ± standard error of 2 independent experiments, each with duplicate plates for each condition. **$p < 0.01$, ***$p < 0.001$ relative to untreated, Student's t test with Welch's correction. (D) Representative colonies of NB4 after 11 days in ATRA-free methylcellulose. (E) PU.1 immunoblot of NB4 cells after 6 days of ATRA, and subsequent 6 days of ATRA withdrawal, with Actin loading control. (F) Clonogenic frequency (red) of single index-sorted NB4 cells following an ATRA time course, with total viable sorted cells (top) or $CD11B^{+}CD15^{+}$ cells (bottom) plated into ATRA-free (left) or ATRA (right) medium. Results from single experiment with multiple 96-well plate. (G) Surface CD11B and CD15 expression of individual untreated (top) or ATRA-treated (bottom) NB4 cells index-sorted into ATRA-free culture medium in multiwall plates, with subsequently clonogenic cells shown in red and non-clonogenic cells in black. (H) CD11B/CD15 flow cytometry of clones G12 and H9 derived from single cells shown in (G). Clones were expanded in ATRA-free medium and then ATRA-treated for 4 days before analysis.

4.4 *En masse* de-differentiation of HT93 cells upon ATRA withdrawal

Withdrawing ATRA from mature NB4 revealed a capacity for de-differentiation in human APL. However, like AML246 the cell line NB4 is deficient in the tumour suppressor TP53, which may influence maturational plasticity (Tschaharganeh et al. 2014). Therefore, we obtained the p53 proficient cell line HT93 to verify the potential for de-differentiation.

One of the most intriguing qualities of HT93 cells is their expression of the classical LSC marker CD34 (Bonnet and Dick 1997). Upon ATRA treatment of HT93, CD34 is downregulated as CD11B is upregulated (Figure 4.3A). In contrast to NB4, HT93 exhibit a remarkable neutrophil morphology following 6 days ATRA differentiation (Figure 4.3A).

Mimicking our previous experiments, viable untreated (mostly $CD11B^{-}/CD34^{+}$) and 6 day ATRA-treated mature ($CD11B^{+}/CD34^{-}$) HT93 were sorted and plated into untreated or ATRA-treated methylcellulose (Figure 4.3A). Unlike NB4 cells, only 10% of viable untreated HT93 cells were clonogenic (Figure 4.3B). Even so, 1% of sorted $CD11B^{+}/CD34^{-}$ mature cells from 6 day ATRA pre-treated cultures could still form colonies in untreated methylcellulose (Figure 4.3B). The colonies derived from mature HT93 were smaller although morphologically similar to their immature counterparts (Figure 4.3C). As with NB4 cells, ATRA maintenance prevented any further growth of secondary HT93 cultures (Figures 4.3B-C). Washing the remaining cells out of methylcellulose revealed that withdrawal of ATRA reverted HT93 cells to an immature morphology (Figure 4.3D). Curiously, despite the ATRA-treated methylcellulose preventing colony formation, some viable $CD11B^{+}/CD34^{-}$cells with neutrophilic morphology remained suggesting that these mature APL-derived granulocytes can persist without proliferation for some time under these conditions (Figure 4.3D-E).

Single cell sorting was not well tolerated by HT93 cells, therefore we could not address de-differentiation at a single cell level. Rather, de-differentiation was analysed at regular intervals in bulk cultures to discern the homogeneity of immunophenotypic reversion. HT93 cells were treated with ATRA for 6 days and thereafter treatment was either maintained or withdrawn. In the cells maintained on ATRA, the culture had a complete loss of culture viability within 12 days (Figure 4.3F). In contrast, viability improved 4 days after day 6 ATRA withdrawal, demonstrating a rapid recovery of mature HT93 upon therapy cessation (Figure 4.3F). As with NB4, PU.1 protein in HT93 also correlates with ATRA treatment, further suggesting the

potential control of AML maturation (Figure 4.3G). However, some PU.1 protein lingered 6 days after withdrawal hinting at mechanistic differences in PU.1 regulation between NB4 and HT93 cells (Figure 4.3G).

In addition to CD11B and CD15, ATRA-induced HT93 cell maturation was assessed by the expression of the monocyte and neutrophil marker FCGR3 (CD16). Following 6 days of ATRA therapy HT93 exhibited high expression of CD11B, along with moderate CD15 and CD16 expression (Figures 4.3H-I). Continued treatment for 6 more days maintained CD11B expression and further increased CD15 and CD16 (Figures 4.3H-I). Conversely, withdrawal of ATRA at day 6 revealed a synchronous incremental reduction in CD11B, CD15, and CD16 levels over days 8, 10, and 12 (Figures 4.3H-I). Although not analysed at a single cell level, ATRA withdrawal resulted in a population-wide homogenous response in HT93 cells, consistent with *en masse* de-differentiation. The use of HT93 has verified that de-differentiation is possible in p53 proficient cells, and further demonstrated that differentiation therapy induced APL plasticity is a conserved phenomenon.

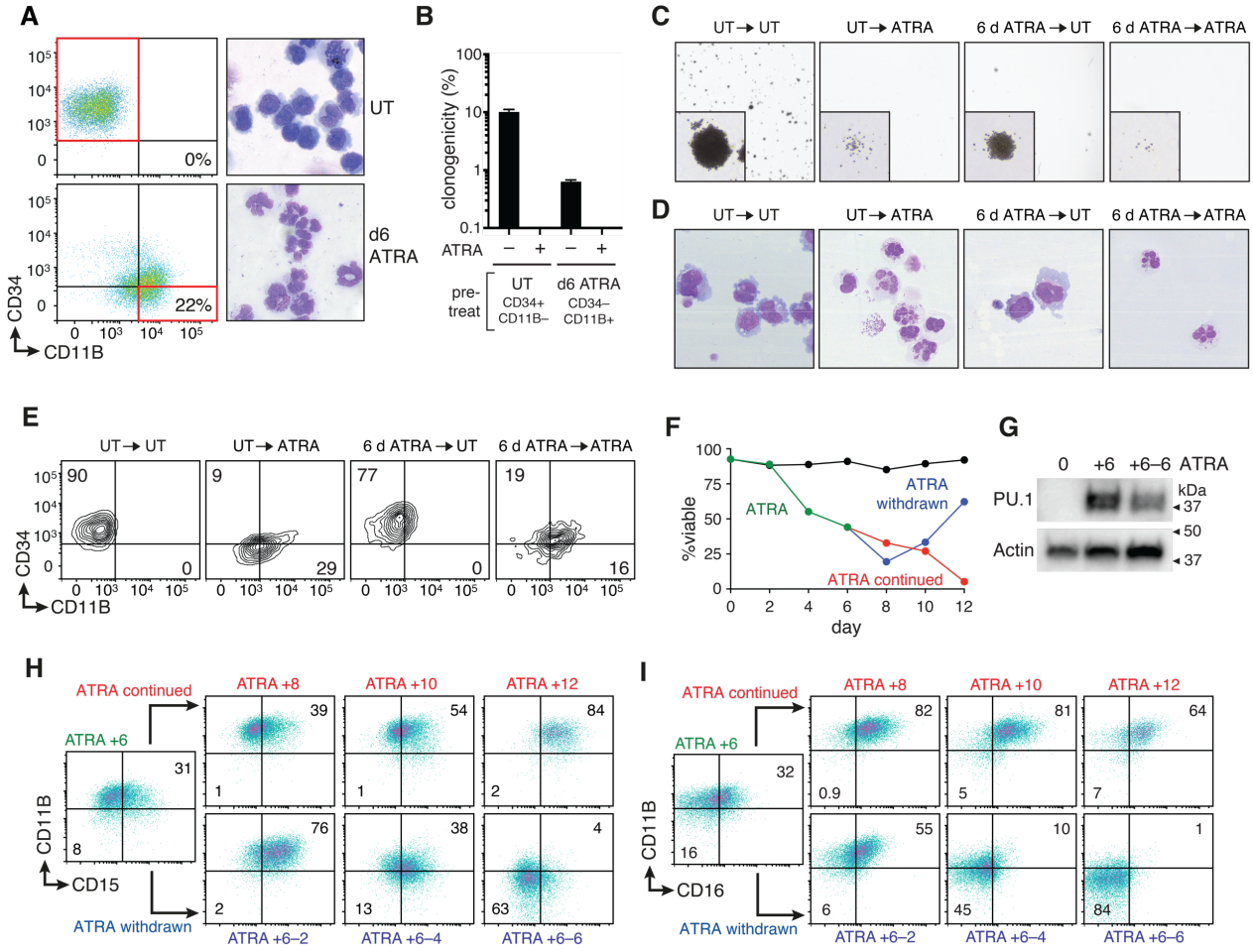

Figure 4.3: HT93 reacquires the leukaemia stem cell marker CD34 following ATRA withdrawal

(A) CD11B/CD34 flow cytometry of HT93 cells showing sort gates in red (left; $CD11B^-/CD34^+$ for untreated; $CD11B^+/CD34^-$ for ATRA) and MGG stained cytospins of sorted cells (right). (B) Clonogenic frequency of sorted HT93 cells from (A) in methylcellulose with or without ATRA as indicated and imaged 19 days later. Mean ± SEM of 3 plates per condition, from one of two similar experiments. (C) HT93 methylcellulose colony morphology with individual colony insets. (D) MGG stained cytospins and (E) CD11B/CD34 profiles for corresponding cells washed out from methylcellulose. (F) Viability of HT93 cultures comparing untreated (black) to 6 days ATRA treatment (green) followed by 6 days of either ATRA continuation (red) or withdrawal (blue). Results represent singleton data. (G) PU.1 immunoblot of HT93 cells after 6 days of ATRA, and subsequent 6 days of ATRA withdrawal, with actin loading control. CD11B/CD15 (H) and CD11B/CD16 (I) profiles of HT93 cells described in (F) showing response to initial ATRA treatment and subsequent continuation (red) or withdrawal (blue).

4.5 *In vitro* culture and differentiation of human primary APL samples

APL presents as an aggressive disease in patients, and prior to the introduction of ATRA resulted in a median survival of under one week (Coombs, Tavakkoli, and Tallman 2015). Even so, primary APL samples rarely engraft in mouse xenotransplants and are notoriously difficult to culture *in vitro*. To examine maturational plasticity in primary human APL, 6 frozen bone marrow samples derived from APL patients comprising ~90% of blasts were evaluated by Giovanna Pomilio from Professor Andrew Wei's Group at the Australian Centre for Blood Diseases (ACBD). These primary samples were cultured in media optimised for haematopoietic stem cell growth, supplemented with the stem cell and myeloid cytokines IL-3, SCF, GM-CSF, and EPO. Two of six primary samples remained viable and modestly proliferative for several weeks in these culture conditions, hereafter termed APL1 and APL3 (Figure 4.4A). These cultures were obtained for further investigation.

Approximately one week after thawing of the original cryopreserved patient samples, primary APL cells were treated with ATRA for 7 days to investigate ex vivo differentiation. Based on the high blast counts, initial experiments were performed under the assumption that the majority of cells were APL derived (Figure 4.4A). In bulk cytospins, APL1 appeared to undergo monocytic differentiation while APL3 more closely resembled neutrophils (Figures 4.4B-C). To further validate differentiation of the APL fraction of the samples, ATRA responses were compared to healthy CD34+ isolated haematopoietic cells. Flow cytometry revealed that a large proportion of the untreated cultures were $CD11B^{mid}/CD15^{mid}$, likely to be APL cells based on blast counts (Figure 4.4A, D). Following 7 days of ATRA treatment, no response was observed in wild type cells whereas a sizable fraction of the APL1 and APL3 cultures upregulated CD11B, indicating that this ATRA-sensitive population is likely to be the APL cells (Figure 4.4D). Despite survival in liquid culture, primary APL cells did not fare well in methylcellulose, with samples regardless of treatment overwhelmed by a rapid expansion of apparently foamy macrophages likely due to the outgrowth of residual non-AML monocytes from the original sample (Figure 4.4E). Furthermore, multiple attempts at enrichment of the APL from the primary samples using cell sorting only led to loss of proliferation and survival.

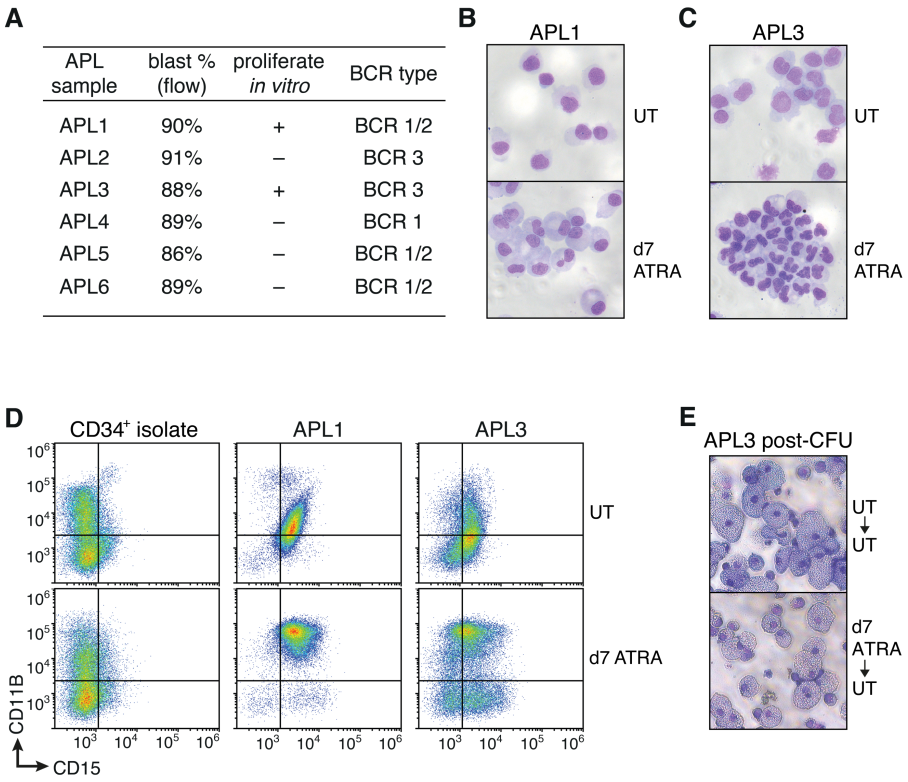

Figure 4.4: Human APL primaries can be transiently grown and differentiated with ATRA in culture

(A) List of APL primary samples thawed, with diagnosis blast counts, BCR isoforms, and whether or not they can be cultured *in vitro*. MGG cytospins of the primary patient samples APL1 (B) and APL3 (C) after 7 days untreated or 1 µM ATRA-treated. (D) CD11B/CD15 flow cytometry of APL1, APL3, and $CD34^+$ isolated bone marrow cells cultured for 7 days untreated or 1 µM ATRA. (E) MGG cytospins of APL3 recovered from untreated methylcellulose, following 7 days untreated or 1 µM ATRA before viability (untreated) or $CD11B^+/CD15^+$ (ATRA) sorting.

4.6 Immunophenotypic plasticity in primary APL samples

The arduous nature of culturing primary APL samples was reminiscent of experiences with the APL cell line HT93, hence further investigation of de-differentiation was performed by observing bulk changes in unsorted cells to keep any disturbance to a minimum. Due to a larger reserve of cryopreserved sample vials, experiments were restricted to APL3.

Primary APL3 cells were cultured with ATRA for 4 days then ATRA was either maintained or ceased. Within the first 4 days of treatment ATRA had minimal influence on growth, and cells continued to proliferate thereafter whether or not treatment was withdrawn (Figure 4.5A). Concurrent fluorescence in situ hybridization (FISH) for t(15;17) performed by Dr. Meg Wall at the Victorian Clinical Genetics Services revealed that the proliferation in these cultures was mostly due to the outgrowth of non-APL cells (Figure 4.5B). Conversely, growth in the untreated culture plateaued after 4 days, although the percentage of cells harbouring t(15;17) as assessed by FISH remained high (Figures 4.5A-B).

Immunophenotypic analysis revealed that untreated APL3 remained $CD11B^{-}/CD15^{low/mid}$ across the time course (Figure 4.5C). However, 4 days of ATRA treatment drove a marked increase in CD11B expression, with the culture evenly split between $CD15^{+}$ and $CD15^{-}$ (Figure 4.5C). In cultures maintained on ATRA, the double positive fraction of cells diminished over time, replaced by rapid outgrowth of a new $CD11B^{-}/CD15^{+}$ population (Figure 4.5C). Coupled with FISH analysis, this indicates a dilution of APL cells by the contaminant cells (Figures 4.5B-C). Strikingly, in the culture withdrawn from ATRA the $CD11B^{+}/CD15^{+}$ cells showed a migration through a $CD11B^{mid}/CD15^{mid}$ stage and back to $CD11B^{low}/CD15^{-}$, consistent with de-differentiation of the population of t(15;17) positive APL cells (Figure 4.5B-C). The distinction between ATRA maintenance and withdrawal indicate that immunophenotypic maturation is reversible in primary APL. It remains to be confirmed that this population is certainly APL via sorting and t(15;17) FISH. The assay does not demonstrate restoration of leukaemic proliferation, possibly impacted by the difficulty in culturing primary APL. Therefore, leukaemic propagation/self-renewal from mature APL remains to be determined and will form the basis of future experiments.

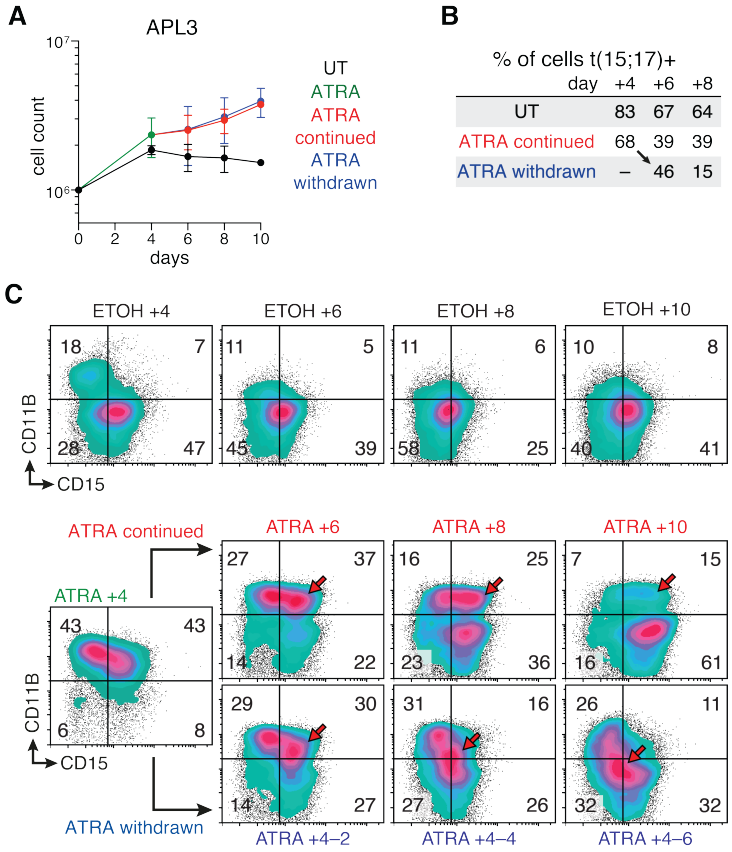

Figure 4.5: Ceasing ATRA-treatment induces immunophenotypic reversion in a human APL primary sample

(A) Proliferation of APL3 cells comparing untreated (black) or 4 days 1uM ATRA (green) followed by ATRA continuation (red) or ATRA withdrawal (blue). Results from 2 independent experiments, with error bars representing max/min values. (B) Percentage of $t(15;17)^{+}$ APL3 cells as assessed by FISH from an independent ATRA withdrawal experiment. (C) CD11B/CD15 flow cytometry for APL3 treated with untreated (black) or 1uM ATRA for 4 days (green), followed by ATRA maintenance (red) or ATRA withdrawal (blue). Red arrow indicates $CD11B^{+}CD15^{+}$ population of interest that reverts to $CD11B^{-}CD15^{-}$ following ATRA withdrawal.

4.7 Discussion and Conclusion

This Chapter expands upon the observation that maturational plasticity occurs in a mouse model of AML differentiation, exploring the concept in human APL maturation following treatment with the therapeutic differentiation agent ATRA. Following withdrawal of ATRA, mature APL cells underwent immunophenotypic and morphologic de-differentiation, restoring both clonogenicity and viability. This was recapitulated in both human APL cell lines *in vitro* and primary patient samples *ex vivo*. The reversibility of therapy-induced maturation has implications for all AML differentiation therapies, and impacts how we consider the role of immature leukaemia stem cells (LSCs) in intratumoural heterogeneity.

4.7.1 Maturational plasticity challenges the Leukaemic Stem Cell model

It has been proposed that leukaemia is arranged in a hierarchical manner similar to standard haematopoiesis, with LSCs at the apex of the hierarchy giving rise to more differentiated bulk leukaemia cells in a unidirectional manner. Based on early AML xenotransplantation assays, it was believed that a rare population of immature LSCs propagate the leukaemia, giving rise to a more mature cancer bulk that itself is not capable of sustaining the tumour (Bonnet and Dick 1997). This fraction of LSCs could be defined purely through the immunophenotypic markers $CD34^{+}/CD38^{-}$, however further investigation uncovered a host of additional markers including CD25, CD32, CD96, CD123, and TIM3 (Ding, Gao, and Zhang 2017). With the discovery of a rare stem cell like population in glioma, the LSC model has been expanded to phenotypically heterogeneous solid cancers maintained by a cancer stem cell (CSC) (Ignatova et al. 2002; Ayob and Ramasamy 2018). The concept has driven extensive investigation of methods to selectively target and ablate CSCs, without which the tumour cannot sustain itself (Shibata and Hoque 2019). However, as of yet there are no effective LSC-targeting therapies in clinical use (Pollyea and Jordan 2017).

In direct contrast with the LSC model, which assumes unidirectional differentiation, we demonstrate by immunophenotypic, mechanistic, transcriptomic, and morphologic measures that mature and non-proliferative AML-derived cells can harbour latent leukaemic potential through de-differentiation. Our results illustrate an avenue by which the differentiated bulk can contribute to tumour progression, indicating that immunophenotype alone is insufficient to determine leukaemic potential. Our experiments support other findings that contradict the LSC model, where refinement of xenotransplantation assays have shown the capacity for mature

leukaemic cells to not only engraft, but also reconstitute the entire heterogeneous leukaemic tumour (Sarry et al. 2011). Furthermore, de-differentiation has been described in solid tumours, whereby models of colorectal cancer have shown mature cells replenishing the immature fraction following the selective ablation of the CSC (de Sousa e Melo et al. 2017; Shimokawa et al. 2017).

The present observation of maturational plasticity is in some part limited by the use of only one molecular subtype of AML, however we intend in future to examine de-differentiation in models of AML responsive to the more novel differentiation agents such as the inhibitors of FLT3 and mutant IDH1/IDH2.

4.7.2 Intratumoural maturational heterogeneity in AML

The data presented in Chapter 4 reveal maturational plasticity in APL cells with addition and withdrawal of ATRA, which as discussed further in Chapter 5 is dependent in-part through PU.1 perturbation. PU.1 expression is modulated by numerous myeloid cytokines and recurrent AML mutations (Mossadegh-Keller et al. 2013; Vangala et al. 2003; Mueller et al. 2006; Huang et al. 2008; Gu et al. 2018). Therefore, the frequent perturbation of PU.1 in AML may be in part responsible for the intratumoural spectrum of immature and mature leukaemic cells through fluctuation of PU.1 repression. Importantly, the resulting phenotypic variability within a tumour may be a factor influencing sensitivity to certain therapeutic agents. For instance, it has been proposed that quiescent LSC have a survival advantage over their more proliferative progeny following genotoxic chemotherapy (Ishikawa et al. 2007). However, our data suggest the intriguing possibility that the most mature and non-dividing cells may also evade chemotherapy and seed relapse through de-differentiation.

Future studies beyond the scope of this PhD may address these questions by evaluating responses to genotoxic chemotherapeutic agents in an ATRA sensitive APL cell line through a range of ATRA-induced differentiation states.

4.7.3 Persistent and mature AML-derived cells may seed relapse via de-differentiation

As illustrated in both APL cell lines and primary samples, cessation of ATRA treatment is sufficient to reverse differentiation of mature cells, separating the link between immaturity and tumour progression.

Historically, the transitory remissions by ATRA monotherapy has been attributed to the continued survival of immature and therapy-resistant LSCs (Zheng et al. 2007). However, the absence of relapse resistance mutations in matched diagnosis samples suggests that resistance emerges following a successful response to the therapy (Marasca et al. 1999; Fasan et al. 2017). Our data proposes that persistent and mature AML-derived cells may be an avenue of relapse through the acquisition of these resistance mutations and subsequent reversion.

Curiously, while maturation state reversion was apparent following acute withdrawal of ATRA in our experiments, in APL patients relapse can occur many years after therapy has been discontinued (Sakurai et al. 2018). These circumstances may point to means of survival independent of ATRA-resistance, however late relapses can also harbour ATRA-resistance mutations in PML-RARA (Gallagher et al. 2006). One possible explanation is that ATRA-resistance mutations can independently promote persistence of leukaemia cells without driving reversion, and an additional transformative event might sometimes be required to fully restore leukaemogenicity.

It may be of worth in future to investigate whether spontaneous acquisition of PML-RARA resistance mutations in mature APL cells can overcome sustained ATRA treatment, linking together the concepts of resistance and relapse to reversion. While one could inducibly overexpress a version of PML-RARA harbouring an ATRA-resistance mutation in ATRA-treated APL cells, overexpression systems may not adequately represent the endogenous levels of oncoprotein found in APL necessary for the differentiation block without ablating PU.1. Circumventing this, in the future we intend to utilise the CRISPR/Cas9 system to introduce random mutations into the ligand binding domain of PML-RARA in mature APL pre-treated with ATRA. The acquisition of any ATRA-resistance mutations in mature APL may subsequently allow reversion.

This process of de-differentiation has important implications in the use and development of novel differentiation agents in the treatment of AML. These include the mutant IDH1 and IDH2 inhibitors ivosidenib and enasidenib, the FLT3 inhibitors quizartinib and gilteritinib, and the HDAC inhibitor panobinostat in AML1-ETO leukaemia, all of which have shown differentiating effects capable of inducing deep remission in patients and AML mouse models (Stein et al. 2017; DiNardo et al. 2018; Sexauer et al. 2012; Bots et al. 2014; Salmon et al.

2015). Furthermore, early trials with the nuclear export inhibitor selinexor have shown limited differentiation effects in AML harbouring NPM1c (Garzon et al. 2017). Unfortunately, similar to ATRA monotherapy, while these novel differentiating agents induce remission it is often transient, with relapses frequently arising from clones that have acquired resistance mutations in the target oncogene (Intlekofer et al. 2018; Lehmann-Che et al. 2018). Although these therapies are capable of restoring myeloid differentiation, our results suggest that without complete clearance of the entire mature population, cells may persist and act as a source of relapse through de-differentiation. However, relapse in these cases may also derive from persistent immature leukaemic cells reacquiring proliferative potential, especially in the context of treatments with a limited duration of therapy therefore requiring further investigation.

4.7.4 Differentiation lineage may influence persistence and relapse

ATRA therapy typically induces differentiation of APL cells overwhelmingly into the neutrophilic lineage. It is generally accepted that the NB4 and HT93 cell lines also undergo ATRA-induced neutrophilic differentiation. However, it is possible for APL to mature into other myeloid lineages, including monocytes or eosinophils (Naeem et al. 2006; Riccioni et al. 2003; Yamamoto et al. 2007). This was apparent in one of the APL primary samples investigated, with ATRA triggering robust morphological differentiation into monocyte-like cells. In addition, some APLs may harbour the potential for multilineage differentiation, with lineage choice influenced by cytokine signalling or alternative differentiation agents (Kishi et al. 1998; Jensen et al. 2015).

Other AML-derived mature lineages may be much more long-lived compared to neutrophils, with certain monocyte-derived macrophages capable of persisting for life (Patel et al. 2017). This raises the intriguing possibility that lineage may influence the likelihood of AML-derived cells to persist following differentiation therapy, potentially impacting the probability of relapse through de-differentiation. Both very late relapse and extra-medullary relapse in APL is associated with monocytic differentiation, owing to the long life-span of monocytes and the capacity to extravasate into tissues and become macrophages (Watts et al. 2016). These correlations would not occur without the mature fraction of cells in some way influencing leukaemic progression, further supporting the idea of mature cells seeding relapse through reversion.

4.7.5 Terminal differentiation

The efficacy of differentiation therapies is dependent on AML cells reaching a 'point of no-return', otherwise known as terminal differentiation, beyond which a cell permanently leaves the cell cycle. In the myeloid lineage, this is driven in part through an auto-regulatory loop of lengthened cell cycles resulting in accumulated PU.1, which further lengthens cell division (Kueh et al. 2013). Although we observed immunophenotypically mature AML cells reacquiring clonogenicity, this does not suggest there is no state of terminal differentiation. Rather, the point of no return may be further down the stream of differentiation than previously appreciated. Notably, in both the AML246 and NB4 index-sorting reversion experiments, longer pre-treatments prior to the withdrawal of Dox or ATRA decreased the frequency of cells reacquiring clonogenicity. The diminishing frequency implies a greater proportion of cells could be locked into a terminal fate.

4.7.6 Conclusion

In conclusion, this Chapter demonstrates that immunophenotypically and morphologically mature APL cells can revert to an immature state through cessation of differentiation therapy, after which they reacquire the ability to proliferate. This was achieved in both human APL cell lines *in vitro* and primary patient samples *ex vivo*, indicating that maturation plasticity by addition and withdrawal of ATRA is conserved in APL.

CHAPTER 5. Generating models of inducible PU.1 restoration in human APL

5.1 Introduction

As reviewed in Chapter 1, PU.1 dysfunction is a hallmark of AML development. Although rarely mutated itself, its function is impeded by several recurrent mutually exclusive class II mutations, including the APL oncoprotein PML-RARA which binds and interferes with PU.1 transcription (Mueller et al. 2006; Wang et al. 2010; Zhu et al. 2012). Upon treatment with the ATRA, PU.1 protein is upregulated and function is restored, in part contributing to restored differentiation (Mueller et al. 2006). However, the influence of PU.1 suppression versus the other oncogenic functions of PML-RARA in APL pathogenesis remains ill-defined. Furthermore, the relative contribution of PU.1 restoration, PML-RARA degradation, and retinoic acid receptor signalling in ATRA efficacy is incompletely understood.

This Chapter focuses on the generation of novel human AML models driven by reversible PU.1 knockdown to address these questions. Furthermore, these models can be used to replicate the results of Chapter 3 in a human context.

5.2 PU.1 knockdown in NB4 confers resistance to ATRA

It has previously been reported that transient PU.1 knockdown with siRNA dampened ATRA-induced differentiation responses in APL cells at early time points (Mueller et al. 2006). However, whether sustained downregulation of PU.1 can confer a permanent differentiation block in ATRA-treated APL remains unclear. To explore this possibility, NB4 cells were transduced with constitutively expressed retroviral mCherry-linked miR-E shRNA targeting PU.1 (PU.1.885 or PU.1.1384) or the control Renilla Luciferase shRNA (Ren.713) in the LENC construct, resulting in heterogeneous cultures of infected mCherry^{+} and uninfected mCherry^{-} cells (Figure 5.1A) (Fellmann et al. 2013). Following 3 days of culture recovery, cells were plated treated with ATRA (Figure 5.1B).

To first verify knockdown, quantitative real time PCR (qRT-PCR) was used to measure PU.1 transcript in mCherry^{-} and mCherry^{+} sorted cells 4 days after ATRA treatment (Figure 5.1C). In the untransduced mCherry^{-} cells of each culture, ATRA reproducibly increased PU.1 transcript (Figure 5.1C). In mCherry^{+} sorted cells, PU.1 expression was unaffected by the expression of the Ren.713 control shRNA, however transcript was repressed to near-undetectable levels by both PU.1 shRNAs indicating strong on-target suppression (Figure 5.1C).

Flow cytometry was employed to track changes in viability, mCherry, and expression of differentiation markers. ATRA treatment of the Ren.713-transduced culture revealed the typical loss of viability seen in NB4 cells (Figure 5.1D). After an initial drop in viability, representing the death of uninfected NB4 cells, cultures transduced with PU.1.885 and PU.1.1384 recovered soon after ATRA treatment with viability equal to that of the untreated cells (Figure 5.1D). Proliferation similarly was maintained in these cultures (data not shown). This demonstrated for the first time that PU.1 knockdown maintains the NB4 differentiation block indefinitely in the presence of the ATRA.

From the outset, all three shRNA were transduced to approximately 50% of the starting culture (Figures 5.1E-F). Over time, the proportion of Ren.713-expressing mCherry^{+} cells did not change regardless of treatment conditions (Figures 5.1E-F). However, as both PU.1.885 and PU.1.1384 protected from ATRA, the proportion of mCherry^{+} cells rose to 60-80% of the culture (Figures 5.1E-F). Curiously, neither PU.1 shRNA culture was 100% mCherry^{+},

possibly revealing a disconnect between expression of the reporter and the shRNA, or a novel adaptation of the mCherry$^-$ NB4 cells conferring survival (Figures 5.1E-F). Interestingly, PU.1 knockdown in the absence of ATRA was not well tolerated by NB4, with the mCherry$^+$ fraction of cells lost over time (Figures 5.1E-F). This reflects the degree of PU.1 suppression but not ablation required to support AML growth and survival without terminating cell viability (Rosenbauer et al. 2004).

Immunophenotypic analysis revealed that PU.1 knockdown dulled the induction of the differentiation markers CD11B and CD15 (Figure 5.1G). Although difficult to determine which shRNA was stronger from qRT-PCR, PU.1.885 more greatly repressed the expression of CD11B and CD15 (Figures 5.1C, G), therefore PU.1.855 became the focus of further experiments. Regardless, both shRNAs behaved relatively similarly, giving confidence that the phenotypic effects are the result of PU.1 knockdown rather than off-target effects.

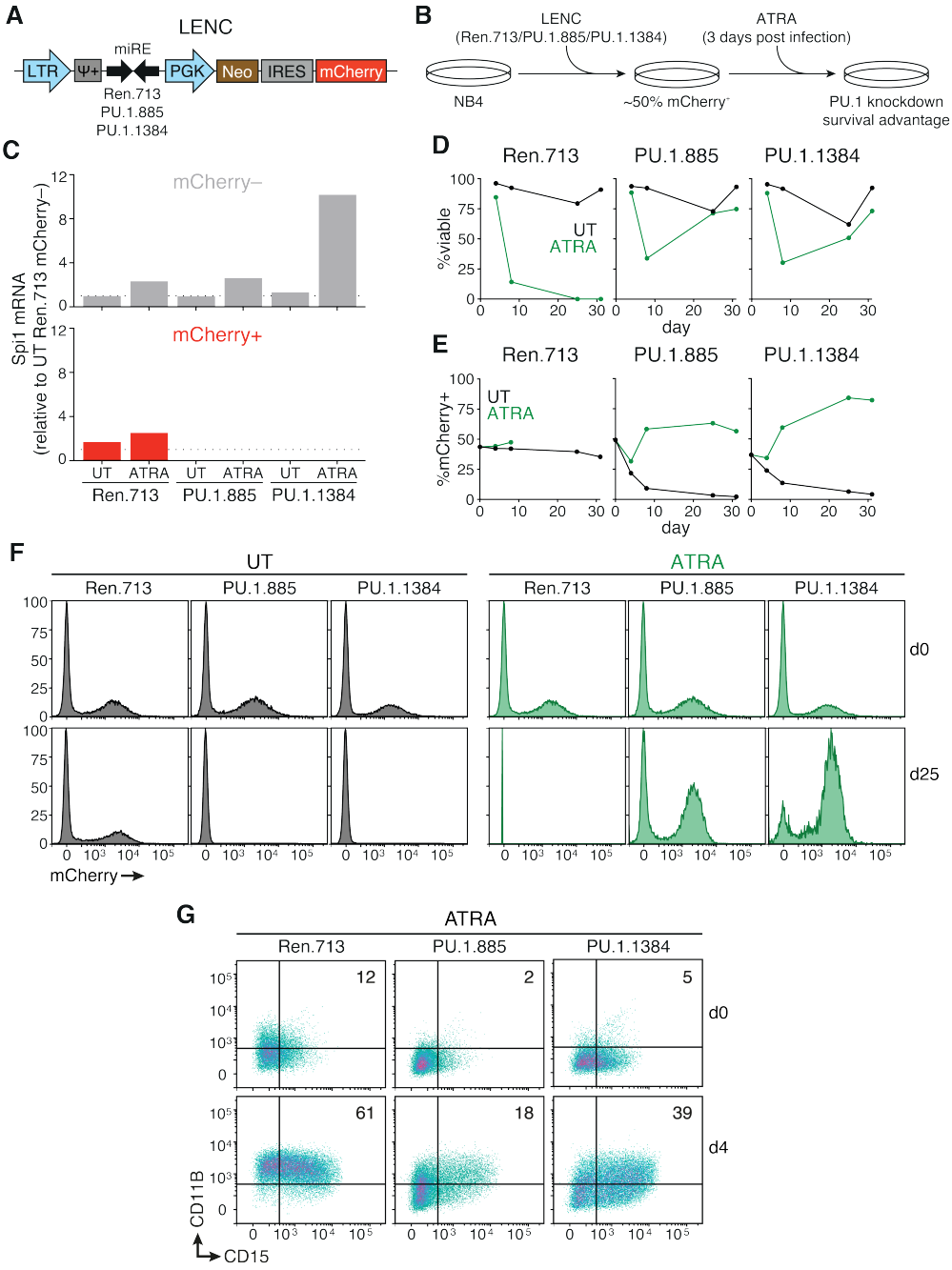

Figure 5.1: PU.1 knockdown in NB4 cells is sufficient to block ATRA differentiation
(A) LENC vector map for constitutive expression of shRNAs with mCherry reporter. (B) Strategy for assessing ATRA survival advantage by PU.1 knockdown. (C) Spi1 (PU.1) mRNA qRT of mCherry positive and negative LENC Ren.713, PU.1.885, and PU.1.1384 infected NB4 cells after 4 days untreated or ATRA treatment. (D) Viability of the NB4 cells infected with LENC Ren.713 (negative control), PU.1.885, and PU.1.1384 untreated (black) or ATRA-treated (green). (E) Percentage of mCherry positive cells. Results from D and E represent singleton data. (F) Flow cytometry of mCherry expression on days 0 and 25 of treatment. (G) CD11B/CD15 flow cytometry of the LENC Ren.713, PU.1.885, and PU.1.1384 mCherry^{+}-gated cells on days 0 and 4 of ATRA.

5.3 Lentiviral tet-on shRNAs targeting PU.1 tightly control PU.1 knockdown

The stable expression of PU.1.885 and PU.1.1384 revealed that PU.1 suppression alone sustained APL survival following ATRA administration. However, the system did not provide the opportunity to inducibly restore human PU.1 in a manner possible in our mouse model AML246 in Chapter 1.

NB4 cells were transduced with the miR-E shRNA Ren.713 or PU.1.885 in the LT3-GEPIR construct (Figure 5.2A). LT3-GEPIR is a lentiviral vector with that expresses a GFP-linked shRNA under the control of the TRE3G promoter. Concurrently, the vector stably expresses rtTA3 and puromycin resistance. Normally dormant, rtTA3 will only bind the TRE3G promoter in the presence of Dox, initiating transcription of the GFP-linked shRNA (tet-on) (Figure 5.2A). Next, cells were treated with the antibiotic puromycin for 7 days for selection.

To verify successful PU.1 knockdown with the LT3-GEPIR construct, Ren.713 and PU.1.885 expressing NB4 cells were subjected to simultaneous treatment of Dox and ATRA. Approximately 60% of cells expressed GFP indicating antibiotic selection only partially enriched for expression of LT3-GEPIR transduced cells, and these GFP^+ cells were sorted and processed for PU.1 immunoblots. As expected from acute Dox treatment, the inducible PU.1 shRNA strongly reduced but did not ablate levels of PU.1 protein in the presence of ATRA, affirming results previously seen by qRT-PCR (Figures 5.1F, 5.2B). Conversely, both parental uninfected and Ren.713 transduced NB4 robustly upregulated PU.1 protein upon ATRA treatment (Figure 5.2B).

To verify whether reversing the PU.1 knockdown in ATRA-treated NB4 can restore the differentiation process, Ren.713 and PU.1.885 transduced cells were subjected to Dox, ATRA, or the combination of treatments. Treatment with Dox rapidly induced GFP expression though there was minimal impact on total culture viability (Figures 5.2C-D). PU.1.885 transduced cells gradually lost GFP expression over time, again revealing the selection pressure of PU.1 suppression (Figure 5.2D). However, Ren.713-expressing GFP^+ cells gradually increased from 60% to 80% of the culture (Figure 5.2D). While unexpected, this may have been due to lingering effects of the puromycin selection. Interestingly, PU.1 knockdown suppressed the basal expression of CD11B, implying that the minimal CD11B expression in untreated NB4 cells is driven by a low but present PU.1 activity in the immature myeloid blasts (Figures 5.2F).

In the absence of Dox, both Ren.713 and PU.1.885 transduced cultures responded to ATRA similar to that of parental NB4, emphasising the lack of leakiness of the PU.1.885 shRNA in the LT3-GEPIR construct (Figure 5.2C-D). However, concurrent Dox-treatment eventually lead to the outgrowth of viable GFP^+ PU.1.885-expressing cells while eradicating the Ren.713 culture (Figures 5.2C-D). Remarkably, although 50% of the culture expressed the PU.1.885 shRNA following acute Dox-treatment, only a small fraction of viable cells lingered after 12 days of ATRA treatment (Figures 5.2C-D). Furthermore, the culture remained stagnant for another 12 days before a drawn-out period of recovery and growth (Figures 5.2C). Over time, this culture stabilised close to 100% GFP^+ implying complete dependence on the knockdown of PU.1 (Figure 5.2D). Dox-induced expression of PU.1.885 dulled the ATRA-induction of CD11B, with the differentiation marker eventually settling to the basal levels seen in the untreated cells (Figures 5.2E-F). This may represent a process of adaptation and stabilisation to an optimal level of PU.1 suppression, and thus maturation state, to maintain APL growth and survival with ATRA.

Overall, these results further support that PU.1 suppression alone can drive ATRA resistance, however the process is dependent on the selection for an optimal degree of PU.1 knockdown.

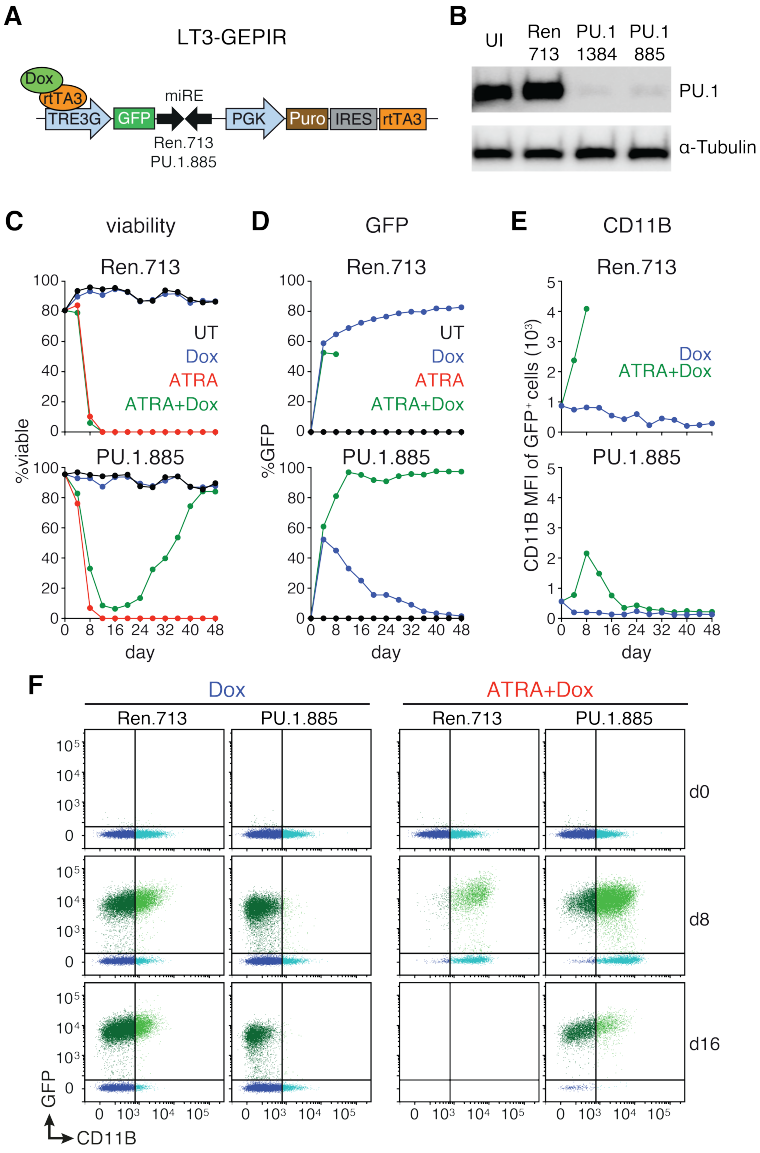

Figure 5.2: Inducible PU.1 knockdown provides stable ATRA resistance
(A) LT3-GEPIR vector map for all-in-one tetON expression of a GFP-linked shRNA (Ren.713 or PU.1.885). (B) PU.1 immunoblot of uninfected NB4 (UI) treated for 4 days with ATRA, and GFP positive NB4 transduced with LT3-GEPIR Ren.713, PU.1.885, or PU.1.1384 after 4 days of ATRA and Dox treatment. (C) Viability of NB4 cells infected with LT3-GEPIR Ren.713 or PU.1.885 in untreated (black), Dox (blue), ATRA (red), or ATRA+Dox (green) treated culture. (D) Percentage of GFP positive cells untreated or ATRA-treated with or without Dox. (E) GFP/CD11B flow cytometry of Ren.713 (left) and PU.1.885 (right) cells over 16 days untreated or ATRA-treated with Dox. (F) CD11B MFI over time of Ren.713 and PU.1.855 cells untreated or ATRA-treated with Dox. All results represent singleton data.

5.4 ATRA-adapted NB4 cell lines differentiate upon PU.1 restoration

The long-term treatment of NB4 cells expressing tet-on PU.1.885 with ATRA and Dox resulted in a new model for testing the conditional restoration of endogenous PU.1. In these cells, Dox provides the PU.1 shRNA which sustains a state of low PU.1 expression, whereas ATRA restrains the activity of PML-RARA (Figure 5.3A). This reveals a delicate balance in NB4 cells whereby PU.1 knockdown is required for cells to tolerate ATRA, and only with ATRA can cells tolerate PU.1 knockdown. By withdrawing ATRA and/or Dox, the individual components maintaining the viability and differentiation state of the cells can be explored.

In the combined ATRA and Dox-treated state, the cells remain 100% GFP^+ and harbour a middling CD11B expression reminiscent of the untreated parental NB4 cells, however they also display a slightly lower viability than parental NB4 (Figures 5.3B-D). This implies subtle differences between normal NB4 cells that have a PML-RARA driven differentiation block, and these ATRA-treated cells maintained through PU.1 knockdown.

ATRA and Dox were withdrawn individually or together from the cells. ATRA withdrawal caused a gradual loss in viability and basal CD11B, mimicking upfront PU.1 knockdown in untreated NB4 (Figures 5.3B, D). Possibly owing to the non-functional p53 in NB4, there was a prompt adaptation and a GFP^- population emerged signalling the deletion of the shRNA construct by some manner (Figures 5.3C, E). However, the ~40% of cells maintaining GFP expression suggest that there may be various methods of adaptation (Figures 5.3C, E). These results demonstrated that ATRA withdrawal restored PML-RARA protein and thereby increased PU.1 suppression to a degree lethal to myeloid blasts (Figure 5.3A, F).

In contrast, withdrawal of Dox caused a rapid loss of GFP (Figure 5.3C). Loss of the PU.1 shRNA restored PU.1 protein, triggering myeloid differentiation and cell death (Figures 5.3B, D, F). This verifies that, with ATRA treatment, the suppression of PU.1 needs to be maintained indefinitely to sustain the differentiation block (Figure 5.3A). Whereas AML246 was generated using a tet-off vector and differentiate with Dox, here endogenous PU.1 expression was restored through the withdrawal of Dox (tet-on). Nevertheless, this provides a model system for inducibly restoring the endogenous expression of PU.1 in human AML cells, triggering differentiation. However, a fraction of cells remained viable 24 days after PU.1 restoration, suggesting that there is an avenue of adaptation for continued survival on ATRA (Figure 5.3B).

This may be due to prolonged ATRA treatment causing a loss of sensitivity to the normal retinoic acid signalling pathways, dulling ATRA-induced cell death.

Finally, withdrawal of both ATRA and Dox from the cells resulted in a remarkable regression to the parental state without major changes to PU.1 protein (Figures 5.3A-D, F). The enriched viability and stabilisation of CD11B expression further exemplified the plasticity of the AML differentiation block, and the interchangeability between PU.1 knockdown alone versus active PML-RARA fusion oncoprotein.

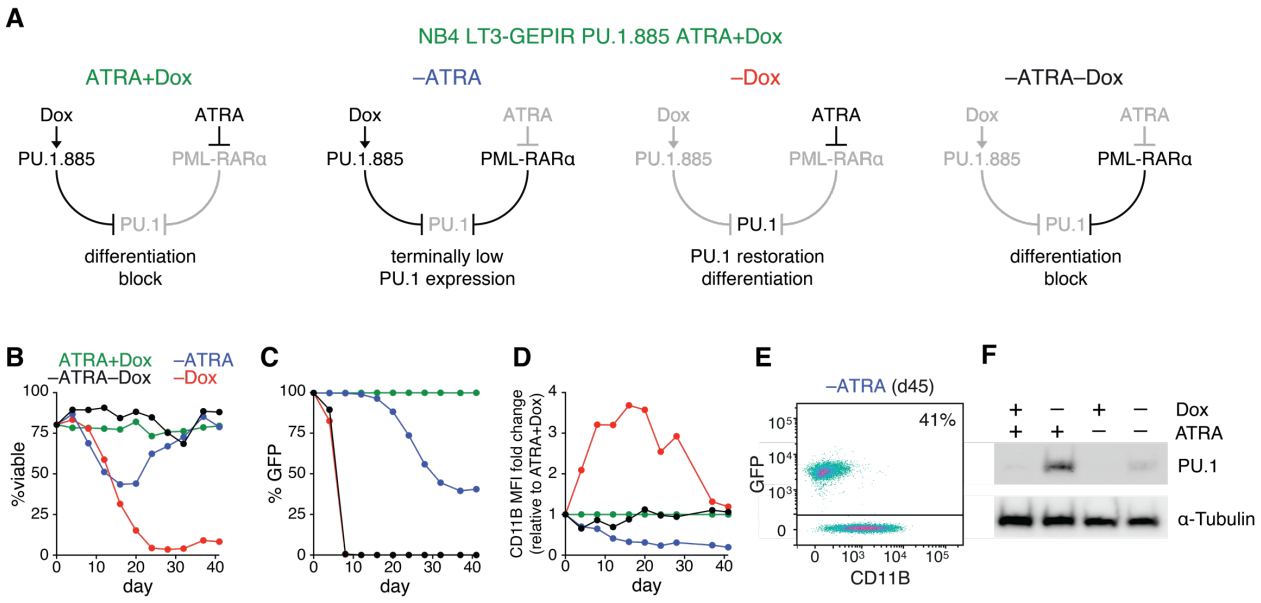

Figure 5.3: PU.1 restoration alone drives differentiation in a human AML cell line
(A) Schematic for the functions of both ATRA and Dox in maintaining the PU.1-knockdown dependent differentiation block. (B) Viability of NB4 LT3-GEPIR PU.1.885 on ATRA and Dox after maintaining treatment (ATRA+Dox; green), withdrawing ATRA (–ATRA; blue), withdrawing Dox (–Dox; red), or withdrawing both (–ATRA–Dox; black). (C and D) Percentage GFP positive cells (C) and CD11B MFI (D) of cultures described in (B). (E) GFP/CD11B flow cytometry of –ATRA cells at day 45. (F) PU.1 immunoblot of LT3-GEPIR PU.1.885 cells on long term ATRA and Dox treatment, 4 days after withdrawal of ATRA and/or Dox. This membrane and image capture is shared with the immunoblot featured in Figure 5.2B. All results represent singleton data.

5.5 PU.1 knockdown is sufficient to revert mature ATRA-treated APL

In §5.3 we demonstrated that PU.1 knockdown can protect cells from ATRA-induced differentiation when Dox and ATRA are added simultaneously. As it has been established that mature NB4 revert to an immature state when ATRA is withdrawn, we sought to further investigate de-differentiation by suppressing PU.1 in NB4 that have already undergone ATRA-induced differentiation.

To verify whether PU.1 knockdown alone was sufficient to reverse ATRA maturation, the NB4 cells transduced with LT3-GEPIR Ren.713 or PU.1.885 were treated with 100nM ATRA, rather than the 1μM normally used, to draw out the differentiation process. During ATRA treatment, the cells were treated with Dox either concurrently with ATRA, or starting at 4 day intervals (days 4, 8, 12).

Regardless of when Dox was added, inducing control Ren.713 shRNA expression did not impact the ATRA response (Figures 5.4A-B). Remarkably, not only did PU.1.885 protect from simultaneous treatment with ATRA, Dox-induced PU.1 knockdown rescued cells even after 12 days of ATRA-induced differentiation (Figures 5.4A-B). There is a lag period before recovery however, as viability continues a downward trajectory for 4 days following Dox addition (Figure 5.4A). Dox treatment triggers an immediate and striking effect on immunophenotype, with reduction of CD11B evident within 4 days and a return to its basal levels after 8 days (Figure 5.4C).

These observations further validate the maturational plasticity of APL cells, however they also uncovered the interesting result that PU.1 suppression alone can drive reversion of mature NB4 cells despite continuous ATRA treatment. This could have implications for the appearance of *de novo* mutations during relapse following differentiation therapy, where the acquisition of any PU.1-repressing genetic lesions may be sufficient to re-initiate leukaemogenicity.

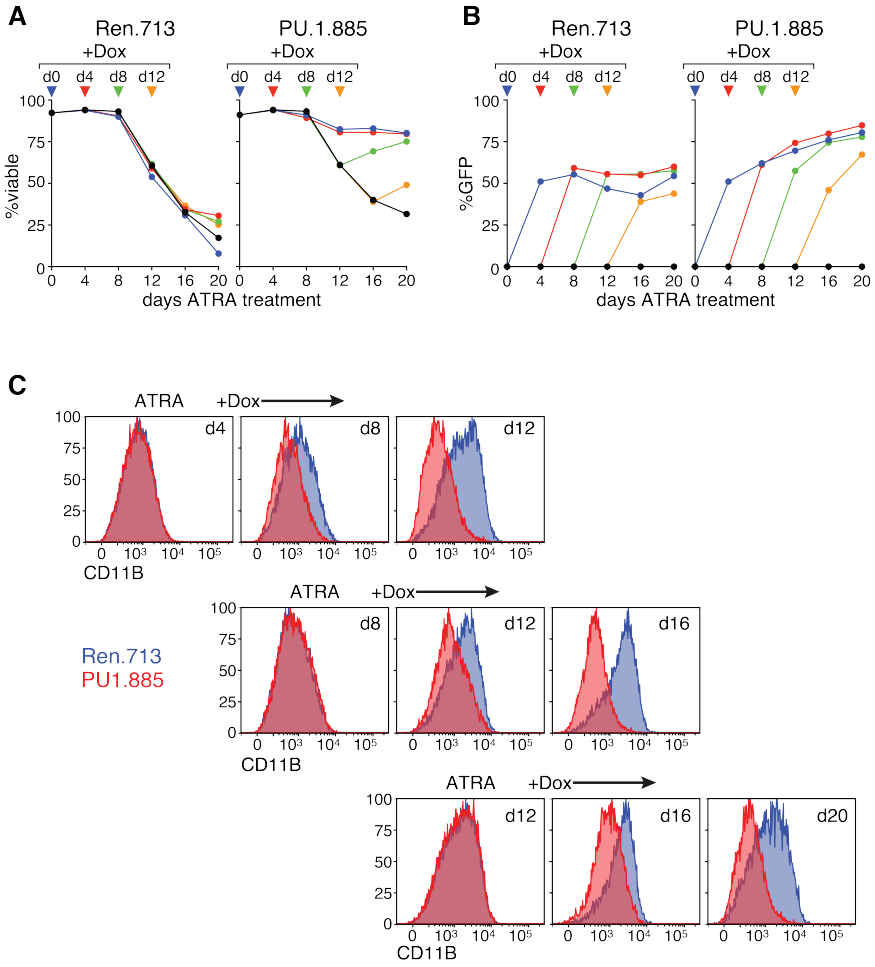

Figure 5.4: PU.1 knockdown in mature ATRA-treated APL restores leukaemogenicity through reversion

(A) Viability for NB4 LT3-GEPIR Ren.713 (left) and PU.1.885 (right) on 100nM ATRA, without (black) or with the addition of Dox on days 0 (blue), 4 (red), 8 (green), and 12 (orange) as indicated by the arrows. (B) The percentage of GFP positive cells from (A). (C) CD11B flow cytometry of GFP positive Ren.713 (blue) and PU.1.885 (red) cells on days 4, 8, and 12 days ATRA (top to bottom, left) before the addition of Dox and the subsequent 8 days (to the right of each graph). All results represent singleton data.

5.6 PU.1 expression does not impact ATO responses in NB4

As detailed in Chapter 1, frontline therapy for APL includes arsenic trioxide (ATO) in conjunction with ATRA (Tallman and Altman 2009). Interestingly, the effects of ATO are two-fold and appear to manifest in a concentration-dependent manner, with lower concentrations inducing a differentiation response, and higher concentrations inducing apoptosis (Miller et al. 2002). To interrogate whether PU.1 knockdown influences responses to ATO, the NB4 LT3-GEPIR cell lines expressing either Ren.713 or PU.1.885 were subjected to a range of ATO concentrations between 200-1000nM with or without Dox.

After 16 days of treatment with ATO, NB4 cell death increased in a concentration dependent manner (Figure 5.5A). However, Dox-induced PU.1 knockdown did not provide any survival advantage at any concentration of ATO (Figure 5.5A). Rather, Dox treatment lowered viability at higher concentrations of ATO, likely an off-target toxicity as this occurred in both PU.1.885 and the Ren.713 control (Figure 5.5A). There was also no apparent induction of the marker CD11B with low concentration ATO, suggesting limited capacity to measure differentiation in this assay (data not shown). The irrelevance of PU.1 suppression could be a potential factor in the high efficacy and deep remission following monotherapy ATO compared to ATRA (Niu et al. 1999).

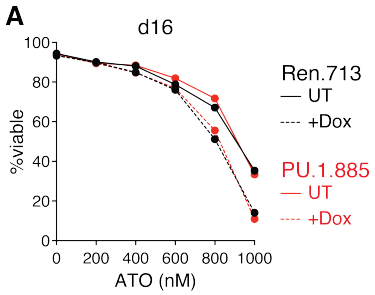

Figure 5.5: PU.1 knockdown does not impact ATO responses
(A) Viability for NB4 LT3-GEPIR Ren.713 (black) and PU.1.885 (red) on day 16 of treatment ranging from 0-1000nM of ATO either without (solid line) or with (dotted line) Dox. Results represent singleton data.

5.7 CRISPR/Cas9-mediated deletion of PML-RARA in NB4

As demonstrated in §5.4, we developed a human model cell line with selective PU.1 restoration using tet-on PU.1 knockdown and ATRA. However, maintaining a state of PML-RARA suppression was a practical hassle due to the labile nature of ATRA in culture. Additionally, constant retinoic acid signalling may also have had an under-appreciated influence on the state of the cells. Therefore, we set out to generate another NB4 model with inducible PU.1 knockdown using CRISPR/Cas9 for the genetic deletion of PML-RARA.

To accomplish this, NB4 were transduced in precise order with four vectors, two for CRISPR/Cas9 deletion of PML-RARA, and two for the tet-off expression of PU.1.885 with GFP (Figure 5.6A). NB4 cells were co-infected with the vector expressing Cas9 with puromycin resistance (Cas9-puro) and the vector for TRE3G GFP-linked PU.1.885 with neomycin resistance (LT3-GEN), then treated with puromycin and neomycin together to select for co-expression of the vectors (Figures 5.6A, C). In the absence of a tetracycline-responsive transactivator, the TRE3G promoter was silent and the cells were GFP^{-}. Furthermore, without short guide RNA (sgRNA), the Cas9 was inactive.

After selection, these cells were co-infected with two more vectors. The first encoded for tTA (MSCV-tTA) allowing tet-off control of PU.1.885 (Figures 5.6A, C). Secondly, the cells received the sgRNA vector (sgETN) harbouring one of three sgRNA (sgCtrl for a scramble control, or sgPML1/sgPML2 targeting exon 2 of both PML and PML-RARA) with Thy1.1 as a reporter (Figures 5.6A-C). As the PML-RARA break point cluster region (BCR) in NB4 resides in an intron, a sgRNA could not be designed that selectively targeted PML-RARA without also targeting the untranslocated PML allele.

The second round of infections resulted in a heterogeneous mix of GFP and Thy1.1 positivity in three distinct cultures, expressing PU.1 knockdown in conjunction with either sgCtrl, sgPML1, or sgPML2 (Figure 5.6D). The relative proportions of the four populations (GFP^{-} /$Thy1.1^{-}$ uninfected cells, GFP^{+} PU.1.885 expressing cells, $Thy1.1^{+}$ sgRNA expressing cells, and GFP^{+}/$Thy1.1^{+}$ co-expressing cells) were tracked over time to identify selective pressures.

Compared to the uninfected cells, the $Thy1.1^{+}$ sgPML1 and sgPML2 cells were negatively selected whereas the proportion of sgCtrl-expressing cells had did not change, indicating that

the PML/PML-RARA-targeting sgRNA were exerting some phenotypic effect (Figures 5.6D-E). Similarly, the proportion of GFP^+ PU.1.885 expressing cells diminished relative to the uninfected cells indicating selection against excessive PU.1 suppression (Figures 5.6D-E).

Crucially, in GFP^+/$Thy1.1^+$ cells expressing both shRNA and sgRNA, PU.1 knockdown was tolerated better with sgPML1 and sgPML2 compared to the sgCtrl scramble control (Figure 5.6E). This implied that PU.1 knockdown aided the survival of cells in the culture that harboured PML-RARA mutations, or that PML-RARA deletion allowed the cells to tolerate PU.1 shRNA.

Interestingly, $Thy1.1^+$ sgPML1 and sgPML2 transduced cells did not upregulate the differentiation marker CD11B, whereas CD15 induction was apparent (Figures 5.6F-G). This effect upon CD15 was reproducibly observed in 6/7 guides tested targeting exons 1-6 of PML/PML-RARA (not shown). Although CD11B induction is the typical ATRA-induced differentiation response, the upregulation of CD15 suggested partial immunophenotypic differentiation from PML-RARA deletion, and this response was moderately reduced by PU.1 knockdown (Figure 5.6G).

During the characterisation of the co-transduced NB4 culture, single cell clones were generated from the GFP^+/$Thy1.1^+$ populations of the sgPML1 and sgPML2 cultures for further examination (Figures 5.6C-D).

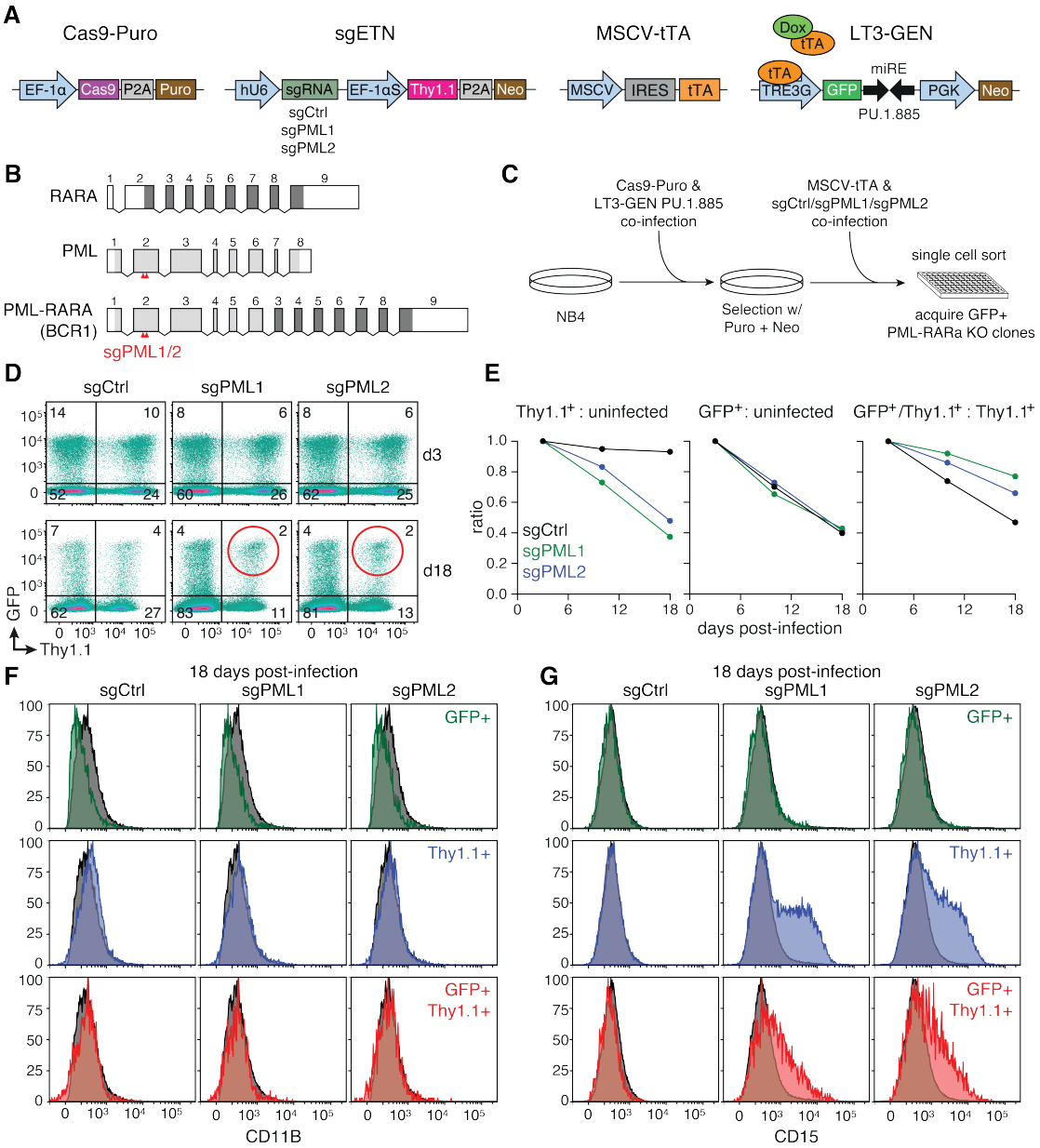

Figure 5.6: Generation of PML-RARA knockout, PU.1 shRNA dependent cell lines using CRISPR-Cas9

(A) Vector maps for constitutive expression of Cas9, TRE3G inducible GFP-linked PU.1.885 shRNA, constitutive tTA expression, and constitutive sgRNA (control, and two PML-targeted guides) with Thy1.1 as a reporter. (B) Gene structure of PML, RARA, and PML-RARA. (C) Strategy for generating ΔPML-RARA clones of NB4 expressing the inducible PU.1 shRNA. (D) Thy1.1/GFP flow cytometry of sgCtrl, sgPML1, and sgPML2 infected NB4, each harbouring Cas9, LT3-GEN PU.1.885, and MSCV-tTA after 3 and 18 days post-infection. Red circle indicates population of interest. (E) Changes in the relative proportional ratio of $Thy1.1^+$ or GFP^+ cells in comparison to uninfected on the left and middle graphs respectively, and the ratio of $GFP^+/Thy1.1^+$ to $Thy1.1^+$ on the right, for cultures infected with sgCtrl (black), sgPML1 (green), and sgPML2 (blue). CD11B (F) and CD15 (G) flow cytometry of the co-infected cells with sgCtrl, sgPML1, and sgPML2. $GFP^+/Thy1.1^+$ in red, GFP^+ in green, $Thy1.1^+$ in blue, uninfected in black.

5.8 Characterising PML-RARA-null clones of NB4

Following single cell sorting, clones were screened for expression of sgPML (Thy1.1) and tet-off PU.1 knockdown (GFP expression). Two clones were identified, termed NB4Δ1 and NB4Δ2. NB4Δ1 was derived from cells infected with sgPML1 and homogenously expressed a high level of GFP (Figure 5.7A). In contrast, NB4Δ2 was generated with sgPML2 and featured a lower GFP expression along with a sizable GFP^- tail (Figure 5.7A).

To verify CRISPR/Cas9-mediated PML-RARA deletion, it was necessary to sequence the sgRNA target site. For this reason, primers were designed to span the translocation region. One pair spanning from exon 1 to exon 8 of PML, the other exon 1 of PML to exon 7 of RARA, allowing for the selective amplification of PML and PML-RARA sequences (Figure 5.7B). Primers resulting in large amplicons from start to finish of PML-RARA were designed to account for the possibility of alternative splicing variants. RNA from both NB4Δ1 and NB4Δ2 was harvested and cDNA was PCR amplified for sequencing. It must be noted that NB4 harbour trisomy of chromosome 15 resulting in one translocated copy of PML-RARA, and two untranslocated PML alleles (Mozziconacci et al. 2002). PCR amplification resulted in bands of various sizes in both parental and knockout clone NB4 cells, however only the bands of the predicted size produced viable sequences. Following Sanger sequencing, the primer pair spanning PML-RARA for both NB4Δ1 and NB4Δ2 produced clean reads, whereas the primer pair for PML resulted in reads representing two different alleles near the sgRNA target site (double peaks). Through careful alignment of the double peak reads to a reference cDNA sequence, the sequences for each PML allele could be determined (Figure 5.7C).

In NB4Δ1 cells, PML-RARA harboured a deletion of 4 base pairs, whereas the PML alleles exhibited deletions of 1 or 11 base pairs, all of which result in frameshifts and premature stop codons (Figure 5.7C). These mutations were likely deleterious for all alleles concerned.

On the other hand, NB4Δ2 displayed a deletion of 16 base pairs in one allele of PML causing a frameshift and premature stop, while the other PML allele as well as the fusion PML-RARA showed identical deletions of 15 base pairs resulting in a 5 amino acid in-frame deletion (Figure 5.7D). The PML-RARA protein encoded by this allele may retain some ability to suppress PU.1 through an otherwise unchanged RARA moiety, potentially explaining the lower GFP expression of the clone through decreased reliance on PU.1 knockdown (Figure 5.7A). It

remains to be determined in both NB4Δ1 and NB4Δ2 whether or not any mutant PML-RARA protein is present, as such this is to be confirmed via a RARA immunoblot in future.

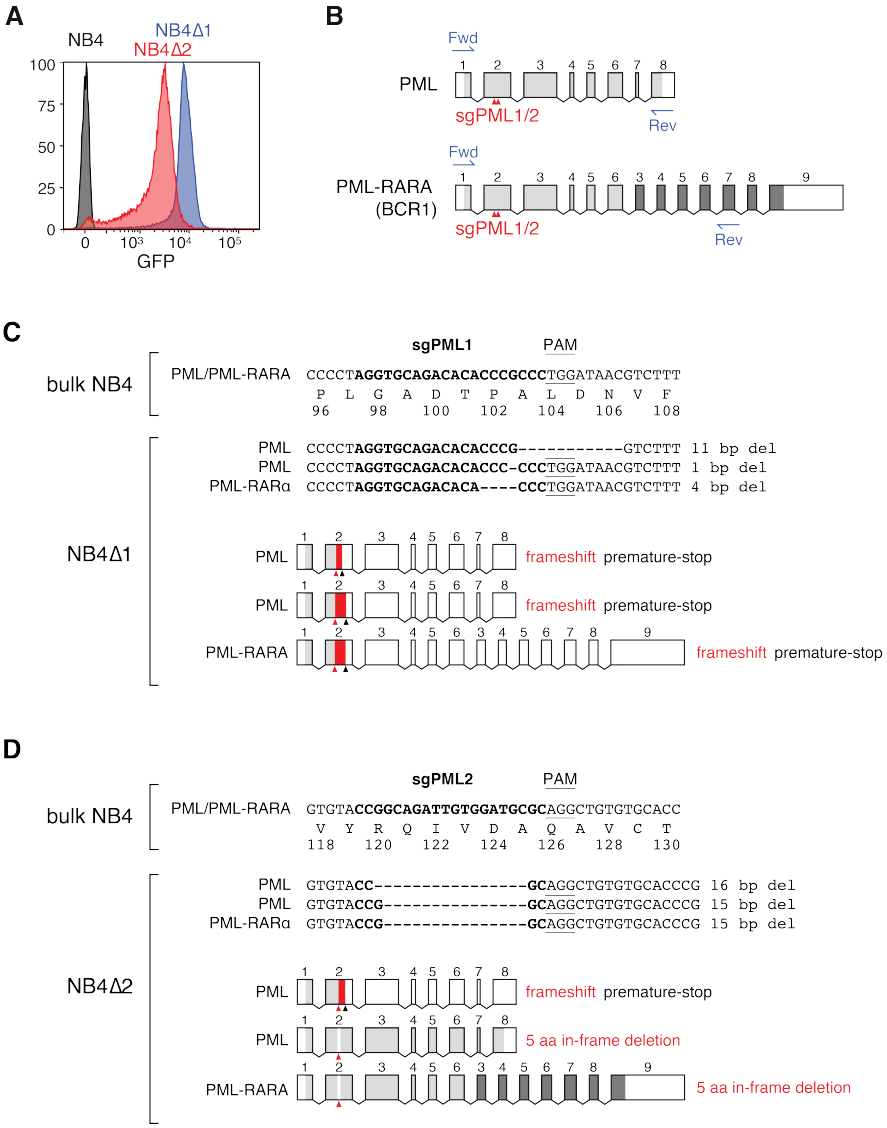

Figure 5.7: NB4 clones can tolerate PU.1 knockdown following deletion of both endogenous PML-RARa and PML

(A) GFP flow cytometry of NB4Δ1 (blue) and NB4Δ2 (red), with NB4 parental control (black). (B) Schematic of primers (blue) for the individual sequencing of the untranslocated PML and PML-RARA separately. (C and D) DNA sequencing results and functional consequences for PML and PML-RARA in NB4Δ1 (C) and NB4Δ2 (D).

5.9 Both PU.1 restoration and ATRA independently drive NB4Δ1 differentiation

Although the status of PML-RARA in NB4Δ2 is ambiguous, NB4Δ1 is likely PML-RARA-null. To assess whether the differentiation block is maintained by PU.1 knockdown, both clones were subjected to Dox. As the PU.1 shRNA is under the control of tet-off system, addition of Dox represses GFP and thus shRNA expression. In parallel, they were treated with 100nM ATRA, or a combination of ATRA plus Dox, to determine whether the PML-RARA-independent effects of ATRA can impact differentiation, and if these responses compound.

Administration of Dox to NB4Δ1 repressed GFP as anticipated and led to a gradual loss in viability (Figure 5.8A). This occurred in conjunction with a faint increase in CD11B, and a more apparent upregulation of CD15 (Figure 5.8B). This demonstrated a mild but homogeneous differentiation response in NB4Δ1 through restoration of endogenous human PU.1. Additionally, unlike the LT3-GEPIR system described in §5.3 above, this was achieved without maintaining ATRA treatment. Hence this more closely resembled the AML246 model system outlined in Chapter 3, where Dox treatment simply restores PU.1 expression and triggers AML differentiation.

Interestingly, a slightly stronger differentiation response was observed following treatment with 100nM of ATRA alone (Figures 5.8A-B). Although the PU.1 shRNA remained expressed in this context as indicated by continued GFP expression, it seems that ATRA may engage normal retinoic acid signalling mechanisms to override PU.1 suppression to a degree sufficient for myeloid differentiation. Therefore, it remains to be determined whether PU.1 protein increases with ATRA in NB4Δ1. Interestingly, the effects of ATRA were more pronounced in conjunction with Dox, indicating that a robust differentiation response in this clone is dependent on both PML-RARA independent effects of ATRA, as well as the full restoration of endogenous PU.1 expression (Figures 5.8A-B). Additionally, the increasing impact upon viability corresponded to the degree of CD11B induction, however CD15 upregulation was more apparent with PU.1 restoration alone than with ATRA which may imply alternative differentiation responses or pathways (Figures 5.8A-B).

In contrast, NB4Δ2 did not appear to undergo Dox-induced differentiation (Figure 5.8C). Despite complete repression of GFP, there was little impact on viability or the expression of

differentiation markers (Figures 5.8C-D). Importantly, where CD15 upregulation was apparent in bulk sgPML transduced cells, NB4Δ2 remained $CD15^{-}$ upon Dox administration (Figure 5.8D). However, the cells, especially the GFP^{-} tail, remained sensitive to ATRA-induced differentiation (Figures 5.8C-D). Interestingly, the response to ATRA was enhanced with Dox indicating that the PU.1 shRNA, although not maintaining the differentiation block, is functional enough to slightly impede ATRA responses (Figures 5.8C-D). Altogether, the data suggests that the in-frame deletion within the NB4Δ2 PML-RARA may not impede its differentiation-blocking function, such that survival of this clone remains independent of PU.1 knockdown. This is consistent with weaker shRNA-linked GFP expression in NB4Δ2 relative to NB4Δ1.

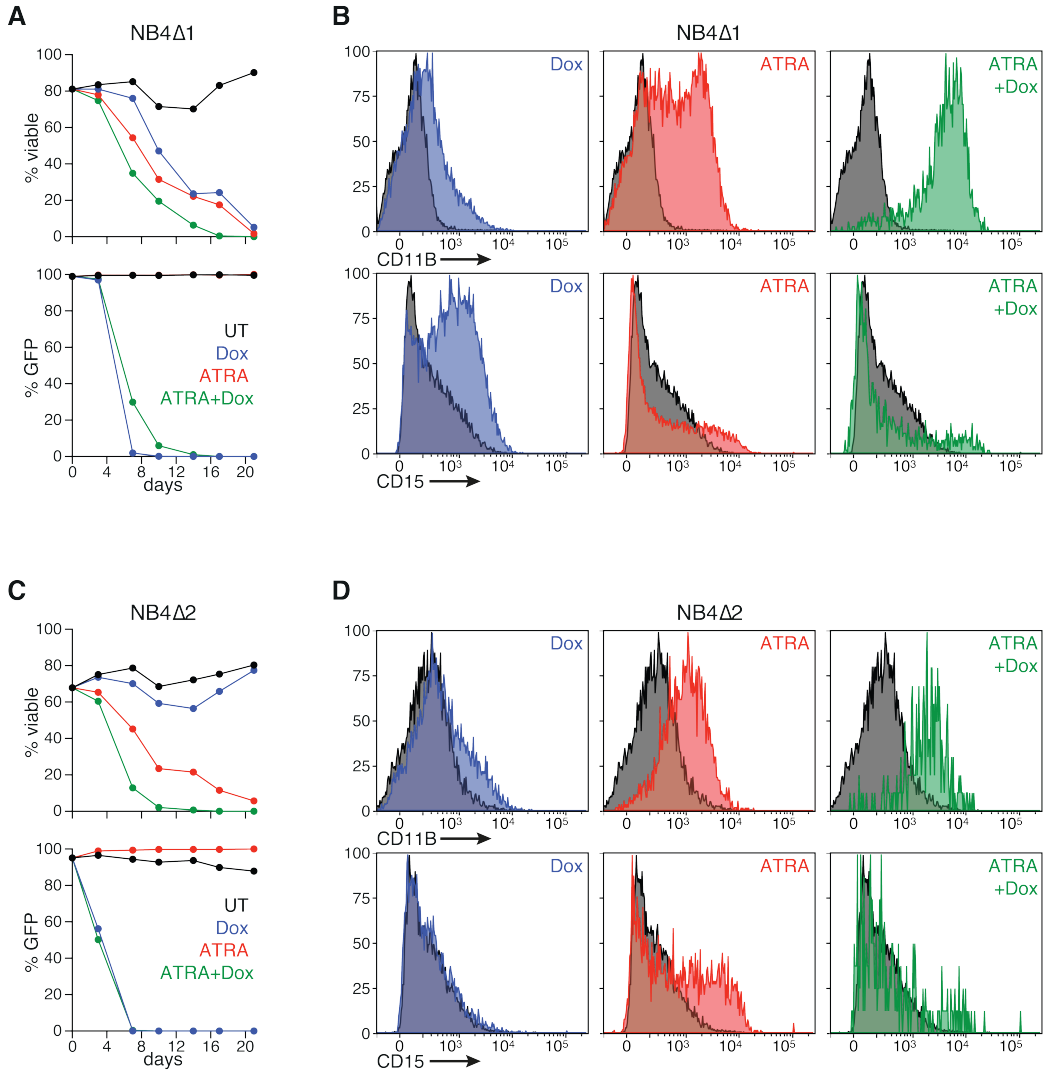

Figure 5.8: NB4Δ1 maturation through both the restoration of PU.1 and PML-RARA-independent effects of ATRA

(A) Viability and GFP% of NB4Δ1 of untreated (black), Dox (blue), 100nM ATRA (red) or 100nM ATRA with Dox (green). (B) CD11B and CD15 flow cytometry of NB4Δ1 after 7 days of culture with treatments described in (A). Viability (C) and CD11B/CD15 flow cytometry (D) of NB4Δ2 treated as in (A) and (B). Results represent singleton data.

5.10 Discussion and Conclusion

APL remains the ideal example of a successful differentiation therapy to be emulated in the treatment of other AML subtypes. In this Chapter, we developed and characterised human model cell lines based on NB4 that separated aspects of APL biology, integrating inducible PU.1 knockdown, CRISPR/Cas9, and ATRA to allow for further investigation into the interplay between PML-RARA, PU.1, RARA and ATRA.

5.10.1 PU.1 knockdown can block ATRA-induced differentiation

In this Chapter, we utilised both stable and inducible PU.1 knockdown to block ATRA-induced differentiation of NB4 cells. This was achieved using two independent PU.1 targeting shRNAs and ATRA concentrations similar to therapeutic levels (0.1-1μM) (Adamson 1996). It has previously been reported that transient PU.1 suppression can blunt ATRA differentiation, however this is the first time that PU.1 knockdown has been shown to maintain the immature state indefinitely.

In addition to PU.1 restoration, ATRA also activates retinoic acid receptor signalling and re-establishes PML nuclear bodies (de The and Chen 2010; Takitani et al. 2003; Mueller et al. 2006). Our results revealed that these were not sufficient to trigger NB4 differentiation in the context of PU.1 knockdown. RARA exerts a differentiation effect through upregulation of OCT-1 and CEBPB, regulators of PU.1 (Mueller et al. 2006). Thus, knockdown of PU.1 blocks downstream signalling of RARA. Moreover, NB4 are a p53 deficient APL cell line, and the therapeutic effect of PML nuclear body restoration may depend on p53. Therefore, PU.1 suppression represents a fundamental aspect of NB4 pathogenesis, however it may need further examination in other APL cell lines.

In the future, we intend to further investigate the role of PU.1 in the p53-proficient cell line HT93 to support our results with NB4. We will also expand into AML driven by other recurrent mutations susceptible to novel targeted differentiation therapies. Chiefly, PU.1 is aberrantly relocated to the cytoplasm in NPM1c leukaemia, which can be counteracted with the nuclear export inhibitor selinexor resulting in AML differentiation (Gu et al. 2018). Therefore, maintaining PU.1 suppression with shRNAs may provide resistance to this differentiation therapy in the classical NPM1c-harbouring and selinexor-sensitive cell line OCI-AML3 (Brunetti et al. 2018). The t(8;21) fusion AML1-ETO binds and inhibits PU.1 function,

however while panobinostat administration results in differentiation of the AML blasts, it is achieved through epigenetic remodelling and global changes in transcription (Vangala et al. 2003; Huang et al. 2008; Salmon et al. 2015). Similarly, inhibition of mutant IDH1 and IDH2 triggers differentiation through epigenetic means, yet it is currently unknown if this therapeutic effect requires PU.1 (Bewersdorf et al. 2019; Raineri and Mellor 2018). Therefore, it will be of interest to explore whether PU.1 restoration is a universal component in these various novel differentiation therapies.

5.10.2 APL differentiation can be reversed through PU.1 knockdown alone

In Chapter 3 we determined that PU.1 suppression was sufficient to drive de-differentiation of mature AML246. However, as this mouse model cell line was generated as a result of PU.1 knockdown, the immature state was already reliant on expression of PU.1 shRNA. In Chapter 4, APL cell lines and primary samples were used to show that withdrawal of ATRA could reverse APL differentiation. Chapter 5 demonstrated that PU.1 suppression not only blocked APL differentiation, but was also capable of rescuing mature ATRA-treated cells through the process of de-differentiation.

Our results raise an intriguing possibility whereby the acquisition of mutations that suppress PU.1, rather than those that specifically confer ATRA resistance, are potential avenues for APL de-differentiation and relapse following ATRA-based therapy. This concept may partially explain the appearance of certain non-PML-RARA mutations discovered at relapse in APL, most notably mutant RUNX1 (Madan et al. 2016). We anticipate that the forced expression of other recurrent class II oncogenes that are mutually exclusive with PML-RARA, particularly AML1-ETO or NPM1c, may potentially restore the immature state of ATRA-treated APL through PU.1 repression.

5.10.3 ATO responses are unaffected by sustained PU.1 repression

As outlined in Chapter 1, the standard of care for APL combines ATO with ATRA to great success. Much like ATRA, ATO directly binds and degrades the PML-RARA fusion protein, in principle unleashing PU.1 function and restoring myeloid differentiation while also re-establishing PML nuclear bodies and triggering apoptosis (Zhu, Lallemand-Breitenbach, and de The 2001). To investigate whether PU.1 restoration was an important mechanism in ATO

responses, PU.1 was suppressed in NB4 cells while simultaneously treated with a range of ATO concentrations.

The therapeutic mechanisms of ATO are two-fold, with low concentrations reportedly inducing mild APL differentiation, and higher concentrations capable of triggering apoptosis (Miller et al. 2002). However, we observed no apparent impact with PU.1 knockdown upon low- or high-concentration ATO responses compared to the negative control, suggesting that ATO therapy functions through PU.1-independent means. It must be again noted that this was performed on the p53 deficient cell line NB4, therefore some typical ATO responses may be disabled. Nevertheless, the irrelevance of PU.1 restoration has intriguing implications regarding the efficacy of ATO as a single-agent compared to ATRA. Furthermore, this raises the question as to whether the reported differentiation effects of ATO contribute to its therapeutic success.

5.10.4 PU.1 knockdown can functionally replace PML-RARA in human APL

PU.1 knockdown can maintain NB4 cells in an immature state even in the presence of ATRA. Following withdrawal of the PU.1 shRNA these cells undergo myeloid differentiation, providing a model for restoration of endogenous PU.1 where it is possible to recapitulate mouse AML246 findings in a human context. However, to avoid a model requiring perpetual ATRA treatment, the CRISPR/Cas9 system was used to genetically remove PML-RARA in NB4 while concurrently expressing a GFP-linked PU.1 shRNA under tet-off control. Following selection and sequencing we identified NB4Δ1, a PML-RARA-null clone. This clone was stably dependent on PU.1 shRNA, and Dox-induced PU.1 restoration triggered myeloid differentiation. While PU.1 knockdown prevented ATRA-induced differentiation in §5.2 and §5.3, CRISPR/Cas9 deletion of PML-RARA demonstrated a direct redundancy between PML-RARA and PU.1 suppression. However, it is also unknown whether additional adaptations have occurred in NB4Δ1 in order to tolerate PML-RARA deletion and PU.1 knockdown, nor how closely it phenotypically resembles the parental NB4, though we intend to address this in the future through comparative RNAseq.

5.10.5 PML-RARA deletion results in a mild differentiation response compared to ATRA

Prior to selection of PML-RARA knockout clones, the co-infected culture of NB4 cells harboured a large population with likely disabling mutations of PML-RARA by CRISPR/Cas9 that simultaneously did not express the PU.1 shRNA (Thy1.1^{+} cells). These cells featured a

marked increase in the expression of CD15, however the PU.1 target and pan-myeloid marker CD11B remained at basal levels. Furthermore, there was a meagre selective disadvantage to this fraction of cells, demonstrating only a mild differentiation response in comparison to ATRA.

Interestingly, one of the main factors for both ATRA and ATO efficacy is regarded to be the degradation of the fusion protein (Lallemand-Breitenbach et al. 2008; Yoshida et al. 1996). However, this limited response in our PML-RARA null NB4 suggests that other functions of ATRA, for instance enhanced retinoic acid signalling, and of ATO, such as PML nuclear body reformation and pro-apoptotic regulation, are critical for sustained responses (Chomienne et al. 1991; Kumar, Yedjou, and Tchounwou 2014; Zhu et al. 1997). While this may be an artefact of extensive *in vitro* culturing of the NB4 cells, selective PML-RARA repression has been reported to initiate a distinct differentiation response to ATRA (Ward, Sternsdorf, and Woods 2011). The specificities of PML-RARA degradation in comparison to the robust differentiation therapy responses in APL remain to be determined.

5.10.6 PML-RARA null NB4 remain ATRA sensitive

Although NB4Δ1 cells lack functional PML-RARA, they remain sensitive to ATRA. ATRA-induced differentiation has been observed in AML devoid of PML-RARA before, most famously in the cell line HL-60 (Breitman, Selonick, and Collins 1980; Thomas 2019). Furthermore, ATRA has been shown to potentiate non-APL AML differentiation and apoptosis when used in combination with other therapies, most often with epigenetic modifiers (Johnson and Redner 2015; Ma, Robinson, and Small 2016). These ATRA responses are likely mediated by functional wild type RARA (Dore and Momparler 1996).

It is possible that NB4 cells select for the optimal level of PU.1 suppression, a balance between too much or too little to maintain a state of proliferation and survival. The ATRA-dependent PU.1 knockdown NB4 cells generated in §5.3 likely selected for a high degree of knockdown to offset the PU.1 induction resulting from both PML-RARA degradation and RARA signalling. Conversely, NB4Δ1 were generated with only PML-RARA deletion and likely selected for a comparatively lower level of PU.1 knockdown. Therefore, ATRA may still upregulate PU.1 in NB4Δ1, which will be address in future PU.1 immunoblots.

5.10.7 PML is a dispensable gene in NB4Δ1 cells

sgRNAs targeting the coding sequence of PML were used to delete PML-RARA in NB4 cells. Although the absence of any PML protein via alternative slicing is yet to be verified by PML immunoblot, sequencing of NB4Δ1 identified mutations resulting in a frameshift and premature stop codon in both alleles of untranslocated PML. As discussed in Chapter 1, PML nuclear bodies are involved in the regulation of DNA replication, transcription, senescence, and apoptosis, whereas $PML^{-/-}$ mice have increased tumourigenesis and impaired apoptotic responses, but otherwise develop as normal (Lallemand-Breitenbach and de The 2010; Wang et al. 1998). In APL, treatment with ATRA restores the fragmented and dysregulated nuclear bodies caused by PML-RARA, possibly aiding therapeutic responses (Koken et al. 1994; Zhu et al. 1997). Nevertheless, deletion of the untranslocated allele of PML in NB4Δ1 did not affect ATRA sensitivity, suggesting that reformation of the nuclear bodies may not be an important facet of differentiation therapy. Rather, the lack of PML may have contributed to the selection of NB4Δ1 where nuclear bodies remain dysfunctional in the absence of PML-RARA. To circumvent this, one must screen for additional clones with silent mutations in PML where function is retained, or find another way to selectively target PML-RARA. It remains to be determined whether NB4Δ1 remain sensitive to ATO.

5.10.8 NB4Δ1 as a platform for investigating APL differentiation

NB4Δ1 cells represent a novel platform to selectively explore different aspects of APL biology. Endogenous PU.1 alone is restored following Dox administration, providing an opportunity to build upon results acquired with AML246, namely human PU.1 targets, but also compare to a classical ATRA differentiation. Furthermore, the PML-RARA-independent effects of ATRA and ATO can be addressed in NB4Δ1. These future results may further elucidate distinct critical targets or interesting pathways that ensure terminal myeloid differentiation.

In addition to NB4Δ1, we intend to generate another model of APL whereby one could selectively downregulate PML-RARA without the other effects of ATRA. This could be made possible using inducible shRNA targeting the fusion site of the transcript, potentially shining a light on the alternative oncogenic functions of the fusion protein.

5.10.9 Conclusion

This Chapter described the generation of several human AML models whereby the myeloid transcription factor PU.1 can be selectively toggled on and off. Using the APL cell line NB4, stable PU.1 knockdown was shown to effectively maintain the immature proliferative state of the cells in spite of continuous ATRA treatment. These models provide the future opportunity to investigate distinct aspects of APL differentiation.

CHAPTER 6. Conclusion

AML is an aggressive malignancy driven by immature and proliferative myeloid blasts with a block in normal differentiation. AML has a particularly poor prognosis. While chemotherapy remains the gold standard-of-care for the majority of patients, several novel targeted therapies have been developed capable of inducing deep yet transient remission. A class of these novel therapeutics behave similarly to the differentiating agent ATRA, a vitamin A analogue capable of restoring normal myeloid maturation leading to the clearance of mature APL cells. While ATRA boasts impressive cure rates when used in conjunction with ATO, the new differentiation therapies as single agents often result in relapse. Therefore, how differentiation in AML contributes to disease clearance is a topic of much interest requiring further investigation.

This thesis interrogates the plasticity of maturation in AML using mouse models, human cell lines and primary patient samples. Throughout, myeloid differentiation is manipulated through the inducible expression of the myeloid transcription factor PU.1, by the differentiation agent ATRA, or through a combination of both. Remarkably, differentiation is revealed to be a highly malleable and bidirectional process by which mature AML cells can revert to an immature state following cessation of the differentiation stimulus. This work establishes that leukaemogenic potential is an inherent but latent property of mature, non-proliferative AML-derived cells, implicating them as a potential source of relapse following differentiation therapy.

Of note, our findings are heavily reliant on immunophenotypic analysis as a determinant of maturity of AML cells. The use of immunophenotypic markers has long been relied on for the investigation of LSCs, to assess maturational heterogeneity of tumours, and to measure the fate of AML cells following differentiation therapy (Bonnet and Dick 1997). However, immunophenotypic markers are limited and do not describe the true functional, transcriptional, or epigenetic heterogeneity present throughout the tumour bulk (Corces et al. 2016; van Galen et al. 2019). Our experiments indicate that reversion is a relatively rare event, therefore future experiments should explore whether there is a unique quality in certain immunophenotypically mature cells that allows this reversibility.

Additionally, the work described herein is largely completed *in vitro*, whereas *in vivo* transplantation remains the gold standard assessment of leukaemic potential. Although this

potentially limits the conclusions that can be drawn from our work, the inability of transplanted mature cells to home to the bone marrow and engraft may ultimately prevent direct measurement of de-differentiation *in vivo*. Nevertheless, an important future direction for this work is to eventually translate and investigate the concept of maturation plasticity in an *in vivo* context, or further scrutinize it in human AML patient samples.

Ultimately though, we hope our unprecedented observation that immunophenotypically, transcriptionally, and morphologically mature, non-clonogenic AML-derived cells can reacquire proliferative capacity may expand the definition of a leukaemia-propagating cell, contributing to the field of leukaemia research and potentially clinical practice.

CHAPTER 7. Bibliography

Ablain, J., M. Leiva, L. Peres, J. Fonsart, E. Anthony, and H. de The. 2013. 'Uncoupling RARA transcriptional activation and degradation clarifies the bases for APL response to therapies', *J Exp Med*, 210: 647-53.

Adamson, P. C. 1996. 'All-Trans-Retinoic Acid Pharmacology and Its Impact on the Treatment of Acute Promyelocytic Leukemia', *Oncologist*, 1: 305-14.

AIHW. 2018. 'Cancer in Australia: Actual incidence data from 1982 to 2013 and mortality data from 1982 to 2014 with projections to 2017', *Asia Pac J Clin Oncol*, 14: 5-15.

Al-Hajj, M., M. S. Wicha, A. Benito-Hernandez, S. J. Morrison, and M. F. Clarke. 2003. 'Prospective identification of tumorigenic breast cancer cells', *Proc Natl Acad Sci U S A*, 100: 3983-8.

Altman, J. K., J. M. Foran, K. W. Pratz, D. Trone, J. E. Cortes, and M. S. Tallman. 2018. 'Phase 1 study of quizartinib in combination with induction and consolidation chemotherapy in patients with newly diagnosed acute myeloid leukemia', *Am J Hematol*, 93: 213-21.

Arber, D. A., A. Orazi, R. Hasserjian, J. Thiele, M. J. Borowitz, M. M. Le Beau, C. D. Bloomfield, M. Cazzola, and J. W. Vardiman. 2016. 'The 2016 revision to the World Health Organization classification of myeloid neoplasms and acute leukemia', *Blood*, 127: 2391-405.

Ayob, A. Z., and T. S. Ramasamy. 2018. 'Cancer stem cells as key drivers of tumour progression', *J Biomed Sci*, 25: 20.

Barozzi, I., M. Simonatto, S. Bonifacio, L. Yang, R. Rohs, S. Ghisletti, and G. Natoli. 2014. 'Coregulation of transcription factor binding and nucleosome occupancy through DNA features of mammalian enhancers', *Mol Cell*, 54: 844-57.

Bewersdorf, J. P., R. Shallis, M. Stahl, and A. M. Zeidan. 2019. 'Epigenetic therapy combinations in acute myeloid leukemia: what are the options?', *Ther Adv Hematol*, 10: 2040620718816698.

Birendra, K. C., and C. D. DiNardo. 2016. 'Evidence for Clinical Differentiation and Differentiation Syndrome in Patients With Acute Myeloid Leukemia and IDH1 Mutations Treated With the Targeted Mutant IDH1 Inhibitor, AG-120', *Clin Lymphoma Myeloma Leuk*, 16: 460-5.

Bonnet, D., and J. E. Dick. 1997. 'Human acute myeloid leukemia is organized as a hierarchy that originates from a primitive hematopoietic cell', *Nat Med*, 3: 730-7.

Bots, M., I. Verbrugge, B. P. Martin, J. M. Salmon, M. Ghisi, A. Baker, K. Stanley, J. Shortt, G. J. Ossenkoppele, J. Zuber, A. R. Rappaport, P. Atadja, S. W. Lowe, and R. W. Johnstone. 2014. 'Differentiation therapy for the treatment of t(8;21) acute myeloid leukemia using histone deacetylase inhibitors', *Blood*, 123: 1341-52.

Boyd, A. L., L. Aslostovar, J. Reid, W. Ye, B. Tanasijevic, D. P. Porras, Z. Shapovalova, M. Almakadi, R. Foley, B. Leber, A. Xenocostas, and M. Bhatia. 2018. 'Identification of Chemotherapy-Induced Leukemic-Regenerating Cells Reveals a Transient Vulnerability of Human AML Recurrence', *Cancer Cell*, 34: 483-98 e5.

Bratton, D. L., and P. M. Henson. 2011. 'Neutrophil clearance: when the party is over, clean-up begins', *Trends Immunol*, 32: 350-7.

Breitman, T. R., S. E. Selonick, and S. J. Collins. 1980. 'Induction of differentiation of the human promyelocytic leukemia cell line (HL-60) by retinoic acid', *Proc Natl Acad Sci U S A*, 77: 2936-40.

Brunetti, L., M. C. Gundry, D. Sorcini, A. G. Guzman, Y. H. Huang, R. Ramabadran, I. Gionfriddo, F. Mezzasoma, F. Milano, B. Nabet, D. L. Buckley, S. M. Kornblau, C. Y. Lin, P. Sportoletti, M. P. Martelli, B. Falini, and M. A. Goodell. 2018. 'Mutant NPM1 Maintains the Leukemic State through HOX Expression', *Cancer Cell*, 34: 499-512 e9.

Burda, P., P. Laslo, and T. Stopka. 2010. 'The role of PU.1 and GATA-1 transcription factors during normal and leukemogenic hematopoiesis', *Leukemia*, 24: 1249-57.

Buss, E. C., and A. D. Ho. 2011. 'Leukemia stem cells', *Int J Cancer*, 129: 2328-36.

Camacho, L. H., S. L. Soignet, S. Chanel, R. Ho, G. Heller, D. A. Scheinberg, R. Ellison, and R. P. Warrell, Jr. 2000. 'Leukocytosis and the retinoic acid syndrome in patients with acute promyelocytic leukemia treated with arsenic trioxide', *J Clin Oncol*, 18: 2620-5.

Cancer Genome Atlas Research, Network, T. J. Ley, C. Miller, L. Ding, B. J. Raphael, A. J. Mungall, A. Robertson, K. Hoadley, T. J. Triche, Jr., P. W. Laird, J. D. Baty, L. L. Fulton, R. Fulton, S. E. Heath, J. Kalicki-Veizer, C. Kandoth, J. M. Klco, D. C. Koboldt, K. L. Kanchi, S. Kulkarni, T. L. Lamprecht, D. E. Larson, L. Lin, C. Lu, M. D. McLellan, J. F. McMichael, J. Payton, H. Schmidt, D. H. Spencer, M. H. Tomasson, J. W. Wallis, L. D. Wartman, M. A. Watson, J. Welch, M. C. Wendl, A. Ally, M. Balasundaram, I. Birol, Y. Butterfield, R. Chiu, A. Chu, E. Chuah, H. J. Chun, R. Corbett, N. Dhalla, R. Guin, A. He, C. Hirst, M. Hirst, R. A. Holt, S. Jones, A. Karsan, D. Lee, H. I. Li, M. A. Marra, M. Mayo, R. A. Moore, K. Mungall, J. Parker, E.

Pleasance, P. Plettner, J. Schein, D. Stoll, L. Swanson, A. Tam, N. Thiessen, R. Varhol, N. Wye, Y. Zhao, S. Gabriel, G. Getz, C. Sougnez, L. Zou, M. D. Leiserson, F. Vandin, H. T. Wu, F. Applebaum, S. B. Baylin, R. Akbani, B. M. Broom, K. Chen, T. C. Motter, K. Nguyen, J. N. Weinstein, N. Zhang, M. L. Ferguson, C. Adams, A. Black, J. Bowen, J. Gastier-Foster, T. Grossman, T. Lichtenberg, L. Wise, T. Davidsen, J. A. Demchok, K. R. Shaw, M. Sheth, H. J. Sofia, L. Yang, J. R. Downing, and G. Eley. 2013. 'Genomic and epigenomic landscapes of adult de novo acute myeloid leukemia', *N Engl J Med*, 368: 2059-74.

Chan, S. M., and R. Majeti. 2013. 'Role of DNMT3A, TET2, and IDH1/2 mutations in pre-leukemic stem cells in acute myeloid leukemia', *Int J Hematol*, 98: 648-57.

Chen, Z., Y. Wang, W. Wang, J. Gong, and Y. Xue. 2002. 'All-trans retinoic acid as a single agent induces complete remission in a patient with acute leukemia of M2a subtype', *Chin Med J (Engl)*, 115: 58-61.

Chomienne, C., N. Balitrand, P. Ballerini, S. Castaigne, H. de The, and L. Degos. 1991. 'All-trans retinoic acid modulates the retinoic acid receptor-alpha in promyelocytic cells', *J Clin Invest*, 88: 2150-4.

Christian, S., C. Merz, L. Evans, S. Gradl, H. Seidel, A. Friberg, A. Eheim, P. Lejeune, K. Brzezinka, K. Zimmermann, S. Ferrara, H. Meyer, R. Lesche, D. Stoeckigt, M. Bauser, A. Haegebarth, D. B. Sykes, D. T. Scadden, J. A. Losman, and A. Janzer. 2019. 'The novel dihydroorotate dehydrogenase (DHODH) inhibitor BAY 2402234 triggers differentiation and is effective in the treatment of myeloid malignancies', *Leukemia*, 33: 2403-15.

Collins, S. J. 2002. 'The role of retinoids and retinoic acid receptors in normal hematopoiesis', *Leukemia*, 16: 1896-905.

Collins, S. J., K. A. Robertson, and L. Mueller. 1990. 'Retinoic acid-induced granulocytic differentiation of HL-60 myeloid leukemia cells is mediated directly through the retinoic acid receptor (RAR-alpha)', *Mol Cell Biol*, 10: 2154-63.

Coombs, C. C., M. Tavakkoli, and M. S. Tallman. 2015. 'Acute promyelocytic leukemia: where did we start, where are we now, and the future', *Blood Cancer J*, 5: e304.

Corces, M. R., J. D. Buenrostro, B. Wu, P. G. Greenside, S. M. Chan, J. L. Koenig, M. P. Snyder, J. K. Pritchard, A. Kundaje, W. J. Greenleaf, R. Majeti, and H. Y. Chang. 2016. 'Lineage-specific and single-cell chromatin accessibility charts human hematopoiesis and leukemia evolution', *Nat Genet*, 48: 1193-203.

Cornelissen, J. J., and D. Blaise. 2016. 'Hematopoietic stem cell transplantation for patients with AML in first complete remission', *Blood*, 127: 62-70.

Cortes, J. E., S. Khaled, G. Martinelli, A. E. Perl, S. Ganguly, N. Russell, A. Kramer, H. Dombret, D. Hogge, B. A. Jonas, A. Y. Leung, P. Mehta, P. Montesinos, M. Radsak, S. Sica, M. Arunachalam, M. Holmes, K. Kobayashi, R. Namuyinga, N. Ge, A. Yver, Y. Zhang, and M. J. Levis. 2019. 'Quizartinib versus salvage chemotherapy in relapsed or refractory FLT3-ITD acute myeloid leukaemia (QuANTUM-R): a multicentre, randomised, controlled, open-label, phase 3 trial', *Lancet Oncol*, 20: 984-97.

Daver, N., R. F. Schlenk, N. H. Russell, and M. J. Levis. 2019. 'Targeting FLT3 mutations in AML: review of current knowledge and evidence', *Leukemia*, 33: 299-312.

Davis, J. N., L. McGhee, and S. Meyers. 2003. 'The ETO (MTG8) gene family', *Gene*, 303: 1-10.

De Kouchkovsky, I., and M. Abdul-Hay. 2016. "Acute myeloid leukemia: a comprehensive review and 2016 update", *Blood Cancer J*, 6: e441.

de Sousa e Melo, F., A. V. Kurtova, J. M. Harnoss, N. Kljavin, J. D. Hoeck, J. Hung, J. E. Anderson, E. E. Storm, Z. Modrusan, H. Koeppen, G. J. Dijkgraaf, R. Piskol, and F. J. de Sauvage. 2017. 'A distinct role for Lgr5(+) stem cells in primary and metastatic colon cancer', *Nature*, 543: 676-80.

de The, H. 2018. 'Differentiation therapy revisited', *Nat Rev Cancer*, 18: 117-27.

de The, H., and Z. Chen. 2010. 'Acute promyelocytic leukaemia: novel insights into the mechanisms of cure', *Nat Rev Cancer*, 10: 775-83.

DiNardo, C. D., E. M. Stein, S. de Botton, G. J. Roboz, J. K. Altman, A. S. Mims, R. Swords, R. H. Collins, G. N. Mannis, D. A. Pollyea, W. Donnellan, A. T. Fathi, A. Pigneux, H. P. Erba, G. T. Prince, A. S. Stein, G. L. Uy, J. M. Foran, E. Traer, R. K. Stuart, M. L. Arellano, J. L. Slack, M. A. Sekeres, C. Willekens, S. Choe, H. Wang, V. Zhang, K. E. Yen, S. M. Kapsalis, H. Yang, D. Dai, B. Fan, M. Goldwasser, H. Liu, S. Agresta, B. Wu, E. C. Attar, M. S. Tallman, R. M. Stone, and H. M. Kantarjian. 2018. 'Durable Remissions with Ivosidenib in IDH1-Mutated Relapsed or Refractory AML', *N Engl J Med*, 378: 2386-98.

Ding, Y., H. Gao, and Q. Zhang. 2017. 'The biomarkers of leukemia stem cells in acute myeloid leukemia', *Stem Cell Investig*, 4: 19.

Dore, B. T., and R. L. Momparler. 1996. 'Mutation in the ligand-binding domain of the retinoic acid receptor alpha in HL-60 leukemic cells resistant to retinoic acid and with increased sensitivity to vitamin D3 analogs', *Leuk Res*, 20: 761-9.

Duprez, E., G. Benoit, M. Flexor, J. R. Lillehaug, and M. Lanotte. 2000. 'A mutated PML/RARA found in the retinoid maturation resistant NB4 subclone, NB4-R2, blocks RARA and wild-type PML/RARA transcriptional activities', *Leukemia*, 14: 255-61.

Eash, K. J., A. M. Greenbaum, P. K. Gopalan, and D. C. Link. 2010. 'CXCR2 and CXCR4 antagonistically regulate neutrophil trafficking from murine bone marrow', *J Clin Invest*, 120: 2423-31.

Esnault, S., and E. A. Kelly. 2016. 'Essential Mechanisms of Differential Activation of Eosinophils by IL-3 Compared to GM-CSF and IL-5', *Crit Rev Immunol*, 36: 429-44.

Fasan, A., C. Haferlach, K. Perglerova, W. Kern, and T. Haferlach. 2017. 'Molecular landscape of acute promyelocytic leukemia at diagnosis and relapse', *Haematologica*, 102: e222-e24.

Fathi, A. T., C. D. DiNardo, I. Kline, L. Kenvin, I. Gupta, E. C. Attar, E. M. Stein, S. de Botton, and Ag C. Study Investigators. 2018. 'Differentiation Syndrome Associated With Enasidenib, a Selective Inhibitor of Mutant Isocitrate Dehydrogenase 2: Analysis of a Phase 1/2 Study', *JAMA Oncol*, 4: 1106-10.

Fellmann, C., T. Hoffmann, V. Sridhar, B. Hopfgartner, M. Muhar, M. Roth, D. Y. Lai, I. A. Barbosa, J. S. Kwon, Y. Guan, N. Sinha, and J. Zuber. 2013. 'An optimized microRNA backbone for effective single-copy RNAi', *Cell Rep*, 5: 1704-13.

Feng, J., T. Liu, B. Qin, Y. Zhang, and X. S. Liu. 2012. 'Identifying ChIP-seq enrichment using MACS', *Nat Protoc*, 7: 1728-40.

Forghieri, F., S. Bigliardi, C. Quadrelli, M. Morselli, L. Potenza, A. Paolini, E. Colaci, P. Barozzi, P. Zucchini, G. Riva, D. Vallerini, I. Lagreca, R. Marasca, F. Narni, A. Venditti, M. P. Martelli, B. Falini, F. Lo Coco, S. Amadori, and M. Luppi. 2016. 'All-trans retinoic acid (ATRA) in non-promyelocytic acute myeloid leukemia (AML): results of combination of ATRA with low-dose Ara-C in three elderly patients with NPM1-mutated AML unfit for intensive chemotherapy and review of the literature', *Clin Case Rep*, 4: 1138-46.

Frasch, S. C., K. Z. Berry, R. Fernandez-Boyanapalli, H. S. Jin, C. Leslie, P. M. Henson, R. C. Murphy, and D. L. Bratton. 2008. 'NADPH oxidase-dependent generation of lysophosphatidylserine enhances clearance of activated and dying neutrophils via G2A', *J Biol Chem*, 283: 33736-49.

Gallagher, R. E., E. L. Schachter-Tokarz, D. C. Zhou, W. Ding, S. H. Kim, B. J. Sankoorikal, W. Bi, K. J. Livak, J. L. Slack, and C. L. Willman. 2006. 'Relapse of acute promyelocytic leukemia with PML-RARalpha mutant subclones independent of proximate all-trans retinoic acid selection pressure', *Leukemia*, 20: 556-62.

Garzon, R., M. Savona, R. Baz, M. Andreeff, N. Gabrail, M. Gutierrez, L. Savoie, P. M. Mau-Sorensen, N. Wagner-Johnston, K. Yee, T. J. Unger, J. R. Saint-Martin, R. Carlson, T. Rashal, T. Kashyap, B. Klebanov, S. Shacham, M. Kauffman, and R. Stone. 2017. 'A phase 1 clinical trial of single-agent selinexor in acute myeloid leukemia', *Blood*, 129: 3165-74.

Gelmetti, V., J. Zhang, M. Fanelli, S. Minucci, P. G. Pelicci, and M. A. Lazar. 1998. 'Aberrant recruitment of the nuclear receptor corepressor-histone deacetylase complex by the acute myeloid leukemia fusion partner ETO', *Mol Cell Biol*, 18: 7185-91.

Gerloff, D., R. Grundler, A. A. Wurm, D. Brauer-Hartmann, C. Katzerke, J. U. Hartmann, V. Madan, C. Muller-Tidow, J. Duyster, D. G. Tenen, D. Niederwieser, and G. Behre. 2015. 'NF-kappaB/STAT5/miR-155 network targets PU.1 in FLT3-ITD-driven acute myeloid leukemia', *Leukemia*, 29: 535-47.

Ghisletti, S., I. Barozzi, F. Mietton, S. Polletti, F. De Santa, E. Venturini, L. Gregory, L. Lonie, A. Chew, C. L. Wei, J. Ragoussis, and G. Natoli. 2010. 'Identification and characterization of enhancers controlling the inflammatory gene expression program in macrophages', *Immunity*, 32: 317-28.

Gu, X., Q. Ebrahem, R. Z. Mahfouz, M. Hasipek, F. Enane, T. Radivoyevitch, N. Rapin, B. Przychodzen, Z. Hu, R. Balusu, C. V. Cotta, D. Wald, C. Argueta, Y. Landesman, M. P. Martelli, B. Falini, H. Carraway, B. T. Porse, J. Maciejewski, B. K. Jha, and Y. Saunthararajah. 2018. 'Leukemogenic nucleophosmin mutation disrupts the transcription factor hub that regulates granulomonocytic fates', *J Clin Invest*, 128: 4260-79.

Gupta, P., G. U. Gurudutta, D. Saluja, and R. P. Tripathi. 2009. 'PU.1 and partners: regulation of haematopoietic stem cell fate in normal and malignant haematopoiesis', *J Cell Mol Med*, 13: 4349-63.

Gustafson, M. P., Y. Lin, M. L. Maas, V. P. Van Keulen, P. B. Johnston, T. Peikert, D. A. Gastineau, and A. B. Dietz. 2015. 'A method for identification and analysis of non-overlapping myeloid immunophenotypes in humans', *PLoS One*, 10: e0121546.

Hahne, F., and R. Ivanek. 2016. 'Visualizing Genomic Data Using Gviz and Bioconductor', *Methods Mol Biol*, 1418: 335-51.

Hankey, B. F., L. A. Ries, and B. K. Edwards. 1999. 'The surveillance, epidemiology, and end results program: a national resource', *Cancer Epidemiol Biomarkers Prev*, 8: 1117-21.

Hashimshony, T., N. Senderovich, G. Avital, A. Klochendler, Y. de Leeuw, L. Anavy, D. Gennert, S. Li, K. J. Livak, O. Rozenblatt-Rosen, Y. Dor, A. Regev, and I. Yanai. 2016. 'CEL-Seq2: sensitive highly-multiplexed single-cell RNA-Seq', *Genome Biol*, 17: 77.

Heng, T. S., M. W. Painter, and Consortium Immunological Genome Project. 2008. 'The Immunological Genome Project: networks of gene expression in immune cells', *Nat Immunol*, 9: 1091-4.

Huang, G., P. Zhang, H. Hirai, S. Elf, X. Yan, Z. Chen, S. Koschmieder, Y. Okuno, T. Dayaram, J. D. Growney, R. A. Shivdasani, D. G. Gilliland, N. A. Speck, S. D. Nimer, and D. G. Tenen. 2008. 'PU.1 is a major downstream target of AML1 (RUNX1) in adult mouse hematopoiesis', *Nat Genet*, 40: 51-60.

Ignatova, T. N., V. G. Kukekov, E. D. Laywell, O. N. Suslov, F. D. Vrionis, and D. A. Steindler. 2002. 'Human cortical glial tumors contain neural stem-like cells expressing astroglial and neuronal markers in vitro', *Glia*, 39: 193-206.

Imperato, M. R., P. Cauchy, N. Obier, and C. Bonifer. 2015. 'The RUNX1-PU.1 axis in the control of hematopoiesis', *Int J Hematol*, 101: 319-29.

Intlekofer, A. M., A. H. Shih, B. Wang, A. Nazir, A. S. Rustenburg, S. K. Albanese, M. Patel, C. Famulare, F. M. Correa, N. Takemoto, V. Durani, H. Liu, J. Taylor, N. Farnoud, E. Papaemmanuil, J. R. Cross, M. S. Tallman, M. E. Arcila, M. Roshal, G. A. Petsko, B. Wu, S. Choe, Z. D. Konteatis, S. A. Biller, J. D. Chodera, C. B. Thompson, R. L. Levine, and E. M. Stein. 2018. 'Acquired resistance to IDH inhibition through trans or cis dimer-interface mutations', *Nature*, 559: 125-29.

Ishikawa, F., S. Yoshida, Y. Saito, A. Hijikata, H. Kitamura, S. Tanaka, R. Nakamura, T. Tanaka, H. Tomiyama, N. Saito, M. Fukata, T. Miyamoto, B. Lyons, K. Ohshima, N. Uchida, S. Taniguchi, O. Ohara, K. Akashi, M. Harada, and L. D. Shultz. 2007. 'Chemotherapy-resistant human AML stem cells home to and engraft within the bone-marrow endosteal region', *Nat Biotechnol*, 25: 1315-21.

Iwasaki, H., C. Somoza, H. Shigematsu, E. A. Duprez, J. Iwasaki-Arai, S. Mizuno, Y. Arinobu, K. Geary, P. Zhang, T. Dayaram, M. L. Fenyus, S. Elf, S. Chan, P. Kastner, C. S. Huettner, R. Murray, D. G. Tenen, and K. Akashi. 2005. 'Distinctive and indispensable roles of PU.1 in maintenance of hematopoietic stem cells and their differentiation', *Blood*, 106: 1590-600.

Jensen, H. A., H. B. Yourish, R. P. Bunaciu, J. D. Varner, and A. Yen. 2015. 'Induced myelomonocytic differentiation in leukemia cells is accompanied by noncanonical transcription factor expression', *FEBS Open Bio*, 5: 789-800.

Johnson, D. E., and R. L. Redner. 2015. 'An ATRActive future for differentiation therapy in AML', *Blood Rev*, 29: 263-8.

Jones, L., G. Wei, S. Sevcikova, V. Phan, S. Jain, A. Shieh, J. C. Wong, M. Li, J. Dubansky, M. L. Maunakea, R. Ochoa, G. Zhu, T. R. Tennant, K. M. Shannon, S. W. Lowe, M. M. Le Beau, and S. C. Kogan. 2010. 'Gain of MYC underlies recurrent trisomy of the MYC chromosome in acute promyelocytic leukemia', *J Exp Med*, 207: 2581-94.

Kastner, P., H. J. Lawrence, C. Waltzinger, N. B. Ghyselinck, P. Chambon, and S. Chan. 2001. 'Positive and negative regulation of granulopoiesis by endogenous RARalpha', *Blood*, 97: 1314-20.

Kelaidi, C., L. Ades, S. Chevret, M. Sanz, A. Guerci, X. Thomas, S. de Botton, E. Raffoux, C. Rayon, N. Fegueux, D. Bordessoule, F. Rigal-Huguet, H. Link, A. Stoppa, A. Vekhoff, S. Meyer-Monard, S. Castaigne, H. Dombret, L. Degos, and P. Fenaux. 2006. 'Late first relapses in APL treated with all-trans-retinoic acid- and anthracycline- based chemotherapy: the European APL group experience (APL 91 and APL 93 trials)', *Leukemia*, 20: 905-7.

Kelly, L. M., and D. G. Gilliland. 2002. 'Genetics of myeloid leukemias', *Annu Rev Genomics Hum Genet*, 3: 179-98.

Kim, H. G., C. G. de Guzman, C. S. Swindle, C. V. Cotta, L. Gartland, E. W. Scott, and C. A. Klug. 2004. 'The ETS family transcription factor PU.1 is necessary for the maintenance of fetal liver hematopoietic stem cells', *Blood*, 104: 3894-900.

Kishi, K., K. Toba, T. Azegami, N. Tsukada, Y. Uesugi, M. Masuko, H. Niwano, S. Hashimoto, M. Sakaue, T. Furukawa, T. Koike, H. Takahashi, T. Maekawa, T. Abe, and Y. Aizawa. 1998. 'Hematopoietic cytokine-dependent differentiation to eosinophils and neutrophils in a newly established acute promyelocytic leukemia cell line with t(15;17)', *Exp Hematol*, 26: 135-42.

Koken, M. H., F. Puvion-Dutilleul, M. C. Guillemin, A. Viron, G. Linares-Cruz, N. Stuurman, L. de Jong, C. Szostecki, F. Calvo, C. Chomienne, and et al. 1994. 'The t(15;17) translocation alters a nuclear body in a retinoic acid-reversible fashion', *EMBO J*, 13: 1073-83.

Krysinska, H., M. Hoogenkamp, R. Ingram, N. Wilson, H. Tagoh, P. Laslo, H. Singh, and C. Bonifer. 2007. 'A two-step, PU.1-dependent mechanism for developmentally regulated chromatin remodeling and transcription of the c-fms gene', *Mol Cell Biol*, 27: 878-87.

Kueh, H. Y., A. Champhekar, S. L. Nutt, M. B. Elowitz, and E. V. Rothenberg. 2013. 'Positive feedback between PU.1 and the cell cycle controls myeloid differentiation', *Science*, 341: 670-3.

Kuley-Bagheri, Y., K. A. Kreuzer, I. Monsef, M. Lubbert, and N. Skoetz. 2018. 'Effects of all-trans retinoic acid (ATRA) in addition to chemotherapy for adults with acute myeloid leukaemia (AML) (non-acute promyelocytic leukaemia (non-APL))', *Cochrane Database Syst Rev*, 8: CD011960.

Kumar, S., C. G. Yedjou, and P. B. Tchounwou. 2014. 'Arsenic trioxide induces oxidative stress, DNA damage, and mitochondrial pathway of apoptosis in human leukemia (HL-60) cells', *J Exp Clin Cancer Res*, 33: 42.

Lallemand-Breitenbach, V., and H. de The. 2010. 'PML nuclear bodies', *Cold Spring Harb Perspect Biol*, 2: a000661.

Lallemand-Breitenbach, V., M. Jeanne, S. Benhenda, R. Nasr, M. Lei, L. Peres, J. Zhou, J. Zhu, B. Raught, and H. de The. 2008. 'Arsenic degrades PML or PML-RARalpha through a SUMO-triggered RNF4/ubiquitin-mediated pathway', *Nat Cell Biol*, 10: 547-55.

Lanotte, M., V. Martin-Thouvenin, S. Najman, P. Balerini, F. Valensi, and R. Berger. 1991. 'NB4, a maturation inducible cell line with t(15;17) marker isolated from a human acute promyelocytic leukemia (M3)', *Blood*, 77: 1080-6.

Lapidot, T., C. Sirard, J. Vormoor, B. Murdoch, T. Hoang, J. Caceres-Cortes, M. Minden, B. Paterson, M. A. Caligiuri, and J. E. Dick. 1994. 'A cell initiating human acute myeloid leukaemia after transplantation into SCID mice', *Nature*, 367: 645-8.

Law, C. W., Y. Chen, W. Shi, and G. K. Smyth. 2014. 'voom: Precision weights unlock linear model analysis tools for RNA-seq read counts', *Genome Biol*, 15: R29.

Lawrence, M., W. Huber, H. Pages, P. Aboyoun, M. Carlson, R. Gentleman, M. T. Morgan, and V. J. Carey. 2013. 'Software for computing and annotating genomic ranges', *PLoS Comput Biol*, 9: e1003118.

Lee, J. J., E. A. Jacobsen, S. I. Ochkur, M. P. McGarry, R. M. Condjella, A. D. Doyle, H. Luo, K. R. Zellner, C. A. Protheroe, L. Willetts, W. E. Lesuer, D. C. Colbert, R. A. Helmers, P. Lacy, R. Moqbel, and N. A. Lee. 2012. 'Human versus mouse eosinophils: "that

which we call an eosinophil, by any other name would stain as red"', *J Allergy Clin Immunol*, 130: 572-84.

Lehmann-Che, J., C. Bally, E. Letouze, C. Berthier, H. Yuan, F. Jollivet, L. Ades, B. Cassinat, P. Hirsch, A. Pigneux, M. J. Mozziconacci, S. Kogan, P. Fenaux, and H. de The. 2018. 'Dual origin of relapses in retinoic-acid resistant acute promyelocytic leukemia', *Nat Commun*, 9: 2047.

Ley, T. J., E. R. Mardis, L. Ding, B. Fulton, M. D. McLellan, K. Chen, D. Dooling, B. H. Dunford-Shore, S. McGrath, M. Hickenbotham, L. Cook, R. Abbott, D. E. Larson, D. C. Koboldt, C. Pohl, S. Smith, A. Hawkins, S. Abbott, D. Locke, L. W. Hillier, T. Miner, L. Fulton, V. Magrini, T. Wylie, J. Glasscock, J. Conyers, N. Sander, X. Shi, J. R. Osborne, P. Minx, D. Gordon, A. Chinwalla, Y. Zhao, R. E. Ries, J. E. Payton, P. Westervelt, M. H. Tomasson, M. Watson, J. Baty, J. Ivanovich, S. Heath, W. D. Shannon, R. Nagarajan, M. J. Walter, D. C. Link, T. A. Graubert, J. F. DiPersio, and R. K. Wilson. 2008. 'DNA sequencing of a cytogenetically normal acute myeloid leukaemia genome', *Nature*, 456: 66-72.

Li, H., B. Handsaker, A. Wysoker, T. Fennell, J. Ruan, N. Homer, G. Marth, G. Abecasis, R. Durbin, and Subgroup Genome Project Data Processing. 2009. 'The Sequence Alignment/Map format and SAMtools', *Bioinformatics*, 25: 2078-9.

Liao, Y., G. K. Smyth, and W. Shi. 2013. 'The Subread aligner: fast, accurate and scalable read mapping by seed-and-vote', *Nucleic Acids Res*, 41: e108.

———. 2014. 'featureCounts: an efficient general purpose program for assigning sequence reads to genomic features', *Bioinformatics*, 30: 923-30.

Litzow, M. R. 2004. 'The therapy of relapsed acute leukaemia in adults', *Blood Rev*, 18: 39-63.

Lu, C., and C. B. Thompson. 2012. 'Metabolic regulation of epigenetics', *Cell Metab*, 16: 9-17.

Lun, A. T., K. Bach, and J. C. Marioni. 2016. 'Pooling across cells to normalize single-cell RNA sequencing data with many zero counts', *Genome Biol*, 17: 75.

Ma, H. S., T. M. Robinson, and D. Small. 2016. 'Potential role for all-trans retinoic acid in nonpromyelocytic acute myeloid leukemia', *Int J Hematol Oncol*, 5: 133-42.

Madan, V., P. Shyamsunder, L. Han, A. Mayakonda, Y. Nagata, J. Sundaresan, D. Kanojia, K. Yoshida, S. Ganesan, N. Hattori, N. Fulton, K. T. Tan, T. Alpermann, M. C. Kuo, S. Rostami, J. Matthews, M. Sanada, L. Z. Liu, Y. Shiraishi, S. Miyano, E. Chendamarai, H. A. Hou, G. Malnassy, T. Ma, M. Garg, L. W. Ding, Q. Y. Sun, W. Chien, T. Ikezoe, M. Lill, A. Biondi, R. A. Larson, B. L. Powell, M. Lubbert, W. J. Chng, H. F. Tien, M.

Heuser, A. Ganser, M. Koren-Michowitz, S. M. Kornblau, H. M. Kantarjian, D. Nowak, W. K. Hofmann, H. Yang, W. Stock, A. Ghavamzadeh, K. Alimoghaddam, T. Haferlach, S. Ogawa, L. Y. Shih, V. Mathews, and H. P. Koeffler. 2016. 'Comprehensive mutational analysis of primary and relapse acute promyelocytic leukemia', *Leukemia*, 30: 2430.

Marasca, R., P. Zucchini, S. Galimberti, G. Leonardi, P. Vaccari, A. Donelli, M. Luppi, M. Petrini, and G. Torelli. 1999. 'Missense mutations in the PML/RARalpha ligand binding domain in ATRA-resistant As(2)O(3) sensitive relapsed acute promyelocytic leukemia', *Haematologica*, 84: 963-8.

Martelli, M. P., I. Gionfriddo, F. Mezzasoma, F. Milano, S. Pierangeli, F. Mulas, R. Pacini, A. Tabarrini, V. Pettirossi, R. Rossi, C. Vetro, L. Brunetti, P. Sportoletti, E. Tiacci, F. Di Raimondo, and B. Falini. 2015. 'Arsenic trioxide and all-trans retinoic acid target NPM1 mutant oncoprotein levels and induce apoptosis in NPM1-mutated AML cells', *Blood*, 125: 3455-65.

Mathews, V., P. Balasubramanian, R. V. Shaji, B. George, M. Chandy, and A. Srivastava. 2002. 'Arsenic trioxide in the treatment of newly diagnosed acute promyelocytic leukemia: a single center experience', *Am J Hematol*, 70: 292-9.

McMahon, C. M., J. Canaani, B. Rea, R. L. Sargent, J. N. Qualtieri, C. D. Watt, J. J. D. Morrissette, M. Carroll, and A. E. Perl. 2019. 'Gilteritinib induces differentiation in relapsed and refractory FLT3-mutated acute myeloid leukemia', *Blood Adv*, 3: 1581-85.

Miles, L. A., R. L. Bowman, T. R. Merlinsky, I. S. Csete, A. T. Ooi, R. Durruthy-Durruthy, M. Bowman, C. Famulare, M. A. Patel, P. Mendez, C. Ainali, B. Demaree, C. L. Delley, A. R. Abate, M. Manivannan, S. Sahu, A. D. Goldberg, K. L. Bolton, A. Zehir, R. Rampal, M. P. Carroll, S. E. Meyer, A. D. Viny, and R. L. Levine. 2020. 'Single-cell mutation analysis of clonal evolution in myeloid malignancies', *Nature*, 587: 477-82.

Miller, W. H., Jr., H. M. Schipper, J. S. Lee, J. Singer, and S. Waxman. 2002. 'Mechanisms of action of arsenic trioxide', *Cancer Res*, 62: 3893-903.

Montesinos, P., J. M. Bergua, E. Vellenga, C. Rayon, R. Parody, J. de la Serna, A. Leon, J. Esteve, G. Milone, G. Deben, C. Rivas, M. Gonzalez, M. Tormo, J. Diaz-Mediavilla, J. D. Gonzalez, S. Negri, E. Amutio, S. Brunet, B. Lowenberg, and M. A. Sanz. 2009. 'Differentiation syndrome in patients with acute promyelocytic leukemia treated with all-trans retinoic acid and anthracycline chemotherapy: characteristics, outcome, and prognostic factors', *Blood*, 113: 775-83.

Morita, K., F. Wang, K. Jahn, T. Hu, T. Tanaka, Y. Sasaki, J. Kuipers, S. Loghavi, S. A. Wang, Y. Yan, K. Furudate, J. Matthews, L. Little, C. Gumbs, J. Zhang, X. Song, E.

Thompson, K. P. Patel, C. E. Bueso-Ramos, C. D. DiNardo, F. Ravandi, E. Jabbour, M. Andreeff, J. Cortes, K. Bhalla, G. Garcia-Manero, H. Kantarjian, M. Konopleva, D. Nakada, N. Navin, N. Beerenwinkel, P. A. Futreal, and K. Takahashi. 2020. 'Clonal evolution of acute myeloid leukemia revealed by high-throughput single-cell genomics', *Nat Commun*, 11: 5327.

Mossadegh-Keller, N., S. Sarrazin, P. K. Kandalla, L. Espinosa, E. R. Stanley, S. L. Nutt, J. Moore, and M. H. Sieweke. 2013. 'M-CSF instructs myeloid lineage fate in single haematopoietic stem cells', *Nature*, 497: 239-43.

Mozziconacci, M. J., A. Rosenauer, A. Restouin, M. Fanelli, W. Shao, F. Fernandez, Y. Toiron, J. Viscardi, C. Gambacorti-Passerini, W. H. Miller, Jr., and M. Lafage-Pochitaloff. 2002. 'Molecular cytogenetics of the acute promyelocytic leukemia-derived cell line NB4 and of four all-trans retinoic acid-resistant subclones', *Genes Chromosomes Cancer*, 35: 261-70.

Mueller, B. U., T. Pabst, J. Fos, V. Petkovic, M. F. Fey, N. Asou, U. Buergi, and D. G. Tenen. 2006. 'ATRA resolves the differentiation block in t(15;17) acute myeloid leukemia by restoring PU.1 expression', *Blood*, 107: 3330-8.

Naeem, M., K. Harrison, K. Barton, S. Nand, and S. Alkan. 2006. 'A unique case of acute promyelocytic leukemia showing monocytic differentiation after ATRA (all-trans retinoic acid) therapy', *Eur J Haematol*, 76: 164-6.

Nakahara, F., C. N. Weiss, and K. Ito. 2014. 'The role of PML in hematopoietic and leukemic stem cell maintenance', *Int J Hematol*, 100: 18-26.

Nassereddine, S., C. J. Lap, F. Haroun, and I. Tabbara. 2017. 'The role of mutant IDH1 and IDH2 inhibitors in the treatment of acute myeloid leukemia', *Ann Hematol*, 96: 1983-91.

Nestorowa, S., F. K. Hamey, B. Pijuan Sala, E. Diamanti, M. Shepherd, E. Laurenti, N. K. Wilson, D. G. Kent, and B. Gottgens. 2016. 'A single-cell resolution map of mouse hematopoietic stem and progenitor cell differentiation', *Blood*, 128: e20-31.

Ng, S. W., A. Mitchell, J. A. Kennedy, W. C. Chen, J. McLeod, N. Ibrahimova, A. Arruda, A. Popescu, V. Gupta, A. D. Schimmer, A. C. Schuh, K. W. Yee, L. Bullinger, T. Herold, D. Gorlich, T. Buchner, W. Hiddemann, W. E. Berdel, B. Wormann, M. Cheok, C. Preudhomme, H. Dombret, K. Metzeler, C. Buske, B. Lowenberg, P. J. Valk, P. W. Zandstra, M. D. Minden, J. E. Dick, and J. C. Wang. 2016. 'A 17-gene stemness score for rapid determination of risk in acute leukaemia', *Nature*, 540: 433-37.

Niu, C., H. Yan, T. Yu, H. P. Sun, J. X. Liu, X. S. Li, W. Wu, F. Q. Zhang, Y. Chen, L. Zhou, J. M. Li, X. Y. Zeng, R. R. Yang, M. M. Yuan, M. Y. Ren, F. Y. Gu, Q. Cao, B. W. Gu, X. Y. Su, G. Q. Chen, S. M. Xiong, T. D. Zhang, S. Waxman, Z. Y. Wang, Z. Chen, J. Hu, Z. X. Shen, and S. J. Chen. 1999. 'Studies on treatment of acute promyelocytic leukemia with arsenic trioxide: remission induction, follow-up, and molecular monitoring in 11 newly diagnosed and 47 relapsed acute promyelocytic leukemia patients', *Blood*, 94: 3315-24.

Nutt, S. L., D. Metcalf, A. D'Amico, M. Polli, and L. Wu. 2005. 'Dynamic regulation of PU.1 expression in multipotent hematopoietic progenitors', *J Exp Med*, 201: 221-31.

Okuno, Y., G. Huang, F. Rosenbauer, E. K. Evans, H. S. Radomska, H. Iwasaki, K. Akashi, F. Moreau-Gachelin, Y. Li, P. Zhang, B. Gottgens, and D. G. Tenen. 2005. 'Potential autoregulation of transcription factor PU.1 by an upstream regulatory element', *Mol Cell Biol*, 25: 2832-45.

Papaemmanuil, E., M. Gerstung, L. Bullinger, V. I. Gaidzik, P. Paschka, N. D. Roberts, N. E. Potter, M. Heuser, F. Thol, N. Bolli, G. Gundem, P. Van Loo, I. Martincorena, P. Ganly, L. Mudie, S. McLaren, S. O'Meara, K. Raine, D. R. Jones, J. W. Teague, A. P. Butler, M. F. Greaves, A. Ganser, K. Dohner, R. F. Schlenk, H. Dohner, and P. J. Campbell. 2016. 'Genomic Classification and Prognosis in Acute Myeloid Leukemia', *N Engl J Med*, 374: 2209-21.

Patel, A. A., Y. Zhang, J. N. Fullerton, L. Boelen, A. Rongvaux, A. A. Maini, V. Bigley, R. A. Flavell, D. W. Gilroy, B. Asquith, D. Macallan, and S. Yona. 2017. 'The fate and lifespan of human monocyte subsets in steady state and systemic inflammation', *J Exp Med*, 214: 1913-23.

Plenderleith, I. H. 1990. 'Treating the treatment: toxicity of cancer chemotherapy', *Can Fam Physician*, 36: 1827-30.

Pollyea, D. A., and C. T. Jordan. 2017. 'Therapeutic targeting of acute myeloid leukemia stem cells', *Blood*, 129: 1627-35.

Purdie, C. A., D. J. Harrison, A. Peter, L. Dobbie, S. White, S. E. Howie, D. M. Salter, C. C. Bird, A. H. Wyllie, M. L. Hooper, and et al. 1994. 'Tumour incidence, spectrum and ploidy in mice with a large deletion in the p53 gene', *Oncogene*, 9: 603-9.

Quek, L., M. D. David, A. Kennedy, M. Metzner, M. Amatangelo, A. Shih, B. Stoilova, C. Quivoron, M. Heiblig, C. Willekens, V. Saada, S. Alsafadi, M. S. Vijayabaskar, A. Peniket, O. A. Bernard, S. Agresta, K. Yen, K. MacBeth, E. Stein, G. S. Vassiliou, R. Levine, S. De Botton, A. Thakurta, V. Penard-Lacronique, and P. Vyas. 2018. 'Clonal heterogeneity of acute myeloid leukemia treated with the IDH2 inhibitor enasidenib', *Nat Med*, 24: 1167-77.

Quignon, F., Z. Chen, and H. de The. 1997. 'Retinoic acid and arsenic: towards oncogene-targeted treatments of acute promyelocytic leukaemia', *Biochim Biophys Acta*, 1333: M53-61.

Quintas-Cardama, A., F. P. Santos, and G. Garcia-Manero. 2011. 'Histone deacetylase inhibitors for the treatment of myelodysplastic syndrome and acute myeloid leukemia', *Leukemia*, 25: 226-35.

Radomska, H. S., D. S. Basseres, R. Zheng, P. Zhang, T. Dayaram, Y. Yamamoto, D. W. Sternberg, N. Lokker, N. A. Giese, S. K. Bohlander, S. Schnittger, M. H. Delmotte, R. J. Davis, D. Small, W. Hiddemann, D. G. Gilliland, and D. G. Tenen. 2006. 'Block of C/EBP alpha function by phosphorylation in acute myeloid leukemia with FLT3 activating mutations', *J Exp Med*, 203: 371-81.

Raineri, S., and J. Mellor. 2018. 'IDH1: Linking Metabolism and Epigenetics', *Front Genet*, 9: 493.

Rayeroux, K. C., and L. J. Campbell. 2009. 'Gene amplification in myeloid leukemias elucidated by fluorescence in situ hybridization', *Cancer Genet Cytogenet*, 193: 44-53.

Riccioni, R., E. Saulle, S. Militi, N. M. Sposi, M. Gualtiero, N. Mauro, M. Mancini, D. Diverio, F. Lo Coco, C. Peschle, and U. Testa. 2003. 'C-fms expression correlates with monocytic differentiation in PML-RAR alpha+ acute promyelocytic leukemia', *Leukemia*, 17: 98-113.

Ritchie, M. E., B. Phipson, D. Wu, Y. Hu, C. W. Law, W. Shi, and G. K. Smyth. 2015. 'limma powers differential expression analyses for RNA-sequencing and microarray studies', *Nucleic Acids Res*, 43: e47.

Riva, L., C. Ronchini, M. Bodini, F. Lo-Coco, S. Lavorgna, T. Ottone, G. Martinelli, I. Iacobucci, C. Tarella, A. Cignetti, S. Volorio, L. Bernard, A. Russo, G. E. Melloni, L. Luzi, M. Alcalay, G. I. Dellino, and P. G. Pelicci. 2013. 'Acute promyelocytic leukemias share cooperative mutations with other myeloid-leukemia subgroups', *Blood Cancer J*, 3: e147.

Robinson, M. D., and A. Oshlack. 2010. 'A scaling normalization method for differential expression analysis of RNA-seq data', *Genome Biol*, 11: R25.

Rosenbauer, F., K. Wagner, J. L. Kutok, H. Iwasaki, M. M. Le Beau, Y. Okuno, K. Akashi, S. Fiering, and D. G. Tenen. 2004. 'Acute myeloid leukemia induced by graded reduction of a lineage-specific transcription factor, PU.1', *Nat Genet*, 36: 624-30.

Ross-Innes, C. S., R. Stark, A. E. Teschendorff, K. A. Holmes, H. R. Ali, M. J. Dunning, G. D. Brown, O. Gojis, I. O. Ellis, A. R. Green, S. Ali, S. F. Chin, C. Palmieri, C. Caldas, and J. S. Carroll. 2012. 'Differential oestrogen receptor binding is associated with clinical outcome in breast cancer', *Nature*, 481: 389-93.

Sakurai, M., S. Watanuki, J. Kato, R. Hashida, Y. Yamane, D. Karigane, T. Mitsuhashi, M. Murata, H. Ueno, T. Nakazato, S. Okamoto, and T. Mori. 2018. 'Very Late Relapse of Acute Promyelocytic Leukemia 17 Years after Continuous Remission', *Intern Med*, 57: 3299-302.

Salmon, J. M., M. Bots, E. Vidacs, K. L. Stanley, P. Atadja, J. Zuber, and R. W. Johnstone. 2015. 'Combining the differentiating effect of panobinostat with the apoptotic effect of arsenic trioxide leads to significant survival benefit in a model of t(8;21) acute myeloid leukemia', *Clin Epigenetics*, 7: 2.

Sarry, J. E., K. Murphy, R. Perry, P. V. Sanchez, A. Secreto, C. Keefer, C. R. Swider, A. C. Strzelecki, C. Cavelier, C. Recher, V. Mansat-De Mas, E. Delabesse, G. Danet-Desnoyers, and M. Carroll. 2011. 'Human acute myelogenous leukemia stem cells are rare and heterogeneous when assayed in NOD/SCID/IL2Rgammac-deficient mice', *J Clin Invest*, 121: 384-95.

Schaefer, E. W., A. Loaiza-Bonilla, M. Juckett, J. F. DiPersio, V. Roy, J. Slack, W. Wu, K. Laumann, I. Espinoza-Delgado, S. D. Gore, and P. C. Phase I. I. Consortium Mayo. 2009. 'A phase 2 study of vorinostat in acute myeloid leukemia', *Haematologica*, 94: 1375-82.

Sexauer, A., A. Perl, X. Yang, M. Borowitz, C. Gocke, T. Rajkhowa, C. Thiede, M. Frattini, G. E. Nybakken, K. Pratz, J. Karp, B. D. Smith, and M. Levis. 2012. 'Terminal myeloid differentiation in vivo is induced by FLT3 inhibition in FLT3/ITD AML', *Blood*, 120: 4205-14.

Shen, Z. X., Z. Z. Shi, J. Fang, B. W. Gu, J. M. Li, Y. M. Zhu, J. Y. Shi, P. Z. Zheng, H. Yan, Y. F. Liu, Y. Chen, Y. Shen, W. Wu, W. Tang, S. Waxman, H. De The, Z. Y. Wang, S. J. Chen, and Z. Chen. 2004. 'All-trans retinoic acid/As2O3 combination yields a high quality remission and survival in newly diagnosed acute promyelocytic leukemia', *Proc Natl Acad Sci U S A*, 101: 5328-35.

Shibata, M., and M. O. Hoque. 2019. 'Targeting Cancer Stem Cells: A Strategy for Effective Eradication of Cancer', *Cancers (Basel)*, 11.

Shimokawa, M., Y. Ohta, S. Nishikori, M. Matano, A. Takano, M. Fujii, S. Date, S. Sugimoto, T. Kanai, and T. Sato. 2017. 'Visualization and targeting of LGR5(+) human colon cancer stem cells', *Nature*, 545: 187-92.

Silvennoinen, O., B. A. Witthuhn, F. W. Quelle, J. L. Cleveland, T. Yi, and J. N. Ihle. 1993. 'Structure of the murine Jak2 protein-tyrosine kinase and its role in interleukin 3 signal transduction', *Proc Natl Acad Sci U S A*, 90: 8429-33.

Smith, L. T., S. Hohaus, D. A. Gonzalez, S. E. Dziennis, and D. G. Tenen. 1996. 'PU.1 (Spi-1) and C/EBP alpha regulate the granulocyte colony-stimulating factor receptor promoter in myeloid cells', *Blood*, 88: 1234-47.

Smyth, G. K. 2004. 'Linear models and empirical bayes methods for assessing differential expression in microarray experiments', *Stat Appl Genet Mol Biol*, 3: Article3.

Stein, E. M., C. D. DiNardo, D. A. Pollyea, A. T. Fathi, G. J. Roboz, J. K. Altman, R. M. Stone, D. J. DeAngelo, R. L. Levine, I. W. Flinn, H. M. Kantarjian, R. Collins, M. R. Patel, A. E. Frankel, A. Stein, M. A. Sekeres, R. T. Swords, B. C. Medeiros, C. Willekens, P. Vyas, A. Tosolini, Q. Xu, R. D. Knight, K. E. Yen, S. Agresta, S. de Botton, and M. S. Tallman. 2017. 'Enasidenib in mutant IDH2 relapsed or refractory acute myeloid leukemia', *Blood*, 130: 722-31.

Sweet, K., R. Komrokji, E. Padron, C. L. Cubitt, J. G. Turner, J. Zhou, A. F. List, D. A. Sallman, J. L. Dawson, D. M. Sullivan, J. Chavez, B. D. Shah, and J. E. Lancet. 2020. 'Phase I Clinical Trial of Selinexor in Combination with Daunorubicin and Cytarabine in Previously Untreated Poor-Risk Acute Myeloid Leukemia', *Clin Cancer Res*, 26: 54-60.

Sykes, D. B., Y. S. Kfoury, F. E. Mercier, M. J. Wawer, J. M. Law, M. K. Haynes, T. A. Lewis, A. Schajnovitz, E. Jain, D. Lee, H. Meyer, K. A. Pierce, N. J. Tolliday, A. Waller, S. J. Ferrara, A. L. Eheim, D. Stoeckigt, K. L. Maxcy, J. M. Cobert, J. Bachand, B. A. Szekely, S. Mukherjee, L. A. Sklar, J. D. Kotz, C. B. Clish, R. I. Sadreyev, P. A. Clemons, A. Janzer, S. L. Schreiber, and D. T. Scadden. 2016. 'Inhibition of Dihydroorotate Dehydrogenase Overcomes Differentiation Blockade in Acute Myeloid Leukemia', *Cell*, 167: 171-86 e15.

Takitani, K., M. Koh, C. L. Zhu, A. Inoue, T. Kuno, H. Tanoue, M. Miyake, T. Nakagawa, and H. Tamai. 2003. 'Expression of retinoic acid receptor-target genes during retinoic acid therapy for acute promyelocytic leukemia', *Leukemia*, 17: 646-8.

Tallman, M. S., and J. K. Altman. 2009. 'How I treat acute promyelocytic leukemia', *Blood*, 114: 5126-35.

Tallman, M. S., C. Nabhan, J. H. Feusner, and J. M. Rowe. 2002. 'Acute promyelocytic leukemia: evolving therapeutic strategies', *Blood*, 99: 759-67.

Thomas, X. 2019. 'Acute Promyelocytic Leukemia: A History over 60 Years-From the Most Malignant to the most Curable Form of Acute Leukemia', *Oncol Ther*, 7: 33-65.

Tschaharganeh, D. F., W. Xue, D. F. Calvisi, M. Evert, T. V. Michurina, L. E. Dow, A. Banito, S. F. Katz, E. R. Kastenhuber, S. Weissmueller, C. H. Huang, A. Lechel, J. B. Andersen, D. Capper, L. Zender, T. Longerich, G. Enikolopov, and S. W. Lowe. 2014. 'p53-dependent Nestin regulation links tumor suppression to cellular plasticity in liver cancer', *Cell*, 158: 579-92.

van Galen, P., V. Hovestadt, M. H. Wadsworth Ii, T. K. Hughes, G. K. Griffin, S. Battaglia, J. A. Verga, J. Stephansky, T. J. Pastika, J. Lombardi Story, G. S. Pinkus, O. Pozdnyakova, I. Galinsky, R. M. Stone, T. A. Graubert, A. K. Shalek, J. C. Aster, A. A. Lane, and B. E. Bernstein. 2019. 'Single-Cell RNA-Seq Reveals AML Hierarchies Relevant to Disease Progression and Immunity', *Cell*, 176: 1265-81 e24.

Vangala, R. K., M. S. Heiss-Neumann, J. S. Rangatia, S. M. Singh, C. Schoch, D. G. Tenen, W. Hiddemann, and G. Behre. 2003. 'The myeloid master regulator transcription factor PU.1 is inactivated by AML1-ETO in t(8;21) myeloid leukemia', *Blood*, 101: 270-7.

Verhaak, R. G., C. S. Goudswaard, W. van Putten, M. A. Bijl, M. A. Sanders, W. Hugens, A. G. Uitterlinden, C. A. Erpelinck, R. Delwel, B. Lowenberg, and P. J. Valk. 2005. 'Mutations in nucleophosmin (NPM1) in acute myeloid leukemia (AML): association with other gene abnormalities and previously established gene expression signatures and their favorable prognostic significance', *Blood*, 106: 3747-54.

Wang, K., P. Wang, J. Shi, X. Zhu, M. He, X. Jia, X. Yang, F. Qiu, W. Jin, M. Qian, H. Fang, J. Mi, X. Yang, H. Xiao, M. Minden, Y. Du, Z. Chen, and J. Zhang. 2010. 'PML/RARalpha targets promoter regions containing PU.1 consensus and RARE half sites in acute promyelocytic leukemia', *Cancer Cell*, 17: 186-97.

Wang, Z. G., D. Ruggero, S. Ronchetti, S. Zhong, M. Gaboli, R. Rivi, and P. P. Pandolfi. 1998. 'PML is essential for multiple apoptotic pathways', *Nat Genet*, 20: 266-72.

Ward, S. V., T. Sternsdorf, and N. B. Woods. 2011. 'Targeting expression of the leukemogenic PML-RARalpha fusion protein by lentiviral vector-mediated small interfering RNA results in leukemic cell differentiation and apoptosis', *Hum Gene Ther*, 22: 1593-8.

Watts, J. M., X. V. Wang, R. T. Swords, E. Paietta, D. Douer, S. M. Lugar, H. F. Fernandez, J. M. Rowe, H. M. Lazarus, M. S. Tallman, and M. R. Litzow. 2016. 'Very late relapse of AML after allogeneic hematopoietic cell transplantation is often extramedullary', *Bone Marrow Transplant*, 51: 1013-5.

Weinreb, C., A. Rodriguez-Fraticelli, F. D. Camargo, and A. M. Klein. 2020. 'Lineage tracing on transcriptional landscapes links state to fate during differentiation', *Science*, 367.

Will, B., T. O. Vogler, S. Narayanagari, B. Bartholdy, T. I. Todorova, M. da Silva Ferreira, J. Chen, Y. Yu, J. Mayer, L. Barreyro, L. Carvajal, D. B. Neriah, M. Roth, J. van Oers, S. Schaetzlein, C. McMahon, W. Edelmann, A. Verma, and U. Steidl. 2015. 'Minimal PU.1 reduction induces a preleukemic state and promotes development of acute myeloid leukemia', *Nat Med*, 21: 1172-81.

Wu, D., E. Lim, F. Vaillant, M. L. Asselin-Labat, J. E. Visvader, and G. K. Smyth. 2010. 'ROAST: rotation gene set tests for complex microarray experiments', *Bioinformatics*, 26: 2176-82.

Yamamoto, K., N. Emi, T. Kajiguchi, S. Yamamori, Y. Ono, and T. Naoe. 2007. 'Eosinophils derived from acute promyelocytic leukemia cells after arsenic trioxide treatment', *Int J Hematol*, 85: 456-7.

Yanada, M., K. Matsuo, N. Emi, and T. Naoe. 2005. 'Efficacy of allogeneic hematopoietic stem cell transplantation depends on cytogenetic risk for acute myeloid leukemia in first disease remission: a metaanalysis', *Cancer*, 103: 1652-8.

Yoshida, H., K. Kitamura, K. Tanaka, S. Omura, T. Miyazaki, T. Hachiya, R. Ohno, and T. Naoe. 1996. 'Accelerated degradation of PML-retinoic acid receptor alpha (PML-RARA) oncoprotein by all-trans-retinoic acid in acute promyelocytic leukemia: possible role of the proteasome pathway', *Cancer Res*, 56: 2945-8.

Zhang, D. E., S. Hohaus, M. T. Voso, H. M. Chen, L. T. Smith, C. J. Hetherington, and D. G. Tenen. 1996. 'Function of PU.1 (Spi-1), C/EBP, and AML1 in early myelopoiesis: regulation of multiple myeloid CSF receptor promoters', *Curr Top Microbiol Immunol*, 211: 137-47.

Zheng, X., A. Seshire, B. Ruster, G. Bug, T. Beissert, E. Puccetti, D. Hoelzer, R. Henschler, and M. Ruthardt. 2007. 'Arsenic but not all-trans retinoic acid overcomes the aberrant stem cell capacity of PML/RARalpha-positive leukemic stem cells', *Haematologica*, 92: 323-31.

Zhu, J., M. H. Koken, F. Quignon, M. K. Chelbi-Alix, L. Degos, Z. Y. Wang, Z. Chen, and H. de The. 1997. 'Arsenic-induced PML targeting onto nuclear bodies: implications for the treatment of acute promyelocytic leukemia', *Proc Natl Acad Sci U S A*, 94: 3978-83.

Zhu, J., V. Lallemand-Breitenbach, and H. de The. 2001. 'Pathways of retinoic acid- or arsenic trioxide-induced PML/RARalpha catabolism, role of oncogene degradation in disease remission', *Oncogene*, 20: 7257-65.

Zhu, X., H. Zhang, M. Qian, X. Zhao, W. Yang, P. Wang, J. Zhang, and K. Wang. 2012. 'The significance of low PU.1 expression in patients with acute promyelocytic leukemia', *J Hematol Oncol*, 5: 22.

CHAPTER 8. Appendix

Article

Cell Stem Cell

Interconversion between Tumorigenic and Differentiated States in Acute Myeloid Leukemia

Graphical Abstract

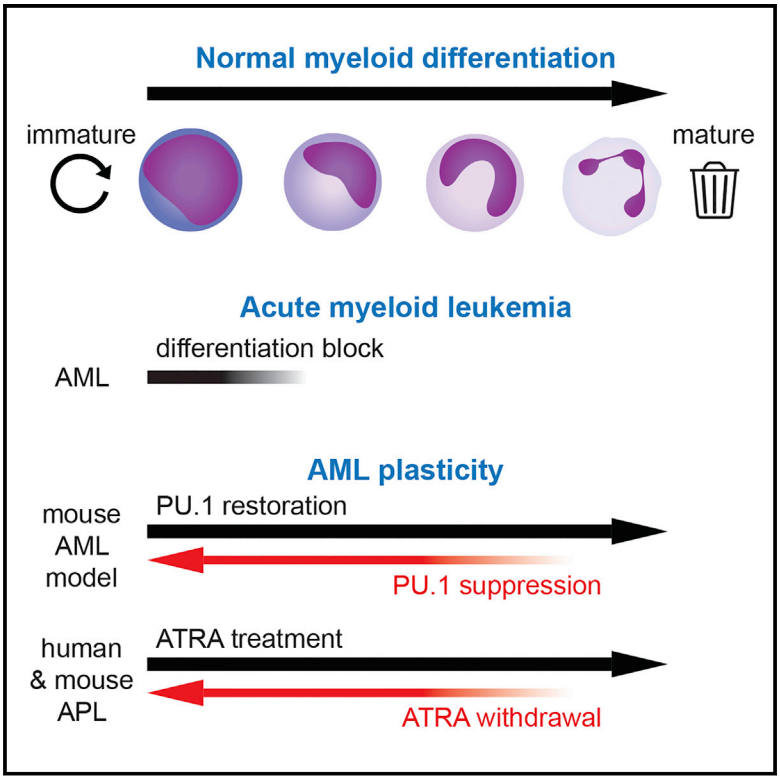

Highlights

- Reversible PU.1 knockdown provides a genetic model of AML differentiation therapy
- Mature AML-derived cells can revert to a leukemogenic state upon PU.1 suppression
- Mouse and human APL cells can regain clonogenicity after ATRA-induced differentiation

Authors

Mark D. McKenzie, Margherita Ghisi, Ethan P. Oxley, ..., Matthew E. Ritchie, Johannes Zuber, Ross A. Dickins

Correspondence

ross.dickins@monash.edu

In Brief

Intratumoral phenotypic heterogeneity in acute myeloid leukemia (AML) and many other cancers is thought to follow a hierarchical cancer stem cell model. Dickins and colleagues show here that mature, non-leukemogenic AML cells can reacquire leukemia-initiating activity and promote disease progression through de-differentiation.

McKenzie et al., 2019, Cell Stem Cell *25*, 258–272
August 1, 2019
https://doi.org/10.1016/j.stem.2019.07.001

CellPress

CellPress

Cell Stem Cell
Article

Interconversion between Tumorigenic and Differentiated States in Acute Myeloid Leukemia

Mark D. McKenzie,[1,24] Margherita Ghisi,[2,23,24] Ethan P. Oxley,[2,24] Steven Ngo,[2] Luisa Cimmino,[3] Cécile Esnault,[4,5,6] Ruijie Liu,[1] Jessica M. Salmon,[2] Charles C. Bell,[7,8] Nouraiz Ahmed,[9] Michael Erlichster,[1,10] Matthew T. Witkowski,[1,2,3,10] Grace J. Liu,[1,2,10] Michael Chopin,[11] Aleksandar Dakic,[11] Emilia Simankowicz,[2] Giovanna Pomilio,[2,12] Tina Vu,[2] Pavle Krsmanovic,[13] Shian Su,[1] Luyi Tian,[1,10] Tracey M. Baldwin,[1] Daniela A. Zalcenstein,[1] Ladina DiRago,[14] Shu Wang,[15] Donald Metcalf,[10,14] Ricky W. Johnstone,[7,8] Ben A. Croker,[15,16] Graeme I. Lancaster,[17,18] Andrew J. Murphy,[17,18] Shalin H. Naik,[1,10] Stephen L. Nutt,[10,11] Vitek Pospisil,[13] Timm Schroeder,[9] Meaghan Wall,[10,19] Mark A. Dawson,[7,8] Andrew H. Wei,[2,12] Hugues de Thé,[4,5,6] Matthew E. Ritchie,[1,10,20] Johannes Zuber,[21,22] and Ross A. Dickins[2,25,*]

[1]Molecular Medicine Division, Walter and Eliza Hall Institute of Medical Research, 1G Royal Parade, Parkville, VIC 3052, Australia
[2]Australian Centre for Blood Diseases, Monash University, Commercial Road, Melbourne, VIC 3004, Australia
[3]Department of Pathology, New York University School of Medicine, 550 1st Avenue, New York, NY 10016, USA
[4]Collège de France, PSL Research University, 75005 Paris, France
[5]INSERM U944, CNRS UMR7212, Université de Paris, Institut de Recherche Saint Louis, 75010 Paris, France
[6]Assistance Publique/Hôpitaux de Paris, Oncologie Moléculaire, Hôpital St. Louis, 75010 Paris, France
[7]Peter MacCallum Cancer Centre, Melbourne, VIC 3000, Australia
[8]Sir Peter MacCallum Department of Oncology, University of Melbourne, Parkville, VIC 3010, Australia
[9]Department of Biosystems Science and Engineering, ETH Zurich, Mattenstrasse 26, 4058 Basel, Switzerland
[10]Department of Medical Biology, University of Melbourne, Parkville, VIC 3010, Australia
[11]Molecular Immunology Division, Walter and Eliza Hall Institute of Medical Research, 1G Royal Parade, Parkville, VIC 3052, Australia
[12]Department of Clinical Haematology, The Alfred Hospital, Melbourne, VIC 3004, Australia
[13]Institute of Pathological Physiology and Biocev, First Faculty of Medicine, Charles University, Prague, Czech Republic
[14]Cancer and Haematology Division, Walter and Eliza Hall Institute of Medical Research, 1G Royal Parade, Parkville, VIC 3052, Australia
[15]Division of Hematology/Oncology, Boston Children's Hospital, Boston, MA, USA
[16]Department of Pediatrics, Harvard Medical School, Boston, MA, USA
[17]Baker Heart and Diabetes Institute, Melbourne, VIC 3004, Australia
[18]Department of Immunology and Pathology, Monash University, Commercial Road, Melbourne, VIC 3004, Australia
[19]Victorian Cancer Cytogenetics Service, St. Vincent's Hospital, 41 Victoria Parade, Fitzroy, VIC 3065, Australia
[20]School of Mathematics and Statistics, University of Melbourne, Parkville, VIC 3010, Australia
[21]Research Institute of Molecular Pathology, Campus Vienna Biocenter 1, 1030 Vienna, Austria
[22]Medical University of Vienna, 1030 Vienna, Austria
[23]Present address: INSERM U1037, Centre de Recherches en Cancérologie de Toulouse, 2 Avenue Hubert Curien, 31037 Toulouse, France
[24]These authors contributed equally
[25]Lead Contact
*Correspondence: ross.dickins@monash.edu
https://doi.org/10.1016/j.stem.2019.07.001

SUMMARY

Tumors are composed of phenotypically heterogeneous cancer cells that often resemble various differentiation states of their lineage of origin. Within this hierarchy, it is thought that an immature subpopulation of tumor-propagating cancer stem cells (CSCs) differentiates into non-tumorigenic progeny, providing a rationale for therapeutic strategies that specifically eradicate CSCs or induce their differentiation. The clinical success of these approaches depends on CSC differentiation being unidirectional rather than reversible, yet this question remains unresolved even in prototypically hierarchical malignancies, such as acute myeloid leukemia (AML). Here, we show in murine and human models of AML that, upon perturbation of endogenous expression of the lineage-determining transcription factor PU.1 or withdrawal of established differentiation therapies, some mature leukemia cells can de-differentiate and reacquire clonogenic and leukemogenic properties. Our results reveal plasticity of CSC maturation in AML, highlighting the need to therapeutically eradicate cancer cells across a range of differentiation states.

INTRODUCTION

Acute myeloid leukemia (AML) is characterized by transformed myeloid progenitors with defective maturation. It is a clinically challenging disease with ~30% 5-year survival, and certain molecular disease subtypes, such as TP53 mutant AML, are resistant to standard genotoxic therapies and are almost invariably

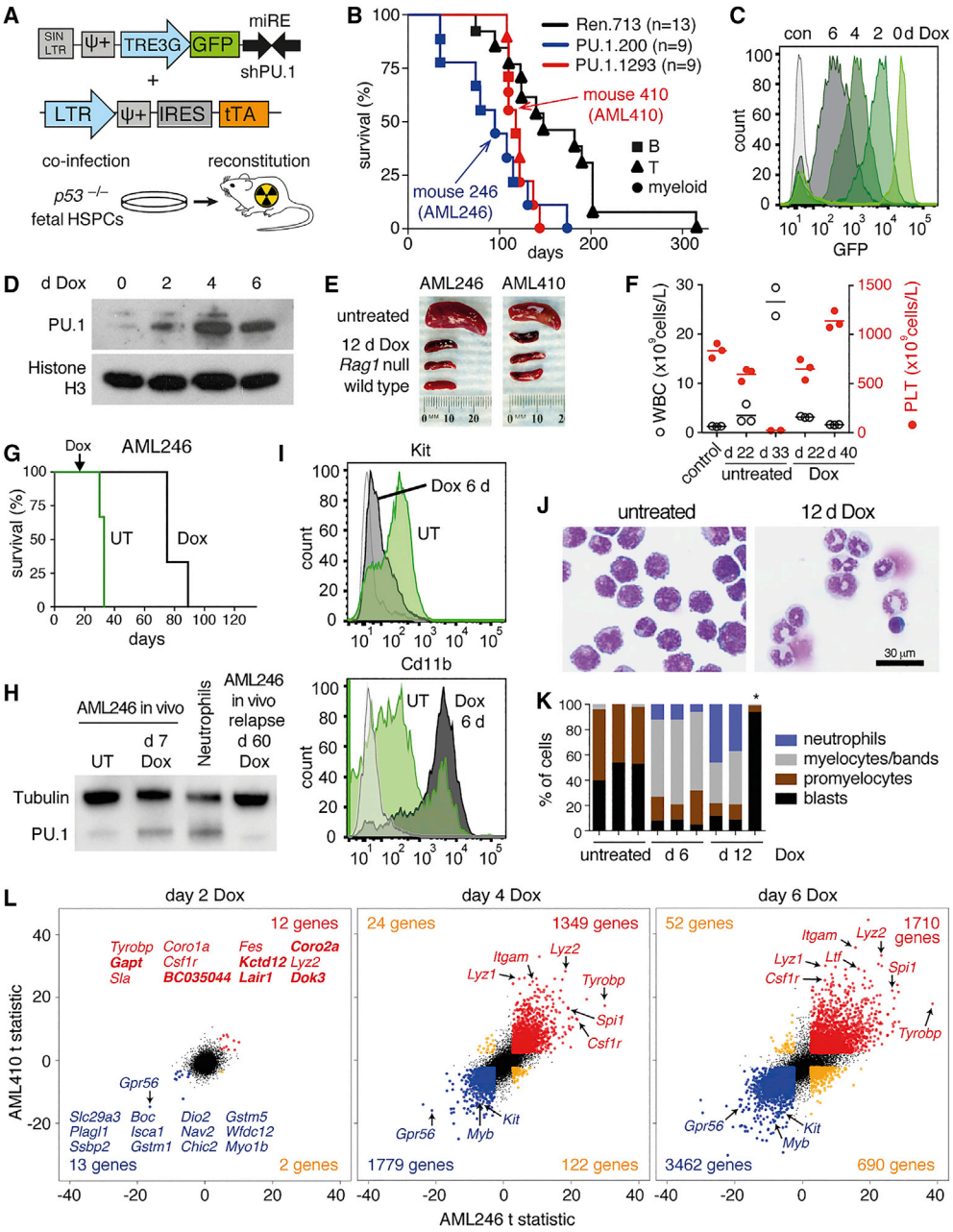

Figure 1. PU.1 Restoration *In Vivo* Triggers Differentiation and Clearance of p53-Deficient AML

(A) Strategy for generating primary AMLs driven by reversible PU.1 knockdown.

(B) Kaplan-Meier survival analysis of mice reconstituted with *Trp53*$^{-/-}$ fetal liver cells from (A) with T3GE shRNA vector indicated. Circles indicate mice developing AML. For shPU1.200 and shPU1.1293 versus shRen.713, p = 0.003 and p = 0.01, respectively (log rank test). n = 9 mice for each PU.1 shRNA and n = 13 for shRen.

(C) GFP flow cytometry of bone marrow cells of *Rag1*$^{-/-}$ mice transplanted with AML246 and Dox treated upon disease establishment.

(D) PU.1 immunoblotting of AML246 cells isolated from bone marrow of leukemic mice following Dox treatment, with histone H3 loading control.

(E) Spleens of mice transplanted with AMLs and treated with Dox following disease establishment, alongside control *Rag1*$^{-/-}$ and wild-type spleens.

(F) Counts of white blood cells (open circles) and platelets (closed red circles) for AML246 leukemic mice. Counts at day 22 indicate disease establishment (slightly elevated white blood cell [WBC] and reduced platelet [PLT] counts) and then groups of mice were either left untreated (harvested with high leukemia burden at day 33) or Dox treated and bled again at day 40. Control counts are from *Rag1*$^{-/-}$ mice.

(G) Kaplan-Meier survival analysis of mice transplanted with 10^6 AML246 cells at day 0 and either untreated (UT) or Dox treated upon disease establishment at day 22 (untreated versus Dox $p < 0.05$; log rank test). n = 3 mice per group.

(H) PU.1 immunoblot of AML246 cells isolated from bone marrow of leukemic mice following Dox treatments as indicated, with control normal mouse Cd11b$^+$Gr1$^+$ neutrophils. Tubulin loading control.

(I) Kit and Cd11b flow cytometry of AML246 cells *in vivo*, sorted from representative mice during Dox treatment. Light gray, unstained control.

(J) Cytospins of AML-derived (Cd45.2$^+$) bone marrow cells sorted from untreated leukemic mice or following 12 days Dox treatment.

(legend continued on next page)

lethal (Rücker et al., 2012). A notable exception is acute promyelocytic leukemia (APL), an AML subtype relatively resistant to standard cytotoxic therapies, where all-*trans* retinoic acid (ATRA) induces leukemia differentiation and transient remission as a single agent and is frequently curative in combination with arsenic trioxide (de Thé, 2018; Lo-Coco et al., 2013). Based on this success, several "differentiation therapies" that induce maturation of diverse AML subtypes are in development, including inhibitors of FLT3, DHODH, and the epigenetic regulator LSD1 (de Thé, 2018; Maes et al., 2018; Sexauer et al., 2012; Sykes et al., 2016). Most notable among these are recently approved targeted inhibitors of mutant IDH1 (ivosidenib) and mutant IDH2 (enasidenib), which produce clinical response in ~40% of cases harboring these mutations by promoting leukemia differentiation (Amatangelo et al., 2017; DiNardo et al., 2018; Stein et al., 2017).

Recent studies of large patient cohorts show that individual AML genomes average only 5 somatic driver mutations; however, two-thirds of cases harbor a mutation of either the transcription factors CEBPA or RUNX1, an NPM1c mutation, or a chromosomal translocation encoding an oncoprotein, including PML-RARA, AML1-ETO (RUNX1-RUNX1T1), MYH11-CBFB, or MLL (KMT2A) fusions (Ley et al., 2013; Papaemmanuil et al., 2016). These genetic alterations are mutually exclusive across patient cohorts, indicating convergent roles in disrupting transcriptional control of myeloid differentiation. Notably, several of these aberrations compromise the activity of PU.1 (SPI1), an ETS family pioneer transcription factor required for myelopoiesis (Carotta et al., 2010; DeKoter et al., 1998; Heinz et al., 2010; Iwafuchi-Doi and Zaret, 2014). In APL, the PML-RARA oncoprotein binds PU.1 protein and inhibits its function (Seshire et al., 2012; Wang et al., 2010). Mutant NPM1c (the commonest genetic lesion found in ~30% of AML cases) and AML1-ETO similarly bind and disable PU.1, and PU.1 expression is also diminished by RUNX1 alterations (Gu et al., 2018; Huang et al., 2008, 2011; Vangala et al., 2003). Hence, although *SPI1/PU.1* gene mutations are infrequent in human AML (Ley et al., 2013; Lavallée et al., 2015), its reduced activity is a common feature of the disease. Accordingly, PU.1 reduction in mice causes a myeloid differentiation block, leading to AML (Basova et al., 2014; Rosenbauer et al., 2004; Will et al., 2015).

Studies of AML in the 1990s showed that tumor cells from an individual patient can be separated into phenotypically distinct subpopulations with different tumorigenic activity (Bonnet and Dick, 1997; Lapidot et al., 1994). This provided the first evidence for a hierarchical model of cancer where tumorigenic cancer stem cells (CSCs) differentiate into relatively mature non-tumorigenic progeny (Kreso and Dick, 2014; Meacham and Morrison, 2013). Although a CSC model has been widely adopted to explain intratumoral heterogeneity in AML and other malignancies, its experimental and clinical predictions depend entirely on whether the differentiation of CSCs is reversible or irreversible. CSC maturation is generally assumed to follow a unidirectional trajectory resembling normal lineage differentiation, which provides rationale for therapeutic strategies in AML designed to specifically eradicate leukemia stem cells or induce their differentiation (de Thé, 2018; Thomas and Majeti, 2017). However, in AML and most other cancers, it remains unclear whether mature cancer cells retain the potential to contribute to tumor progression and/or disease relapse following therapy (Batlle and Clevers, 2017; Kreso and Dick, 2014; Meacham and Morrison, 2013).

Along with its essential role in promoting normal myeloid lineage differentiation, PU.1 is also required for AML differentiation triggered by ATRA or an LSD1 inhibitor (Cusan et al., 2018; Mueller et al., 2006). Given the importance of PU.1 dysregulation in the AML differentiation block, in this study we directly assess leukemia maturation state plasticity using a novel mouse AML model driven by reversible suppression of endogenous PU.1. We also examine AML maturation state interconversion in clinically relevant models of ATRA-based APL differentiation therapy.

RESULTS

PU.1 Knockdown Drives AML Development in Mice

To reversibly control endogenous PU.1 expression in AML, we employed tetracycline (tet)-regulated RNAi. *Trp53*-deficient hematopoietic stem and progenitor cells were co-transduced with two retroviral vectors: one encoding the tTA (tet-off) protein and another harboring a tet-regulated TRE3G promoter controlling a GFP-linked miR-E-based short hairpin RNA (shRNA) targeting PU.1 (T3GE-shPU1) (Figures 1A, S1A, and S1B). 6 months after transplant into lethally irradiated mice, cells expressing negative control shRNAs yielded GFP^- T lineage leukemia resembling spontaneous $Trp53^{-/-}$ disease. In contrast, recipients of shPU.1-transduced cells developed accelerated GFP^+ leukemia that was either myeloid or B lineage at similar frequency, consistent with the known tumor suppressor role of PU.1 in these lineages (Figures 1B, S1C, and S1D). Exome sequencing and spectral karyotyping of two primary myeloid leukemias revealed that AML246 (shPU1.200) was cytogenetically normal but harbored an activating N824K mutation in the receptor tyrosine kinase Kit (Figures S1E–S1H) analogous to high-risk KIT mutations in human $AML1^-ETO^+$ AML (Paschka et al., 2006). AML410 (shPU1.1293) and additional primary shPU.1 *Trp53*-deficient AMLs were karyotypically complex with subclonal genomic heterogeneity (Figures S1G–S1K), consistent with the definition of human monosomal karyotype AML, a disease subtype associated with *TP53* mutation or loss and dismal prognosis (Ley et al., 2013; Papaemmanuil et al., 2016; Rücker et al., 2012).

PU.1 Restoration Triggers AML Differentiation and Clearance *In Vivo*

Although exogenous PU.1 expression using viral vectors promotes differentiation of cultured PU.1-deficient myeloid progenitors or AML cells *in vitro* (Mueller et al., 2006; Rosenbauer et al.,

(K) Morphology scoring of cytospins from (J), with Dox treatments indicated. Each bar represents 100 cells from a single mouse. A non-responsive mouse at day 12 is asterisked.

(L) Scatterplot of differential gene expression (*t*-statistics) in AML246 versus AML410 following 2, 4, or 6 days of Dox-induced PU.1 restoration *in vivo*, comparing each to untreated (7.3-fold upregulation of Spi1/PU.1 at day 6). AML cells were sorted from 3 mice (AML246) or 2 mice (AML410) per time point. Concordantly upregulated genes (5% FDR) are in red, downregulated genes in blue, and discordant genes in orange.

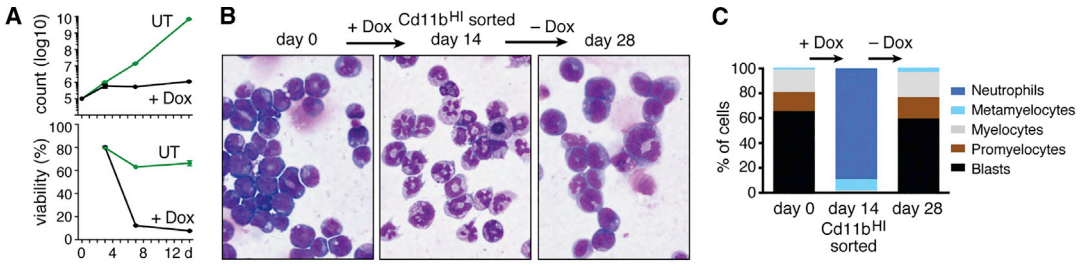

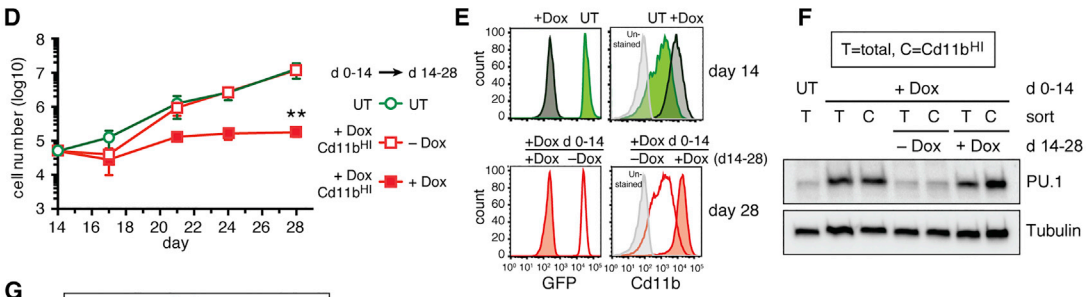

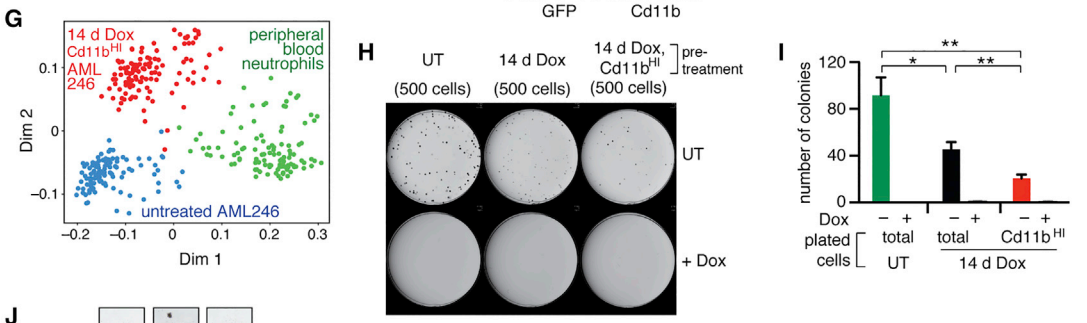

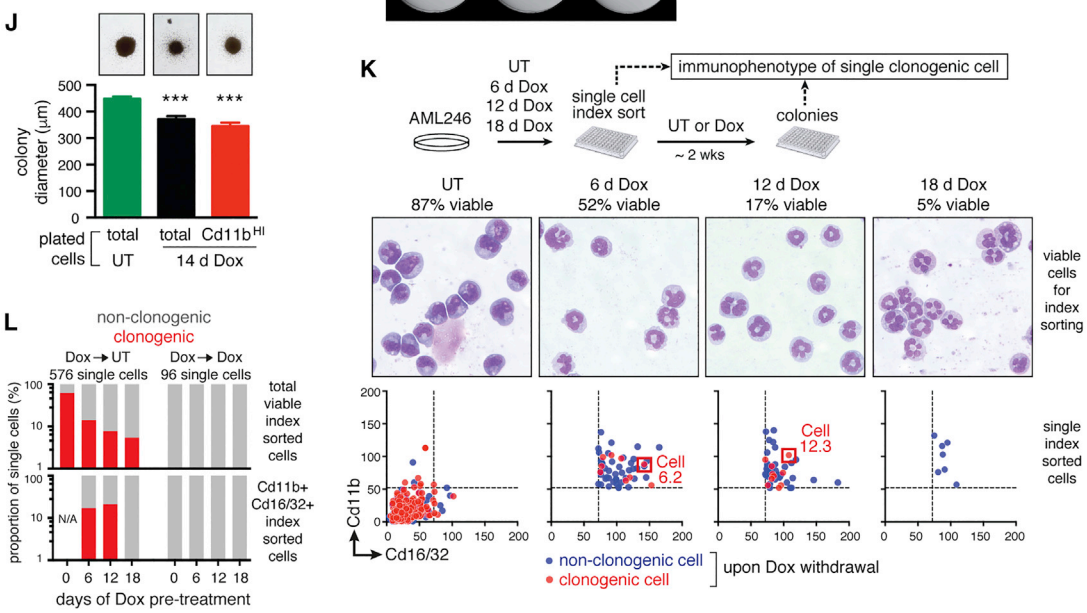

M

AML246 index clone transplants			
clone	UT Clone 0.2	6 d Dox Clone 6.2	12 d Dox Clone 12.3
leukemia	2/2 mice	2/2 mice	2/2 mice

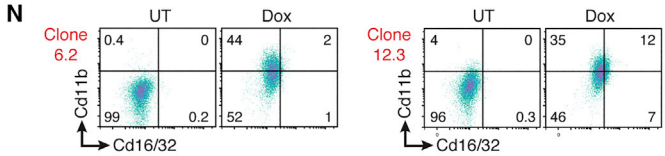

(legend on next page)

2004; Sive et al., 2016; Vangala et al., 2003), the consequences of re-engaging endogenous PU.1 activity in established AML *in vivo* are unknown. To address this, we transplanted primary AML246 or AML410 cells into cohorts of *Rag1*$^{-/-}$ (*Cd45.1*) mice (immunocompromised to allow engraftment), which developed aggressive GFP^{+} leukemia with associated splenomegaly and thrombocytopenia. Administering the tetracycline analog doxycycline (Dox) via the food suppressed GFP in AML cells, restored endogenous PU.1 protein expression, and rapidly normalized spleen size and blood counts in 11 of 12 mice examined (Figures 1C–1F and S2A–S2D). After 2 to 3 months remission, most Dox-treated mice relapsed with GFP^{+} immature AML with Dox-insensitive shRNA activation and PU.1 suppression (Figures 1G, 1H, and S2E), indicating powerful counterselection against PU.1 function.

Acute Dox treatment of leukemic mice induced immunophenotypic and morphological AML differentiation, including downregulation of the stem and progenitor marker Kit and induction of the maturation marker Cd11b (Figures 1I–1K and S2F–S2H). PU.1 restoration in AML246 *in vivo* produced AML-derived (Cd45.2^{+}) granulocytes with segmented nuclei resembling neutrophils, whereas AML410 yielded various mature myeloid cell types (Figures 1J, 1K, S2G, and S2H). We performed RNA sequencing (RNA-seq) of AML cells flow sorted from the bone marrow of multiple transplanted leukemic mice, either untreated (GFP^{high}) or Dox treated for 2, 4, or 6 days (decreasing GFP; Figures 1C and S2D). PU.1 restoration *in vivo* triggered concordant global myeloid differentiation signatures in AML246 and AML410, and MetaCore gene ontology analysis identified neutrophil signaling ($p < 10^{-8}$) and granulocyte development ($p < 10^{-5}$) as top-ranking pathways (Figures 1L and S2I–S2M; Table S1 and S2). Hence, in these 2 models of poor outcome AML, restoring PU.1 triggers leukemia differentiation and induces remission *in vivo*.

PU.1 Suppression in Differentiated AML-Derived Cells Reverts Them to an Immature, Clonogenic, Leukemogenic State

Primary AML246 and AML410 cells grew rapidly in culture, where Dox-induced PU.1 restoration markedly reduced proliferation and viability within 1 week (Figures 2A and S3A–S3C). Dox triggered *in vitro* differentiation of AML246 into neutrophil-like cells, whereas AML410 yielded multiple mature cell types, and a control AML driven by stable PU.1 knockdown was Dox insensitive (Figures S3D–S3I). We then minimized heterogeneity by deriving cultures from single AML246 cells (Figure S4A; Table S3). Similar to parental AML246, clones were highly proliferative, comprising ~60% blasts (Figures 2B–2D). Single-cell tracking and imaging showed that Dox treatment reduced GFP fluorescence within 24 h and reduced proliferation and viability within 1 week, and after 2 weeks PU.1 restoration produced morphologically differentiated cultures devoid of immature blasts and promyelocytes and mostly comprising Cd11b^{+} neutrophil-like cells (Figures 2E, 2F, and S4B–S4E). Single-cell RNA-seq along with phagocytosis and superoxide production assays indicated that *in vitro* Dox-treated AML246 cells did not fully mature into functional neutrophils (Figures 2G and S4F–S4H). However, the distinct transcriptional clustering of Cd11b^{high} Dox-treated AML246 cells relative to their untreated counterparts, both at the transcriptome level and in expression of individual myeloid maturation genes, verified homogeneous AML246 differentiation upon PU.1 restoration (Figures 2G and S4F–S4H).

We then exploited the switchable nature of RNAi to examine whether AML maturation triggered by PU.1 restoration could

Figure 2. PU.1 Suppression Reverts Mature AML-Derived Cells to a Clonogenic State

(A) Proliferation (upper) and viability (lower) of cultured AML246 cells, either UT or Dox treated. Mean ± SD of 3 technical replicates per time point.

(B) Cytospins of AML246 clone 2 cells, untreated (left), after 14 days Dox and flow sorting Cd11b^{high} cells (middle), and then after subsequent Dox withdrawal from Cd11b^{high} cells for 14 days (right).

(C) Morphology scoring of cytospins from (B). Each bar represents 100 cells.

(D) Proliferation of AML246 clone 2 cells over a 2-week period (days 14–28) in Dox-free (open symbols) or Dox (closed symbols) medium, following 2 weeks (days 0–14) pre-culture in Dox-free (circles) or Dox (squares) medium. Viable Cd11b^{high} cells were sorted after 14 days Dox treatment (days 0–14) prior to plating. Mean ± SEM of 3 or 4 biological replicates per time point. Dox pre-treated Cd11b^{high} cells: **$p < 0.01$ for − Dox versus + Dox at day 28; Student's t test with Welch's correction.

(E) GFP (left) and Cd11b (right) expression of AML246 clone 2 cells. Upper panels show untreated or Dox-treated cells at day 14. On day 14, viable Cd11b^{high} cells were sorted from Dox-treated cultures (cytospins in B), cultured for an additional 14 days with or without Dox as indicated, and then analyzed at day 28 (lower panels).

(F) PU.1 immunoblot of flow-sorted viable total "T" or viable Cd11b^{high} "C" cells following *in vitro* Dox pre-treatments (days 0–14) and treatments (days 14–28) as indicated.

(G) Multidimensional scaling plot of RNA-seq expression profiles of 112 single untreated AML246 clone 2 cells (blue), 115 Dox-treated (14 days) Cd11b^{high} cells (red), and 107 Cd11b^{+}Ly6g^{+} peripheral blood neutrophils (green).

(H) Methylcellulose colony formation of AML246 clone 2 cells, untreated or containing Dox as indicated. Plated cells were pre-treated (days 0–14) with Dox as indicated and then 500 viable cells (total or Cd11b^{high}) were plated and colonies imaged 10 days later (day 24).

(I) Colonies arising from 500 plated cells in clonogenic assays from (H) with plated cell pre-treatments indicated. Mean ± SEM of 3 independent experiments each performed in duplicate. *$p < 0.05$; **$p < 0.01$; Student's t test with Welch's correction.

(J) Colony diameter in Dox-free methylcellulose from (H). Mean ± SEM of 3 independent experiments each performed in duplicate. ***$p < 0.001$ relative to untreated; Student's t test with Welch's correction. Representative colonies arising in Dox-free methylcellulose are shown above (20× magnification).

(K) Surface Cd11b and Cd16/32 expression (lower panels) of individual Dox-treated AML246 cells index-sorted into Dox-free culture medium in multiwell plates. Single cells subsequently forming clones are shown in red and non-clonogenic cells in blue. Upper panels show morphology of viable cells at the time of index-sorting.

(L) Clonogenic frequency (red) of single index-sorted AML246 cells following a Dox treatment time course, plated into Dox-free (left) or Dox (right) medium, and showing total viable sorted cells (top) or Cd11b^{+}Cd16/32^{+} cells (bottom).

(M) Fully penetrant leukemogenesis upon transplant of untreated *Rag1*$^{-/-}$ mice with AML246 clones derived from index-sorted single cells in (K).

(N) Cd11b and Cd16/32 profile of single cell clones from (K) expanded in Dox-free medium and Dox treated for 4 days before analysis.

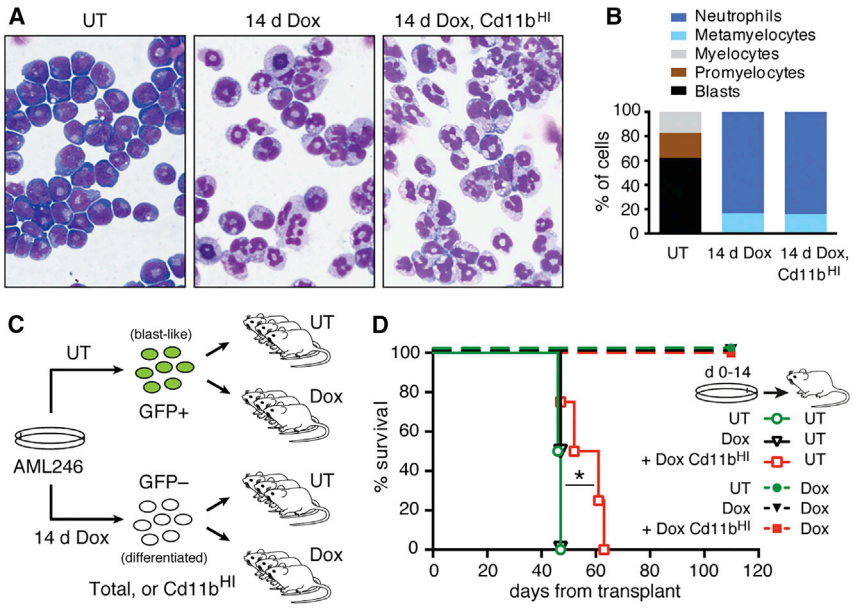

Figure 3. PU.1 Suppression in Mature AML-Derived Cells Restores Their Leukemogenicity

(A) Cytospins of AML246 clone 2 cells at the time of transplant into recipient mice. Cells from untreated (left) or 14 day Dox pre-treated cultures (middle and right) were flow sorted for viability and further sorted based on high Cd11b expression (right).

(B) Morphology scoring of cytospins from (A). Each bar represents 100 cells.

(C) Experimental strategy to examine reversible AML differentiation *in vivo*. 10^5 viable cells were transplanted for each condition.

(D) Kaplan-Meier survival analysis of untreated (solid lines) or Dox-treated (dashed lines) mice transplanted with 10^5 viable AML246 clone 2 cells that were either untreated (green circles) or pre-treated with Dox *in vitro* for 14 days (black triangles) and further sorted for Cd11b^{high} cells (red squares). Untreated mice transplanted with Dox total cells versus Dox Cd11b^{high} cells *$p < 0.05$; log rank test. For all transplanted cells, untreated mice versus Dox-treated mice $p < 0.01$; log rank test. $n = 4$ mice per group. Dox-treated recipients remained disease free for >6 months.

be reversed. Culturing sorted Cd11b^{high} cells in Dox for 14 additional days (total 28 days) maintained their PU.1 expression and mature phenotype (Figures 2D–2F, S4I, and S4J). In striking contrast, withdrawing Dox from sorted Cd11b^{high} cells at day 14 induced GFP within 24 h, reduced PU.1 and Cd11b expression, and within 1 or 2 weeks yielded proliferating blast cultures (Figures 2B–2F, S4C, and S4J). We determined the frequency whereby PU.1 suppression could revert differentiated AML cells to proliferative blasts by assessing mature AML cell clonogenicity in methylcellulose. Approximately 20% of untreated control AML246 cells formed blast colonies 10 days after plating, which was prevented by adding Dox to the methylcellulose (Figures 2H and 2I). Remarkably, sorted Cd11b^{high} (~90% neutrophil-like) cells from 14-day Dox cultures were only 4-fold less clonogenic than untreated cells in Dox-free methylcellulose, with ~5% of cells forming colonies (Figures 2H and 2I). Colonies derived from differentiated cells were indistinguishable in shape but smaller than those seeded by untreated AML cells, consistent with delayed re-engagement of proliferation following Dox withdrawal (Figures 2H–2J). Similar reversion was observed with primary AML246 cultures and an independent AML246 clone (Figures S4D, S4E, and S5A–S5J).

To verify de-differentiation at the single-cell level, we isolated individual AML246 cells after various stages of Dox treatment that progressively increased co-expression of the maturation markers Cd11b and the Fc gamma receptors Cd16/32 (Evrard et al., 2018) and lowered viability (Figures 2K and S5K). Single cells were index-sorted into multiwell plate liquid cultures to assess their clonogenicity. Increasing initial Dox treatment duration reduced AML246 clonogenicity upon subsequent Dox withdrawal; however, 15%–20% of individual Cd11b^{+}Cd16/32^{+} cells from 6- to 12-day Dox-treated cultures formed rapidly growing clones upon Dox withdrawal (Figures 2K and 2L; AML410 results in Figure S5L). Emergent AML246 clones were blast-like, Cd11b^{low}Cd16/32^{low}, leukemogenic, and again differentiated with Dox re-exposure, verifying that de-differentiation of AML246 cells was not due to clonal loss of Dox response (Figures 2M and 2N). Only 5% of AML246 cells were viable after 18 days Dox, and Cd11b^{+} Cd16/32^{+} cells sorted from these cultures failed to form colonies upon Dox withdrawal (Figures 2K and 2L). Together, these results verify that withdrawing Dox allows reversion of individual differentiated AML246 cells to a clonogenic and leukemogenic state but also suggest a potential maturation threshold beyond which de-differentiation is negligible. Importantly, in all assays, continued Dox treatment ablated AML246 clonogenicity.

When transplanted into recipient mice, differentiated AML246 clone cells derived from 2-week Dox cultures (bulk or Cd11b^{high} sorted) produced fully penetrant GFP^{+} leukemia with similar or slightly longer latency to untreated cells, even though they uniformly resembled neutrophils or metamyelocytes and were bereft of immature blasts and (pro)myelocytes at the time of injection (Figures 3A–3D and S5M–S5P). Dox-treated recipients remained disease-free, consistent with tumor suppression by PU.1 (Figure 3D). Hence, reversing transcriptional and phenotypic differentiation of AML cells through PU.1 inhibition can restore their leukemogenicity.

Plasticity of PU.1 Pioneering Transcription Factor Functions in AML

To examine mechanisms of AML246 differentiation and de-differentiation, we tracked dynamic transcription (RNA-seq), PU.1 DNA binding (chromatin immunoprecipitation [ChIP]-seq), and chromatin accessibility (ATAC-seq) at 4-day intervals over 24 days comprising 12 days culture with Dox, sorting of Cd11b^{high} neutrophil-like cells, and then 12 days culture without Dox (Figures 4A, 4B, S6A, and S6B). Dox induced Spi1/PU.1 mRNA 3.9-fold (induction rank 189) and protein at day 4, with levels remaining high at days 8 and 12 despite some fluctuation (Figures 4C–4E). This triggered transcriptional changes in thousands of genes at day 4 with diminishing changes at days 8

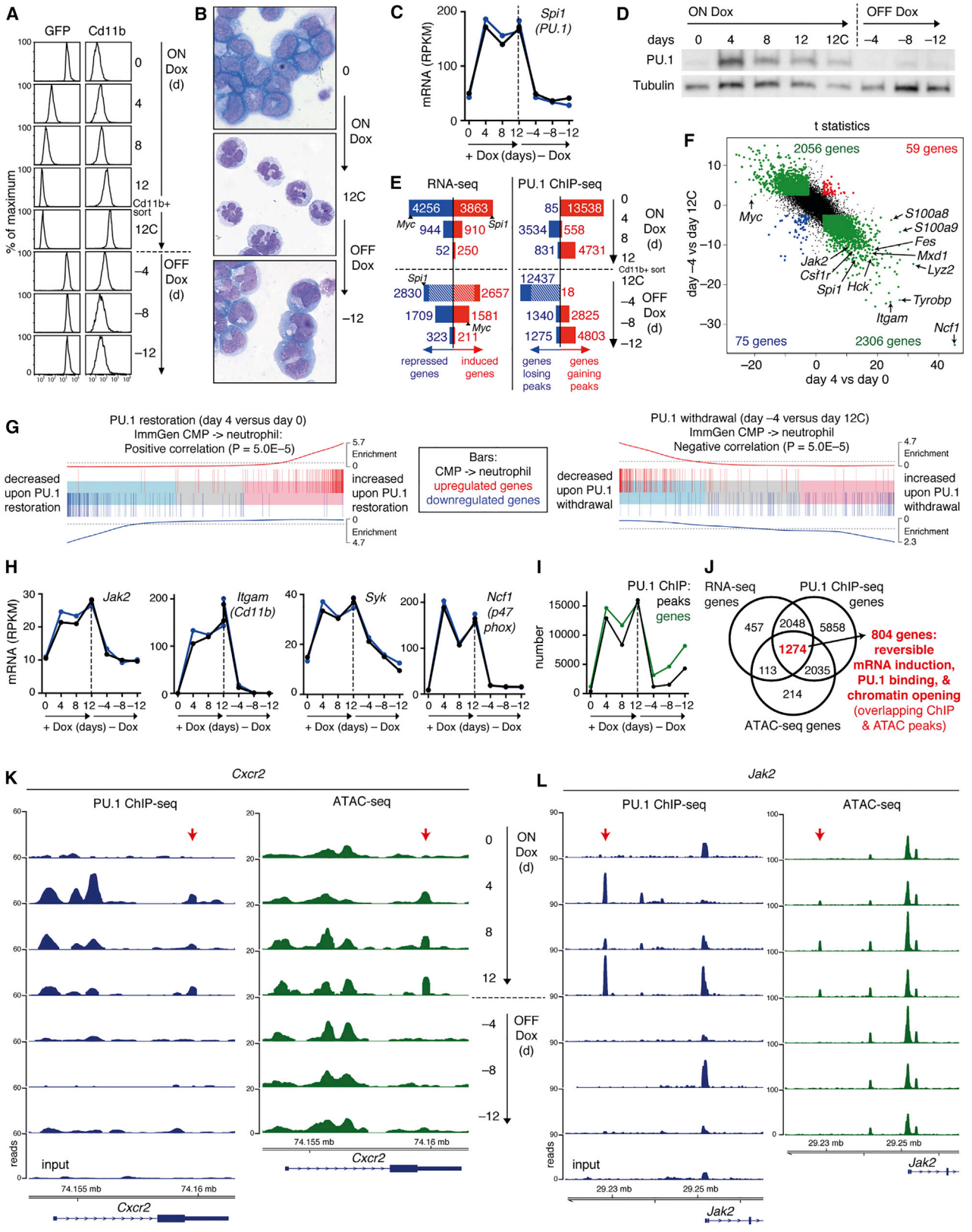

(legend on next page)

and 12 (Figures 4C–4E). In contrast, Dox withdrawal from sorted Cd11b^{high} cells rapidly and synchronously induced shRNA-linked GFP expression, reducing PU.1 mRNA (3.9-fold; repression rank 62) and protein to initial leukemogenic levels within 4 days (Figures 4A and 4C–4E).

Remarkably, the majority of the transcriptional remodeling initially triggered by PU.1 restoration in AML246, including a highly significant myeloid maturation signature, was rapidly reversed upon PU.1 repression in mature AML-derived cells (shaded bars in Figure 4E; Figures 4F and 4G). Of 3,863 genes induced at day 4 Dox (5% false discovery rate [FDR]), 2,306 (60%) had reduced expression 4 days after Dox withdrawal (Figures 4E and 4F). Correlating gene expression with Spi1 across the entire time course revealed that PU.1 not only induces but is then required to sustain transcription of key granulopoietic cytokine response genes, including the GM-CSF receptor β chains Csf2rb/Csf2rb2, Jak1, Jak2, Tyk2, Stat3, and Hcls1, along with important neutrophil function genes, including the integrins Itgam/Cd11b and Itgb2/Cd18 (together comprising Mac1), their adaptor Tyrobp/DAP12, and their signaling kinase Syk (Figures 4F, 4H, S6C, and S6D). Comparing our mouse Spi1-correlated transcriptomic data to human SPI1-correlated genes from a recent profiling study of 173 AML patient samples (Ley et al., 2013) identified conserved global PU.1-correlated gene expression (Pearson's $r = 0.2$; $p < 2.2E-16$), with orthologs of many top PU.1-linked transcriptionally plastic genes in AML246 being strongly SPI1 correlated in human AML, including TYROBP, NCF1, ITGAM, and HCLS1 (Figures S6E–S6G).

Matched time course analysis of AML246 PU.1 ChIP showed the number of PU.1-bound genes (peak within 50 kb of the transcription start site) tracked with levels of PU.1 mRNA and protein throughout, with 13,538 genes acquiring peaks and 12,437 genes losing peaks upon acute PU.1 restoration and withdrawal, respectively (Figures 4E, 4I, and S6H). Acute PU.1 suppression in mature AML cells markedly reduced but did not ablate its binding to the *Spi1* upstream enhancer (URE) and adjacent enhancers (Figure S6I), indicating partial disruption of positive PU.1 autoregulation (Okuno et al., 2005).

Integrating ChIP-seq and ATAC-seq time course data identified genomic locations where PU.1 binding opens chromatin and subsequent PU.1 release reduces chromatin accessibility at the same site. Combining this analysis with dynamic transcriptomic data identified 804 genes where PU.1 restoration triggered simultaneous PU.1 DNA binding (mostly in non-promoter regulatory sequences), chromatin opening, and transcriptional activation, and subsequent PU.1 withdrawal caused PU.1 release, chromatin closing, and transcriptional repression (Figure 4J; Table S4). These 804 transcriptionally plastic PU.1-activated targets were enriched for genes involved in myeloid differentiation and granulocyte function (Figure S6J). These included the chemokine receptor Cxcr2 that promotes neutrophil egress from the bone marrow (Eash et al., 2010; Figure 4K), the key myeloid cytokine signal transducer Jak2 (Figure 4L), and the NADPH oxidase components Ncf1/p47phox, Ncf2/p67phox, Ncf4/p40phox, and Rac2. Building on the known role of PU.1 as a pioneer factor that establishes the myeloid lineage gene expression program (Carotta et al., 2010; Heinz et al., 2010; Iwafuchi-Doi and Zaret, 2014), these results demonstrate that the continuous presence of PU.1 at regulatory sequences, especially enhancers, is required to maintain open chromatin and expression of hundreds of its target genes in mature AML-derived cells.

Differentiated APL Cells Are Leukemogenic upon Cessation of Retinoic Acid Therapy *In Vivo*

In human APL, the PML-RARA fusion oncoprotein physically interferes with PU.1, and all-*trans* retinoic acid (ATRA) treatment triggers APL differentiation (Mueller et al., 2006; Seshire et al., 2012; Wang et al., 2010). However, several studies have shown that differentiation is insufficient for APL eradication (Ablain et al.,

Figure 4. PU.1 Reversibly Regulates Chromatin Accessibility and Expression of Critical Myeloid Maturation Genes in AML

(A) Time course of GFP and Cd11b expression of AML246 clone 2 cells over 12 days Dox treatment followed by Cd11b-high sorting and 12 days Dox withdrawal.

(B) Cytospins of cells from (A).

(C) Time course of Spi1/PU.1 expression (RNA-seq RPKM for 2 replicates), with a dotted line indicating Dox withdrawal.

(D) PU.1 immunoblotting of cells from (A), with tubulin loading control.

(E) Changes in gene expression (5% FDR; left) and PU.1 DNA binding (right) during each 4-day interval across the time course (day 4 versus day 0, day 8 versus day 4, and so on). For day 12C to day −4 (acute Dox withdrawal), shaded regions indicate the proportion of genes where changes in expression or binding reverse changes from day 0 to day 4 (acute Dox treatment). Between day 12 (unsorted) and 12C (Cd11b-high sorted), there was only one differentially expressed gene (5% FDR).

(F) Scatterplot of differential gene expression (*t*-statistics) in AML246 time course cells from day 0 to day 4 (acute Dox treatment) versus day 12C (Cd11b^{high}-sorted) to day −4 (acute Dox withdrawal) based on gene expression from 2 samples per time point. Genes where acute Dox-induced expression changes were reversed upon Dox withdrawal (5% FDR) are green, and genes upregulated or downregulated in both transitions are red and blue, respectively.

(G) Gene set analysis barcode plots for RNA-seq differential gene expression in the time course analysis, showing acute (4 days Dox) PU.1 restoration (left) and subsequent acute (4 days Dox withdrawal) PU.1 suppression (right). Differential expression is shown as a shaded rectangle with genes horizontally ranked by moderated t-statistic. Downregulated genes are shaded blue ($t < 1$) and upregulated genes pink ($t > 1$). Overlaid are sets of the top 200 genes with higher (red bars) or lower (blue bars) expression in neutrophils relative to common myeloid progenitors (CMPs) from the ImmGen expression database (Heng and Painter, 2008). Red and blue traces above and below the barcode represent a moving average of relative enrichment calculated using a tri-cube weight function. p value was computed by the roast method (Wu et al., 2010) using both up- and downregulated genes.

(H) Time course mRNA expression as described in (C) for Jak2, Itgam, Syk, and Ncf1.

(I) Number of PU.1 ChIP-seq peaks (black) and associated genes (green) over the time course.

(J) Venn diagram showing "RNA-seq genes," where expression rises at day 4 (staying up at days 8 and 12) and then falls at day −4 (staying down at day −8 and −12) and "ChIP-seq genes" and "ATAC-seq genes," where peaks are gained then lost at the same time points. For 804 of the common 1,274 genes, ATAC and ChIP peaks overlap, indicating PU.1 directly maintains open chromatin.

(K and L) PU.1 ChIP-seq (left; including input controls) and ATAC-seq (right) tracks for *Cxcr2* (K) and *Jak2* (L). Time course samples are ordered top down with dotted line indicating Dox withdrawal. Arrows indicate enhancers with dynamic, overlapping ChIP and ATAC peaks.

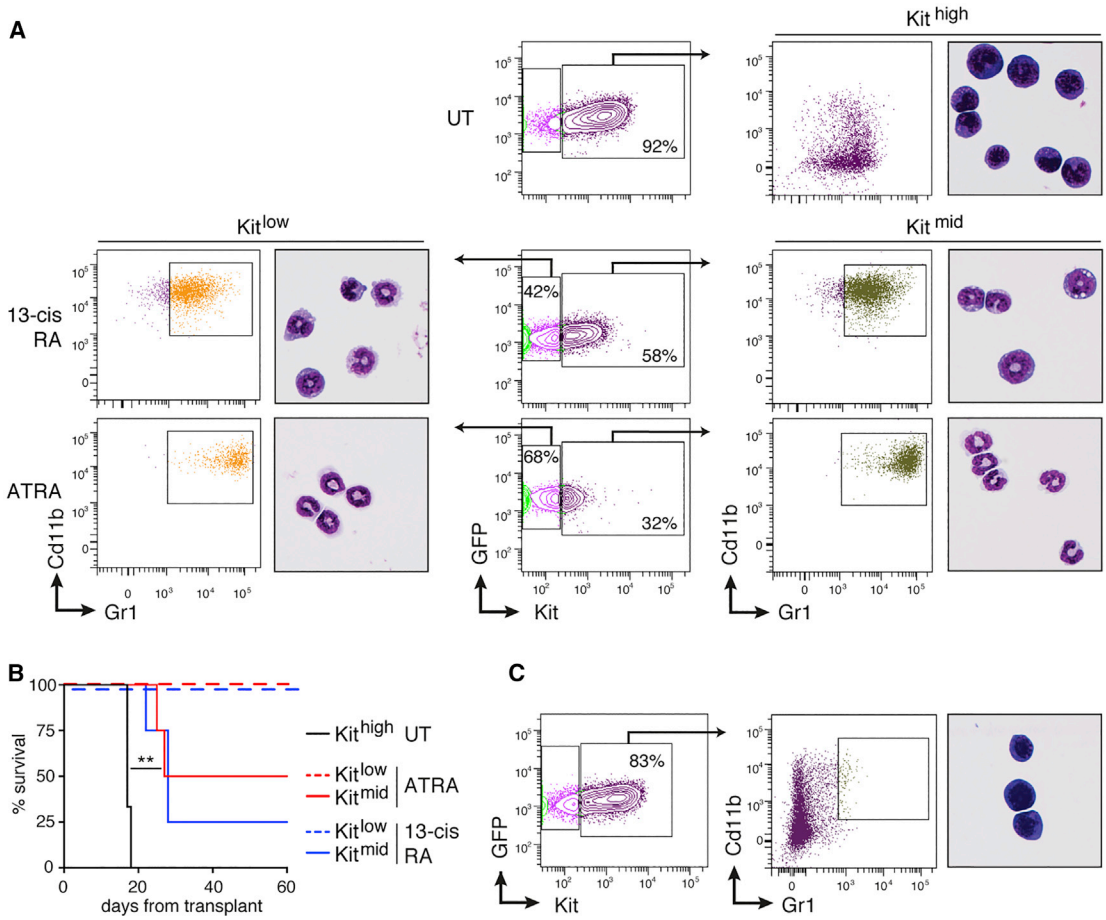

Figure 5. Mature APL Cells Become Leukemogenic upon Cessation of ATRA Differentiation Therapy

(A) Flow cytometry profiles of bone marrow cells from primary APL mice (middle panels), either untreated (UT) or treated for 4 days with 13-*cis* RA or ATRA prior to harvest. Gr1/Cd11b expression of GFP^{+}Kit^{low} (left) or GFP^{+}Kit^{mid} (right) cells is shown along with matched cytospins of Gr1^{high}Cd11b^{high} cells from the indicated sort gate.

(B) Kaplan-Meier survival analysis of untreated secondary recipient mice transplanted with 10^5 sorted APL cells from (A). Mice transplanted with 13-*cis* RA cells or ATRA cells (both n = 4) versus untreated cells (n = 3) **p < 0.01; log rank test.

(C) Flow cytometry profile and cytospin as described in (A) for bone marrow cells from leukemic secondary recipient mice.

2013; de Thé, 2018; Lallemand-Breitenbach et al., 1999; Nasr et al., 2008); therefore, we hypothesized that ATRA-induced APL maturation might be reversible upon ATRA withdrawal.

To examine APL plasticity *in vivo*, we utilized a transplantable, p53 wild-type APL mouse model driven by transgenic PML-RARA (Lallemand-Breitenbach et al., 1999). APL blasts stably expressing GFP were transplanted into syngeneic recipient mice, which developed Kit^{high}Gr1^{low}Cd11b^{low} leukemia (Figure 5A). Treating mice for 4 days with ATRA or its isomer 13-*cis* retinoic acid (13-*cis* RA; isotretinoin) (Warrell et al., 1993) triggered immunophenotypic APL maturation *in vivo*, and flow sorted Gr1^{high}Cd11b^{high} bone marrow APL cells that were either Kit^{mid} or Kit^{low} had uniformly neutrophil-like morphology (Figures 5A and S7A). Notably, transfer of 10^5 differentiated Kit^{mid}Gr1^{high}Cd11b^{high} APL cells into the tail vein of secondary recipient mice caused disease in the majority within 4 or 5 weeks, only 1 or 2 weeks slower than mice engrafted with untreated APL cells (Figure 5B). Secondary leukemias had a similar immature immunophenotype and morphology to untreated primary disease (Figure 5C). In contrast, transplanted Kit^{low}Gr1^{high}Cd11b^{high} APL cells were not leukemogenic despite similar differentiated morphology (Figures 5A and 5B). Together, these results are consistent with maturational reversion upon retinoic acid withdrawal *in vivo* but also suggest a differentiation tipping point associated with loss of leukemogenicity.

Reversible Retinoic-Acid-Induced Differentiation of Human APL Cell Lines and Primary Samples

To assess maturation state plasticity in human APL, we first examined the well-characterized t(15;17) promyelocytic leukemia cell line NB4 (Lanotte et al., 1991), where ATRA treatment reduces proliferation and viability and induces granulocytic morphological changes and the mature surface proteins CD11B and CD15 (Figures 6A and 6B). We examined NB4 cell clonogenic frequency by single-cell index-sorting. Over time, ATRA treatment reduced viability but also progressively reduced the clonogenicity of remaining viable cells upon ATRA withdrawal; however, 1%–3% of single CD11B^{high}CD15^{high} cells

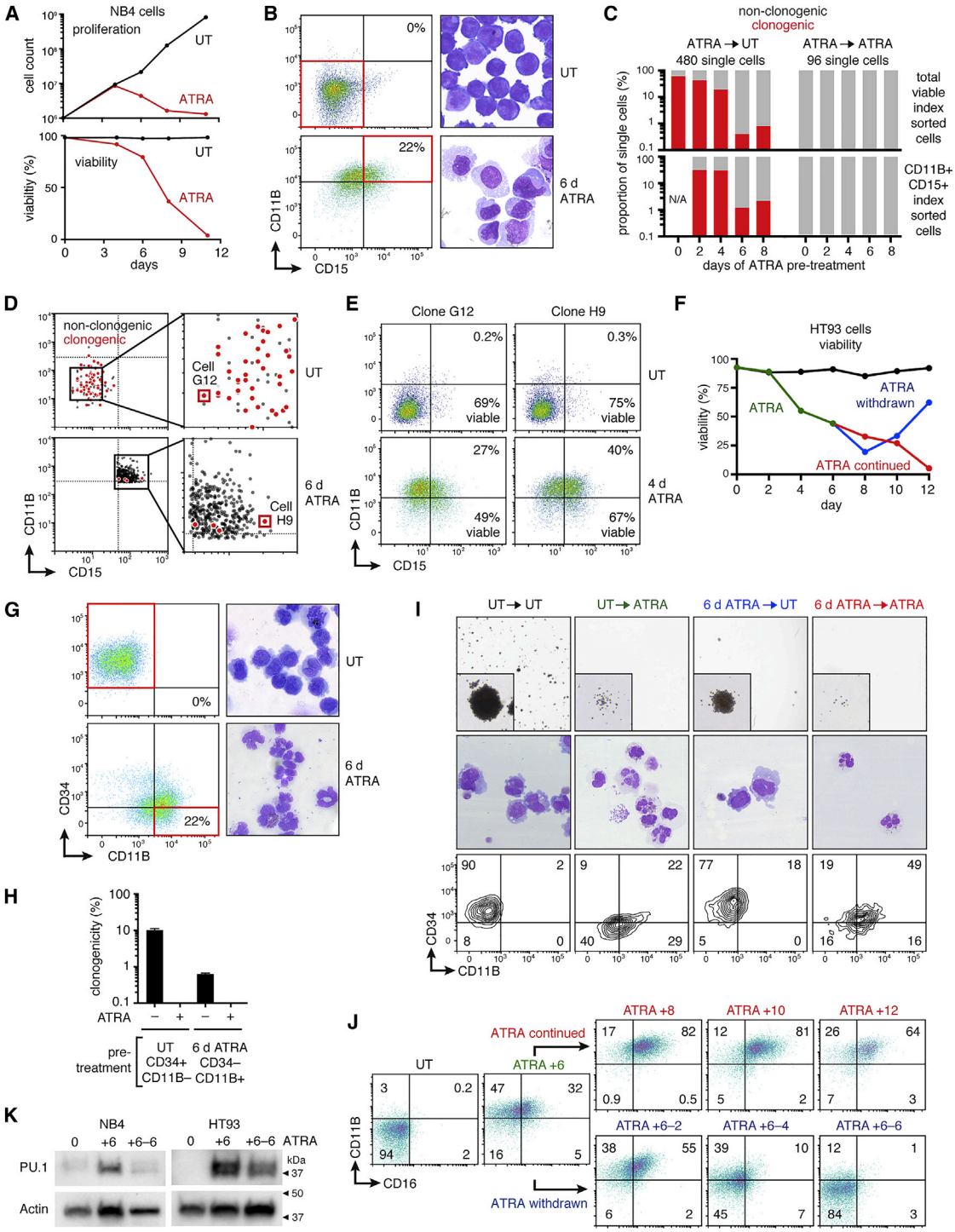

Figure 6. ATRA-Induced Differentiation of Human APL Cell Lines Is Reversible

(A) NB4 cell proliferation and viability time course upon treatment with 1 μM ATRA.

(B) CD15/CD11B flow cytometry of untreated (UT) or 6-day ATRA-treated NB4 cells showing sort gates in red (left) and sorted cell cytospins (right).

(C) Clonogenic frequency (red) of single index-sorted NB4 cells following an ATRA time course, with total viable sorted cells (top) or $CD11B^{+}CD15^{+}$ cells (bottom) plated into ATRA-free (left) or ATRA (right) medium.

(D) Surface CD11B and CD15 expression of individual untreated (top) or ATRA-treated (bottom) NB4 cells index-sorted into ATRA-free culture medium in multiwell plates, with subsequently clonogenic cells shown in red and non-clonogenic cells in black.

(E) CD15/CD11B flow cytometry of clones G12 and H9 derived from single cells G12 and H9 in (D). Clones were expanded in ATRA-free medium and then ATRA treated for 4 days before analysis.

(legend continued on next page)

isolated from 6- to 8-day ATRA cultures generated rapidly growing clones (Figures 6C and 6D). These clones lacked surface CD11B and CD15, but these markers were again induced upon subsequent ATRA exposure (Figure 6E), verifying that mature NB4 de-differentiation was not caused by clonal loss of ATRA response. Indeed, ATRA continuation ablated NB4 clonogenicity in all assays (Figures 6C, S7B, and S7C). In methylcellulose culture, the clonogenic frequency of untreated NB4 cells (~50%) and the reversion frequency of immunophenotypically mature cells upon ATRA withdrawal was similar to liquid culture (Figures S7B and S7C). Notably, methylcellulose colonies derived from differentiated NB4 cells were smaller but similarly shaped to colonies derived from untreated cells, suggesting delayed resumption of proliferation (Figures S7D and S7E).

We also analyzed another human t(15;17) APL cell line HT93 (Kishi et al., 1998; Mueller et al., 2006), which we found to be genetically and functionally *TP53* wild-type in contrast to NB4 cells (Figures S7F–S7H). ATRA-induced differentiation of HT93 cells was associated with reduced viability, downregulation of the stem cell marker CD34, and induction of CD11B, and flow sorted $CD34^{-}CD11B^{+}$ cells uniformly displayed segmented nuclei reminiscent of mature granulocytes (Figures 6F and 6G). Notably, both untreated $CD34^{+}CD11B^{-}$ and ATRA-treated mature $CD34^{-}CD11B^{+}$ flow sorted HT93 cells formed tight blast-like colonies upon ATRA withdrawal in methylcellulose at frequencies of ~10% and 0.5%, respectively (Figures 6H and 6I). Analysis of cells isolated from ATRA-free methylcellulose showed that colonies seeded by mature plated cells had reacquired CD34 expression, lost CD11B expression, and reverted to a blast-like morphology (Figure 6I). In methylcellulose-containing ATRA, only small dispersed groups of cells persisted, and the few cells isolable were $CD34^{-}CD11B^{high}$ and morphologically mature (Figure 6I). HT93 cells were refractory to single-cell index-sorting assays; however, in bulk liquid culture we found that ATRA withdrawal after 6 days of treatment reversed ATRA-induced loss of viability and led to de-induction of the myeloid maturation markers CD15, CD16, and CD11B within 4–6 days (Figures 6J, S7I, and S7J). Immunophenotypic reversion proceeded rapidly and synchronously across the entire cell population (Figures 6J, S7I, and S7J), consistent with *en masse* de-differentiation of mature cells rather than selective expansion of a persistent immature subpopulation. Notably, induction of PU.1 protein by ATRA in NB4 and HT93 cells was partially reversed 6 days after ATRA withdrawal (Figure 6K).

We then examined differentiation plasticity in primary *ex vivo* bone marrow cultures from six different APL patients with ~90% leukemia blast counts. Although most leukemias failed to survive even in optimized culture conditions, samples APL1 and APL3 remained viable for several weeks. In these samples, 7-day ATRA exposure produced a discrete population of mature cells with elevated surface CD11B and CD15 (Figures 7A and S7K). ATRA withdrawal from bulk APL3 cultures resulted in loss of surface CD11B/CD15; however, the APL-derived population was partly obscured by outgrowth of normal bone marrow cells (Figure S7K). To circumvent this, for sample APL1 we flow sorted differentiated APL cells after 7 days ATRA and then monitored surface CD15 upon continued ATRA exposure or ATRA withdrawal. Although prolonged ATRA treatment reinforced CD15 induction, ATRA withdrawal reverted CD15 expression to levels observed in parallel cultures that had never been treated (Figure 7B). This occurred without major changes in proliferation or viability (Figure 7C), consistent with *en masse* de-differentiation of cultured APL1 cells.

DISCUSSION

Using several models of AML differentiation therapy, we have demonstrated that mature leukemia cells can reacquire clonogenic and leukemogenic properties through de-differentiation. Leukemia maturation triggered by PU.1 restoration or ATRA treatment causes widespread cell death and dramatically reduces the clonogenic frequency of remaining viable cells. Yet in several contexts, we identify a minor subpopulation of viable differentiated cells that can propagate disease by reverting to an immature state. Our results do not suggest that "terminal" differentiation can be reversed—indeed, in some contexts, we identify maturation thresholds that preclude AML reversion. However, we observe interconversion across a broad range of transcriptional, immunophenotypic, and morphological states, in contrast to previous studies of leukemia-initiating cells that often stratify maturation stages using one or two surface markers (Bonnet and Dick, 1997; Kreso and Dick, 2014; Lapidot et al., 1994; Meacham and Morrison, 2013). This unforeseen AML maturation state plasticity suggests that leukemia-propagating cells may not exist as a distinct immunophenotypically or morphologically definable cell type, adding important perspective to the CSC model originally founded on this disease and subsequently generalized to solid cancers.

In colorectal cancer models, it was recently shown that CSC ablation can trigger niche-dependent reversion of differentiated cancer cells to a tumor-propagating state (de Sousa e Melo et al., 2017; Shimokawa et al., 2017). Intestinal tumor cell plasticity resembles that of normal intestinal committed progenitor cells, which can revert to a stem cell phenotype upon exposure

(F) Viability of HT93 cultures comparing untreated (black) to 6 days ATRA treatment (green) followed by 6 days of either ATRA continuation (red) or withdrawal (blue).
(G) CD34/CD11B profiles of HT93 cells showing sort gates in red (left; $CD34^{+}CD11B^{-}$ for UT; $CD34^{-}CD11B^{+}$ for ATRA) and cytospins of sorted cells (right).
(H) Clonogenic frequency of sorted HT93 cells from (G) in methylcellulose with or without ATRA as indicated and imaged 19 days later. Mean ± SEM of 3 plates per condition, from one of two similar experiments.
(I) HT93 methylcellulose colony morphology (upper panels; with individual colony insets) and corresponding cells washed out from methylcellulose (middle panels: cytospins; lower panels: CD34/CD11B profiles). For each column, labels at left indicate initial sorted populations (UT: $CD34^{+}CD11B^{-}$ cells; ATRA: $CD34^{-}CD11B^{+}$ cells) and arrows indicate transfer into methylcellulose with or without ATRA.
(J) CD11B/CD16 profiles of HT93 cells described in (F) showing response to initial ATRA treatment and subsequent continuation (red) or withdrawal (blue).
(K) PU.1 immunoblotting of NB4 (left) or HT93 (right) cells after 6 days ATRA treatment and then 6 days after ATRA withdrawal from the same cells. Actin loading control is shown.

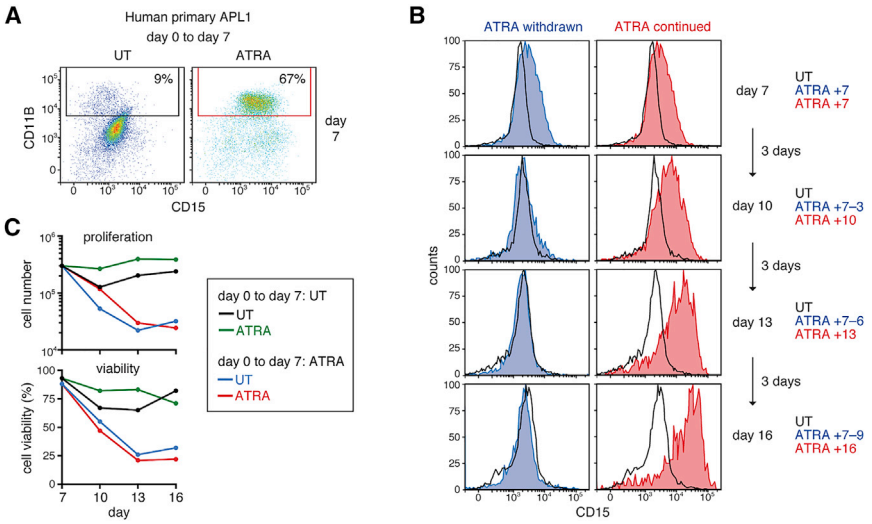

Figure 7. Immunophenotypic Reversion of Primary Human APL Cells following ATRA Withdrawal

(A) CD11B/CD15 flow cytometry of primary human APL cells (patient APL1) after 7 days *ex vivo* culture in the absence (UT) or presence of ATRA, with the sorting gate for mature APL-derived cells shown in red.

(B) CD15 expression of sorted CD11B-high ATRA-treated APL1 cells from (A) at 3-day intervals following ATRA withdrawal (blue) or continuation (red) from day 7 onward. Black line indicates control cells from parallel UT cultures.

(C) Proliferation and viability of primary APL1 cells cultured with or without ATRA from day 7 to day 16, following 7 day pre-treatments (days 0–7) as indicated in the legend.

to crypt base niche signals (Batlle and Clevers, 2017). In contrast, our findings in AML do not imply that the maturation of normal myeloid lineage progenitors is reversible, rather they suggest that CSC plasticity in leukemia is a unique consequence of mutational deregulation of a pioneer transcription factor. We find that simply perturbing endogenous PU.1 activity can regulate AML state interconversion by reversibly modulating enhancer accessibility of its direct target genes *en masse*. The abundance and activity of PU.1 in myeloid lineage cells is influenced by myeloid cytokines along with AML fusion oncoproteins and therapies that target them, exemplified in this study by PML-RARA and ATRA (Mossadegh-Keller et al., 2013; Mueller et al., 2006; Seshire et al., 2012; Vangala et al., 2003; Wang et al., 2010). Our findings suggest these factors may dynamically influence the phenotypic heterogeneity and plasticity of tumor-propagating cells within and between individual AML patients.

An uncoupling of differentiation state from leukemia-initiating activity suggests that morphological and/or immunophenotypic criteria may underestimate effective AML burden (cells capable of propagating disease) at diagnosis and following therapy. The potential of mature AML-derived cells to seed leukemia relapse via de-differentiation emphasizes the importance of molecular level disease monitoring, particularly for emerging therapies that induce AML differentiation including FLT3 inhibitors or mutant IDH1/2 inhibitors (Amatangelo et al., 2017; DiNardo et al., 2018; Sexauer et al., 2012; Stein et al., 2017). Resistance to the differentiation therapies ATRA, ivosidenib, and enasidenib has recently been associated with acquired mutations in PML-RARA, IDH1, and IDH2, respectively (Intlekofer et al., 2018; Lehmann-Che et al., 2018). Our results suggest that, in some cases, these resistance mutations may arise in differentiated AML-derived cells that persist during therapy, rather than in immature AML blasts. Although our study does not directly examine human AML *in vivo*, collectively, our genetic and pharmacological findings are consistent with previous observations in ATRA-treated APL where differentiation per se is insufficient for cure (Ablain et al., 2013; de Thé, 2018; Lallemand-Breitenbach et al., 1999; Nasr et al., 2008). They also raise the intriguing possibility that in certain circumstances, potentially during exposure to genotoxic therapy, mature tumor cells may have a selective advantage over immature CSCs that allows them to subsequently re-initiate disease through de-differentiation. Hence, our observations emphasize the need to eradicate tumor cells irrespective of their maturation state.

STAR★METHODS

Detailed methods are provided in the online version of this paper and include the following:

- KEY RESOURCES TABLE
- LEAD CONTACT AND MATERIALS AVAILABILITY
- EXPERIMENTAL MODEL AND SUBJECT DETAILS
  - Animal studies
  - Mouse AML transplantation
  - Mouse APL experiments
  - Mouse AML proliferation, viability and clonogenic assays
  - Human AML cell line culture
  - Human AML cell line analysis
  - Human primary APL analysis
- METHOD DETAILS
  - Retroviral vectors
  - Fetal liver cell transduction and transplant
  - Flow cytometry, blood analysis, and cytospins
  - Single cell tracking
  - Neutrophil function assays
  - Spectral karyotyping
  - Immunoblotting
  - RNA sequencing
  - Mouse and human AML transcriptome comparison
  - Single cell RNA sequencing
  - ChIP sequencing
  - ATAC sequencing
  - Combined RNA-seq, ChIP-seq, and ATAC-seq analysis
  - Exome sequencing

SUPPLEMENTAL INFORMATION

Supplemental Information can be found online at https://doi.org/10.1016/j.stem.2019.07.001.

ACKNOWLEDGMENTS

We thank B. Coghlan, S. Brown, K. Stoev, C. Alvarado, L. Whitehead, M. Scott, M. Lee, S. Dietrich, and M. Halemba for technical assistance; G. Paukovics, E. Orlowski-Oliver, and M. Costa at the AMREP Flow Facility; S. Wilcox, M. Everest, Y. Zhang, B. Whittle, S. Macraild, and F. Brown for NGS; S. Fleming, M. Gorniak, and A. Ivey at the Alfred Hospital; S. Lowe and L. Dow for MSCV-IRES-tTA; and B. Kile, D. Curtis, S. Ting, J. Hamilton, A. Perkins, M. Plebanski, and members of the Dickins laboratory for insights. This study was supported by the National Health and Medical Research Council of Australia (NHMRC) project grant 1057854, Australian Government NHMRC IRIISS, Victorian State Government OIS grants, an Australian Research Council Future Fellowship (S.L.N.), Gabrielle's Angel Foundation for Cancer Research (B.A.C.), SNF grant 179490 (T.S.), AZV 16-31586A UNCE/MED/016 Progres Q26 (V.P.), Boehringer Ingelheim (J.Z.), Leukaemia Foundation of Australia Postdoctoral Fellowship (M.D.M.), NHRMC Career Development Fellowship 1104924 (M.E.R.), a Sylvia and Charles Viertel Charitable Foundation Fellowship (R.A.D.), and a Victorian Endowment for Science, Knowledge and Innovation (VESKI) Fellowship (R.A.D. and M.A.D.).

AUTHOR CONTRIBUTIONS

Conceptualization, M.D.M., M.G., E.P.O., and R.A.D.; Investigation, M.D.M., M.G., E.P.O., S.N., L.C., C.E., R.L., J.M.S., C.C.B., N.A., M.E., M.T.W., G.J.L., M.C., A.D., E.S., G.P., T.V., P.K., S.S., L.T., T.M.B., D.A.Z., L.D., S.W., D.M., G.I.L., V.P., M.W., and M.E.R.; Writing, M.D.M., M.G., E.P.O., and R.A.D.; Supervision and Funding Acquisition, R.W.J., B.A.C., A.J.M., S.H.N., S.L.N., V.P., T.S., M.W., M.A.D., A.H.W., H.D.T., M.E.R., J.Z., and R.A.D.

DECLARATION OF INTERESTS

The authors declare no competing interests.

Received: June 25, 2018
Revised: January 28, 2019
Accepted: July 1, 2019
Published: August 1, 2019

SUPPORTING CITATIONS

The following references appear in the Supplemental Information: Breems et al. (2008); Fleckenstein et al. (2002); Gao et al. (2013); Leddin et al. (2011); Li et al. (2001); Staber et al. (2013).

REFERENCES

Ablain, J., Leiva, M., Peres, L., Fonsart, J., Anthony, E., and de Thé, H. (2013). Uncoupling RARA transcriptional activation and degradation clarifies the bases for APL response to therapies. J. Exp. Med. *210*, 647–653.

Alhamdoosh, M., Law, C.W., Tian, L., Sheridan, J.M., Ng, M., and Ritchie, M.E. (2017). Easy and efficient ensemble gene set testing with EGSEA. F1000Res. *6*, 2010.

Amatangelo, M.D., Quek, L., Shih, A., Stein, E.M., Roshal, M., David, M.D., Marteyn, B., Farnoud, N.R., de Botton, S., Bernard, O.A., et al. (2017). Enasidenib induces acute myeloid leukemia cell differentiation to promote clinical response. Blood *130*, 732–741.

Andrews, T.D., Whittle, B., Field, M.A., Balakishnan, B., Zhang, Y., Shao, Y., Cho, V., Kirk, M., Singh, M., Xia, Y., et al. (2012). Massively parallel sequencing of the mouse exome to accurately identify rare, induced mutations: an immediate source for thousands of new mouse models. Open Biol. *2*, 120061.

Basova, P., Pospisil, V., Savvulidi, F., Burda, P., Vargova, K., Stanek, L., Dluhosova, M., Kuzmova, E., Jonasova, A., Steidl, U., et al. (2014). Aggressive acute myeloid leukemia in PU.1/p53 double-mutant mice. Oncogene *33*, 4735–4745.

Batlle, E., and Clevers, H. (2017). Cancer stem cells revisited. Nat. Med. *23*, 1124–1134.

Bonnet, D., and Dick, J.E. (1997). Human acute myeloid leukemia is organized as a hierarchy that originates from a primitive hematopoietic cell. Nat. Med. *3*, 730–737.

Breems, D.A., Van Putten, W.L., De Greef, G.E., Van Zelderen-Bhola, S.L., Gerssen-Schoorl, K.B., Mellink, C.H., Nieuwint, A., Jotterand, M., Hagemeijer, A., Beverloo, H.B., and Löwenberg, B. (2008). Monosomal karyotype in acute myeloid leukemia: a better indicator of poor prognosis than a complex karyotype. J. Clin. Oncol. *26*, 4791–4797.

Buenrostro, J.D., Giresi, P.G., Zaba, L.C., Chang, H.Y., and Greenleaf, W.J. (2013). Transposition of native chromatin for fast and sensitive epigenomic profiling of open chromatin, DNA-binding proteins and nucleosome position. Nat. Methods *10*, 1213–1218.

Carotta, S., Wu, L., and Nutt, S.L. (2010). Surprising new roles for PU.1 in the adaptive immune response. Immunol. Rev. *238*, 63–75.

Cusan, M., Cai, S.F., Mohammad, H.P., Krivtsov, A., Chramiec, A., Loizou, E., Witkin, M.D., Smitheman, K.N., Tenen, D.G., Ye, M., et al. (2018). LSD1 inhibition exerts its antileukemic effect by recommissioning PU.1- and C/EBPα-dependent enhancers in AML. Blood *131*, 1730–1742.

de Sousa e Melo, F., Kurtova, A.V., Harnoss, J.M., Kljavin, N., Hoeck, J.D., Hung, J., Anderson, J.E., Storm, E.E., Modrusan, Z., Koeppen, H., et al. (2017). A distinct role for $Lgr5^{+}$ stem cells in primary and metastatic colon cancer. Nature *543*, 676–680.

de Thé, H. (2018). Differentiation therapy revisited. Nat. Rev. Cancer *18*, 117–127.

DeKoter, R.P., Walsh, J.C., and Singh, H. (1998). PU.1 regulates both cytokine-dependent proliferation and differentiation of granulocyte/macrophage progenitors. EMBO J. *17*, 4456–4468.

Dickins, R.A., Hemann, M.T., Zilfou, J.T., Simpson, D.R., Ibarra, I., Hannon, G.J., and Lowe, S.W. (2005). Probing tumor phenotypes using stable and regulated synthetic microRNA precursors. Nat. Genet. *37*, 1289–1295.

DiNardo, C.D., Stein, E.M., de Botton, S., Roboz, G.J., Altman, J.K., Mims, A.S., Swords, R., Collins, R.H., Mannis, G.N., Pollyea, D.A., et al. (2018). Durable remissions with ivosidenib in IDH1-mutated relapsed or refractory AML. N. Engl. J. Med. *378*, 2386–2398.

Dow, L.E., Premsrirut, P.K., Zuber, J., Fellmann, C., McJunkin, K., Miething, C., Park, Y., Dickins, R.A., Hannon, G.J., and Lowe, S.W. (2012). A pipeline for the generation of shRNA transgenic mice. Nat. Protoc. *7*, 374–393.

Eash, K.J., Greenbaum, A.M., Gopalan, P.K., and Link, D.C. (2010). CXCR2 and CXCR4 antagonistically regulate neutrophil trafficking from murine bone marrow. J. Clin. Invest. *120*, 2423–2431.

Evrard, M., Kwok, I.W.H., Chong, S.Z., Teng, K.W.W., Becht, E., Chen, J., Sieow, J.L., Penny, H.L., Ching, G.C., Devi, S., et al. (2018). Developmental analysis of bone marrow neutrophils reveals populations specialized in expansion, trafficking, and effector functions. Immunity *48*, 364–379.e8.

Fellmann, C., Hoffmann, T., Sridhar, V., Hopfgartner, B., Muhar, M., Roth, M., Lai, D.Y., Barbosa, I.A., Kwon, J.S., Guan, Y., et al. (2013). An optimized microRNA backbone for effective single-copy RNAi. Cell Rep. *5*, 1704–1713.

Feng, J., Liu, T., Qin, B., Zhang, Y., and Liu, X.S. (2012). Identifying ChIP-seq enrichment using MACS. Nat. Protoc. *7*, 1728–1740.

Fleckenstein, D.S., Uphoff, C.C., Drexler, H.G., and Quentmeier, H. (2002). Detection of p53 gene mutations by single strand conformational

polymorphism (SSCP) in human acute myeloid leukemia-derived cell lines. Leuk. Res. *26*, 207–214.

Gao, J., Aksoy, B.A., Dogrusoz, U., Dresdner, G., Gross, B., Sumer, S.O., Sun, Y., Jacobsen, A., Sinha, R., Larsson, E., et al. (2013). Integrative analysis of complex cancer genomics and clinical profiles using the cBioPortal. Sci. Signal. *6*, pl1.

Gu, X., Ebrahem, Q., Mahfouz, R.Z., Hasipek, M., Enane, F., Radivoyevitch, T., Rapin, N., Przychodzen, B., Hu, Z., Balusu, R., et al. (2018). Leukemogenic nucleophosmin mutation disrupts the transcription factor hub that regulates granulomonocytic fates. J. Clin. Invest. *128*, 4260–4279.

Hahne, F., and Ivanek, R. (2016). Visualizing genomic data using Gviz and Bioconductor. Methods Mol. Biol. *1418*, 335–351.

Hashimshony, T., Senderovich, N., Avital, G., Klochendler, A., de Leeuw, Y., Anavy, L., Gennert, D., Li, S., Livak, K.J., Rozenblatt-Rosen, O., et al. (2016). CEL-Seq2: sensitive highly-multiplexed single-cell RNA-seq. Genome Biol. *17*, 77.

Heinz, S., Benner, C., Spann, N., Bertolino, E., Lin, Y.C., Laslo, P., Cheng, J.X., Murre, C., Singh, H., and Glass, C.K. (2010). Simple combinations of lineage-determining transcription factors prime cis-regulatory elements required for macrophage and B cell identities. Mol. Cell *38*, 576–589.

Heng, T.S., and Painter, M.W.; Immunological Genome Project Consortium (2008). The Immunological Genome Project: networks of gene expression in immune cells. Nat. Immunol. *9*, 1091–1094.

Hilsenbeck, O., Schwarzfischer, M., Skylaki, S., Schauberger, B., Hoppe, P.S., Loeffler, D., Kokkaliaris, K.D., Hastreiter, S., Skylaki, E., Filipczyk, A., et al. (2016). Software tools for single-cell tracking and quantification of cellular and molecular properties. Nat. Biotechnol. *34*, 703–706.

Hoppe, P.S., Schwarzfischer, M., Loeffler, D., Kokkaliaris, K.D., Hilsenbeck, O., Moritz, N., Endele, M., Filipczyk, A., Gambardella, A., Ahmed, N., et al. (2016). Early myeloid lineage choice is not initiated by random PU.1 to GATA1 protein ratios. Nature *535*, 299–302.

Huang, G., Zhang, P., Hirai, H., Elf, S., Yan, X., Chen, Z., Koschmieder, S., Okuno, Y., Dayaram, T., Growney, J.D., et al. (2008). PU.1 is a major downstream target of AML1 (RUNX1) in adult mouse hematopoiesis. Nat. Genet. *40*, 51–60.

Huang, G., Zhao, X., Wang, L., Elf, S., Xu, H., Zhao, X., Sashida, G., Zhang, Y., Liu, Y., Lee, J., et al. (2011). The ability of MLL to bind RUNX1 and methylate H3K4 at PU.1 regulatory regions is impaired by MDS/AML-associated RUNX1/AML1 mutations. Blood *118*, 6544–6552.

Intlekofer, A.M., Shih, A.H., Wang, B., Nazir, A., Rustenburg, A.S., Albanese, S.K., Patel, M., Famulare, C., Correa, F.M., Takemoto, N., et al. (2018). Acquired resistance to IDH inhibition through trans or cis dimer-interface mutations. Nature *559*, 125–129.

Iwafuchi-Doi, M., and Zaret, K.S. (2014). Pioneer transcription factors in cell reprogramming. Genes Dev. *28*, 2679–2692.

Jacks, T., Remington, L., Williams, B.O., Schmitt, E.M., Halachmi, S., Bronson, R.T., and Weinberg, R.A. (1994). Tumor spectrum analysis in p53-mutant mice. Curr. Biol. *4*, 1–7.

Kishi, K., Toba, K., Azegami, T., Tsukada, N., Uesugi, Y., Masuko, M., Niwano, H., Hashimoto, S., Sakaue, M., Furukawa, T., et al. (1998). Hematopoietic cytokine-dependent differentiation to eosinophils and neutrophils in a newly established acute promyelocytic leukemia cell line with t(15;17). Exp. Hematol. *26*, 135–142.

Kojima, K., Konopleva, M., Samudio, I.J., Shikami, M., Cabreira-Hansen, M., McQueen, T., Ruvolo, V., Tsao, T., Zeng, Z., Vassilev, L.T., and Andreeff, M. (2005). MDM2 antagonists induce p53-dependent apoptosis in AML: implications for leukemia therapy. Blood *106*, 3150–3159.

Kreso, A., and Dick, J.E. (2014). Evolution of the cancer stem cell model. Cell Stem Cell *14*, 275–291.

Lallemand-Breitenbach, V., Guillemin, M.C., Janin, A., Daniel, M.T., Degos, L., Kogan, S.C., Bishop, J.M., and de Thé, H. (1999). Retinoic acid and arsenic synergize to eradicate leukemic cells in a mouse model of acute promyelocytic leukemia. J. Exp. Med. *189*, 1043–1052.

Lanotte, M., Martin-Thouvenin, V., Najman, S., Balerini, P., Valensi, F., and Berger, R. (1991). NB4, a maturation inducible cell line with t(15;17) marker isolated from a human acute promyelocytic leukemia (M3). Blood *77*, 1080–1086.

Lapidot, T., Sirard, C., Vormoor, J., Murdoch, B., Hoang, T., Caceres-Cortes, J., Minden, M., Paterson, B., Caligiuri, M.A., and Dick, J.E. (1994). A cell initiating human acute myeloid leukaemia after transplantation into SCID mice. Nature *367*, 645–648.

Lavallée, V.P., Baccelli, I., Krosl, J., Wilhelm, B., Barabé, F., Gendron, P., Boucher, G., Lemieux, S., Marinier, A., Meloche, S., et al. (2015). The transcriptomic landscape and directed chemical interrogation of MLL-rearranged acute myeloid leukemias. Nat. Genet. *47*, 1030–1037.

Law, C.W., Chen, Y., Shi, W., and Smyth, G.K. (2014). voom: precision weights unlock linear model analysis tools for RNA-seq read counts. Genome Biol. *15*, R29.

Lawrence, M., Huber, W., Pagès, H., Aboyoun, P., Carlson, M., Gentleman, R., Morgan, M.T., and Carey, V.J. (2013). Software for computing and annotating genomic ranges. PLoS Comput. Biol. *9*, e1003118.

Leddin, M., Perrod, C., Hoogenkamp, M., Ghani, S., Assi, S., Heinz, S., Wilson, N.K., Follows, G., Schönheit, J., Vockentanz, L., et al. (2011). Two distinct auto-regulatory loops operate at the PU.1 locus in B cells and myeloid cells. Blood *117*, 2827–2838.

Lehmann-Che, J., Bally, C., Letouzé, E., Berthier, C., Yuan, H., Jollivet, F., Ades, L., Cassinat, B., Hirsch, P., Pigneux, A., et al. (2018). Dual origin of relapses in retinoic-acid resistant acute promyelocytic leukemia. Nat. Commun. *9*, 2047.

Ley, T.J., Miller, C., Ding, L., Raphael, B.J., Mungall, A.J., Robertson, A., Hoadley, K., Triche, T.J., Jr., Laird, P.W., Baty, J.D., et al.; Cancer Genome Atlas Research Network (2013). Genomic and epigenomic landscapes of adult de novo acute myeloid leukemia. N. Engl. J. Med. *368*, 2059–2074.

Li, Y., Okuno, Y., Zhang, P., Radomska, H.S., Chen, H., Iwasaki, H., Akashi, K., Klemsz, M.J., McKercher, S.R., Maki, R.A., and Tenen, D.G. (2001). Regulation of the PU.1 gene by distal elements. Blood *98*, 2958–2965.

Li, H., and Durbin, R. (2009). Fast and accurate short read alignment with Burrows-Wheeler Transform. Bioinformatics *25*, 1754–1760.

Li, H., Handsaker, B., Wysoker, A., Fennell, T., Ruan, J., Homer, N., Marth, G., Abecasis, G., and Durbin, R.; 1000 Genome Project Data Processing Subgroup (2009). The Sequence Alignment/Map format and SAMtools. Bioinformatics *25*, 2078–2079.

Liao, Y., Smyth, G.K., and Shi, W. (2013). The Subread aligner: fast, accurate and scalable read mapping by seed-and-vote. Nucleic Acids Res. *41*, e108.

Liao, Y., Smyth, G.K., and Shi, W. (2014). featureCounts: an efficient general purpose program for assigning sequence reads to genomic features. Bioinformatics *30*, 923–930.

Liu, R., Holik, A.Z., Su, S., Jansz, N., Chen, K., Leong, H.S., Blewitt, M.E., Asselin-Labat, M.L., Smyth, G.K., and Ritchie, M.E. (2015). Why weight? Modelling sample and observational level variability improves power in RNA-seq analyses. Nucleic Acids Res. *43*, e97.

Lo-Coco, F., Avvisati, G., Vignetti, M., Thiede, C., Orlando, S.M., Iacobelli, S., Ferrara, F., Fazi, P., Cicconi, L., Di Bona, E., et al.; Gruppo Italiano Malattie Ematologiche dell'Adulto; German-Austrian Acute Myeloid Leukemia Study Group; Study Alliance Leukemia (2013). Retinoic acid and arsenic trioxide for acute promyelocytic leukemia. N. Engl. J. Med. *369*, 111–121.

Lun, A.T., McCarthy, D.J., and Marioni, J.C. (2016). A step-by-step workflow for low-level analysis of single-cell RNA-seq data with Bioconductor. F1000Res. *5*, 2122.

Maes, T., Mascaró, C., Tirapu, I., Estiarte, A., Ciceri, F., Lunardi, S., Guibourt, N., Perdones, A., Lufino, M.M.P., Somervaille, T.C.P., et al. (2018). ORY-1001, a potent and selective covalent KDM1A inhibitor, for the treatment of acute leukemia. Cancer Cell *33*, 495–511.e12.

Meacham, C.E., and Morrison, S.J. (2013). Tumour heterogeneity and cancer cell plasticity. Nature *501*, 328–337.

Mossadegh-Keller, N., Sarrazin, S., Kandalla, P.K., Espinosa, L., Stanley, E.R., Nutt, S.L., Moore, J., and Sieweke, M.H. (2013). M-CSF instructs myeloid lineage fate in single haematopoietic stem cells. Nature *497*, 239–243.

Mueller, B.U., Pabst, T., Fos, J., Petkovic, V., Fey, M.F., Asou, N., Buergi, U., and Tenen, D.G. (2006). ATRA resolves the differentiation block in t(15;17) acute myeloid leukemia by restoring PU.1 expression. Blood *107*, 3330–3338.

Nasr, R., Guillemin, M.C., Ferhi, O., Soilihi, H., Peres, L., Berthier, C., Rousselot, P., Robledo-Sarmiento, M., Lallemand-Breitenbach, V., Gourmel, B., et al. (2008). Eradication of acute promyelocytic leukemia-initiating cells through PML-RARA degradation. Nat. Med. *14*, 1333–1342.

Okuno, Y., Huang, G., Rosenbauer, F., Evans, E.K., Radomska, H.S., Iwasaki, H., Akashi, K., Moreau-Gachelin, F., Li, Y., Zhang, P., et al. (2005). Potential autoregulation of transcription factor PU.1 by an upstream regulatory element. Mol. Cell. Biol. *25*, 2832–2845.

Papaemmanuil, E., Gerstung, M., Bullinger, L., Gaidzik, V.I., Paschka, P., Roberts, N.D., Potter, N.E., Heuser, M., Thol, F., Bolli, N., et al. (2016). Genomic classification and prognosis in acute myeloid leukemia. N. Engl. J. Med. *374*, 2209–2221.

Paschka, P., Marcucci, G., Ruppert, A.S., Mrózek, K., Chen, H., Kittles, R.A., Vukosavljevic, T., Perrotti, D., Vardiman, J.W., Carroll, A.J., et al.; Cancer and Leukemia Group B (2006). Adverse prognostic significance of KIT mutations in adult acute myeloid leukemia with inv(16) and t(8;21): a Cancer and Leukemia Group B Study. J. Clin. Oncol. *24*, 3904–3911.

Ritchie, M.E., Phipson, B., Wu, D., Hu, Y., Law, C.W., Shi, W., and Smyth, G.K. (2015). limma powers differential expression analyses for RNA-sequencing and microarray studies. Nucleic Acids Res. *43*, e47.

Robinson, M.D., and Oshlack, A. (2010). A scaling normalization method for differential expression analysis of RNA-seq data. Genome Biol. *11*, R25.

Robinson, J.T., Thorvaldsdóttir, H., Winckler, W., Guttman, M., Lander, E.S., Getz, G., and Mesirov, J.P. (2011). Integrative genomics viewer. Nat. Biotechnol. *29*, 24–26.

Rosenbauer, F., Wagner, K., Kutok, J.L., Iwasaki, H., Le Beau, M.M., Okuno, Y., Akashi, K., Fiering, S., and Tenen, D.G. (2004). Acute myeloid leukemia induced by graded reduction of a lineage-specific transcription factor, PU.1. Nat. Genet. *36*, 624–630.

Ross-Innes, C.S., Stark, R., Teschendorff, A.E., Holmes, K.A., Ali, H.R., Dunning, M.J., Brown, G.D., Gojis, O., Ellis, I.O., Green, A.R., et al. (2012). Differential oestrogen receptor binding is associated with clinical outcome in breast cancer. Nature *481*, 389–393.

Rücker, F.G., Schlenk, R.F., Bullinger, L., Kayser, S., Teleanu, V., Kett, H., Habdank, M., Kugler, C.M., Holzmann, K., Gaidzik, V.I., et al. (2012). TP53 alterations in acute myeloid leukemia with complex karyotype correlate with specific copy number alterations, monosomal karyotype, and dismal outcome. Blood *119*, 2114–2121.

Samur, M.K. (2014). RTCGAToolbox: a new tool for exporting TCGA Firehose data. PLoS ONE *9*, e106397.

Seshire, A., Rößiger, T., Frech, M., Beez, S., Hagemeyer, H., and Puccetti, E. (2012). Direct interaction of PU.1 with oncogenic transcription factors reduces its serine phosphorylation and promoter binding. Leukemia *26*, 1338–1347.

Sexauer, A., Perl, A., Yang, X., Borowitz, M., Gocke, C., Rajkhowa, T., Thiede, C., Frattini, M., Nybakken, G.E., Pratz, K., et al. (2012). Terminal myeloid differentiation in vivo is induced by FLT3 inhibition in FLT3/ITD AML. Blood *120*, 4205–4214.

Shimokawa, M., Ohta, Y., Nishikori, S., Matano, M., Takano, A., Fujii, M., Date, S., Sugimoto, S., Kanai, T., and Sato, T. (2017). Visualization and targeting of LGR5^{+} human colon cancer stem cells. Nature *545*, 187–192.

Sive, J.I., Basilico, S., Hannah, R., Kinston, S.J., Calero-Nieto, F.J., and Göttgens, B. (2016). Genome-scale definition of the transcriptional programme associated with compromised PU.1 activity in acute myeloid leukaemia. Leukemia *30*, 14–23.

Skylaki, S., Hilsenbeck, O., and Schroeder, T. (2016). Challenges in long-term imaging and quantification of single-cell dynamics. Nat. Biotechnol. *34*, 1137–1144.

Smyth, G.K. (2004). Linear models and empirical bayes methods for assessing differential expression in microarray experiments. Stat. Appl. Genet. Mol. Biol. *3*, Article3.

Staber, P.B., Zhang, P., Ye, M., Welner, R.S., Nombela-Arrieta, C., Bach, C., Kerenyi, M., Bartholdy, B.A., Zhang, H., Alberich-Jordà, M., et al. (2013). Sustained PU.1 levels balance cell-cycle regulators to prevent exhaustion of adult hematopoietic stem cells. Mol. Cell *49*, 934–946.

Stein, E.M., DiNardo, C.D., Pollyea, D.A., Fathi, A.T., Roboz, G.J., Altman, J.K., Stone, R.M., DeAngelo, D.J., Levine, R.L., Flinn, I.W., et al. (2017). Enasidenib in mutant *IDH2* relapsed or refractory acute myeloid leukemia. Blood *130*, 722–731.

Sykes, D.B., Kfoury, Y.S., Mercier, F.E., Wawer, M.J., Law, J.M., Haynes, M.K., Lewis, T.A., Schajnovitz, A., Jain, E., Lee, D., et al. (2016). Inhibition of dihydroorotate dehydrogenase overcomes differentiation blockade in acute myeloid leukemia. Cell *167*, 171–186.e15.

Thomas, D., and Majeti, R. (2017). Biology and relevance of human acute myeloid leukemia stem cells. Blood *129*, 1577–1585.

Thorvaldsdóttir, H., Robinson, J.T., and Mesirov, J.P. (2013). Integrative Genomics Viewer (IGV): high-performance genomics data visualization and exploration. Brief. Bioinform. *14*, 178–192.

Vangala, R.K., Heiss-Neumann, M.S., Rangatia, J.S., Singh, S.M., Schoch, C., Tenen, D.G., Hiddemann, W., and Behre, G. (2003). The myeloid master regulator transcription factor PU.1 is inactivated by AML1-ETO in t(8;21) myeloid leukemia. Blood *101*, 270–277.

Wang, K., Wang, P., Shi, J., Zhu, X., He, M., Jia, X., Yang, X., Qiu, F., Jin, W., Qian, M., et al. (2010). PML/RARalpha targets promoter regions containing PU.1 consensus and RARE half sites in acute promyelocytic leukemia. Cancer Cell *17*, 186–197.

Warrell, R.P., Jr., de Thé, H., Wang, Z.Y., and Degos, L. (1993). Acute promyelocytic leukemia. N. Engl. J. Med. *329*, 177–189.

Will, B., Vogler, T.O., Narayanagari, S., Bartholdy, B., Todorova, T.I., da Silva Ferreira, M., Chen, J., Yu, Y., Mayer, J., Barreyro, L., et al. (2015). Minimal PU.1 reduction induces a preleukemic state and promotes development of acute myeloid leukemia. Nat. Med. *21*, 1172–1181.

Wu, D., Lim, E., Vaillant, F., Asselin-Labat, M.-L., Visvader, J.E., and Smyth, G.K. (2010). ROAST: rotation gene set tests for complex microarray experiments. Bioinformatics *26*, 2176–2182.

STAR★METHODS

KEY RESOURCES TABLE

REAGENT or RESOURCE	SOURCE	IDENTIFIER
Antibodies		
Ter119	WEHI	N/A
BioMag Goat Anti-Rat IgG	QIAGEN	Cat#310107
CD16/CD32 (clone 2.4G2)	WEHI	N/A
CD16/CD32-PacBlue (clone 2.4G2)	WEHI	N/A
CD11b-PE (clone M1/70)	eBioscience	Cat#12-0112-82; RRID:AB_2734869
Ly6G-APC (clone 1A8-Ly6G)	eBioscience	Cat#17-9668-82; RRID:AB_2573307
F4/80-PECy7 (clone BM8)	eBioscience	Cat#25-4801-82; RRID:AB_469653
CD117-APC (clone ACK2)	WEHI	N/A
CD11b-PacBlue (clone M1/70)	WEHI	N/A
CD19-PE (clone 1D3)	WEHI	N/A
CD3-PE (clone 145-2C11)	eBioscience	Cat#12-0031-82; RRID:AB_465496
CD4-PE (clone GK1.5)	WEHI	N/A
TCRβ-PE (clone H57-597)	BD Biosciences	Cat#561081; RRID:AB_10563767
CD16/CD32 (clone 93)	eBioscience	Cat#14-0161-82; RRID:AB_467133
CD117-APC (clone 2B8)	eBioscience	Cat#17-1171-82; RRID:AB_469430
CD11b-APC/Cy7 (clone M1/70)	BioLegend	Cat#101225; RRID:AB_830641
Gr1-PE (clone RB6-8C5)	eBioscience	Cat#12-5931-82; RRID:AB_466045
Gr1-PerCP-Cy5.5 (clone RB6-8C5)	BD Biosciences	Cat#552093; RRID:AB_394334
CD115-APC (clone AFS98)	eBioscience	Cat#17-1152-80; RRID:AB_1210790
CD11b-PECy7 (clone 6068C2)	BioLegend	Cat#101215; RRID:AB_312798
CD45-PacBlue (clone 30-F11)	BioLegend	Cat#103125; RRID:AB_493536
CD11B-APC (clone Bear1)	Beckman Coulter	Cat#A87782
CD15-BV605 (clone W6D3)	BioLegend	Cat#323031; RRID:AB_2562131
CD16-PE (clone 3G8)	BD Biosciences	Cat#555407; RRID:AB_395807
CD34-PECy7 (clone 581)	BD Biosciences	Cat#560710; RRID:AB_1727470
PU.1 (clone C-3)	Santa Cruz Biotechnology	Cat#sc-390405
PU.1 (clone T-21) [discontinued]	Santa Cruz Biotechnology	Cat#sc-352; RRID:AB_632289
α-tubulin (clone B-5-1-2)	Sigma	Cat#T6074; RRID:AB_477582
Acetyl Histone H3 (clone 06-599)	Millipore	Cat#06-599; RRID:AB_2115283
Biological Samples		
Patient-derived primary APL samples APL1-APL6	Alfred Hospital Haematology Tissue Bank	N/A
Chemicals, Peptides, and Recombinant Proteins		
Meat Free Rat and Mouse plus 600 mg/kg Doxycycline	Specialty Feeds	SF08-026
rhG-CSF	Filgrastim; Hospira	N/A
ATRA	Sigma	CAS:302-79-4
Retronectin	WEHI	N/A
mSCF	Peprotech	Cat#250-03
mIL6	WEHI	N/A
mFlt3L	WEHI	N/A
mTPO	WEHI	N/A
Doxycycline hyclate	Sigma	CAS:24390-14-5
Propidium Iodide	Thermo Fisher Scientific	Cat#P3566

(*Continued on next page*)

Continued

REAGENT or RESOURCE	SOURCE	IDENTIFIER
13-*cis*-Retinoic Acid	Sigma	CAS:4759-48-2
mIL-3	Peprotech	Cat#213-13
DAPI	Sigma	CAS:28718-90-3
MethoCult GF M3434	StemCell Technologies, Inc.	Cat#03434
pHrodo red zymosan bioparticles	Thermo Fisher Scientific	Cat#P35364
Cytochalasin D	Sigma	CAS:22144-77-0
Zombie NIR	BioLegend	Cat#423105
MethoCult H4434	StemCell Technologies, Inc.	Cat#04434
Methocult SF H4236	StemCell Technologies, Inc.	Cat#04326
Nutlin-3a	Selleckchem	Cat#S8059
SYTOX Blue	Life Technologies	Cat#S34857
Idarubicin	Selleckchem	Cat#S1228
Trizol	Invitrogen	Cat#15596026
SuperScript III reverse transcriptase	Thermo Fisher Scientific	Cat#18080093
StemSpan SFEM II	StemCell Technologies, Inc.	Cat#09605
rhFLT3 ligand	R&D Systems	Cat#308-FK-005
rhSCF	R&D Systems	Cat#255-SC-010
rhIL-3	R&D Systems	Cat#203-IL-010
rhIL-6	R&D Systems	Cat#206-IL-010
Critical Commercial Assays		
Cytofix/Cytoperm kit	BD Biosciences	N/A
Sphero AccuCount Blank Beads	Spherotech	N/A
TaqMan primer/probe sets	Applied Biosystems	N/A
21XMouse probe kit	MetaSystems	N/A
RNeasy Plus Mini Kit	QIAGEN	Cat#74134
Illumina TruSeq Kit	Illumina	N/A
NEBNext Second Strand Synthesis Module	New England Biolabs	N/A
NucleoMag NGS Clean-up and size select	Macherey-Nagel	N/A
ProteinG DynaBeads	Thermo Fisher	N/A
Illumina Nextera Kit	Illumina	N/A
DNeasy Blood and Tissue kit	QIAGEN	Cat#69504
Agilent SureSelect Mouse All Exon V1 kit	Agilent	N/A
Deposited Data		
RNA-seq: AML246 *in vivo*	This paper	GEO: GSE76874
RNA-seq: AML410 *in vivo*	This paper	GEO: GSE76875
RNA-seq: AML246 *in vitro* time course	This paper	GEO: GSE108946
RNA-seq: AML246 single cell RNA-seq	This paper	GEO: GSE109100
ChIP-seq: AML246 *in vitro* time course	This paper	GEO: GSE108945
ATAC-seq: AML246 *in vitro* time course	This paper	GEO: GSE108944
Exome sequencing: AML246 and AML410	This paper	https://www.ncbi.nlm.nih.gov/bioproject/?term=PRJNA308523
Experimental Models: Cell Lines		
NB4	Lanotte et al., 1991	N/A
HT93	Kishi et al., 1998; Cell Resource Center for Biomedical Research, Tohuku University, Japan	N/A
Experimental Models: Organisms/Strains		
Mouse: C57BL/6J wild type	WEHI	N/A
Mouse: C57BL/6J-Trp53$^{+/-}$	Jacks et al., 1994; WEHI	N/A

(*Continued on next page*)

Continued

REAGENT or RESOURCE	SOURCE	IDENTIFIER
Mouse: Rag1$^{-/-}$ Ptprc$^{Ly5.1}$ (Cd45.1)	WEHI	N/A
Mouse: FVB/N wild type	Janvier	N/A
Oligonucleotides		
Ren.713 shRNA sequence: TGCTGTTGACAGT GAGCGCAGGAATTATAATGCTTATCTATAGTG AAGCCACAGATGTATAGATAAGCATTATAATT CCTATGCCTACTGCCTCGGA	Fellmann et al., 2013	N/A
PU.1.200 shRNA sequence: TGCTGTTGACAGT GAGCGAATCGGATGACTTGGTTACTTATAGTG AAGCCACAGATGTATAAGTAACCAAGTCATC CGATGTGCCTACTGCCTCGGA	This paper	N/A
PU.1.1293 shRNA sequence: TGCTGTTGACA GTGAGCGCAACCACTAAAGACAAGTAAAAT AGTGAAGCCACAGATGTATTTTACTTGTCTT TAGTGGTTATGCCTACTGCCTCGGA	This paper	N/A
Recombinant DNA		
MSCV-IRES-tTA	SW Lowe and LE Dow	N/A
LMP	Dickins et al., 2005	N/A
T3GM	Dickins et al., 2005	N/A
T3GE	Fellmann et al., 2013	N/A
RT3GEP	Fellmann et al., 2013	N/A
Software and Algorithms		
FlowLogic	Inivai Technologies	N/A
Prism	GraphPad	N/A
Isis image analysis software	MetaSystems	N/A
subread algorithm	Liao et al., 2013	N/A
featureCounts	Liao et al., 2014	N/A
TMM method	Robinson and Oshlack, 2010	N/A
limma package	Ritchie et al., 2015	N/A
voom	Law et al., 2014	N/A
MetaCore	GeneGo	N/A
roast method	Wu et al., 2010	N/A
gplots package	CRAN	https://cran.r-project.org/web/packages/gplots/index.html
scPipe	https://github.com/LuyiTian/scPipe	http://bioconductor.org/packages/release/bioc/html/scPipe.html
RTCGAToolbox package	Samur, 2014	N/A
scran	Lun et al., 2016	N/A
SAMtools	Li et al., 2009	N/A
MACS2	Feng et al., 2012	N/A
Gyiz	Hahne and Ivanek, 2016	N/A
GenomicRanges	Lawrence et al., 2013	N/A
DiffBind	Ross-Innes et al., 2012	N/A
BWA	Li and Durbin, 2009	N/A
IGV	Robinson et al., 2011; Thorvaldsdóttir et al., 2013	N/A
Other		
Advia 2120 hematological analyzer	Bayer	N/A
BD FACSCalibur	BD Biosciences	N/A
BD LSRII	BD Biosciences	N/A
BD LSRFortessa	BD Biosciences	N/A

(*Continued on next page*)

Continued

REAGENT or RESOURCE	SOURCE	IDENTIFIER
BD Influx	BD Biosciences	N/A
BD FACSAria	BD Biosciences	N/A
BD FACSAria III	BD Biosciences	N/A
Aperio ScanScope XT microscope	Leica Biosystems	N/A
Aperio ImageScope software v11.2	Leica Biosystems	N/A
GelCount colony counter	Oxford Optromix	N/A
LightCycler 480 II	Roche	N/A
Axiopla2 fluorescent microscope	Zeiss	N/A
HiSeq 2000	Illumina	N/A
NextSeq 500	Illumina	N/A
PippinPrep	Sage Science	N/A

LEAD CONTACT AND MATERIALS AVAILABILITY

Further information and requests for resources and reagents should be directed to and will be fulfilled by the Lead Contact, Ross Dickins (ross.dickins@monash.edu).

EXPERIMENTAL MODEL AND SUBJECT DETAILS

Animal studies

p53-deficient embryos were generated by intercrossing *Trp53*$^{+/-}$ mice (Jacks et al., 1994). Doxycycline (Sigma-Aldrich, St Louis, MO) was administered in the diet at 600 mg/kg food (Specialty Feeds, Glen Forrest, Western Australia). All mouse experiments were approved by the AMREP, Walter and Eliza Hall Institute, and Université Paris Diderot Animal Ethics Committees.

Mouse AML transplantation

To generate secondary leukemias, primary splenocytes from leukemic mice (predominantly leukemia cells) were transplanted by tail vein injection into immunocompromised *Ptprc*$^{Ly5.1}$ (*Cd45.1*) *Rag1*$^{-/-}$ recipient mice (~10^6 cells/mouse). After approximately 4-6 weeks transplant recipients generally developed signs of leukemia including loss of activity or weight, breathing difficulty, palpable splenomegaly, and elevated peripheral blood white cell counts and low platelet counts. For *in vivo* PU.1 restoration experiments Dox treatment *in vivo* was commenced upon detection of GFP$^+$ tumor cells in peripheral blood and/or reduced platelet counts. For leukemia-initiation experiments Dox treatment *in vivo* was commenced upon leukemia transplant. For differentiation reversion experiments 100,000 FACS-sorted AML246 Clone 2 cells were pre-cultured *in vitro* in the presence or absence of Dox (1 μg/ml) for 14 days. Viable (PI-negative) untreated cells and viable total or Mac-1^{high} Dox-treated cells were FACS-sorted at day 14 prior to intravenous injection into *Rag1*$^{-/-}$ recipient mice.

Mouse APL experiments

6 week old FVB/N mice were purchased from Janvier. For primary transplantations, 3 × 10^5 PML-RARA (GFP+) bone marrow cells were intravenously injected into recipient mice. One untreated and two treated mice were used for each treatment modality. All-*trans* Retinoic Acid (ATRA, Innovative Research of America) was administered as subcutaneous 10 mg pellets that consistently released a daily quantity of drug (0.5 mg). 50 mg/kg/d of 13-*cis*-Retinoic Acid (Isotretinoin, Sigma R3255) were administered by intraperitoneal injection daily for 4 days. The drug was previously resuspended in ethanol at 50 mg/mL and then extemporaneously diluted in sunflower oil at 10 mg/mL before use (100 μL per 20 g mouse). After 4 days of treatment, primary mice were sacrificed and bone marrow cells recovered and stained for flow cytometry analysis and sorting. Cellular Fc receptors were blocked with normal rat IgG (Fc Block, anti-CD16/32 Clone 93, eBioscience), then immunophenotypically analyzed using fluorochrome-conjugated monoclonal antibodies (1:1000): APC-conjugated anti-CD117 (cKit) (Clone 2B8, eBioscience), APC-Cy7-conjugated anti-CD11b (Mac1) (Clone M1/70, BioLegend) and PE-conjugated anti-Gr1 (Clone RB6-8C5, eBioscience). Cells were stained for 1 h at 4°C, washed once, and resuspended in PBS. FACS analysis and sorting were performed on a BD FACSAria III cells analyzer (BD Biosciences). For secondary transplantation, 10^5 sorted cells were intravenously injected into recipient mice and survival was monitored. 50,000 sorted cells were cytospun and stained with May Grünwald Giemsa (MGG).

Mouse AML proliferation, viability and clonogenic assays

Primary mouse AML cells (usually splenocytes) and AML246 subclones were cultured in IMDM supplemented with 10% FBS, penicillin (100 U/mL), streptomycin (100 mg/mL) and 10 ng/mL IL-3 (Peprotech). Single cell clones were generated by sorting individual cells into 96 well plates using a FACSAria (BD Biosciences, San Jose, CA) followed by 3-4 weeks of culture. For cell

proliferation analysis, 50,000 AML cells were plated in a 48-well plate. Untreated cells were split 1:4 at day 3, 7 and 10, while Dox-treated cells were split 1:4 at day 3 only. Dox medium was refreshed every 7 days. Absolute AML cell counts were assessed by flow cytometry using Sphero AccuCount Blank Beads (Spherotech) adjusting for the dilution factor. For cell viability analysis, cells were resuspended in FACS buffer (PBS supplemented with 5% FCS) with propidium iodide (PI, Thermo Fisher Scientific) at a concentration of 1 μg/mL, and the proportion of viable (PI-negative) cells was quantified by flow cytometry. For DNA content analysis, cultured cells were permeabilized and fixed using the Cytofix/Cytoperm kit (BD Biosciences), stained with DAPI (49,6-diamidino-2-phenylindole dihydrochloride) (Sigma-Aldrich), and analyzed by flow cytometry. For colony-forming assays 500 FACS-purified viable AML246 cells were plated in duplicate cultures of 1 mL of Dox-free or 1 μg/mL Dox-supplemented methylcellulose (MethoCult GF M3434, StemCell Technologies, Inc.) in 35 mm culture dishes. Colony number and diameter was assessed 10 days after plating using a GelCount colony counter (Oxford Optromix). For single-cell clonogenic assays, AML246 or AML410 cells were single cell index sorted by Influx (BD Biosciences) into 96-well plates containing 200 μL of Dox-free or Dox-treated medium, and cultured for 3-4 weeks to allow clonal outgrowth.

Human AML cell line culture

Human APL cell lines NB4 (Lanotte et al., 1991) and HT93 (Kishi et al., 1998) (obtained from the Cell Resource Center for Biomedical Research, Tohoku University, Japan) were authenticated at CellBank Australia. Both cell lines were cultured in RPMI (GIBCO) supplemented with 10% FBS, penicillin (100 U/mL), and streptomycin (100 mg/mL), and HT93 were further supplemented with 50 ng/mL rhG-CSF (Filgrastim; Hospira). Cells were treated with 1 μM ATRA (Sigma) as required.

Human AML cell line analysis

NB4 and HT93 cells were screened for DNA mutations in 54 genes relevant to myeloid malignancy using the TruSight Myeloid Sequencing Panel (Illumina). For clonogenic assays NB4 cells were plated in MethoCult H4434 (StemCell Technologies, Inc.) and HT93 cells were plated in MethoCult SF H4236 (StemCell Technologies, Inc.) supplemented with 100 ng/mL rhG-CSF (Filgrastim; Hospira). NB4 colonies were counted using a GelCount colony counter (Oxford Optromix), and HT93 blast-like colonies were counted by eye with a microscope. For single-cell clonogenic assays, NB4 cells were single cell index sorted by Influx (BD Biosciences) into 96-well plates containing 200 μL of untreated or ATRA-treated medium, and cultured for 2-3 weeks to allow clonal outgrowth. For *in vitro* drug response assays, cell lines were plated at 2.5×10^5 cells/mL and drugs tested over a 5-log concentration range. Nutlin-3a (Kojima et al., 2005) was purchased from Selleckchem. After 48 h, cell viability was determined by flow cytometry by exclusion of SYTOX Blue Dead Cell Stain (Life Technologies) using an LSR-Fortessa (BD Biosciences). Data was analyzed using FlowJo and GraphPad Prism software. For CDKN1A expression analysis, cell lines were plated at 5×10^5 cells/mL and treated with vehicle (DMSO) or 100 nM Idarubicin (Selleckchem) for 6 h. Total RNA was extracted using Trizol (Invitrogen), and 2 μg of total RNA was used for reverse transcription using SuperScript III reverse transcriptase (Thermo Fisher Scientific). TaqMan primer/probe sets (Applied Biosystems) were used to assess *CDKN1A* (Hs00355872_m1) and *HPRT* (Hs01003267_m1) expression. qRT-PCR was performed on a LightCycler 480 II (Roche), and *CDKN1A* expression was determined using the comparative ΔΔCT method normalizing to *HPRT*.

Human primary APL analysis

Studies were approved by the Alfred Hospital Human Research Ethics Committee. AML patients were consented according to institutional guidelines before obtaining bone marrow samples. Approximately 3 million Ficoll-purified primary APL cells were thawed and cultured for 7 days in StemSpan SFEM II (StemCell Technologies, Inc.) supplemented with 50 ng/mL FLT3 ligand, 50 ng/mL rhSCF, 10 ng/mL rhIL-3, and 10 ng/mL rhIL-6 (all from R&D Systems). Following this 7 day pre-culture, cells were either continuously cultured in the same medium (untreated) or 1 μM ATRA was added as required for an additional 7 days (day 0 to day 7). At day 7, $CD11B^{high}$ cells were flow sorted using an Influx (BD Biosciences) with a 100 μm nozzle and replated with or without 1 μM ATRA (Sigma). Surface CD15 expression was monitored every 3 days for 9 days. Control untreated cultures were propagated in parallel for the duration and viable (PI-negative) cells were sorted at day 7.

METHOD DETAILS

Retroviral vectors

MSCV-IRES-tTA was provided by S.W. Lowe and L.E. Dow (Memorial Sloan Kettering Cancer Centre, New York, USA). LMP and T3GM vectors were described previously (Dickins et al., 2005). The T3GE shRNA vector was derived from RT3GEP (Fellmann et al., 2013). shRNA inserts were cloned using established protocols (Dow et al., 2012; Fellmann et al., 2013) using the following 97-mer oligonucleotide templates (5′ to 3′): Ren.713 as previously described (Fellmann et al., 2013); PU.1.200 (TGCTGTTGACAGTGAGCGAATCGGATGACTTGGTTACTTATAGTGAAGCCACAGATGTATAAGTAACCAAGTCATCCGATGTGCCTACTGCCTCGGA); and PU.1.1293 (TGCTGTTGACAGTGAGCGCAACCACTAAAGACAAGTAAAATAGTGAAGCCACAGATGTATTTTACTTGTCTTTAGTGGTTATGCCTACTGCCTCGGA).

Fetal liver cell transduction and transplant

Retroviral supernatants were produced by calcium phosphate transfection of 293T cells using standard protocols. For fetal liver reconstitutions, freshly harvested embryonic day 13.5-14.5 fetal liver cells were dispersed and incubated with 10 μg/mL monoclonal

rat anti-mouse Ter119 antibody (WEHI) for 15 min. Washed cells were incubated with goat anti-rat IgG biomagnetic beads (QIAGEN) and erythroid cells were magnetically depleted. Cells were plated onto retronectin-coated plates that had previously been coated with retrovirus by spinning at 4,000 rpm at 4°C for 2 hours. Following centrifugation, cells were incubated overnight in IMDM (Sigma-Aldrich) supplemented with 15% FCS (Sigma-Aldrich), 100 ng/mL mSCF (Peprotech), 10 ng/mL mIL6 (WEHI), 5 ng/mL mFlt3L (WEHI), and 50 ng/mL mTPO (WEHI) at 37°C and 10% CO_2. Cells were transplanted by tail vein injection into lethally irradiated (2 × 550 rad) wild-type C57BL/6J recipient mice.

Flow cytometry, blood analysis, and cytospins

Blood was collected by retro-orbital or mandible bleed or by tail prick, and parameters were measured with an Advia 2120 hematological analyzer (Bayer, Leverkusen, Germany). For analysis of leukemia in mice, single cell suspensions derived from bone marrow, spleen, and peripheral blood were treated with red cell lysis buffer (15 mM NH_4Cl, 1 mM $KHCO_3$, 0.01 mM EDTA) and washed twice in FACS staining buffer (PBS supplemented with 5% FCS) before incubation with fluorochrome-conjugated antibodies. For all immunophenotyping flow cytometry analysis of mouse and human leukemias, cell aliquots were incubated for 5 min with anti-CD16/CD32 (unlabelled, clone 2.4G2, WEHI), and subsequently incubated for 30 min on ice with the following antibodies against mouse antigens: CD11b-PE (clone M1/70, eBioscience), Ly6G (Gr-1)-APC (clone 1A8-Ly6G, eBioscience), F4/80-PECy7 (clone BM8, eBioscience), CD117-APC (clone ACK2, WEHI), CD11b-PacBlue (clone M1/70, WEHI), CD16/CD32-Pac-Blue (clone 2.4G2, WEHI, without unlabelled anti-CD16/CD32 pre-incubation), CD19-PE (clone 1D3, WEHI), CD3-PE (clone 145-2C11, eBioscience), CD4-PE (clone GK1.5, WEHI) and TCRbeta-PE (clone H57-597, BD Biosciences); or the following antibodies against human antigens: CD11B-APC (clone Bear-1, Beckman Coulter), CD15-BV605 (clone W6D3, BioLegend), CD16-PE (clone 3G8, BD Biosciences), and CD34-PECy7 (clone 581, BD Biosciences). Cell pellets were resuspended in 300 μL FACS staining buffer with PI (Thermo Fisher Scientific, 1 μg/ml). Flow cytometry of surface marker expression was performed on gated viable (PI-negative) cells using BD FACSCalibur, LSRII or Fortessa LSR flow cytometers, and FACS-sorting was performed on a FACSAria (BD Biosciences, San Jose, CA). All human cell line sorts were performed using an Influx (BD Biosciences) with a 100 μm nozzle. For cytospins, 50,000-100,000 AML cells were spun onto SuperFrost Plus microscope slides (Menzel Gläser) at 800 rpm for 5 min. After drying, cytospins were stained with May-Grünwald Giemsa, mounted, and imaged with the Aperio ScanScope XT microscope. Representative images were taken using Aperio ImageScope software v11.2 (Leica) and scored blind.

Single cell tracking

Single AML246 cells were longitudinally tracked using previously established protocols (Hilsenbeck et al., 2016; Hoppe et al., 2016; Skylaki et al., 2016). Briefly, AML246 Clone 2 cells were treated with Dox for 6 days, then $Cd11b^{high}$ cells were sorted and imaged for up to 3 days.

Neutrophil function assays

To measure phagocytosis, 100,000 cells per well of untreated or 14 day Dox-treated AML246 cells or whole blood positive control cells were plated in a 96-well tissue culture plate with or without 0.5 mg/mL pHrodo red zymosan bioparticles (ThermoFisher Scientific). To confirm the fluorescence signal from pHrodo red was due to phagocytosis, some samples were treated with 20 μM cytochalasin D (Sigma-Aldrich) for 30 min prior to, and during, incubation. After 2 h incubation at 37°C red blood cells were lysed (whole blood sample only), and cells centrifuged and washed in FACS buffer (HBSS containing 0.05% BSA, 0.5 mM EDTA). Cells were stained with the following antibodies for 30 min on ice: Gr1-PerCP-Cy5.5 (RB6-8C5, BD Biosciences), CD115-APC (AFS98, eBioscience), CD11b-PeCy7 (6068C2, BioLegend), and CD45-pacific blue (30-F11, BioLegend). Cells were washed in FACS buffer before determination of surface staining and pHrodo fluorescence on a BD Fortessa (BC Biosciences). To measure superoxide production, AML246 cells were treated with Dox for 9 days and immunophenotypic maturation was verified using Cd11b and Ly6g flow cytometry. Cells were stimulated with 100 ng/mL rhG-CSF (Filgrastim; Hospira) overnight, and loaded with dihydrorhodamine 123 (DHR) prior to fMLF stimulation. 100,000 untreated or Dox-treated AML246 cells or control whole peripheral blood leukocytes were resuspended in DMEM with 0.05% FBS and loaded with 1 μM DHR 123 for 15 min at 37°C, followed by stimulation with 10 μM fMLF for 15 min at 37°C. Peripheral white blood cells were then stained with Ly6g and Zombie NIR viability stain (BioLegend) and analyzed by flow cytometry.

Spectral karyotyping

Multi-color fluorescent *in situ* hybridization (M-FISH) was performed on metaphase spreads using the 21XMouse probe kit (MetaSystems). Images were captured on an Axioplan2 fluorescent microscope (Zeiss) interfaced with Isis image analysis software (MetaSystems).

Immunoblotting

Western blotting was performed using rabbit polyclonal (T-21) or mouse monoclonal anti-PU.1 antibody (C-3; both Santa Cruz Biotechnology), mouse monoclonal anti α-tubulin antibody (B-5-1-2, Sigma-Aldrich), and rabbit polyclonal anti-acetyl Histone H3 antibody (06-599, Millipore).

RNA sequencing

For *in vivo* leukemia gene expression analysis GFP+ leukemia cells were flow sorted from mice that were either untreated (GFP^{high} cells) or Dox treated for 2, 4, or 6 days (decreasing GFP expression). For *in vitro* AML246 gene expression time course analysis, duplicate samples (from parallel cultures) of viable (PI-negative) cells or Cd11b-high viable cells were flow sorted at each time point. Total RNA was extracted using the RNeasy Plus Mini Kit (QIAGEN, Valencia, CA). RNA libraries for *in vivo* and *in vitro* samples were prepared from 200 ng total RNA using the Illumina TruSeq Kit and sequenced on Illumina HiSeq 2000 (100 base single end reads) or NextSeq 500 (86 base single end reads) respectively. Reads were aligned to the mouse genome (mm10) using the subread algorithm (Liao et al., 2013) then summarized at the gene-level using featureCounts (Liao et al., 2014) from the Rsubread package. Genes with low expression (less than 0.5 counts per million in fewer than 3 samples) were removed from further analysis. Compositional differences between libraries were normalized using the trimmed mean of *M*-values (TMM) method (Robinson and Oshlack, 2010). Differential expression analysis was performed using the *limma* package (Ritchie et al., 2015). Counts were transformed to log2-CPM values (with an offset of 0.5) with associated precision weights using voom (Law et al., 2014) or voom with sample quality weights (Liu et al., 2015). Linear models with effects for different treatments at different time-points were fitted. Contrasts between conditions were estimated and differential expression was assessed using moderated *t*-statistics (Smyth, 2004). Genes with false discovery rate (FDR) < 0.05 were considered differentially expressed. Gene ontology analysis was performed using MetaCore software (https://portal.genego.com/). Gene set testing used the *roast* method (Wu et al., 2010) for gene signatures obtained from the ImmGen expression database (GSE15907) (Heng and Painter, 2008) comparing neutrophils to common myeloid progenitors (CMPs – Derrick Rossi laboratory). For the ImmGen comparisons, logFCs of the ImmGen data were used as gene weights for *roast* and all differentially expressed genes (FDR < 0.05, $|logFC| > 1$) were used. Heatmaps of the expression values on a log2 scale that were row-scaled were generated using the *gplots* package (https://cran.r-project.org/web/packages/gplots/index.html). To determine genes whose expression correlated with *Spi1* across the AML246 time course, linear model analysis was performed that included log2-CPM *Spi1* expression as a covariate in the design matrix using the limma-voom pipeline described above. RNA-seq data are available through the Gene Expression Omnibus under accession numbers GSE76874 (AML246 *in vivo*), GSE76875 (AML410 *in vivo*), and GSE108946 (AML246 *in vitro* time course).

Mouse and human AML transcriptome comparison

Gene-wise RNA-seq counts for human AML samples from The Cancer Genome Atlas (TCGA) project (Ley et al., 2013) were retrieved using the RTCGAToolbox package (Samur, 2014). Data from the 20160128 release were downloaded and analyzed using the limma-voom pipeline described above to identify genes with expression patterns correlated with SPI1. Genes were matched between species using homology mapping information obtained from the MGI database (http://www.informatics.jax.org). The moderated *t*-statistics and Spi1/SPI1 coefficients from the mouse and human linear model fits were then compared for genes with a cross species match.

Single cell RNA sequencing

Single untreated or 14 day Dox-treated AML246 cells were flow sorted (PI-negative or PI-negative Cd11b-high cells respectively) into 384-well plates using a BD FACSAria III flow cytometer (BD Biosciences). Single cell transcriptome libraries were generated using the CEL-Seq2 protocol (Hashimshony et al., 2016) with adaptations: second strand synthesis was performed using NEBNext Second Strand Synthesis Module in a final reaction volume of 8 μL, and NucleoMag NGS Clean-up and Size select magnetic beads (Macherey-Nagel) were used for DNA purification and size selection. CEL-Seq2 scRNA-sequencing reads were mapped to the GRCm38 mouse genome using the *Rsubread* aligner (Liao et al., 2013) and assigned to genes using *scPipe* (http://bioconductor.org/packages/release/bioc/html/scPipe.html) with ENSEMBL v86 annotation. Gene counts were exported as a matrix by *scPipe* with UMI-aware counting and imported into R. Cells were removed from further analysis if they failed to achieve 1000 total counts or 1000 total genes detected. Genes were filtered out if they failed to achieve 1 count in at least 20% of a particular cell condition group. Multi-dimensional scaling was performed on normalized log2-CPM expression values with size factors calculated by the computeSumFactors function in scran (Lun et al., 2016). These data are available through the Gene Expression Omnibus under accession number GSE109100.

ChIP sequencing

For *in vivo* leukemia PU.1 ChIP, whole splenocytes were isolated from heavily leukemic mice that were either untreated (n = 2 mice) or Dox treated (n = 3) for 2 days, where > 90% of splenocytes were AML246 cells. For *in vitro* leukemia ChIP time course analysis $\sim 10^7$ viable (PI-negative) cells or Cd11b-high viable cells were flow sorted using a FACSAria (BD Bioscience). Cells were cross-linked for 10 min at room temperature in 0.1 volumes of fresh formaldehyde solution (11% formaldehyde, 1 mM EDTA, 0.5 mM EGTA, 50 mM HEPES-KOH, 100 mM NaCl). Formaldehyde was quenched with 0.1 volumes of 1.25 M glycine. Cross-linked cells were washed twice with PBS and snap-frozen. ChIP samples were prepared according to the modified Millipore/Upstate protocol using the polyclonal anti-PU.1 IgG (T-21 X, Santa Cruz Biotechnology: sc-352 X). Briefly, cells were lysed and the chromatin sonicated (Branson Sonifier) in SDS lysis buffer (1% SDS, 10 mM EDTA, 50 mM Tris-HCl pH 8.1) containing protease inhibitors (Roche). Sonicated chromatin was incubated at 4°C overnight in dilution buffer (0.01% SDS, 1% Triton-X, 1.2 mM EDTA, 16.5 mM Tris-HCl pH 8.1, 165 mM NaCl) containing anti-PU.1 antibody and protease inhibitors, then for another hour with ProteinG DynaBeads. Immunoprecipitated chromatin was washed sequentially in low salt buffer (0.1% SDS, 1% Triton-X, 2 mM EDTA, 20 mM Tris-HCl pH 8.1, 150 mM

NaCl), high salt buffer (low salt buffer with 500mM NaCl), LiCl buffer (1% NP-40, 1% Na deoxycholic acid, 1 mM EDTA, 10 mM Tris-Hcl pH 8.1, 0.25 M LiCl), then twice in TE buffer. Chromatin was eluted from DynaBeads by two rounds of incubation in elution buffer (1% SDS, 0.1 M $NaHCO_3$) at 65°C for 15 min with occasional vortexing. Protein-DNA crosslinks were reversed by incubating the eluate at 65°C for 6 hours in the presence of 0.2 M NaCl and 0.02 mg/ml RNase A, followed by another hour of incubation at 45°C in the presence of 0.04 mg/ml Proteinase K, 10mM EDTA, and 40mM Tris-HCl. DNA was extracted using ChIP DNA clean and concentrator columns (Zymo Research). DNA libraries were prepared from 10 ng ChIP DNA using the Illumina TruSeq DNA Sample Kit and sequenced on NextSeq 500 (86 base single end reads). Reads were aligned to the mouse genome (mm10) using the *Rsubread* program and bam files were sorted using SAMtools (Li et al., 2009). For *in vivo* ChIP samples, MACS2 (Feng et al., 2012) was used to identify differentially bound peaks between the Dox treated and untreated samples by treating the latter samples as background and using a q-value cut-off of 0.05. For *in vitro* time course ChIP samples, peaks were identified by MACS2 using an input control sample as background with a q-value cut-off of 0.05 and fold-enrichment < 10. Remaining peaks were plotted using *Gviz* (Hahne and Ivanek, 2016) and assigned to genes from the RNA-seq analysis with TSS within ± 50 kb using *GenomicRanges* software (Lawrence et al., 2013). Peaks with low values for all samples were filtered out. Changes in PU.1 binding at particular genomic locations over time were determined using *DiffBind* (Ross-Innes et al., 2012), merging ChIP peaks across samples that overlap by at least one base then calculating reads within a binding site interval ('superpeak') for each sample. ChIP-seq data are available through the Gene Expression Omnibus under accession number GSE108945.

ATAC sequencing

Cells were isolated as described for the ChIP time course. Libraries were prepared from 50,000 cells using the Illumina Nextera Kit and standard ATAC-seq protocols (Buenrostro et al., 2013). Libraries were size selected from 200-700 bp on a PippenPrep and sequenced on an Illumina NextSeq 500 (75 base paired end reads). Reads were aligned to the mouse genome (mm10) using the *Rsubread* program and bam files were sorted using SAMtools. Peaks were identified using MACS2 with a q-value cut-off of 0.05. Changes in chromatin accessibility at particular genomic locations over time were determined using *DiffBind* as described above. ATAC-seq data are available through the Gene Expression Omnibus under accession number GSE108944.

Combined RNA-seq, ChIP-seq, and ATAC-seq analysis

Three criteria were used to identify direct PU.1-activated genes where PU.1 binding and release correlates with chromatin opening and closing respectively: (1) Increased expression (5% FDR) at Dox d4 versus d0 (staying up at d8 and d12 relative to d0), followed by decreased expression at d–4 versus d12 (staying down at d–8 and d–12 relative to d12); (2) ChIP superpeak counts increasing at Dox d4 versus d0 (staying up at d8 and d12 relative to d0), and decreasing at d–4 versus d12 (staying down at d–8 and d–12 relative to d12); and (3) ATAC superpeak counts increasing at Dox d4 versus d0 (staying up at d8 and d12 relative to d0), and decreasing at d–4 versus d12 (staying down at d–8 and d–12 relative to d12). These 1274 genes corresponded to 6127 ChIP superpeaks and 11029 ATAC superpeaks. For these genes, combined DiffBind analysis of ChIP and ATAC superpeaks was used to identify sites where PU.1 binding correlates with chromatin opening, yielding 958 sites corresponding to 804 genes (Table S3). For 24 of these genes (including *Csf1r*, *Itgam*, *Ncf1*, *Tlr9*, *Bcl2a1a*) PU.1 binding and chromatin accessibility were correlated within ± 500 bp of the TSS. Enrichment of pathways (REACTOME, KEGG) among these 804 genes was assessed using the egsea.ora method from *EGSEA* (Alhamdoosh et al., 2017).

Exome sequencing

Genomic DNA was extracted from sorted leukemia cells using the DNeasy Blood and Tissue kit (QIAGEN, Valencia, CA). Exome sequencing libraries were prepared using the Agilent SureSelect Mouse All Exon V1 kit, and were sequenced on an Illumina HiSeq 2000 (100 base paired end reads). Sequence reads were aligned using BWA (v 0.6.1) with default settings to the reference mouse genome mm10. Reads aligning to multiple genomic locations and potential CPR duplicates were removed and raw SNV calls were made using Samtools (v 0.1.18). Raw SNV calls were then annotated and filtered as previously described (Andrews et al., 2012). Allele counts for particular SNVs were extracted from the bam files and visualized using IGV (Robinson et al., 2011; Thorvaldsdóttir et al., 2013). Exome sequencing data are available through NCBI BioProject PRJNA308523.

QUANTIFICATION AND STATISTICAL ANALYSIS

Bioinformatic analysis of RNA-seq, ChIP-seq, and ATAC-seq data are included in the relevant methods sections above. All other statistical analyses were performed using GraphPad Prism software. The Mantel-Cox log-rank test was used for statistical assessment of survival (Figures 1B, 1G, 3D, 5B, and S2E). Student's t test was used for comparison of groups of samples of equal variance. The unpaired Student's t test with Welch's correction was used to compare groups of samples with significantly different variance (for $n < 6$). For each experiment the number of mice and experimental replicates along with the statistical test and p value are indicated in the figure legend.

DATA AND CODE AVAILABILITY

RNA-seq, ChIP-seq, and ATAC-seq data are available from NCBI GEO as part of SuperSeries GSE76934:

https://www.ncbi.nlm.nih.gov/geo/query/acc.cgi?acc=GSE76934

RNA-seq

GEO: GSE76874 (AML246 *in vivo*):

https://www.ncbi.nlm.nih.gov/geo/query/acc.cgi?acc=GSE76874

GEO: GSE76875 (AML410 *in vivo*)

https://www.ncbi.nlm.nih.gov/geo/query/acc.cgi?acc=GSE76875

GEO: GSE108946 (AML246 *in vitro* time course):

https://www.ncbi.nlm.nih.gov/geo/query/acc.cgi?acc=GSE108946

GEO: GSE109100 (AML246 single cell RNA-seq):

https://www.ncbi.nlm.nih.gov/geo/query/acc.cgi?acc=GSE109100

ATAC-seq

GEO: GSE108944 (AML246 *in vitro* time course)

https://www.ncbi.nlm.nih.gov/geo/query/acc.cgi?acc=GSE108944

ChIP-seq

GEO: GSE108945 (AML246 *in vitro* time course)

https://www.ncbi.nlm.nih.gov/geo/query/acc.cgi?acc=GSE108945

Exome sequencing (AML246 and AML410)

https://www.ncbi.nlm.nih.gov/bioproject/?term=PRJNA308523

blood®
Regular Article

MYELOID NEOPLASIA

The EMT modulator SNAI1 contributes to AML pathogenesis via its interaction with LSD1

Catherine L. Carmichael,[1,*] Jueqiong Wang,[1] Thao Nguyen,[1] Oluseyi Kolawole,[1] Aissa Benyoucef,[2,3] Charlotte De Mazière,[1,4] Anna R. Milne,[1] Sona Samuel,[1] Kevin Gillinder,[1] Soroor Hediyeh-zadeh,[5] Anh N. Q. Vo,[1] Yizhou Huang,[6,7] Kathy Knezevic,[7] William R. L. McInnes,[1] Benjamin J. Shields,[1] Helen Mitchell,[1] Matthew E. Ritchie,[5] Tim Lammens,[8,9] Beatrice Lintermans,[9,10] Pieter Van Vlierberghe,[9,10] Nicholas C. Wong,[1,11] Katharina Haigh,[1-3] Julie A. I. Thoms,[12] Emma Toulmin,[1] David J. Curtis,[1,13] Ethan P. Oxley,[1] Ross A. Dickins,[1] Dominik Beck,[6,7] Andrew Perkins,[1] Matthew P. McCormack,[1] Melissa J. Davis,[5,14,15] Geert Berx,[4,9] Johannes Zuber,[16] John E. Pimanda,[7,12,17] Benjamin T. Kile,[18] Steven Goossens,[1,4,9,10,19,*] and Jody J. Haigh[1-3,*]

[1]Australian Centre for Blood Diseases, Monash University, Melbourne, VIC, Australia; [2]Department of Pharmacology and Therapeutics, Rady Faculty of Health Sciences, University of Manitoba, Winnipeg, MB, Canada; [3]Research Institute in Oncology and Hematology, CancerCare Manitoba, Winnipeg, MB, Canada; [4]Department for Biomedical Molecular Biology, Ghent University, Ghent, Belgium; [5]Walter and Eliza Hall Institute of Medical Research, Melbourne, VIC, Australia; [6]Centre for Health Technologies and School of Biomedical Engineering, University of Technology Sydney, Sydney, NSW, Australia; [7]Lowy Cancer Research Centre and Prince of Wales Clinical School, Faculty of Medicine, University of New South Wales, Sydney, NSW, Australia; [8]Department of Pediatric Hematology-Oncology and Stem Cell Transplantation, Ghent University Hospital, Ghent, Belgium; [9]Cancer Research Institute Ghent, Ghent, Belgium; [10]Department of Biomolecular Medicine, Ghent University, Ghent, Belgium; [11]Monash Bioinformatics Platform, Monash University, Melbourne, VIC, Australia; [12]Lowy Cancer Research Centre and School of Medical Sciences, Faculty of Medicine, University of New South Wales, Sydney, NSW, Australia; [13]Department of Clinical Haematology, Alfred Health, Melbourne, Australia; [14]Department of Medical Biology, University of Melbourne, Melbourne, VIC, Australia; [15]Department of Biochemistry and Molecular Biology, Faculty of Medicine, Dentistry and Health Sciences, University of Melbourne, Melbourne, VIC, Australia; [16]Research Institute of Molecular Pathology, Vienna, Austria; [17]Department of Haematology, Prince of Wales Hospital, Randwick, NSW, Australia; [18]Department of Anatomy and Developmental Biology, Monash Biomedicine Discovery Institute, Monash University, Melbourne, VIC, Australia; and [19]Department of Diagnostic Sciences, Ghent University, Ghent, Belgium;

KEY POINTS

- **KDM1A/LSD1 is a new therapeutic target for AML; we have identified SNAI1 as a pathological modulator of KDM1A/LSD1 target selection in AML.**
- **Targeting the SNAI1-LSD1 complex or its downstream targets may be a novel and potent therapeutic strategy for the treatment of AML.**

Modulators of epithelial-to-mesenchymal transition (EMT) have recently emerged as novel players in the field of leukemia biology. The mechanisms by which EMT modulators contribute to leukemia pathogenesis, however, remain to be elucidated. Here we show that overexpression of SNAI1, a key modulator of EMT, is a pathologically relevant event in human acute myeloid leukemia (AML) that contributes to impaired differentiation, enhanced self-renewal, and proliferation of immature myeloid cells. We demonstrate that ectopic expression of Snai1 in hematopoietic cells predisposes mice to AML development. This effect is mediated by interaction with the histone demethylase KDM1A/LSD1. Our data shed new light on the role of SNAI1 in leukemia development and identify a novel mechanism of LSD1 corruption in cancer. This is particularly pertinent given the current interest surrounding the use of LSD1 inhibitors in the treatment of multiple different malignancies, including AML. (*Blood*. 2020;136(8):957-973)

Introduction

Acute myeloid leukemia (AML) is a genetically heterogeneous disease with an average 5-year overall survival (OS) of <40%. Comprehensive genomic profiling of AML patients has resulted in a clearer understanding of the recurrent genetic lesions that underpin the development and pathogenesis of this aggressive leukemia.[1,2] The frequent mutation of epigenetic regulators, such as DNMT3a, TET1/2, and IDH1/2, highlights a critical role for deregulated epigenetic mechanisms in AML pathogenesis.[3] In contrast to genetic changes, epigenetic modifications are potentially reversible and thus provide unique opportunities for targeted therapy.[4] Lysine-specific demethylase 1A (LSD1/KDM1A), hereafter referred to as LSD1, is an H3K4Me1/2 histone demethylase that regulates gene expression through its involvement in various transcriptional complexes such as CoREST and the nucleosome remodelling and deacetylase complex.[5,6] LSD1 has emerged as a viable therapeutic target in AML[7] because its activity is frequently perturbed in this disease, and studies have demonstrated that LSD1 inhibition and/or downregulation can induce AML cell differentiation in vitro and reduce tumor burden in vivo.[8,9] However, the mechanisms by which LSD1 activity is perturbed in AML, and the identity of the key downstream events that contribute to AML pathogenesis, remain unclear.

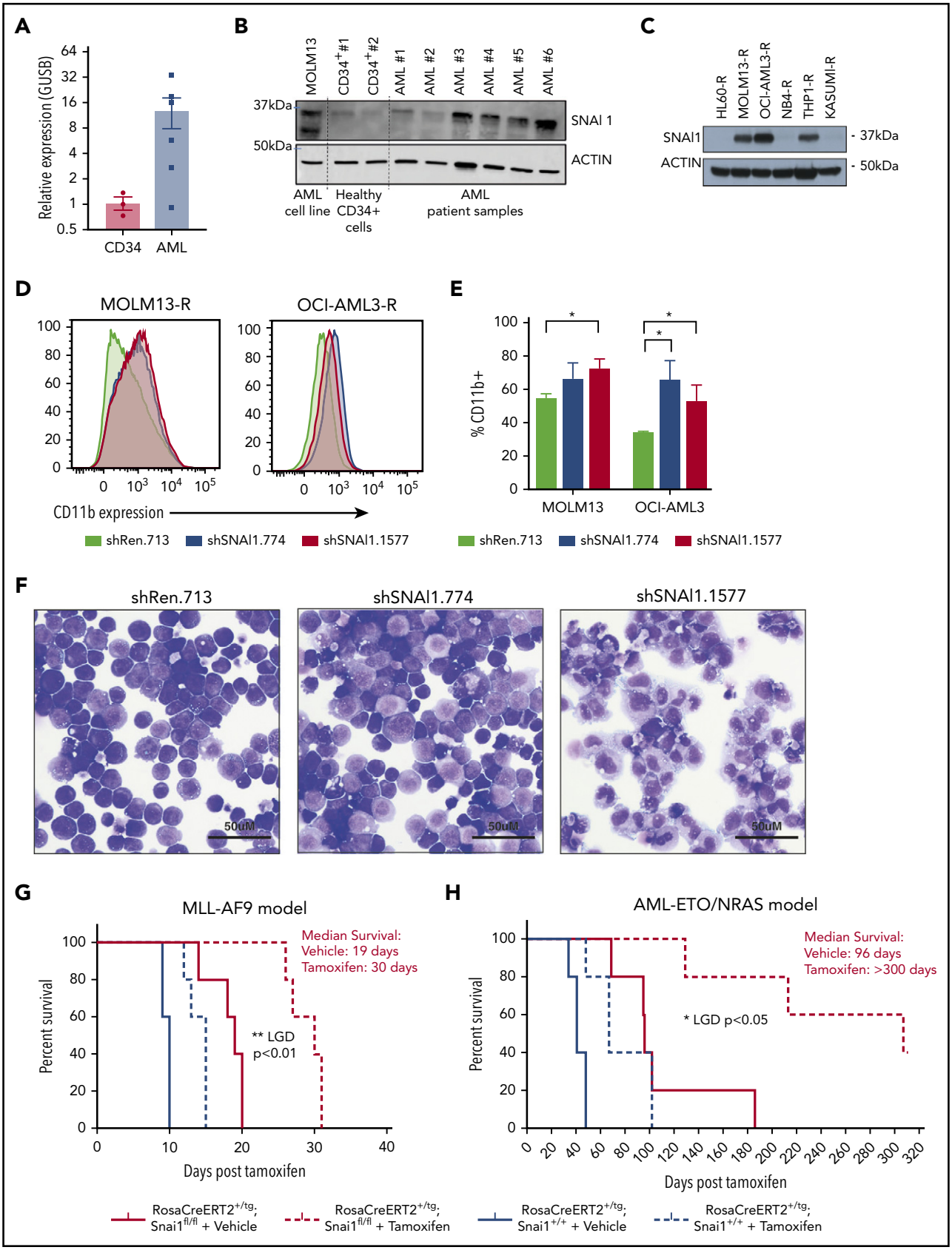

Figure 1. A putative role for *SNAI1* in human AML. (A) Quantitative real-time PCR analysis showing *SNAI1* mRNA is expressed ~12-fold higher in human AML patient samples compared with normal hematopoietic stem and progenitor cells ($CD34^+$, n = 3; AML, n = 6; $P < .05$ Mann-Whitney nonparametric 1-tailed test). SNAI1 expression is normalized to the expression of the housekeeping gene GUSB. (B) SNAI1 protein expression is higher in AML patient samples compared with healthy $CD34^+$ control cells. The MOLM13 cell line is also shown as a comparison. (C) Western blot analysis showing MOLM13-R, OCI-AML3-R, and THP1-R AML cell lines express SNAI1 protein, whereas HL60-R, NB4-R, and Kasumi-R do not. (D) shRNA-mediated *SNAI1* knockdown in OCI-AML3-R and MOLM13-R AML cell lines results in upregulation of the myeloid maturation marker CD11b (red

Epithelial-to-mesenchymal transition (EMT) modulators of the SNAIL (SNAI1/2/3) and ZEB (ZEB1/2) families are key regulators of epithelial tumor biology by facilitating cancer cell invasion and metastasis, acquiring cancer stem cell properties, and activating survival pathways responsible for increased chemotherapy and radiotherapy resistance.[10,11] In hematological malignancies, however, the role of these proteins has been largely overlooked because of their perceived lack of relevance in non-EMT contexts. Recently, we and others have begun to show that deregulated expression of EMT modulators represents a previously unrecognized pathogenic event in acute leukemia.[12-14] Increased levels of ZEB1 in AML are associated with a more aggressive and invasive phenotype and subsequently poorer OS,[13] and ZEB2 has been shown to be a novel regulator of AML differentiation and proliferation[12] as well as a driver of early thymic progenitor T-cell acute lymphoblastic leukemia.[14] The mechanisms by which EMT modulators contribute to leukemia development and pathogenesis, however, remain to be elucidated.

In this current study, we have discovered a novel oncogenic role for SNAI1 in AML development and show that increased expression of EMT modulators, such as SNAI1, are key contributors to the perturbation of LSD1 activity that is critical for AML pathogenesis.

Materials and methods

Cell culture

RIEP-modified human AML cell lines[15] were maintained in RPMI medium supplemented with 10% fetal bovine serum (Sigma), penicillin (100 U/mL-1) and streptomycin (100 μg/mL-1), and 2 mM of L-glutamine (Gibco). HPC-7 cells were kindly provided by Leif Carlsson (Umea University, Umea, Sweden) and grown in Iscove modified Dulbecco medium supplemented with 10% fetal bovine serum (Sigma), penicillin (100 U/mL-1) and streptomycin (100 μg/mL-1), 2 mM of L-glutamine (Gibco), 0.05 mM of 2-mercaptoethanol, and 100 ng/mL of mouse stem cell factor (mSCF; peprotech). Fetal liver cells were cultured in Dulbecco's modified Eagle medium supplemented with 10% (volume/volume) fetal calf serum, mSCF (100 ng/mL), mouse interleukin-6 (mIL-6; 10 ng/mL), mouse Flt3L (5 ng/mL), and mouse thrombopoietin (mTPO; 50 ng/mL).

Retroviral production and cell transduction

The top 3 predicted short hairpin RNAs (shRNAs) for SNAI1 (shSNAI1.774, shSNAI1.1577, and shSNAI1.1633) were cloned into the LMP-miR-E vector,[16] and murine wild-type (WT) and mutant Snai1 complementary DNA (cDNA) were subcloned with a 5′FLAG tag into the MSCV-IRES-GFP vector (Addgene). HEK293T packaging cells were transfected with target viral vectors and packaging plasmids using Lipofectamine reagent (Invitrogen), and supernatant was collected after 48 hours and stored in aliquots at −80°C degrees. Retroviral transduction of fetal liver cells and HPC7 cells was performed in 12-well plates coated with 32 μg/mL of retronectin (Takara Bio) using the spin infection protocol. Briefly, retroviral supernatant was spun onto retronectin-coated plates for 2 hours, followed by addition of cells in culture medium supplemented with 4 μg/mL of polybrene (Sigma).

Flow cytometry

Cells were run on an LSR Fortessa (BD Biosciences) flow cytometric machine and data analyzed using FACSDiva or FlowJo software (BD Biosciences). Dead cells were excluded from analysis using either propidium iodide or the fixable viability dye eFluor780 or eFluor450 (eBioscience). Antibodies used for flow cytometry are listed in supplemental Table 6.

Human patient samples

Human patient samples were obtained and used in accordance with the Declaration of Helsinki guidelines, and investigations were performed only after local ethical committee approval and with informed written patient consent. Patient sample details are provided in supplemental Table 1.

Mice and animal procedures

All animal experiments were performed according to the regulations and guidelines in the Australian Code for the care and use of animals for scientific purposes 2013 and approved by the Alfred Medical Research and Education Precinct Animal Ethics Committee. Bone marrow transplantation and Cre induction experiments are described in the supplemental Methods.

Mouse pathology and blood cell analysis

Hematopoietic organs were fixed in 10% buffered formalin and stained with hematoxylin and eosin for histopathological examination. Spleen and bone marrow cytospins (Cytospin 4; Thermo Fisher Scientific) and peripheral blood smears were stained with Wright-Giemsa. Submandibular blood samples were collected into EDTA-coated tubes, and differential counts were performed on a HemaVet 950FS automated blood analysis machine (Drew-Scientific).

Quantitative Real-time polymerase chain reaction

RNA was isolated using the RNeasy midi- or minikit (Qiagen), and RNA concentration was measured on the NanoDrop 1000 Spectrophotometer according to the manufacturer's instructions (Bio-Rad). cDNA was generated using the SuperScript III reverse transcriptase kit according to the manufacturer's instructions (Sigma). Relative gene expression of SNAI1 was calculated using the δ-Ct method.[17]

Figure 1 (continued) and blue lines) compared with the control shRen.713 shRNA (black line). (E) Quantification of the percentage of $CD11b^+$ cells in shRen.713 infected cells (black bars) compared with shSNAI1 infected cells (red bars). Data are represented as mean + standard error of the mean; n = 3 independent replicates. (F) Wright-Giemsa staining analysis of MOLM13-R cells shows evidence of myeloid differentiation, such as increased cytoplasmic/nuclear ratio and presence of cytoplasmic granules, upon SNAI1 knockdown in shSNAI1.774 and shSNAI1.1577 cells compared with control shRen.713 cells. Kaplan-Meier plots showing that Cre (tamoxifen)–mediated loss of *Snai1* in MLL-AF9 (G) and AML-ETO/NRAS–driven (H) AML models leads to a significant reduction in the survival of recipient mice as determined by leukemia growth delay (LGD)[52] analysis (AML-ETO, $P < .05$; MLL-AF9, $P < .01$). Red lines indicate $Snai1^{fl/fl}$ cells, and black lines indicate $Snai1^{+/+}$ cells. Dotted lines indicate mice treated with tamoxifen vs solid lines indicated mice treated with vehicle. Data are from 5 recipient mice per cohort, each transplanted with 300 000 (MLL-AF9) or 500 000 (AML-ETO/NRAS) AML cells combined from 2 to 3 primary tumors. $^*P < .05$ Student 2-sided unpaired *t* test, $^{**}P < .01$ Mantel-Cox test.

Methylcellulose culture and replating

Methylcellulose cultures were incubated for 7 days at 37°C and 5% carbon dioxide in duplicate 1.1-mL, 35-mm dishes of Methylcult 3234 (Stem Cell Technologies) supplemented with 100 ng/mL of SCF, 10 ng/mL of IL-3, and 4 IU/mL of erythropoietin. Methylcellulose colonies were dissociated into Dulbecco's modified Eagle medium/10% fetal calf serum and stained for flow cytometric analysis or cytocentrifuged for cytological analysis (antibodies used are given in supplemental Table 1). For replating assays, cells were washed out of methylcellulose using 6× phosphate-buffered saline (PBS) washes and then replated in Methocult 3234 and cultured for another 7 days.

RNA-seq analysis

At 7 to 10 days posttransduction, RNA was extracted using an RNeasy midikit and quality assessed using a BioAnalyzer machine (Agilent). Library preparation was performed using the Truseq stranded messenger RNA (mRNA) kit (Illumina), and single-end 100-bp reads were generated on an Illumina HiSeq 2500. Details of RNA sequencing (RNA-seq) data analysis are included in the supplemental Methods. RNA-seq data are available from Gene Expression Omnibus (GEO; GSE132724).

ChIP

Chromatin immunoprecipitation (ChIP) assays were performed as previously described[18] with 2×10^7 cells per condition using an antibody against H3K4me1 (Abcam #ab8895), H3K4me2 (Millipore #07-030), SNAI1 (Cell Signaling #3879), or LSD1 (Abcam #ab17721). More detailed protocols are given in the supplemental Methods.

ChIP-seq

Library preparation for H3K4me1/2 ChIP samples was performed by BGI (Hong Kong) using a variation of Illumina's standard protocol. The libraries were sequenced by BGI using a HiSeq2500 analyzer. Library preparation for the Snai1 ChIP samples was performed using the Illumina Truseq ChIP library preparation kit (Illumina), and sequencing was performed on an Illumina NextSeq analyzer. ChIP-seq data are available from GEO (GSE132990).

Western blotting and immunoprecipitation

Western blot analysis was performed using standard protocols with the following antibodies: rabbit polyclonal α-SNAI1 (C15D3; Cell Signaling Technology #3879), HRP-conjugated α-B-Actin (Sigma #ab49900), and secondary HRP-conjugated rabbit α-mouse (Calbiochem #401353) and goat α-rabbit (Calbiochem #402335) antibodies. Detection was performed using an ECL detection kit (GE Healthcare). Immunoprecipitations were performed using the α-LSD1 antibody (Abcam #ab17721) conjugated to Dynabeads Protein G (Invitrogen #1003D). More detailed protocols are given in the supplemental Methods.

ATAC-seq

A total of 100 000 cells per sample were collected and washed with PBS, pelleted by centrifugation, and washed with lysis buffer (10 mM of tris[hydroxymethyl]aminomethane hydrochloride; pH, 7.4; 10 mM of sodium chloride; 3 mM of magnesium chloride; 0.1% Tween 20) after a 3-minute incubation on ice. The tagmentation reaction (1× Tagment DNA buffer, 0.3× PBS, 0.1% Tween 20, and 2.5 μL of Tn5 [Illumina]) was performed at 37°C for 30 minutes using a thermocycler in a 50-μL volume as previously described.[19] Reactions were immediately purified using a MinElute PCR Kit (Qiagen) and underwent 13 cycles of amplification with indexing adapters before being sequenced on the NovaSeq 6000 platform (Illumina). Replicate sample libraries (3×) were generated on successive days. Assay for transposase-accessible chromatin (ATAC)–seq data are available from GEO (GSE147873).

Results

Increased SNAI1 expression plays a key role in human AML pathogenesis

Using the BloodSpot database, we discovered that *SNAI1* expression is significantly increased in AML compared with normal hematopoietic stem/progenitor cells irrespective of presence of genetic abnormality/driver mutation (supplemental Figure 1A). To confirm this result, we performed quantitative real-time polymerase chain reaction (qRT-PCR) on 6 AML patient samples (supplemental Table 1) and 3 human $CD34^+$ control hematopoietic stem/progenitor cell preparations and found that *SNAI1* mRNA levels were on average ~12-fold higher in the AML samples (Figure 1A). A recent study by Shousha et al[20] also found an increased level of *SNAI1* in AML patients compared with healthy controls. In their study, they observed only a 2.6-fold increase in *SNAI1* mRNA; however, they analyzed whole-blood samples rather than bone marrow, which may explain their lower fold change result. Furthermore, we could also observe a clear increase in protein levels for SNAI1 in a separate cohort of 4 of 6 primary AML patient samples compared with normal $CD34^+$ cells (Figure 1B) and in 3 of 6 AML cell lines (Figure 1C). Because of dynamic and rapid degradation of SNAI1 protein, primary AML and $CD34^+$ cells had to first be treated with a proteasome inhibitor (MG132) for 24 hours to stabilize the SNAI1 protein before western blot analysis.

Using 2 independent AML patient gene expression data sets (available from the online databases PROGgene[21,22] and UCSC Cancer Browser[23]), we identified a significant correlation between high *SNAI1* expression (above the median) in AML patients with normal cytogenetics and reduced OS (supplemental Figure 1B). This survival advantage was only observed in patients with normal-/intermediate-risk cytogenetics, and no correlation with common AML mutations could be observed (data not shown).

To determine how increased *SNAI1* expression contributes to AML biology, we performed shRNA-mediated *SNAI1* knockdown using existing optimized miR-E-shRNA murine retroviral vectors[16] in 6 human AML cell lines that were modified (AML-RIEP) to express the retroviral ecotropic receptor (rtTA3-IRES-EcoR-PGK-Puro).[15] Three of these AML-RIEP cell lines (OCI-AML3-R, MOLM13-R, and THP1-R) expressed SNAI1 protein, whereas the other 3 cell lines (HL60-R, NB4-R, and KASUMI-R) were negative for SNAI1 under steady-state conditions (Figure 1C). We tested the top 3 predicted shRNAs for human SNAI1 according to Fellman et al[16] in MOLM13-R cells and identified a 60% to 90% knockdown at the RNA level for all 3 shRNAs (supplemental Figure 1C). A concomitant reduction in SNAI1 protein level was seen for shSNAI1.774 and shSNAI1.1577 vs the

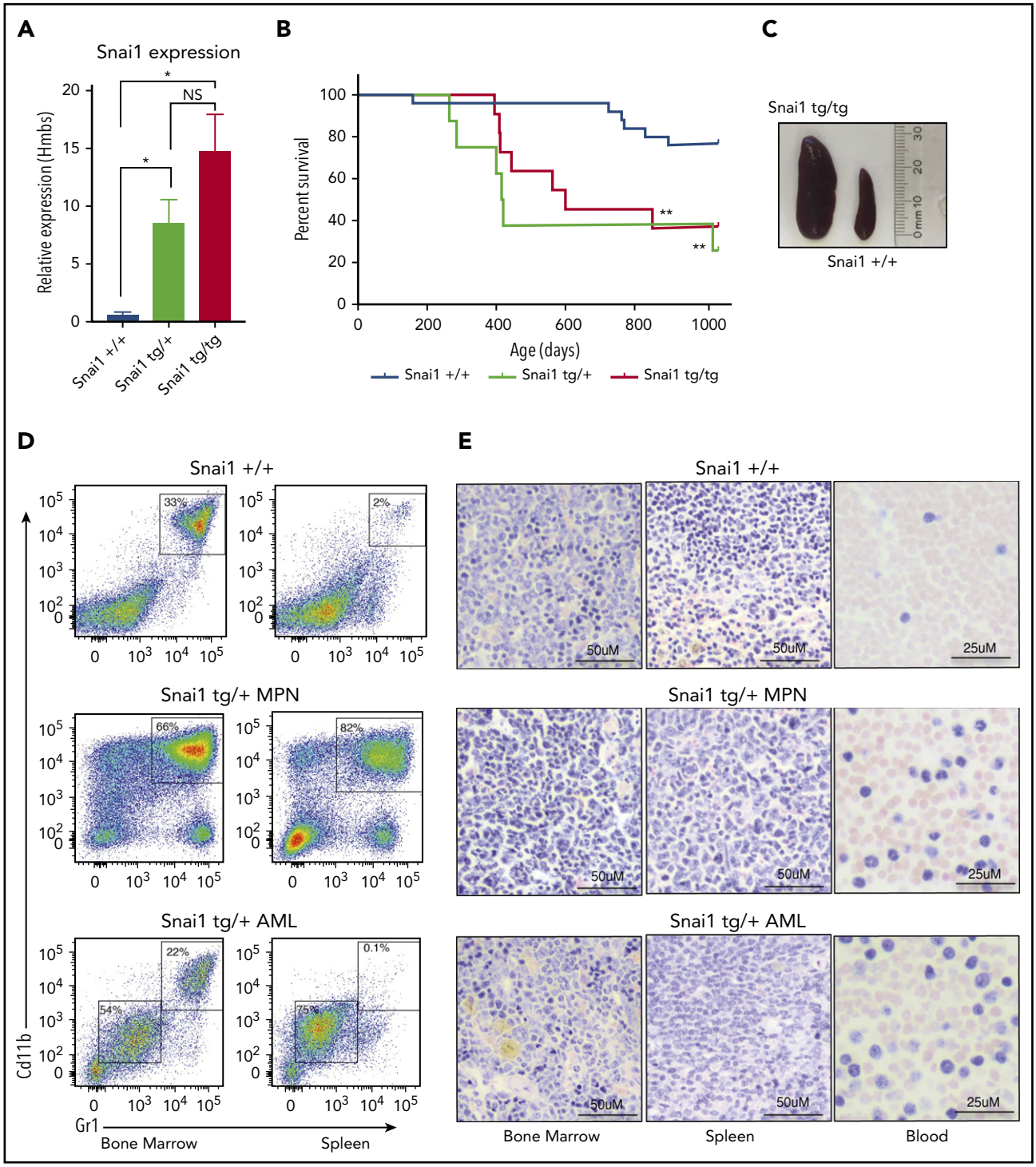

Figure 2. Enforced hematopoietic expression of Snai1 predisposes mice to AML development. (A) Quantitative real-time PCR analysis showing *Snai1* mRNA levels were approximately eightfold to 15-fold higher in transgenic mouse bone marrow, as compared with WT controls (*Snai1*$^{+/+}$, n = 3; *Snai1*$^{tg/+}$, n = 3; *Snai1*$^{tg/tg}$, n = 3). Data are presented as mean + standard error of the mean. (B) Kaplan-Meier plot showing *Snai1* transgenic mice become moribund from ~12 months of age, with a median age of 601 days for *Snai1*$^{tg/tg}$ and 418 days for *Snai1*$^{tg/+}$. No significant difference in survival was observed between heterozygous and homozygous transgenic mice. (C) Pictograph showing splenomegaly in an *Snai1*$^{tg/tg}$ mouse. (D) Representative flow cytometric plots with predominant CD11b^{+}GR1^{+} cell populations in both the bone marrow and spleen. Flow cytometric profiles of CD11b and GR1 expression on bone marrow and spleen cells are shown for a representative WT mouse in the top panel, a moribund mouse with a myeloproliferative disease in the middle panel, and a mouse with AML in the bottom panel. (E) Hematoxylin and eosin staining of bone marrow, spleen, and peripheral blood histological sections of the same mice as in panel D are shown. A representative WT mouse is depicted in the top panel. A representative mouse with myeloproliferative disease is shown in the middle panel, with evidence of granulocytic cell infiltration in the spleen and blood, increased numbers of granulocytic precursor and mature cells in the bone marrow and spleen, and reduced erythropoiesis. In the bottom panel, a representative mouse with AML is shown as evidenced by myeloid blast cell infiltration into bone marrow, spleen, and peripheral blood, along with loss of normal hematopoiesis in the bone marrow and spleen. *$P < .05$ 1-tailed Student unpaired *t* test, **$P < .01$ Mantel-Cox test.

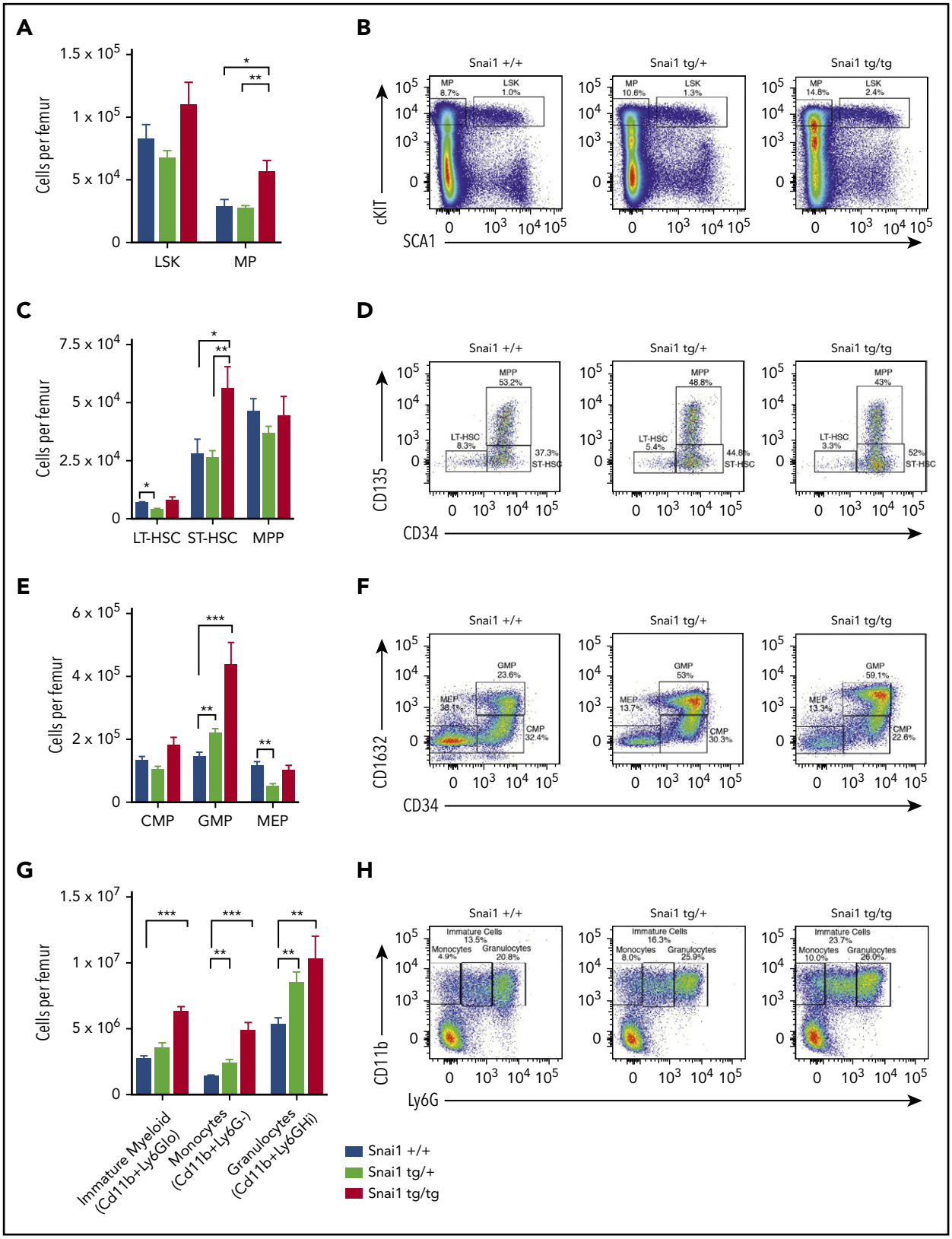

Figure 3. *Snai1* overexpression perturbs myeloid lineage development. (A) Immunophenotypic characterization of hematopoietic stem (LSK) and myeloid progenitor (MP) cell populations within the bone marrow of *Snai1* transgenic mice. (B) Flow cytometric analysis showing representative dot plots of LSK gated cells. (C) Within the stem cell compartment, there was a significant increase in the number of short-term HSCs (ST-HSCs; LIN$^-$cKIT$^+$SCA1$^+$CD34$^+$CD135$^-$) but no change in the number of long-term HSCs (LT-HSCs; lin$^-$cKit$^+$Sca1$^+$CD34$^-$-CD135$^-$) or multipotent progenitors (MPPs; LIN$^-$cKIT$^+$SCA1$^+$CD34$^+$CD135$^+$). (D) Representative dot plots of LT-HSC, ST-HSC, and MPP gated cells are shown. (E) A significant increase in the number of common myeloid progenitors (CMPs; LIN$^-$cKIT$^+$SCA1$^-$CD34$^+$CD16/32$^-$) GMPs (LIN$^-$cKIT$^+$SCA1$^-$CD34$^+$CD16/32$^+$) was observed; however, the megakaryocyte/erythroid progenitor (MEP; LIN$^-$cKIT$^+$SCA1$^-$CD34$^-$CD16/32$^-$) population was slightly reduced (significant only in the

control shREN.713, an shRNA targeting the *Renilla* gene (supplemental Figure 1D). Because no effect on SNAI1 protein levels was seen for shSNAI1.1663, we excluded this from future experiments. We successfully transduced 5 of 6 of these AML cell lines (THP1-R was refractory to transduction, suggesting the inserted ecotropic receptor gene had been shut down or lost) with either 1 of the 2 best-performing shRNAs (shSNAI1_774 and shSNAI1_1577) or a control shRNA targeting the *Renilla* gene (shRen_713). Two weeks posttransduction, shRNA-expressing OCI-AML3-R and MOLM13-R (SNAI1^{+}; Figure 1C) cells showed significantly increased levels of CD11b on their surface (indicative of myeloid maturation; Figure 1D-E), whereas no change in CD11b expression was observed in the SNAI1^{-} (Figure 1C) NB4-R, HL60-R, or Kasumi-R cell lines (supplemental Figure 1E-F). The increase in CD11b expression observed in the MOLM13-R cell line further correlated with morphological changes consistent with partial myeloid differentiation, including an increased cytoplasmic/nuclear ratio and presence of cytoplasmic granules (Figure 1F).

Snai1 expression is required for AML pathogenesis driven by common AML oncogenes

To investigate whether endogenous expression of *Snai1* is required for the pathogenesis of common AML oncogenes, we generated mouse AMLs driven by either the *MLL-AF9* (t9;11) or *AML/ETO* (t8;21)/*NRAS* human oncogenes on a tamoxifen-inducible *RosaCreERT2-Snai1*$^{fl/fl}$ background.[24] Tumor latency was significantly increased for the MLL-AF9 model when *Snai1* was deleted (median survival of 30 days for tamoxifen compared with 19 days for vehicle-treated mice; Figure 1G red lines). The delay in development of the AML-ETO/NRAS model was even more profound (96 days for vehicle-treated and >300 days for tamoxifen-treated mice), with 3 of 5 mice remaining alive at the end of the experiment (300 days posttransplantation; Figure 1H red lines). Importantly, the delay in tumor latency after *Snai1* deletion was significantly longer in both models than that induced by Cre toxicity alone[25] (Figure 1G-H black lines).

Ectopic Snai1 induces myeloproliferation and predisposes mice to leukemia development

To determine the effect of increased *Snai1* expression on hematopoietic development, we used our published conditional gain-of-function *Snai1* transgenic mice[26] (supplemental Figure 2A). Expression of the *Snai1-IRES-EGFP* transgene from the *Rosa26* promoter was induced specifically in the hematopoietic lineage by breeding transgenic mice onto a *Vav-iCre*$^{tg/+}$ transgenic background.[27] *Vav-iCre*$^{+/-}$*Snai1*$^{tg/+}$ (Snai1 heterozygous) or *Vav-iCre*$^{+/-}$*Snai1*$^{tg/tg}$ (Snai1 homozygous) transgenic mice were born at normal Mendelian ratios (data not shown). The levels of *Snai1* mRNA in the bone marrow of transgenic mice were approximately eightfold (*Snai1*$^{tg/+}$) to 15-fold (*Snai1*$^{tg/tg}$) greater than those observed in WT littermate controls (Figure 2A), comparable to the increased levels of *SNAI1* we observed in human AML samples.

We aged a cohort of *Snai1* transgenic mice up to 34 months of age (952 days) and found that from 12 months onward, mice progressively became moribund with evidence of anemia and splenomegaly (Figure 2B-C). In *Snai1* transgenic mice analyzed upon terminal disease development (*Snai1*$^{tg/+}$, n = 7; *Snai1*$^{tg/tg}$, n = 2), flow cytometry of hematopoietic organs revealed an expanded population of myeloid cells with variable levels of CD11b^{+}GR1^{+} expression (Figure 2D; supplemental Figure 2B) or, in 1 case, cells expressing CD71^{+}Ter119^{+} (supplemental Figure 2C). Histological analysis revealed the presence of myeloproliferation in all mice, including hypercellularity and disordered architecture of bone marrow and spleen, increased granulopoiesis, expanded erythropoiesis, and an increase in immature myeloid forms (Figure 2E; supplemental Figure 2Di). Three mice further demonstrated clear AML development, with excessive blast cells evident in bone marrow, spleen, and/or peripheral blood (Figure 2E; supplemental Figure 2Dii). Two of the AMLs (1 *Snai1*$^{tg/+}$ and 1 *Snai1*$^{tg/tg}$) as well as one of the myeloproliferative diseases (Snai1$^{tg/+}$) could be transplanted into NSG mice, with recipient mice showing development of a disease similar to that of the primary donors (supplemental Figure 2E).

Ectopic Snai1 significantly perturbs myeloid cell development

To gain a better understanding of how Snai1 expression predisposes to leukemia, we analyzed myeloid development in preleukemic *Snai1* transgenic mice at 8 months of age. Peripheral blood counts of transgenic animals did not differ from those of WT littermate controls (supplemental Figure 3A), and hematopoietic organ cellularity and architecture were also normal (supplemental Figure 3B-C). Flow cytometric analysis of bone marrow identified a slight but nonsignificant increase in the number of hematopoietic stem cell (HSC)–enriched LSK cells, as well as a significant expansion of the myeloid progenitor (MP) compartment in *Snai1*$^{tg/tg}$ mice (Figure 3A-B). Within the LSK compartment, *Snai1*$^{tg/tg}$ mice further displayed a significant increase in the number of short-term HSCs (ST-HSCs) but no difference in multipotent progenitors (MPPs) or long-term HSCs (LT-HSCs) (Figure 3C-D). Within the myeloid progenitor compartment, both the *Snai1*$^{tg/+}$ and *Snai1*$^{tg/tg}$ mice were found to have a significant increase in the number of granulocyte macrophage progenitor cells (GMPs) but no change in the number of common myeloid progenitor cells (CMPs). A slight but significant decrease in the number of megakaryocyte erythroid progenitor cells (MEPs) was observed in the *Snai1*$^{tg/+}$ mice (Figure 3E-F).

Further downstream of the GMPs, we identified a significant increase in the number of myeloid lineage cells (CD11b^{+}) in the bone marrow and spleen of *Snai1* transgenic mice. Ly6G levels on Cd11b^{+} cells can distinguish immature myeloid cells and monocytes, which are Ly6G^{low} or Ly6G^{-}, respectively, from mature granulocytes, which are Ly6G^{high}. All myeloid cell populations were found to be expanded in both *Snai1*$^{tg/+}$ and *Snai1*$^{tg/tg}$ mice, suggesting an overall increase in myeloid cell output (Figure 3G-H).

Figure 3 (continued) heterozygous mice). (F) Representative FACs plots of myeloid progenitor gating are shown. (G) A significant increase in the number of immature (CD11b^{+}Ly6G^{lo}) and mature myeloid cells (monocytes CD11b^{+}GR1^{-} and granulocytes CD11b^{+}Ly6G^{hi}) was also evident in the bone marrow of *Snai1* transgenic mice. (H) Flow cytometric analysis showing representative dot plots of myeloid gated cells. (A,C,E,G) Data are represented as mean + standard error of the mean for *Snai1*$^{+/+}$ (n = 13), *Snai1*$^{tg/+}$ (n = 8), and *Snai1*$^{tg/tg}$ (n = 7) biological replicates.*$P < .05$, **$P < .01$, ***$P < .001$ Student 2-sided unpaired *t* test.

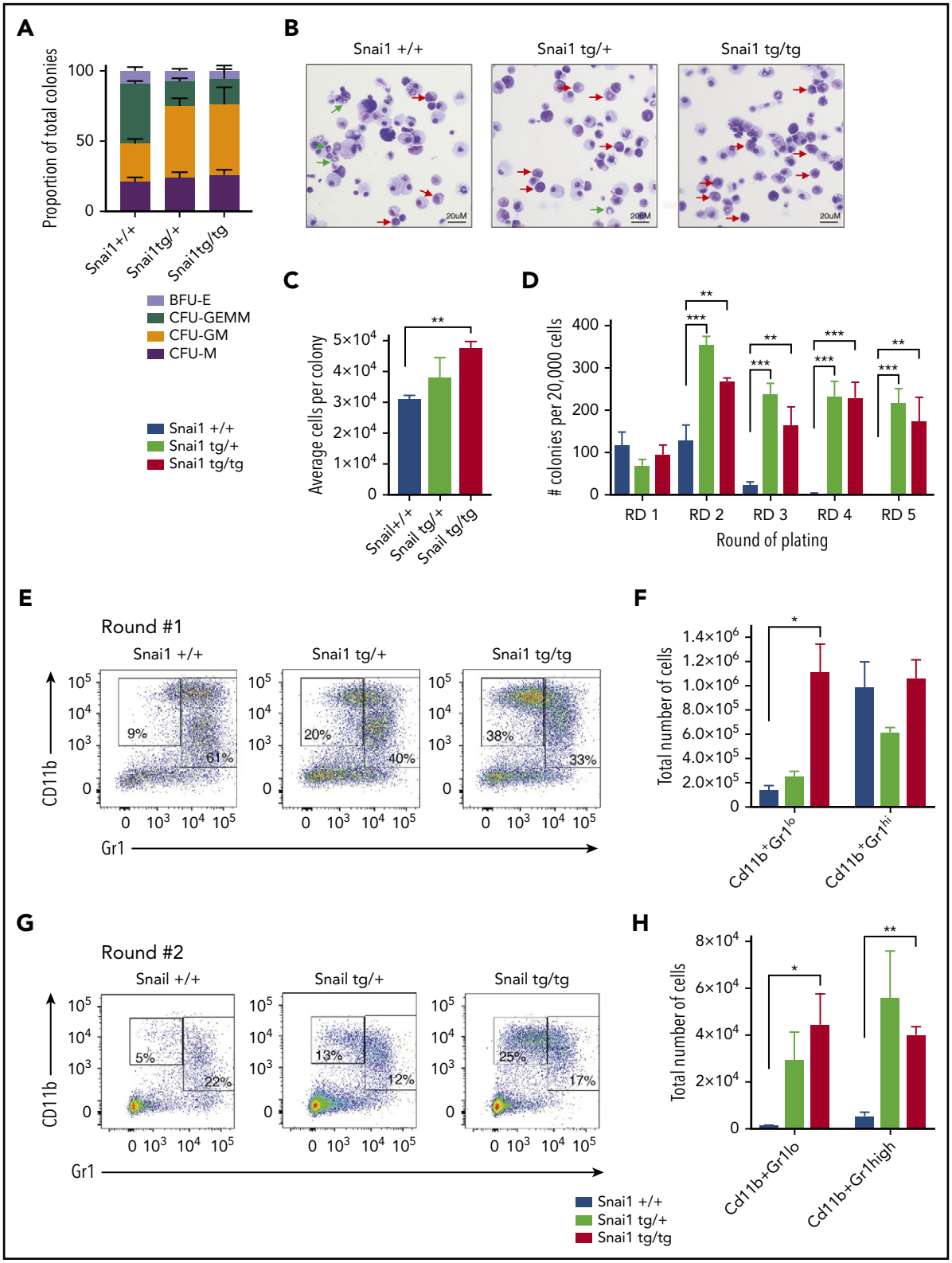

Figure 4. *Snai1* overexpression induces self-renewal potential in immature myeloid cells and impairs granulocytic differentiation. (A) *Snai1*$^{tg/+}$ and *Snail*$^{tg/tg}$ bone marrow generate significantly more colony-forming unit (CFU) granulocyte/macrophage (GM) colonies and significantly fewer CFU granulocyte/erythroid/macrophage/megakaryocyte (GEMM) colonies as compared with *Snai1*$^{+/+}$ bone marrow. (B) Wright-Giemsa staining analysis of *Snai1*$^{tg/+}$ and *Snail*$^{tg/tg}$ methylcellulose colony cytospins showing almost complete lack of mature granulocytes (green arrows) and an increase in immature myeloid cells (red arrows) as compared with *Snai1*$^{+/+}$ colonies. (C) The number of cells per colony (calculated as total number of cells per total number of colonies) was significantly increased in *Snail*$^{tg/tg}$ cultures compared with *Snai1*$^{+/+}$ cultures. *Snai1*$^{tg/+}$ cultures also showed a trend toward an increased number of cells per colony; however, this was not significant. (D) Quantification of bone marrow methylcellulose colonies showing that *Snai1*$^{tg/+}$ hematopoietic progenitor cells have increased self-renewal capability compared with *Snai1*$^{+/+}$ controls, with *Snai1*$^{tg/+}$ and *Snai1*$^{tg/tg}$ cells able to generate colonies in methylcellulose up to 5 rounds of replating. *Snai1*$^{+/+}$ cells were only able to replate up to 3 rounds. (E) Flow cytometric analysis of methylcellulose-derived hematopoietic cells

Snai1-induced perturbed myelopoiesis is a cell-intrinsic phenotype

To further explore this perturbed myeloid differentiation phenotype and compare *Snai1* transgenic stem and progenitor cell fitness with that of WT control cells, we performed a competitive bone marrow transplantation. Test bone marrow from 6- to 8-month-old *Snai1*$^{+/+}$, *Snai1*$^{tg/+}$, or *Snai1*$^{tg/tg}$ mice (CD45.2^{+}) was transplanted alongside competitor bone marrow from *Snai1*$^{+/+}$ C567BL/6 (CD45.1^{+}) mice into lethally irradiated C57BL/6 mice (supplemental Figure 4A). Mice were then analyzed at 12 and 20 weeks posttransplantation.

Particularly evident in the spleen, both the *Snai1*$^{tg/+}$ and *Snai1*$^{tg/tg}$ cells contributed to a significantly higher proportion of myeloid cells at both time points compared with *Snai1*$^{+/+}$ cells (supplemental Figure 4B-C). These data demonstrate that the perturbed myelopoiesis in the *Snai1* transgenic animals is a cell-intrinsic effect.

In the bone marrow, there was no significant difference in the contribution of *Snai1*$^{tg/+}$ or *Snai1*$^{tg/tg}$ cells to the stem and progenitor cell compartment, with the exception of a mild increase in the contribution of the *Snai1*$^{tg/+}$ cells to the GMP lineage at 12 weeks posttransplantation (supplemental Figure 4D-E). These data indicate that the changes in the stem and progenitor populations seen in the transgenic mice may be compensatory because of an altered bone marrow microenvironment.

To confirm that the myeloid differentiation defects were indeed cell intrinsic, we performed methylcellulose colony-forming assays. Whole bone marrow from *Snai1*$^{tg/+}$ and *Snai1*$^{tg/tg}$ mice generated normal numbers of hematopoietic colonies compared with *Snai1*$^{+/+}$ mice (data not shown). However, the colony type was significantly skewed toward the granulocyte/macrophage lineage, with a higher number of colony-forming unit granulocyte/macrophage (CFU-GM) and a concomitant reduction in colony-forming unit granulocyte/erythroid/macrophage/megakaryocyte (CFU-GEMM) in both the *Snai1*$^{tg/+}$ and *Snai1*$^{tg/tg}$ cultures (Figure 4A). Furthermore, cytocentrifuge and flow cytometric analysis of cells washed out of methylcellulose revealed an increase in the number of immature myeloid cells (red arrows) within the transgenic colonies and a reduction in the number of mature granulocytes (green arrows) compared with WT colonies (Figure 4B), suggesting terminal myeloid differentiation was impaired. Colony size also seemed larger in the transgenic cultures, with the number of cells per colony being higher in the *Snai1* transgenic cultures, although this was only significant for the *Snai1*$^{tg/tg}$ cultures (Figure 4C).

Ectopic Snai1 increases self-renewal of myeloid progenitors

Given that *Snai1* expression has previously been associated with promoting stemness in mammary tumors,[28] we sought to determine whether the expanded myeloid progenitor cell compartment of transgenic mice displayed increased self-renewal capacity. We performed serial replating methylcellulose assays on bone marrow from *Snai1*$^{+/+}$, *Snai1*$^{tg/tg}$, and *Snai1*$^{tg/+}$ mice and observed that although colony numbers after the first round of colony formation were similar between WT and transgenic cultures, the subsequent rounds of replating all resulted in an increase in the number of colonies generated by the transgenic cells (Figure 4D). Furthermore, although transgenic cells were capable of replating up to at least 5 rounds in methylcellulose, all self-renewal capacity was exhausted in the WT cells after the third round of replating (Figure 4D). The colonies generated at round 2 were again larger in the transgenic cultures, with a concomitant increase in the total number of cells per culture dish (data not shown). Immunophenotypic analysis of cells washed out of methylcellulose revealed a significant increase in the number of immature (CD11b^{+}, GR1^{lo}) myeloid cells in the transgenic colonies after round 1 of replating (Figure 4E-F), which was also evident after round 2 (Figure 4G-H). Morphological analysis further demonstrated that WT colonies from round 2 consisted predominantly of mast cells (supplemental Figure 4F green arrows), whereas transgenic cultures still retained a large number of immature myeloid cells (supplemental Figure 4F red arrows).

Ectopic SNAI1 perturbs normal myeloid differentiation via its interaction with the histone demethylase LSD1

In epithelial tumor contexts, SNAI1 is known to exert its predominantly gene-repressive functions via interactions with histone modifying complexes, including the CoREST/HDAC complex.[29,30] A key component of this complex is the histone demethylase LSD1, which has been shown to directly bind SNAI1 via its SNAG (SNAIL/GFI) protein interaction domain.[30] LSD1 is an integral cofactor of the SNAG domain–containing hematopoietic transcription factors GFI1/1B and has also been shown to cooperate with other key hematopoietic transcription factors, including RUNX1, GATA2, SCL/TAL1, and SALL4.[31-34] Through these interactions, LSD1 is essential for maintaining normal hematopoietic stem cell function and self-renewal, as well as for driving myeloid differentiation.[34-36] Importantly, loss of LSD1 function in mice results in similar myeloid differentiation defects (eg, impaired granulocytic development and expansion of immature myeloid cells and GMPs), as we observed in our *Snai1* transgenic mice, suggesting that increased expression of SNAI1 in the hematopoietic system may affect LSD1 function.[35,36] To test whether ectopic SNAI1 can physically interact with LSD1 in the hematopoietic context, we performed coimmunoprecipitation studies in the murine hematopoietic progenitor cell line, HPC7, which had been transduced with a retroviral vector encoding FLAG-tagged SNAI1.[37] Immunoprecipitation with an anti-LSD1 antibody was able to pull down both endogenous and ectopic SNAI1 (Figure 5A), consistent with previous studies in epithelial cells.[30] To determine whether this SNAI1/LSD1 interaction is required for the myeloid defects induced by *Snai1*, we cloned either WT *Snai1* (MIG-Snai1) or a mutant form of *Snai1* (MIG-mut5Snai1), which is unable to bind

Figure 4 (continued) showing a higher percentage of immature and mature myeloid cells generated from *Snai1*$^{tg/+}$ and *Snai1*$^{tg/tg}$ progenitor cells at the first round of culture. (F) Quantification of immature (CD11b^{+}GR1^{lo}) and mature (CD11b^{+}GR1^{hi}) myeloid cell populations in *Snai1*$^{+/+}$, *Snai1*$^{tg/+}$, and *Snai1*$^{tg/tg}$ cultures showing a significant increase in immature myeloid cells in the *Snai1*$^{tg/tg}$ cultures at the first round of culture. (G-H) A similar increase in immature myeloid cells was also observed after the second round of replating. (A,C,D,F,H) Data are represented as mean + standard error of the mean; n = 3 biological replicates. *$P < .05$, **$P < .01$, ***$P < .001$ Student 2-tailed unpaired *t* test.

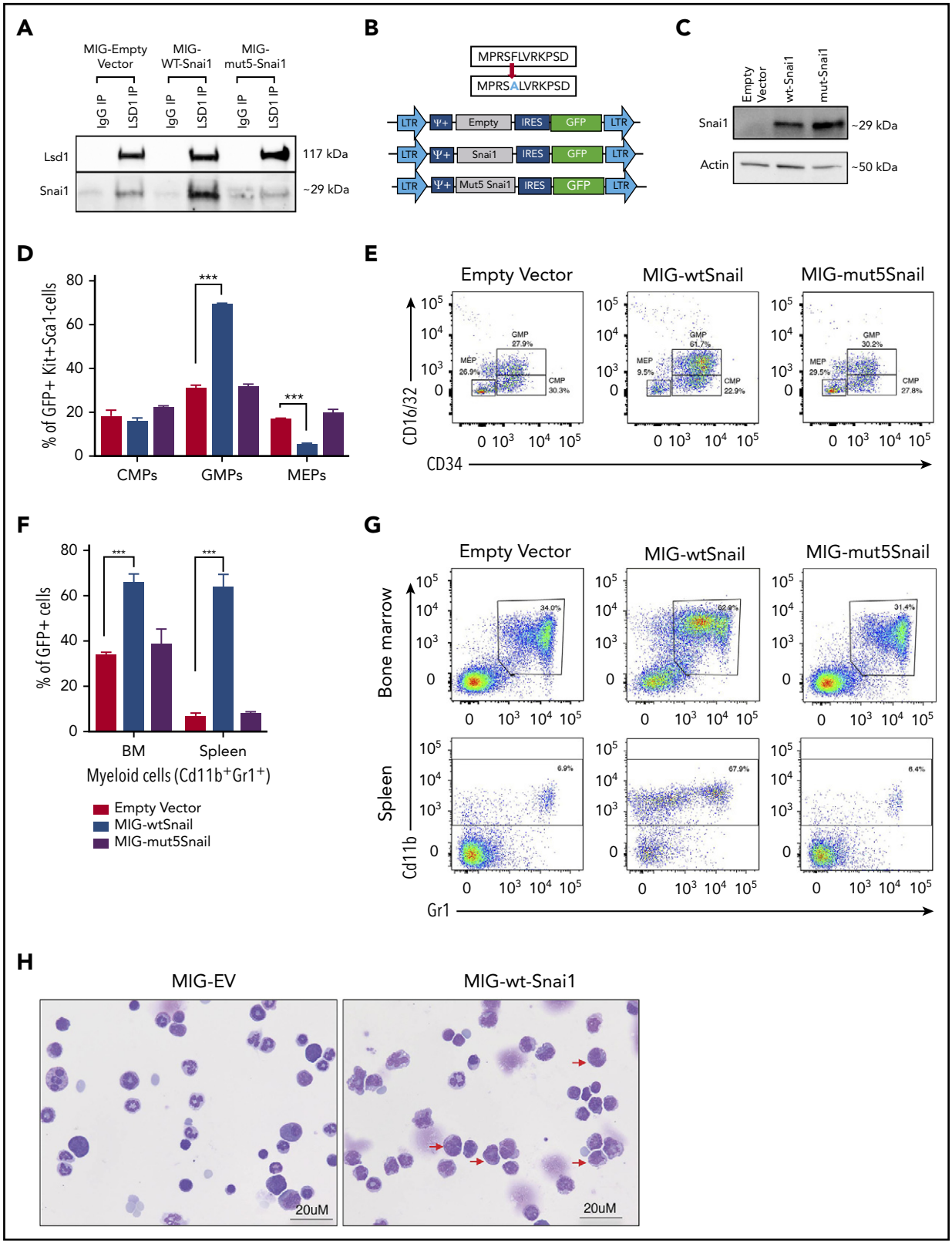

Figure 5. SNAI1 requires interaction with LSD1 to induce myeloid development defects. (A) Western blot analysis showing that LSD1 immunoprecipitation is able to pull down SNAI1 in the mouse hematopoietic progenitor cell line (HPC7). Empty vector control (MIG-EV)–transduced cells and MIG-mut5Snai1–transduced cells show a low level of endogenous SNAI1 pulldown, whereas the MIG-Snai1–transduced cells show a much higher level of SNAI1 pulldown because of the overexpressed WT-SNAI1 protein also being pulled down. The overexpressed mut5SNAI1 protein is not able to be pulled down by LSD1. (B) Overview (upper panel) of the mutant version of Snai1 that was generated with a phenylalanine (F) to alanine (A) amino acid change at position 5 of the SNAI1 protein. WT *Snai1* cDNA and the mutant *Snai1* cDNA were individually cloned into the MSCV-IRES-GFP retroviral vector. An empty MSCV-IRES-GFP vector was used as a transduction control. (C) MIG-Snai1– and MIG-mut5-Snai1–transduced cells both show high levels of SNAI1 protein, whereas the endogenous SNAI1 protein is unable to be detected in the empty vector–transduced cells. The western blot also demonstrates that the F→A

LSD1, into an MSCV-IRES-GFP retroviral vector backbone (Figure 5B). The mutant *Snai1* cDNA encodes a protein with a single amino acid change at position 5 (A>F) of the N-terminal SNAG domain that blocks LSD1 binding but does not impair protein stability, localization, or folding[30] (Figure 5C; data not shown). Coimmunoprecipitation analysis confirmed the inability of this mutant form of SNAI1 to bind LSD1 (Figure 5A). Next, we generated mouse bone marrow chimeras using C57BL/6 fetal liver cells transduced with MIG-Snai1, MIG-mut5Snai1, or empty vector MIG-EV retrovirus. At 12 weeks posttransplantation, GFP$^+$ cells from MIG-Snai1 bone marrow chimeric mice displayed the same myeloid developmental defects and cell expansion we had previously identified in the *Snai1* transgenic mice (Figure 5D-G blue bars). The phenotype, however, was much more profound in the retroviral setting, with an expansion of immature myeloid cells and a reduction in mature granulocytes also readily apparent upon morphological analysis of GFP$^+$ bone marrow cells from MIG-Snai1 mice (Figure 5H red arrows). These data further confirm that the *Snai1*-induced myeloid defects are due to cell-intrinsic effects of *Snai1* expression on myeloid cell development.

Notably, the myeloid defects observed in the MIG-Snai1 mice were completely absent in the MIG-mut5Snai1 mice (Figure 5D-G purple bars). Combined, these data verify that the 5F>A mutation in the SNAG domain completely abolishes the ability of SNAI1 to perturb myeloid development both in vivo and in vitro, signifying a requirement for LSD1 binding in SNAI1-induced myeloid defects.

Ectopic SNAI1 induces an altered myeloid differentiation gene expression program through perturbed LSD1 activity

Increased levels of SNAI1 in stem/progenitor cells may: (1) sequester LSD1 away from its normal hematopoietic interacting partners (ie, GFI1/1b, RUNX1, GATA2, SCL/TAL1, and SALL4[31-34]), leading to reduced demethylation of its H3K4me1/2 histone substrates at promoter/enhancer elements of target genes, and/or (2) result in binding of SNAI1/LSD1 complexes at promoters and enhancers containing SNAI1 E-box binding motifs. LSD1 may then demethylate SNAI itself and/or enhance the demethylation of H3K4me1/2 marks specifically at SNAI1 target genes. To investigate these proposed models further, we performed RNA and ChIP-seq as well as ATAC-seq analysis on the HPC7 cell line transduced with either MIG-Snai1, MIG-mut5Snai1, or MIG-EV retroviral vectors.

Using a false discovery rate (FDR) cutoff of $P < .05$, we identified 474 significantly upregulated genes (the second highest being *Snai1* itself) and 361 significantly downregulated genes upon ectopic expression of WT *Snai1* (supplemental Figure 5A; supplemental Table 2). In contrast, the mut5-Snai1–expressing cells showed no differentially expressed genes (other than mutant *Snai1* itself) compared with MIG-EV-transduced control cells (supplemental Figure 5B).

Differentially expressed genes (FDR < 0.05) in the MIG-Snai1–transduced HPC7 cells cover a broad spectrum of biological processes, including, but not limited to, alterations in cytokine signaling (eg, *Il1b*, *Il1r2*, *Csf1r*, and *Csf2rb*), transcriptional regulation (eg, AP-1 family members Jun/Fos, Hes1, Cebpb, and Gata1), migration/adhesion/invasion (eg, *Mmp8/9/19*, *Ccl2/Ccr2*, and *Cxcr4*), and emerging tumor suppressor genes (eg, *Ssbp2*, *Zdhhc14*, *Sik1*, and *Hook1*[38-41]; supplemental Figure 5C [activated genes, red; repressed genes, blue). Unbiased gene set enrichment analysis using the Hallmark Gene Set panel in the Molecular Signatures Database found that the top gene sets enriched in differentially expressed genes (FDR < 0.05) from MIG-Snai1 HPC7 cells included the TNFα-NFκB, Il2-STAT5, KRAS, apoptosis, hypoxia, p53 signaling, and expected EMT pathway components (Figure 6A; supplemental Table 3), all of which have been previously implicated in AML development/progression.[42-46] This analysis further revealed upregulation of a distinct myeloid differentiation gene expression program in MIG-Snai1 cells (Figure 6B), which was further demonstrated by an increased expression of key myeloid cell surface markers (CD11b, Ly6G, and Ly6C) as detected by flow cytometric analysis (supplemental Figure 6A).

In agreement with our working model of LSD1 inhibition by SNAI1, we observed a significant correlation between genes upregulated as a result of LSD1 chemical inhibition in 2 human AML cell lines (HEL and CMK) and those upregulated by *Snai1* overexpression in HPC7 cells (Figure 6C). Notably, we also identified a significant correlation between those genes upregulated in MIG-Snai1 HPC7 cells and genes upregulated in AML patient samples expressing high levels of endogenous *SNAI1* (Figure 6D; patient data taken from GSE10358).

To determine the genome-wide effects of *Snai1* overexpression on methylation level of the LSD1 histone substrates H3K4me1 and H3K4me2, we performed ChIP-seq analysis using antibodies for the H3K4me1 and H3K4me2 marks. We limited our analysis to regions surrounding the annotated transcription start site (± 5 kb) encompassing proximal and distal regulatory regions, where predominant peaks were observed (supplemental Figure 6B). This analysis identified 629 and 127 genes with associated differential H3K4me1 or H3K4me2 methylation, respectively (supplemental Table 4). Because these 2 histone marks are commonly associated with transcriptional activation,

Figure 5 (continued) mutation in the mut5-SNAI1 protein does not affect its overall protein stability or antibody recognition. (D) Flow cytometric quantification of the GFP$^+$ bone marrow cell population in MIG-Snai1–recipient mice at 12 weeks posttransplantation, showing a significantly increased proportion of granulocyte/macrophage progenitor cells (GMPs) and a significantly decreased proportion of megakaryocyte/erythroid progenitor cells (MEPs) compared with GFP$^+$ cells in MIG-EV–recipient mice (blue bars compared with black bars). The common myeloid progenitor cell (CMP) population was not different between the 2 mouse cohorts (left panel). No difference was observed in MIG-mut5Snai1 bone marrow compared with MIG-EV control bone marrow (purple bars compared with black bars). (E) Representative myeloid progenitor flow cytometric plots from empty vector, MIG-Snai1, and MIG-mut5Snail mice. (F) A significant increase in the proportion of mature myeloid cells was also observed within the GFP$^+$ cell population in MIG-Snai1–recipient mouse bone marrow and spleen (blue bars compared with black bars). These myeloid abnormalities were completely absent in the MIG-mut5Snai1–recipient mice (purple bars). Data are represented as mean + standard error of the mean (SEM); n = 3 biological replicates. (G) Representative myeloid cell flow cytometric plots from bone marrow and spleens of MIG-EV, MIG-Snai1, and MIG-mut5Snail mice. (H) Wright-Giemsa staining of GFP$^+$ bone marrow cytocentrifuge preparations shows normal myeloid development in MIG-EV–recipient mice, whereas in MIG-Snai1–recipient mice, there is a significant increase in the number of immature myeloid cells (red arrows), and a significant reduction of mature granulocytes. (D-E) Data are presented as mean + SEM; n = 3 mice from each cohort ***$P < .001$ Student 2-sided unpaired *t* test.

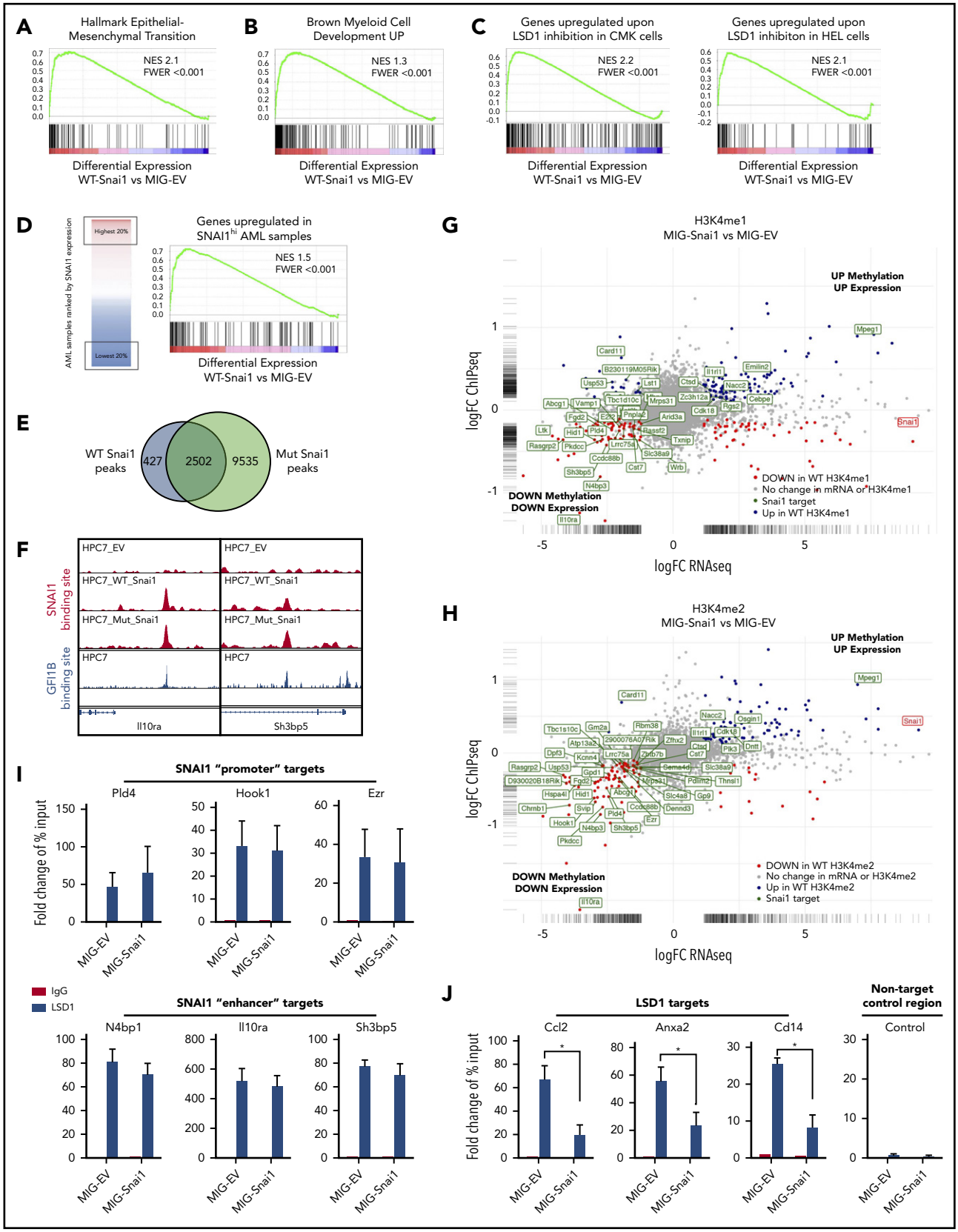

Figure 6. Genomic analysis of HPC7 cells transduced with either MIG-Snai1, MIG-mut5Snai1, or MIG-EV. Gene set enrichment analysis (GSEA) on RNA-seq data from MIG-Snai1 vs MIG-EV identified a significant correlation between genes upregulated in HPC7 cells expressing *Snai1* (MIG-Snai1) and genes involved in the EMT (GSEA: hallmark epithelial mesenchymal transition) (A), genes upregulated upon myeloid development (GSEA: brown myeloid cell development up), genes upregulated upon LSD1 inhibition in HEL and CMK leukemia cell lines (GSE68348) (C), and genes upregulated in SNAI1 high AML patient samples (GSE10358) (D). (E) Overlap between WT SNAI1 and mut5-SNAI1 binding sites in HPC7 cells indicates that mut5SNAI1 protein is still capable of binding DNA. (F) Sample IGV tracks showing clear overlap of WT SNAI1 and mut5SNAI1 binding

an increased level of methylation at promoters and/or enhancers would be expected to correspond to an increase in gene expression and vice versa. We indeed saw that 21% (135 of 629) of genes with H3K4me1 changes and 48% (61 of 127) of genes with H3K4me2 changes showed significant differential expression in our RNA-seq analysis (supplemental Table 4). Furthermore, we observed a clear trend for increased levels of methylation to correspond with increased gene expression and decreased levels of methylation to correspond with reduced gene expression, which was particularly evident for the H3K4me2 mark (supplemental Figure 6C).

Because LSD1 is predominantly associated with gene repression (via demethylation of the active H3K4me1/2 marks), we hypothesized that genes with decreased methylation (and decreased gene expression) may be SNAI1 targets that had become demethylated (and therefore repressed) as a result of binding of LSD1 to SNAI1-bound promoter or enhancer sites. To test this, we performed SNAI1 ChIP-seq analysis to identify SNAI1-bound sites within the MIG-Snai1 HPC7 cells. MACS2 analysis identified 2932 peaks in MIG-Snai1 cells, 12 054 peaks in MIG-Mut5-Snai1 cells, and 137 peaks in MIG-EV cells (supplemental Table 5). Importantly, a majority of WT SNAI1 peaks overlapped entirely with the Mut5-SNAI1 peaks (Figure 6E-F), demonstrating that the mutant form of SNAI1 maintains DNA binding ability but is unable to regulate gene transcription. MEME motif discovery analysis[47] further revealed that 92% of WT SNAI1 binding sites contained a central canonical E-box sequence (CAGGTG), which is known to be the preferred DNA binding motif of SNAI1 (supplemental Figure 6D).[48] In contrast, only 62% of Mut5-SNAI1 binding sites contained this E-box sequence (data not shown), suggesting that reduced specificity of binding may be partly responsible for the increased number of ChIP-seq peaks identified in MIG-Mut5-Snai1 cells. A higher level of expression and stability of the Mut5-SNAI1 protein (data not shown) may also explain the increased peak number. SNAI1 binding sites were predominantly promoter associated (44%) or intergenic (40%), with only 16% of peaks being intragenic (supplemental Figure 6E). WT SNAI1 was bound to 15% of differentially expressed genes (126 of 835), a majority of which were repressed genes (supplemental Figure 6F; 90 of 126 were repressed compared with 36 of 126 being activated). When we overlaid WT SNAI1 binding sites onto our gene expression FC vs histone methylation FC chart (Figure 6G-H), we could clearly see an extensive overlap of WT SNAI1 binding sites in the genes with decreased histone methylation and decreased gene expression. In contrast, we saw very little overlap of binding to activated genes.

ChIP–quantitative PCR for LSD1 in our MIG-Snai1 HPC7 cells further confirmed that LSD1 was indeed also bound at downregulated SNAI1 target sites (*Pld4*, *Hook1*, *Ezr*, *N4bp1*, *Il10ra*, and *Sh3bp5*; Figure 6I), and ATAC-seq analysis demonstrated that WT SNAI-bound gene promoters frequently had reduced chromatin accessibility correlating with reduced transcriptional activity (supplemental Figure 6G). In MIG-EV cells, LSD1 was also found to be bound at these sites, suggesting that it may be recruited in the absence of ectopic SNAI1 by another hematopoietic cofactor, such as GFI1B. Indeed, using previously published data,[49] we were able to identify an overlapping binding site for GFI1B in 50% of WT SNAI1-bound sites that had significant changes in H3K4me2 methylation (Figure 6F; supplemental Table 4). These data suggest possible competition between SNAI1 and GFI1B for LSD1 binding at these sites, particularly as they interact with LSD1 via exactly the same SNAG protein domain.

Finally, ChIP–quantitative PCR for LSD1 at 3 upregulated LSD1 targets with increased H3K4me1/2 methylation (*Ccl2, Cd14*, and *Anxa2*) confirmed that there was a significant reduction of LSD1 binding at these sites in MIG-Snai1 HPC7 cells (Figure 6J), supporting our model that overexpressed SNAI1 can also sequester LSD1 away from its normal gene targets.

Discussion

Deregulated expression of EMT modulators is emerging as a novel theme in AML biology; however, our understanding of how these key developmental regulators and epithelial tumor oncogenes contribute to malignancy of the hematopoietic system is still lacking. In this current study, we have demonstrated a previously unknown association between ectopic EMT factor expression and altered LSD1 activity during malignant transformation of hematopoietic and myeloid stem/progenitors.

SNAI1 is overexpressed throughout a broad spectrum of primary AML patient samples, irrespective of presence of driver mutation or genetic abnormality, and higher levels of *SNAI1* are correlated with decreased OS in this disease (also recently demonstrated for *ZEB1*[13]). Furthermore, we have shown that increased expression of *SNAI1* is functionally relevant for AML biology and contributes to the differentiation block in AML cells in a fashion similar to that demonstrated for *ZEB2*.[12] Using in vivo transgenic and retroviral *Snai1* overexpression systems, we discovered that increased expression of *Snai1* drives an expanded myelopoiesis, enhances self-renewal and proliferative capacity of immature myeloid cells, and ultimately results in the development of a myeloproliferative-like disease that can transform into AML over a prolonged period of time (Figure 7). We identified several AML-relevant biological pathways that are upregulated by SNAI1, including the TNFα-NFκβ pathway[42] and key cytokine/signaling pathways such as those involving RAS and IL-2/Stat5,[43-45] as well as decreased expression of emerging (and thus less well studied) AML tumor suppressors such as *Ssbp2*.[38] The

Figure 6 (continued) sites in 2 representative gene regulatory elements for *Il10ra* and *Sh3bp5*, as well as with published binding sites for GFI1B.[49] FC-FC plot showing differentially expressed genes on the x-axis and differential H3K4me1 (G) or H3K4me2 (H) methylation levels on the y-axis. A correlation between differential methylation and differential expression in MIG-Snai1 cells is evident in both plots. Genes in green have an identified SNAI1 binding site in the ChIP-seq data. Red and blue dots indicate genes with significantly reduced or significantly increased respectively gene expression and methylation in MIG-Snai1 cells using a *P* value cut off <.05. (I) LSD1 ChIP–quantitative PCR (qPCR) results for 6 SNAI1 target genes that have reduced gene expression and reduced H3K4 methylation in MIG-Snai1 HPC7 cells. ChIP-qPCR data show binding of LSD1 directly overlapping SNAI1 binding sites in both the MIG-EV and MIG-Snai1 cells at all sites analyzed. (J) LSD1 ChIP-qPCR results for 3 LSD1 target sites showing significantly reduced LSD1 binding upon SNAI1 expression in MIG-Snai1 HPC7 cells. Control immunoglobulin G (IgG) samples were used as a control for nonspecific ChIP enrichment, and a nontarget control region was used to show specific pulldown at LSD1-bound sites compared with other sites within the genome. Data analyzed using a Mann-Whitney 1-tailed *t* test. $^*P < .01$.

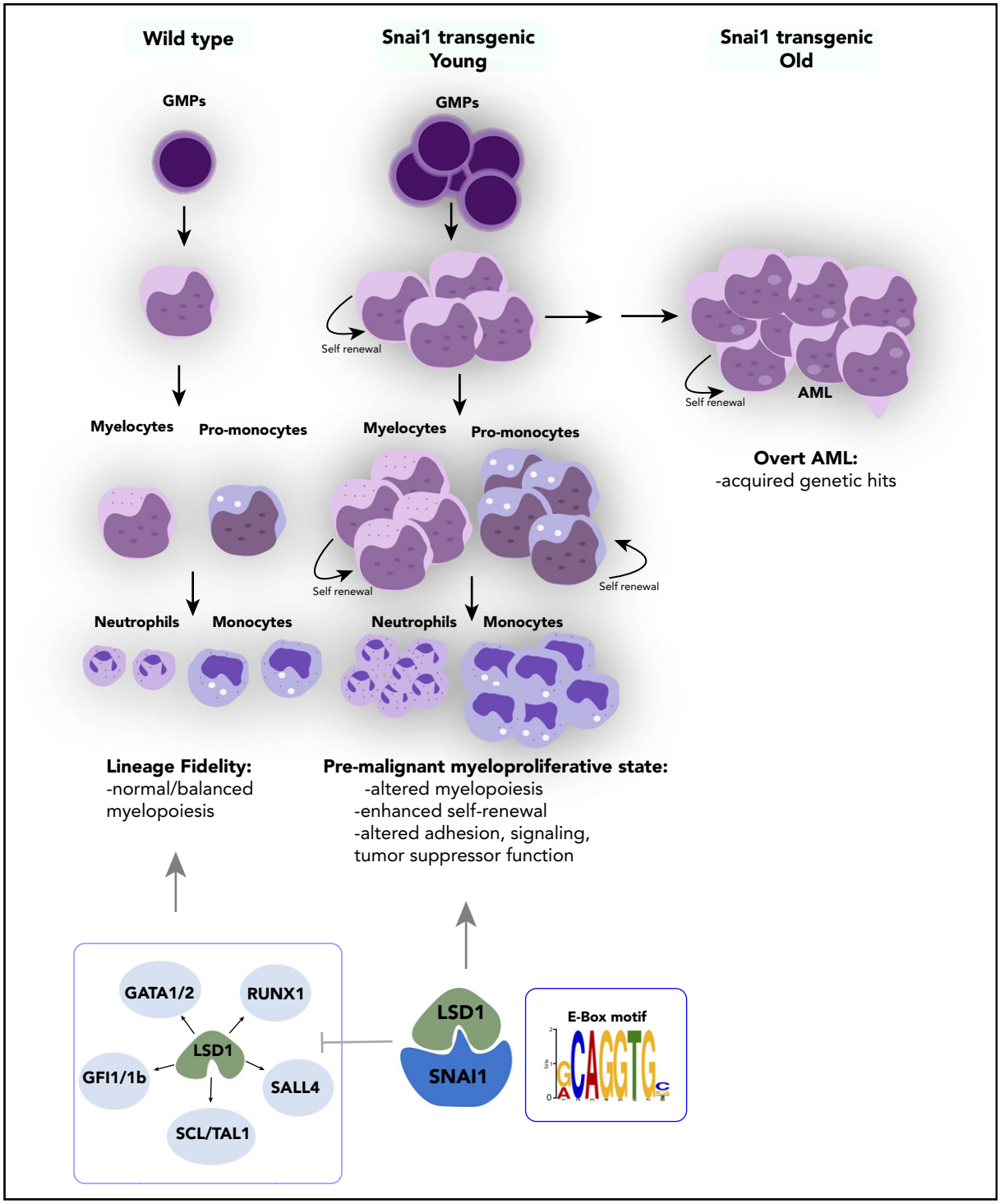

Figure 7. Proposed model of the effect of ectopically expressed SNAI1 on normal hematopoiesis and LSD1 function. During normal hematopoiesis, balanced myeloid development is observed, resulting in normal numbers of mature myeloid cells. Ectopic SNAI1 in hematopoietic cells interacts with LSD1 and subsequently leads to inhibition promotion of myeloid differentiation along the granulocyte and macrophage lineages. This complex drives expanded myeloid cell differentiation and production of excessive numbers of mature myeloid cells, resulting in myeloproliferative phenotypes. SNAI1/LSD1 complex also imbues enhanced self-renewal capacity on immature myeloid cells, allowing these cells to expand and potentially accumulate additional mutations that can result in AML development over an extended period of time. We propose that the interaction between SNAI1 and LSD1 drives myeloid developmental defects through physical interaction at SNAI1 gene targets containing the canonical E-box motif and subsequent modulation of LSD1 function and inhibition of LSD1 binding to its normal hematopoietic transcription factor partners, such as GATA1/2, SALL4, and GFI1/1b, and subsequently compromising the function of these key hematopoietic transcription factors.

altered expression of these key pathways likely cooperates with *Snai1* overexpression to drive full-scale transformation of immature myeloid cells that have enhanced self-renewal properties.

Interestingly, we found that SNAI1-induced myeloid developmental changes were completely dependent on the SNAG domain–mediated interactions with LSD1. This interaction led to not only loss of LSD1 demethylase activity at normal hematopoietic gene targets, but also acquisition or modulation of LSD1 demethylase/gene repression activity at other gene targets that were also bound by SNAI1. In both scenarios, competition for LSD1 binding between SNAI1 and other LSD1 cofactors, such as GFI1B, likely also contributes to the phenotype; however, additional studies will be required to test this further.

LSD1 has garnered much interest over the past few years as a putative therapeutic target in multiple cancer types, including solid tumors and AML, because of its frequently altered expression and/or activity in malignant cells.[50,51] The mechanism of action of LSD1 in AML, however, seems to be in conflict with its known biological roles during normal hematopoietic development. Although loss of LSD1 in hematopoietic cells results in derepression of stem cell–associated genes, acquisition of enhanced stem cell function, and reduced hematopoietic cell differentiation,[35] inhibition/loss of LSD1 in AML cells instead drives myeloid differentiation and switches off expression of oncogenic stem cell genes.[9] Presumably, these conflicting roles suggest that LSD1 function can be altered by malignant mechanisms such as the expression of key AML oncogenes. Indeed, Harris et al[8] showed that LSD1 function specifically at MLL-AF9–bound promoters was important for sustaining leukemia stem cell activity in a mouse model of AML. Our data now suggest that during malignant hematopoiesis, ectopic expression of SNAI1 (and potentially other EMT modulators) is able to perturb normal LSD1 function, not only by interfering with its ability to interact with its normal hematopoietic partners, such as GFI1B (Figure 7), but also by coopting its histone demethylase activity to repress expression of SNAI1 target genes that play key roles in regulating adhesion, signaling, and tumor suppressor functions.

Although our study has focused primarily on the role of LSD1/SNAI1 interactions, it should be noted that other known interactions between SNAI1 and epigenetic modifiers, such as HDAC1/2 and SIN3A, may also be altered upon aberrant SNAI1 expression. Further investigation into the common/specific target genes and pathways regulated by SNAI1/LSD1 and other SNAI/ZEB-containing repression complexes, as well as their functional characterization, is therefore warranted and will enable a greater understanding of the mechanism by which LSD1 and EMT transcription factors contribute to AML biology. Given the known dose-limiting effects of LSD1 inhibition on normal blood cell development, our study suggests that targeting the SNAI1/LSD1 complex or its downstream targets, rather than LSD1 itself, may be a more viable therapeutic option in AML.

Acknowledgments

The authors thank Lief Carlsson (Umea University, Sweden) for providing the HPC7 cells and Andrew Wei (Australian Centre for Blood Diseases, Monash University, Australia) for providing access to primary AML samples.

This work was supported by the Multi-modal Australian Sciences Imaging and Visualisation Environment high-performance computing facility and National eResearch Collaboration Tools and Resources project and funded by project grants G1141081 (J.J.H.); 1102589, 1139787, 11398111, and 1160110 (J.E.P.); program grants 1016647 and 1113577 (B.T.K.), and Senior Research Fellowship (D.J.C) and Independent Research Institutes Infrastructure Support Scheme grant 361646 (B.T.K.) from the Australian National Health and Medical Research Council. T.L. received funding from vzw Kinderkankerfonds and D.B. received funding from Cancer Institute NSW. J.J.H. also received funding from the Canadian Institute of Health Research (project grant 419220). S.G. and P.V.V. received funding from the European Hematology Association (EHA), the Research Foundation Flanders (FWO), the Basic Research Fund of Ghent University and the Belgian Foundation Against Cancer. J.E.P. is also supported by the Anthony Rothe Leukemia Foundation, Translational Cancer Research Network, Cancer Institute NSW, NSW Health Pathology, and South Eastern Area Laboratory Services.

Authorship

Contribution: C.L.C., S.G., and J.J.H. were responsible for study conception and design; C.L.C., J.W., O.K., A.B., T.N., C.D.M., A.R.M., S.S., K.G., W.R.L.M., A.N.Q.V., T.L., B.L., B.J.S., H.M., K.H., Y.H., J.A.I.T., and K.K. acquired the data; C.L.C., K.G., S.H.-z., M.J.D., M.E.R., N.C.W., S.G., and J.J.H. analyzed and interpreted the data; A.P. provided histological review of pathology specimens; C.L.C., S.G., and J.J.H. wrote, reviewed, and revised the manuscript; and P.V.V., E.T., D.J.C., D.B., M.P.M., E.P.O., R.A.D., G.B., J.E.P., J.Z., and B.T.K provided other critical samples, reagents, and/or technical support.

Conflict-of-interest disclosure: The authors declare no competing financial interests.

ORCID profiles: C.L.C., 0000-0002-6751-153X; A.R.M., 0000-0002-1092-4309; K.G., 0000-0002-1221-9718; S.H.-z., 0000-0001-7513-6779; Y.H., 0000-0002-7003-3110; K.K., 0000-0002-3940-3363; W.R.L.M., 0000-0003-4831-4722; H.M., 0000-0002-8359-9279; M.E.R., 0000-0002-7383-0609; T.L., 0000-0001-8733-4027; P.V.V., 0000-0001-9063-7205; N.C.W., 0000-0003-4393-7541; J.A.I.T., 0000-0002-4876-7230; D.J.C., 0000-0001-9497-0996; R.A.D., 0000-0003-4112-5304; A.P., 0000-0003-3644-7093; M.P.M., 0000-0003-1536-5611; M.J.D., 0000-0003-4864-7033; G.B., 0000-0001-5770-2458; S.G., 0000-0002-5693-8570.

Correspondence: Jody J. Haigh, CancerCare Manitoba, ON5029, 675 McDermot Ave, Winnipeg, MB, Canada, R3E 0V9; e-mail: jody.haigh@umanitoba.ca; and Catherine L. Carmichael, Australian Centre for Blood Diseases, Monash University, 99 Commercial Rd, Prahran, Melbourne, VIC, Australia, 3004; e-mail: catherine.carmichael@monash.edu.

Footnotes

Submitted 18 July 2019; accepted 15 April 2020; prepublished online on *Blood* First Edition 5 May 2020. DOI 10.1182/blood.2019002548.

*C.L.C., S.G., and J.J.H. provided equal intellectual contribution to this work.

Contact the corresponding author for original data.

The online version of this article contains a data supplement.

There is a *Blood* Commentary on this article in this issue.

The publication costs of this article were defrayed in part by page charge payment. Therefore, and solely to indicate this fact, this article is hereby marked "advertisement" in accordance with 18 USC section 1734.

REFERENCES

1. Ley TJ, Miller C, Ding L, et al; Cancer Genome Atlas Research Network. Genomic and epigenomic landscapes of adult de novo acute myeloid leukemia [published correction appears in *N Engl J Med*. 2013;369(1):98]. *N Engl J Med*. 2013;368(22):2059-2074.
2. Papaemmanuil E, Gerstung M, Bullinger L, et al. Genomic Classification and Prognosis in Acute Myeloid Leukemia. *N Engl J Med*. 2016; 374(23):2209-2221.
3. Greenblatt SM, Nimer SD. Chromatin modifiers and the promise of epigenetic therapy in acute leukemia. *Leukemia*. 2014;28(7): 1396-1406.
4. Tsai CT, So CW. Epigenetic therapies by targeting aberrant histone methylome in AML: molecular mechanisms, current preclinical and clinical development. *Oncogene*. 2017; 36(13):1753-1759.
5. Shi Y, Lan F, Matson C, et al. Histone demethylation mediated by the nuclear amine oxidase homolog LSD1. *Cell*. 2004;119(7): 941-953.
6. Shi Y, Sawada J, Sui G, et al. Coordinated histone modifications mediated by a CtBP corepressor complex. *Nature*. 2003;422(6933): 735-738.
7. Magliulo D, Bernardi R, Messina S. Lysine-specific demethylase 1A as a promising target in acute myeloid leukemia. *Front Oncol*. 2018; 8:255.
8. Harris WJ, Huang X, Lynch JT, et al. The histone demethylase KDM1A sustains the oncogenic potential of MLL-AF9 leukemia stem cells [published correction appears in *Cancer Cell*. 2012;21(6):856]. *Cancer Cell*. 2012;21(4): 473-487.
9. Schenk T, Chen WC, Göllner S, et al. Inhibition of the LSD1 (KDM1A) demethylase reactivates the all-trans-retinoic acid differentiation pathway in acute myeloid leukemia. *Nat Med*. 2012;18(4):605-611.
10. Puisieux A, Brabletz T, Caramel J. Oncogenic roles of EMT-inducing transcription factors. *Nat Cell Biol*. 2014;16(6):488-494.
11. Stemmler MP, Eccles RL, Brabletz S, Brabletz T. Non-redundant functions of EMT transcription factors. *Nat Cell Biol*. 2019;21(1): 102-112.
12. Li H, Mar BG, Zhang H, et al. The EMT regulator ZEB2 is a novel dependency of human and murine acute myeloid leukemia. *Blood*. 2017;129(4):497-508.
13. Stavropoulou V, Kaspar S, Brault L, et al. MLL-AF9 expression in hematopoietic stem cells drives a highly invasive AML expressing EMT-related genes linked to poor outcome. *Cancer Cell*. 2016;30(1):43-58.
14. Goossens S, Radaelli E, Blanchet O, et al. ZEB2 drives immature T-cell lymphoblastic leukaemia development via enhanced tumour-initiating potential and IL-7 receptor signalling. *Nat Commun*. 2015;6:5794.
15. Zuber J, Shi J, Wang E, et al. RNAi screen identifies Brd4 as a therapeutic target in acute myeloid leukaemia. *Nature*. 2011;478(7370): 524-528.
16. Fellmann C, Hoffmann T, Sridhar V, et al. An optimized microRNA backbone for effective single-copy RNAi. *Cell Rep*. 2013;5(6): 1704-1713.
17. Livak KJ, Schmittgen TD. Analysis of relative gene expression data using real-time quantitative PCR and the 2(-Delta Delta C(T)) method. *Methods*. 2001;25(4):402-408.
18. Diffner E, Beck D, Gudgin E, et al. Activity of a heptad of transcription factors is associated with stem cell programs and clinical outcome in acute myeloid leukemia [published correction appears in *Blood*. 2014;123(18):2901]. *Blood*. 2013;121(12):2289-2300.
19. Corces MR, Trevino AE, Hamilton EG, et al. An improved ATAC-seq protocol reduces background and enables interrogation of frozen tissues. *Nat Methods*. 2017;14(10):959-962.
20. Shousha WG, Ramadan SS, El-Saiid AS, Abdelmoneim AE, Abbas MA. Expression and clinical significance of SNAI1 and ZEB1 genes in acute myeloid leukemia patients. *Mol Biol Rep*. 2019;46(4):4625-4630.
21. Goswami CP, Nakshatri H. PROGgene: gene expression based survival analysis web application for multiple cancers. *J Clin Bioinforma*. 2013;3(1):22.
22. Goswami CP, Nakshatri H. PROGgeneV2: enhancements on the existing database. *BMC Cancer*. 2014;14:970.
23. Zhu J, Sanborn JZ, Benz S, et al. The UCSC Cancer Genomics Browser. *Nat Methods*. 2009;6(4):239-240.
24. Murray SA, Oram KF, Gridley T. Multiple functions of Snail family genes during palate development in mice. *Development*. 2007; 134(9):1789-1797.
25. Li Y, Choi PS, Casey SC, Felsher DW. Activation of Cre recombinase alone can induce complete tumor regression. *PLoS One*. 2014;9(9):e107589.
26. Nyabi O, Naessens M, Haigh K, et al. Efficient mouse transgenesis using Gateway-compatible ROSA26 locus targeting vectors and F1 hybrid ES cells. *Nucleic Acids Res*. 2009;37(7):e55.
27. de Boer J, Williams A, Skavdis G, et al. Transgenic mice with hematopoietic and lymphoid specific expression of Cre. *Eur J Immunol*. 2003;33(2):314-325.
28. Mani SA, Guo W, Liao MJ, et al. The epithelial-mesenchymal transition generates cells with properties of stem cells. *Cell*. 2008;133(4): 704-715.
29. Lin T, Ponn A, Hu X, Law BK, Lu J. Requirement of the histone demethylase LSD1 in Snai1-mediated transcriptional repression during epithelial-mesenchymal transition. *Oncogene*. 2010;29(35):4896-4904.
30. Lin Y, Wu Y, Li J, et al. The SNAG domain of Snail1 functions as a molecular hook for recruiting lysine-specific demethylase 1. *EMBO J*. 2010;29(11):1803-1816.
31. Guo Y, Fu X, Huo B, et al. GATA2 regulates GATA1 expression through LSD1-mediated histone modification. *Am J Transl Res*. 2016; 8(5):2265-2274.
32. Li Y, Deng C, Hu X, et al. Dynamic interaction between TAL1 oncoprotein and LSD1 regulates TAL1 function in hematopoiesis and leukemogenesis. *Oncogene*. 2012;31(48): 5007-5018.
33. Liu L, Souto J, Liao W, et al. Histone lysine-specific demethylase 1 (LSD1) protein is involved in Sal-like protein 4 (SALL4)-mediated transcriptional repression in hematopoietic stem cells. *J Biol Chem*. 2013;288(48): 34719-34728.
34. Saleque S, Kim J, Rooke HM, Orkin SH. Epigenetic regulation of hematopoietic differentiation by Gfi-1 and Gfi-1b is mediated by the cofactors CoREST and LSD1. *Mol Cell*. 2007;27(4):562-572.
35. Kerenyi MA, Shao Z, Hsu YJ, et al. Histone demethylase Lsd1 represses hematopoietic stem and progenitor cell signatures during blood cell maturation. *eLife*. 2013;2:e00633.
36. Sprüssel A, Schulte JH, Weber S, et al. Lysine-specific demethylase 1 restricts hematopoietic progenitor proliferation and is essential for terminal differentiation. *Leukemia*. 2012;26(9): 2039-2051.
37. Pinto do O P, Wandzioch E, Kolterud A, Carlsson L. Multipotent hematopoietic progenitor cells immortalized by Lhx2 self-renew by a cell nonautonomous mechanism. *Exp Hematol*. 2001;29(8):1019-1028.
38. Liang H, Samanta S, Nagarajan L. SSBP2, a candidate tumor suppressor gene, induces growth arrest and differentiation of myeloid leukemia cells. *Oncogene*. 2005;24(16): 2625-2634.
39. Sun X, Zhang Q, Chen W, et al. Hook1 inhibits malignancy and epithelial-mesenchymal transition in hepatocellular carcinoma. *Tumour Biol*. 2017;39(7):1010428317711098.
40. Yang L, Xie N, Huang J, et al. SIK1-LNC represses the proliferative, migrative, and invasive abilities of lung cancer cells. *OncoTargets Ther*. 2018;11:4197-4206.
41. Yeste-Velasco M, Mao X, Grose R, et al. Identification of ZDHHC14 as a novel human tumour suppressor gene. *J Pathol*. 2014; 232(5):566-577.
42. Kagoya Y, Yoshimi A, Kataoka K, et al. Positive feedback between NF-κB and TNF-α promotes leukemia-initiating cell capacity. *J Clin Invest*. 2014;124(2):528-542.
43. Allan JN, Roboz GJ, Askin G, et al. CD25 expression and outcomes in older patients with acute myelogenous leukemia treated with plerixafor and decitabine. *Leuk Lymphoma*. 2018;59(4):821-828.
44. Wingelhofer B, Maurer B, Heyes EC, et al. Pharmacologic inhibition of STAT5 in acute myeloid leukemia. *Leukemia*. 2018;32(5): 1135-1146.
45. Zhou JD, Yao DM, Li XX, et al. *KRAS* overexpression independent of *RAS* mutations confers an adverse prognosis in cytogenetically normal acute myeloid leukemia. *Oncotarget*. 2017;8(39):66087-66097.
46. Post SM, Kornblau SM, Quintás-Cardama A. p53 pathway dysfunction in AML: beyond *TP53* mutations. *Oncotarget*. 2017;8(65): 108288-108289.

47. Bailey TL, Boden M, Buske FA, et al. MEME SUITE: tools for motif discovery and searching. *Nucleic Acids Res*. 2009;37: W202-W208.

48. Chiang C, Ayyanathan K. Characterization of the E-box binding affinity to snag-zinc finger proteins. *Mol Biol (Mosk)*. 2012;46(6):907-914.

49. Wilson NK, Foster SD, Wang X, et al. Combinatorial transcriptional control in blood stem/progenitor cells: genome-wide analysis of ten major transcriptional regulators. *Cell Stem Cell*. 2010;7(4):532-544.

50. Niebel D, Kirfel J, Janzen V, Höller T, Majores M, Gütgemann I. Lysine-specific demethylase 1 (LSD1) in hematopoietic and lymphoid neoplasms. *Blood*. 2014;124(1):151-152.

51. Schulte JH, Lim S, Schramm A, et al. Lysine-specific demethylase 1 is strongly expressed in poorly differentiated neuroblastoma: implications for therapy. *Cancer Res*. 2009;69(5): 2065-2071.

52. Szymanska B, Wilczynska-Kalak U, Kang MH, et al. Pharmacokinetic modeling of an induction regimen for in vivo combined testing of novel drugs against pediatric acute lymphoblastic leukemia xenografts. *PLoS One*. 2012;7(3):e33894.